NASA CR-174738
AVSCOM TR-84-C-14
EDR 11683

Analytical Fuel Property Effects--
Small Combustors

by

R. D. Sutton, D. L. Troth, and G. A. Miles

Allison Gas Turbine Division
General Motors Corporation
P. O. Box 420
Indianapolis, Indiana 46206-0420

prepared for

National Aeronautics and Space Administration
NASA Lewis Research Center
Contract NAS 3-23165

NASA CR-174738
AVSCOM TR-84-C-14
EDR 11683

Analytical Fuel Property Effects--
Small Combustors

by

R. D. Sutton, D. L. Troth, and G. A. Miles

Allison Gas Turbine Division
General Motors Corporation
P. O. Box 420
Indianapolis, Indiana 46206-0420

prepared for

National Aeronautics and Space Administration
NASA Lewis Research Center
Contract NAS 3-23165

TABLE OF CONTENTS

TABLE OF CONTENTS (CONT)

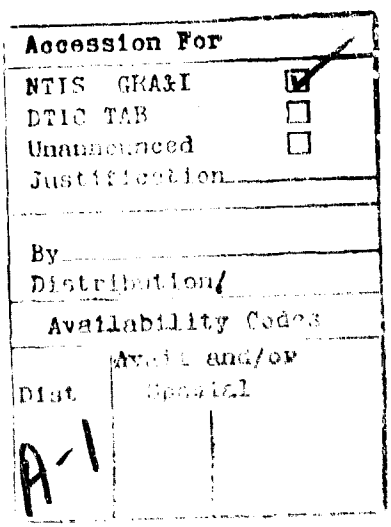

LIST OF ILLUSTRATIONS

LIST OF ILLUSTRATIONS (CONT)

LIST OF ILLUSTRATIONS (CONT)

LIST OF ILLUSTRATIONS (CONT)

LIST OF ILLUSTRATIONS (continued)

LIST OF TABLES

SUMMARY

The purpose of this program--under Contract No. NAS3-23165--was to assess analytically the consequences of using broad-property fuels in both conventional and advanced state-of-the-art small gas turbine combustors. Predictions were made regarding the extent to which these fuels affected performance, emissions, operational characteristics, and durability of these small combustors. Five fuels, Jet A, ERBS 12.8, ERBS 12.3, ERBS 11.8, and DF-2, were selected to represent the range in fuel properties that may characterize small gas turbine fuels in the late 1980s and beyond.

Eight combustor concepts were initially selected for considerations in this program. Three of the combustors represented modifications to the existing baseline combustor (a current production combustor from the 250-C30 engine). The remaining four combustors represented advanced concepts. Each combustor concept was defined through the preliminary design phase to determine general sizing, basic dimensions, hole sizes, and airflow distribution.

Selection of four combustor concepts for further detailed analysis was made objectively on the basis of the merits of each of the eight combustor concept candidates. A total of 17 concept selection criteria were established in five major areas for evaluation: fuel systems, performance, emissions, system effects, and development time and cost. Four combustor concepts were considered to have sufficient merit to warrant further analysis. These included the pressure fed dual orifice injector baseline combustor (as a control concept for the analysis), two baseline airblast injected modifications, the short and piloted prechamber combustors, and an advanced concept--the airblast injected, variable geometry air staged combustor.

Final predictions--regarding the effect of the five fuels on performance, emissions, durability, and operational characteristics of the four selected final combustor candidate concepts--employed the use of the STAC-I computer code developed during this program. This quasi 2-D streamtube (surrounding a central recirculation zone) type model includes real fuel properties, effects of injector type on atomization and drop size distribution, detailed droplet dynamics, and multistep chemical kinetics. The model was specifically developed to assess combustor performance, unburned hydrocarbon, carbon monoxide and thermal nitric oxide emissions, ignition and lean-blowout characteristics, and pattern factor trends when operating over a wide range of fuels. The computer code predicts these combustor traits as a function of combustor concept, operating condition, and fuel type.

Analysis of the processes occurring within the combustors indicates that although the impact of fuel type on combustion performance and liner durability is small in comparison with the effects of combustor concept, liner geometry, and combustor operating conditions, it is nevertheless of sufficient magnitude to warrant serious consideration.

In general fuel property effects on various combustor concepts can be classified as chemical or physical in nature. Predictions from STAC-I and correlations indicate that fuel chemistry, as delineated primarily by hydrogen content, has a significant effect on flame radiation, liner wall temperature, and smoke emissions.

Fuel physical properties that govern atomization quality and evaporation rates are predicted to affect ignition characteristics, lean-blowout limits, combustion efficiency, unburned hydrocarbon, and carbon monoxide emissions. Just as these parameters, and thermal nitric oxide emissions, are predicted to be nearly unaffected by fuel chemistry, flame radiation, liner wall temperature, smoke emissions, and even thermal nitric oxide emission are predicted to be sensible independent of physical properties. Thermal nitric oxide emission is important only at high power levels and neither the chemical nor physical properties of the fuel have significant effects on this type of NO_x formation in this operating regime. Thermal nitric oxide formation is predicted to be dependent primarily on the combustion gas temperature and available oxygen concentration. Fuel bound nitrogen effects with respect to NO_x production are not significant for the fuels considered in this report.

Fuel chemistry also is predicted to have no direct influence on pattern factor. Physical properties affect the pattern factor at low power through decreased evaporation of the spray. The importance of the effects of this physical property diminish with engine power becoming very small at the highest power setting where the effect of pattern factor on engine life is most significant.

Finally, STAC-I predicted results clearly indicate that any deteriorated performance characteristics of the ERBS fuels and DF-2, as compared with Jet A, are primarily due to the physical properties of the fuels as they affect atomization. The thermodynamic properties of the fuels, therefore, have little effect on performance; however, the physical properties, viscosity, surface tension, and liquid density, as they affect the atomization process, also determine the level of performance.

As expected, the combustor candidates that employ hybrid airblast atomization are predicted to be less sensitive to the properties of alternate fuel type, and performance deterioration can be nearly negligible.

The four combustor concept candidates were analyzed by STAC-I (or combinations of STAC-I results and correlations) and ranked, relative to one another with respect to fuel type sensitivity, according to their predicted combustion efficiency, emissions, ignition and lean-blowout characteristics, liner wall temperature and durability, and pattern factor.

With respect to combustion efficiency, unburned hydrocarbon, and carbon monoxide emissions, the relative ranking order of the combustors was unchanged: variable geometry, short prechamber, piloted prechamber, and baseline.

The airblast injected combustors were clearly superior to the baseline combustor and their overall performance was nearly identical.

Both the baseline and variable geometry combustors exhibited better predicted ignition and lean-blowout stability characteristics than either the piloted or short prechamber combustors.

Combustor concept ranking with respect to liner wall temperature effects, thermal nitric oxide, and smoke emissions was predicted to be a function of the individual combustor's internal combustion gas temperature. The ranking

of the combustors is, therefore, in inverse order of their combustion gas temperature: variable geometry, piloted prechamber, short prechamber, and baseline.

Liner wall temperature effects as a function of fuel type would be minimized for the airblast injected concepts since they are to be constructed of Lamilloy, which provides enhanced cooling effectiveness. Soot emission (smoke) is expected to be low for these three combustors, again due to their use of airblast injection. The variable geometry combustor exhibited a clear advantage in regard to decreased thermal nitric oxide emission.

The predicted pattern factor of all three airblast injected combustor concepts was superior to that of the baseline combustor, reflecting the increased spray evaporation rate for all fuel types. Predicted pattern factor differences between the piloted and short prechamber concepts was very small, followed closely by the variable geometry combustor. The baseline combustor was predicted to exhibit considerable sensitivity to fuel type.

On an overall basis, without regard to cost or operating complexity, the analyses would rank the combustors in this order: variable geometry, piloted prechamber, short prechamber, and baseline

The piloted prechamber combustor exhibited a clear, but admittedly small, advantage with respect to ignition and lean-blowout stability, and thermal nitric oxide emission compared with the short prechamber combustor.

When cost and/or operating complexity is included in the analysis, the order of ranking would change: short prechamber, piloted prechamber, variable geometry, and baseline.

The short prechamber concept represents a very simple modification to the baseline combustor, while the variable geometry would require extensive controls for fuel and airflow rate scheduling.

The conclusions from this study indicate that combustors can be modified easily to operate satisfactorily when projected future fuels are used as the energy source for the gas turbine engine. However, other factors such as potential fuel tank freezing should probably be given more consideration than combustor requirements when official fuel property specifications are established. Technical and cost considerations indicate that it will be simpler and less expensive to modify the combustor to meet future fuel specifications than it will be to modify most other engine/airframe systems.

At least one or two of the final airblast injected combustor candidate concepts (short and/or piloted prechamber) should be constructed and a test program initiated to evaluate and verify the predictions resulting from the STAC-1 computer code.

I. INTRODUCTION

The supply, quality, and cost of future aviation gas turbine fuels may be adversely affected by diminishing crude oil supplies, increased demand for middistillates, and deterioration in the quality of the crude oil supply. To ensure a continuing supply of aviation fuel, use of jet fuels with a broader range of properties may be necessary in the future.

The use of fuels with broad ranges of properties in small gas turbine engines by the general aviation industry could adversely affect engine performance, combustor durability, and reliability. These general aviation engines, which have their own special problems and requirements, were the subjects of this analytical study.

The purpose of this program--under contract No. NAS3-23165--was to analytically assess the consequences of using broad-property fuels in both conventional and advanced state-of-the-art small gas turbine combustors. Predictions were made regarding the extent to which these fuels affected performance, emissions, durability, and operational characteristics of these small combustors. For this program five fuels representing the range in fuel properties that may characterize small gas turbine fuels in the late 1980s and beyond were selected.

A series of eight combustor concepts were initially selected for consideration in this program. These combustors represented three levels of technology. The current production combustor from the small gas turbine engine selected for this study represented the first level; three combustor concepts representing baseline combustor modifications, which could be easily substituted for the existing baseline combustor, were considered to reflect a second level of technology. Finally, four advanced combustor concepts, which could depart significantly from the baseline combustor design and which were to exhibit tolerance to alternate fuel types while providing improved performance, were selected as representative of the third level of technology.

Final predictions--regarding the effect of the five fuels on performance, emissions, durability, and operational characteristics of four selected final combustor candidate concepts--employed the use of the STAC-I computer code developed during this program. This quasi-2-D model includes real fuel properties, effects of injector type on atomization and drop size distribution, detailed droplet dynamics, and multistep chemical kinetics. The model was specifically developed to assess combustor performance, emissions, and durability when operating over a wide range of fuels. STAC-I also serves as a design tool for initial sizing and selection of engine combustor candidates.

1.1 ENGINE AND CYCLE CONDITIONS

Allison Gas Turbine Division is one of the world's largest producers of small gas turbine engines for general aviation and military helicopters. Through 1983 Allison has produced over 23,000 Model 250 gas turbine engines. The Model 250 engine, shown in Figure 1, evolved from the T63 engine originally developed for the U.S. Army Light Observation Helicopter (LOH) competition in the early 1960s.

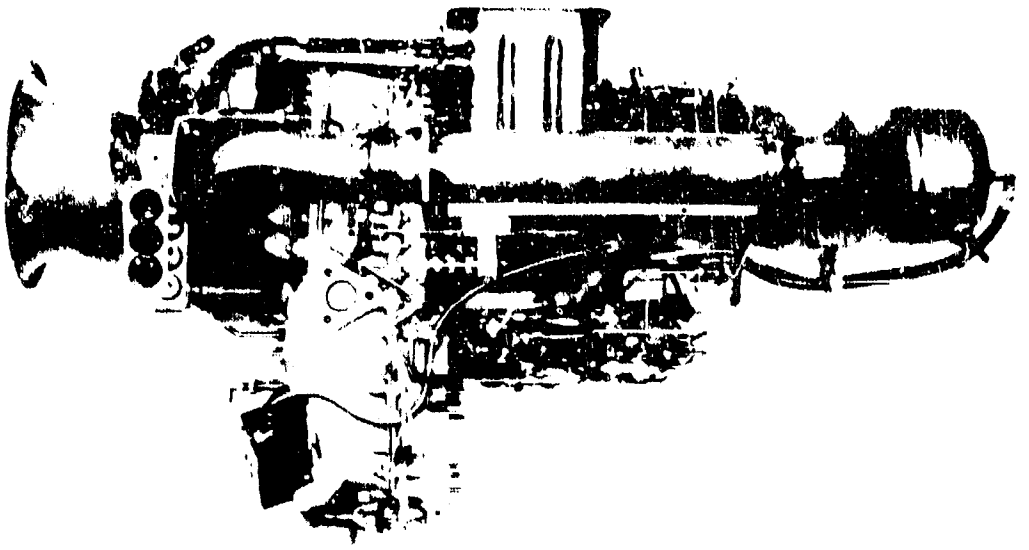

TE80-1538

Figure 1. Allison Model 250 turboshaft gas turbine engine.

From this military beginning the T63 engine moved into the commercial marketplace in 1965 to power the Bell 206 Jet Ranger. These original Model 250-series engines were rated at 236 kW [317 shaft horsepower (shp)]. With subsequent modifications and growth steps, the engine has developed into three major models in production--including the Model 250-C20B, rated at 313 kW (420 shp); the Model 250-C28, rated at 373 kW (500 shp); and the Model 250-C30, rated at 485 kW (650 shp).

The Allison Model 250 engine production now constitutes 68% of all gas turbine engines between 298 and 820 kW (400 and 1100 shp) in use in the U.S. and 40% of those in the world. The Model 250-series engine is recognized worldwide as a well-tested, reliable product. Thus, the Model 250-C30 turboshaft engine, shown in Figure 2, was selected for the baseline production engine on this program. The Model 250-C30 is a 485 kW (650 shp) engine the latest in a series of Model 250 engines produced for general aviation use. The unique engine arrangement of the Model 250 engine series permits use of a highly simplified combustion system consisting of a simple can combustion chamber and a single fuel injector. The production Model 250-C30 prechamber combustion system is shown in Figure 3.

Important mechanical features of the combustion system include the following:

- o prechamber fed by axially swirled airflow
- o dual-orifice, pressure-atomizing fuel injector
- o water shield over primary air feed holes
- o film-cooled barrel
- o dual spark ignitors

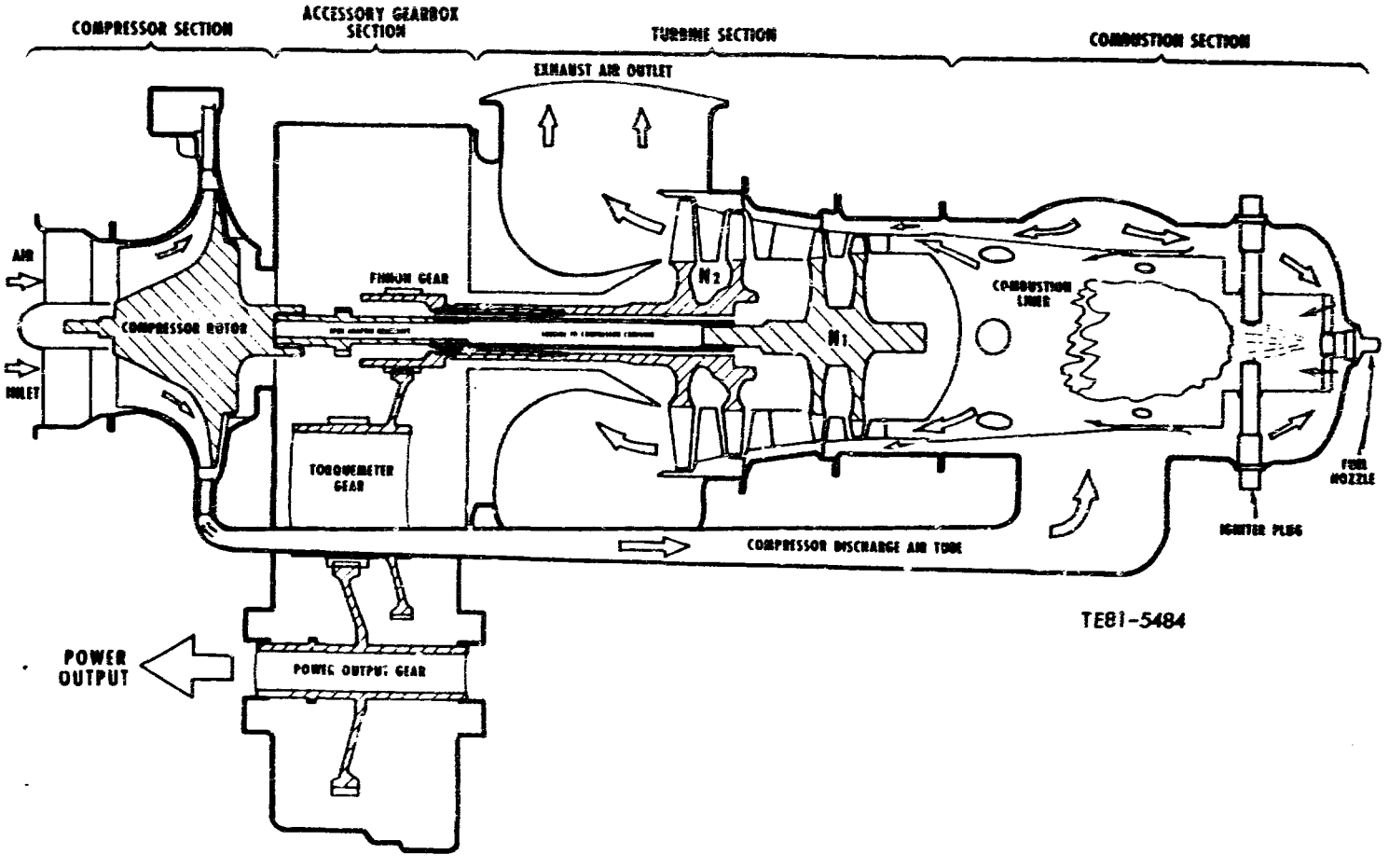

Figure 2. Cross section and airflow schematic of the Allison Model 250-C30 gas turbine engine.

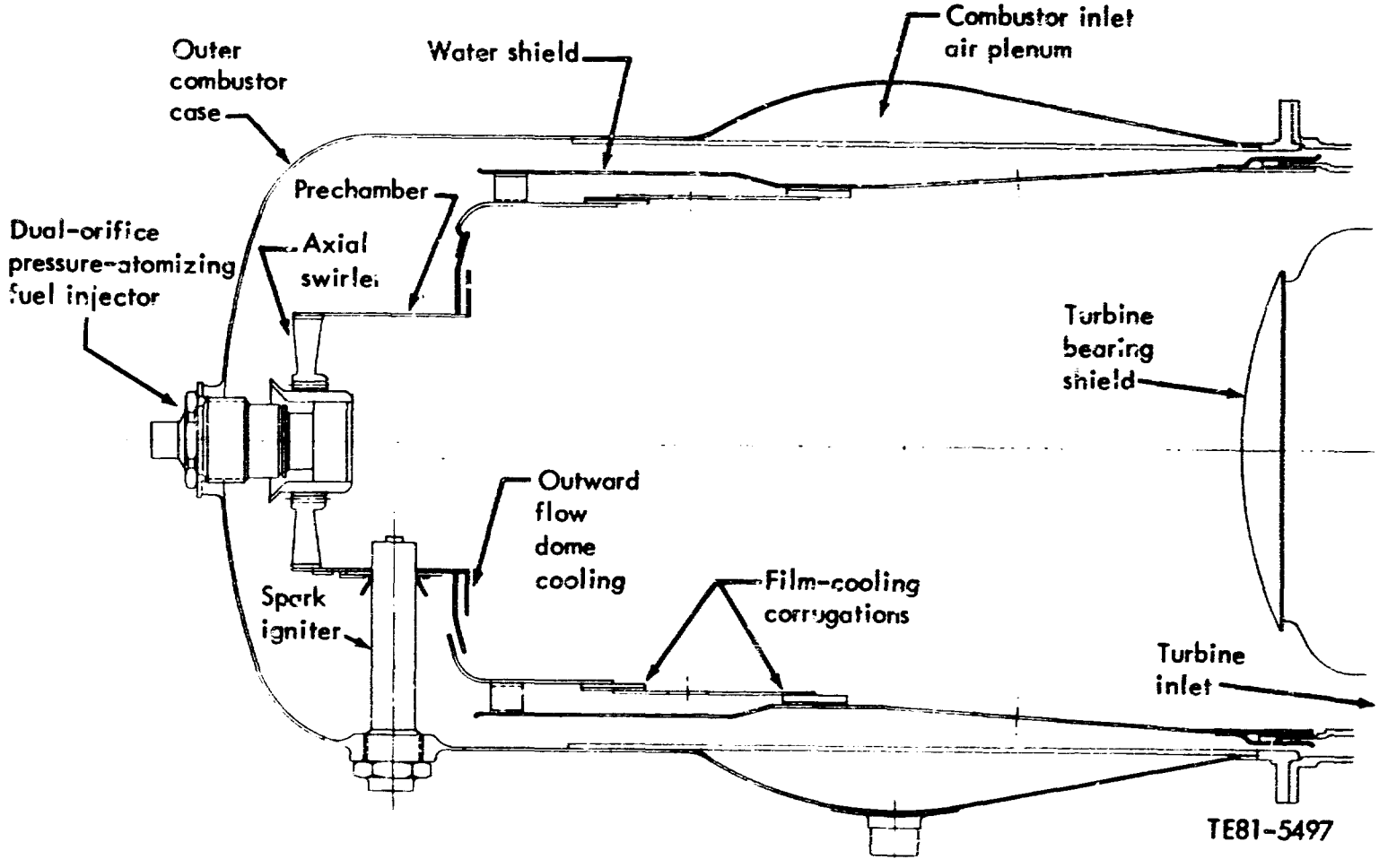

Figure 3. Cross section of production Model 250-C30 combustion system.

Prechamber combustors have demonstrated the following advantages:

- o reliable altitude/cold starting
- o reduced emission levels
- o increased tolerance to water ingestion
- o reduced noise

The prechamber is a good candidate for burning wide specification fuels because of its dual burning-zone feature consisting of the small-diameter prechamber expanding into a larger-diameter reaction zone. There is a smooth transition between the burning zones. The stoichiometry for this combustor was designed to be fuel-rich in the primary zone to improve idle emissions. A reaction-zone equivalence ratio of almost 1.8 occurs at the maximum power condition. The measured smoke level of the combustor at this condition, an Environmental Protection Agency (EPA) smoke number of 45, is faintly visible in helicopter applications. The combustor operating conditions for the Model 250-C30 engine are given in Table I.

Table I.
Model 250-C30 combustor operating conditions for LOH duty cycle and JP-4 fuel.

	kW--shp	Hp--%	Airflow rate, W_a--kg/s (lb/sec)	Burner inlet temperature--°C (°F)	Burner outlet temperature--°C (°F)
Takeoff	484.7 (650)	100	2.48 (5.47)	321 (610)	989 (1812)
Cruise	415.4 (557)	86	2.37 (5.22)	306 (582)	931 (1708)
Hover	372.9 (500)	77	2.29 (5.04)	297 (566)	899 (1651)
Air taxi	279.6 (375)	58	2.08 (4.59)	275 (527)	831 (1527)
Descent	186.4 (250)	38	1.84 (4.05)	252 (485)	755 (1391)
Flight idle	93.2 (125)	19	0.98 (2.15)	179 (354)	560 (1040)
Ground idle	29.8 (40)	6	0.91 (2.00)	149 (300)	516 (960)

	T_{rise}--°C (°F)	Burner inlet pressure--kPa (psia)	Corrected flow--$W_a R\sqrt{T}/P$	Fuel flow, W_f--kg/h (lb/hr)	Fuel/air ratio
Takeoff	650 (1202)	872 (126.5)	1.4145	167.9 (370.1)	0.01879
Cruise	608 (1126)	812 (117.8)	1.4304	148.4 (327.2)	0.01741
Hover	585 (1085)	774 (112.2)	1.4388	137.0 (302.0)	0.01664
Air taxi	538 (1000)	685 (99.3)	1.4522	113.5 (250.3)	0.01515
Descent	486 (906)	583 (84.6)	1.4716	89.5 (197.3)	0.01353
Flight idle	363 (686)	304 (44.1)	1.3910	38.3 (84.4)	0.01090
Ground idle	349 (660)	292 (42.4)	1.3004	31.8 (70.0)	0.00972

As denoted in Table I, the Allison Model 250-C30 engine consumes approximately 2.48 kg/s (5.5 lb/sec) of air while operating at an 8.6:1 maximum power pressure ratio. The combustor outlet temperature is approximately 982°C (1800°F), allowing for future thermal growth. The Model 250-C30 turboshaft engine has wide usage and is representative of the present state of the art; the model, therefore, was chosen as the characteristic small gas turbine engine for this study.

1.2 FUELS

To distinguish fuel property effects on various combustor designs for a gas turbine engine, both physical and thermodynamic fuel data are required. Physical data, i.e., liquid viscosity and surface tension, are used in conjunction with injection models to determine spray drop size distribution and location. These particular properties have been determined for many of the alternate fuels. However, the thermodynamic and some additional physical properties of hydrocarbon mixtures required by the spray combustion model STAC-I include, as a minimum, the following as a function of the droplet internal temperature:

- o liquid
  - o molal mass
  - o density
  - o specific heat and enthalpy
  - o vapor pressure
  - o latent heat of vaporization
- o vapor
  - o molal mass
  - o specific heat and enthalpy
  - o thermal conductivity
  - o viscosity

For hydrocarbon fuels such as JP-4, JP-5, JP-8, Jet A, and DF-2, such properties are tabulated or can be determined using the methods of Ref 1, 2, 3, 4, and 5. However, the various specifications for the family of Experimental Referee Broadened Specification (ERBS) fuels, such as ERBS 11.8 and ERBS 12.3 (weight percent of hydrogen), result from the fact that these fuels are blends. Both of these blends are composed of different mixtures of ERBS 12.8 (which is already high in aromatic content having a hydrogen-carbon ratio of 1.76) and a light blending stock, which has an extremely high volumetric aromatic content (above 80%) and a low hydrogen content--10.26% by weight. The high aromatic content of the blending stock is composed of very volatile compounds (more than 20% by weight naphthalenes). As a consequence, the distillation curves of all three ERBS blends, as presented in Figure 4, deviate considerably from those of the more usual hydrocarbon fuels, also shown in Figure 4. The deviation is more pronounced for the ERBS 11.8 and ERBS 12.3 blends below the 50% distillation point because they reflect larger concentrations of the blending stock. Above the 50% distillation point, all of the ERBS blends appear to have approximately the same properties resulting from the heavier, low volatility fuels from which the parent fuel, ERBS 12.8, was made.

The most definitive data obtained describing the physical and thermodynamic properties of the ERBS fuels have been gathered through the characterization work of F. N. Hodson at Monsanto (Ref 6) under contract to Major D. Potter, Air Force Wright Aeronautical Laboratory (AFWAL)/POSF, Aero Propulsion Labora

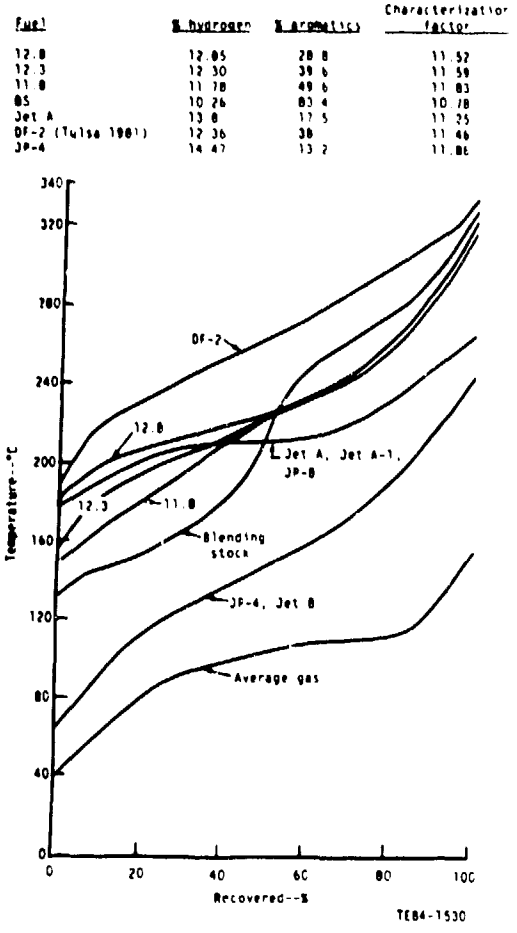

Figure 4. Fuel distillation curves using ASTM D86 method.

tory, Wright-Patterson Air Force Base, Ohio. Communications with both of these men led to the conclusion that very few ERBS 11.8 and ERBS 12.3 thermodynamic property data exist at elevated temperatures. Due to the constituency of these fuels these properties were thought to be incalculable by the standard methods of Ref 1 through 5. In fact, very few ERBS 12.8 thermodynamic data exist in this temperature regime. But due to the lack of the blending stock, the methods of Ref 1 through 5 were thought usable to obtain most of the thermal properties of this fuel. Thus, to model the effects of these broad property fuels, representative fuels were initially selected that bracket the properties of the ERBS blends and for which thermodynamic data were available.

The fuels initially selected for use in this analysis are listed along with some of their pertinent combustion-related characteristics in Table II.

The DF-2 chosen for analysis differs from that presented in Figure 4. While the Tulsa 1981 DF-2 is closer in hydrogen percent by weight and aromatics percent by volume to ERBS 12.3, very few thermodynamic data were available for this particular DF-2. Further, this fuel was not representative of typical commercially available DF-2 fuels. The DF-2 fuel chosen resulted from a

Table II.
Selected broad-specification fuel types.

	JP-4	Jet A	ERBS 12.8	ERBS 12.3	ERBS 11.8	DF-2 (Navy fuels survey, 1982)
Molal H/C	2.02	1.91	1.76	1.67	1.59	1.82
H% by weight	14.47	13.80	12.85	12.30	11.78	13.22
Aromatic % by vol	13.2	17.5	28.8	39.6	49.6	25.0
Stoichiometric weight f/a	0.06751	0.06822	0.06924	0.06987	0.07046	0.06882

characterization study of the effect of fuel composition on Navy T56 aircraft hot section components (Ref 7). The thermodynamic data for this fuel were available. Though it more closely resembles ERBS 12.8 characteristics, the ASTM D86 method distillation data curve is nearly identical to that of the Tulsa 1981 DF-2 fuel. The single exception is the initial boiling point (IBP). The IBP for the selected fuel is 34°C lower (153°C) than that for the Tulsa 81 DF-2. Temperature values for the 10% distillation point and beyond, however, are virtually identical for the two fuels.

As additional data and test results pertaining to the use of ERBS fuels became available (Ref 8), the ERBS fuels appeared to be acting as normal distillate fuels when burned in gas turbine combustors. The aromatic concentration of the fuels did not affect temperature contours appreciably within the combustor; rather the enhanced heat transfer to the liner walls was due to increased radiation flux to the walls. This radiation flux increases as aromatic concentration increases; but such an effect can be computed by a heat transfer model that includes the effects of the C/H ratio (or H%) of the fuel on the flame emissivity, ϵ.

As far as the actual combustion process is concerned, chemical reaction rates were found to vary only slightly between the various hydrocarbon fuels of interest to the aircraft gas turbine (Ref 9). This slight variation is partly because these fuels exhibit only slight differences in adiabatic flame temperature. The variation is also due to the fact that the fuels are largely pyrolyzed to simple hydrocarbons and hydrogen entering the true reaction zone. Hence, the gas composition in the reaction zone is substantially independent of the parent fuel. Any differences that occur in ignition performance, lean-blowout (LBO) limits, and combustion efficiency should then be caused mainly by differences in the physical properties, viscosity, surface tension, and density, of the fuel insofar as they control the quality of atomization and the ensuing rate of evaporation. These same physical properties, along with critical liner design features, and the combustor operating conditions determine the level of emissions. (With the exception of smoke, soot formation is strongly dependent on fuel chemistry.)

These results prompted a review of the initial conclusions that the thermodynamic properties of ERBS 12.3 and 11.8 could not be calculated by standard distillate fuel techniques. Both Maxwell's (Ref 4) method of fuel property

determination and the characterization factor (KF) techniques of Ref 2 treat a range of petroleum fractions that consider paraffin hydrocarbons, having a maximum hydrogen content, as one end and aromatics, which have a minimum hydrogen content, as the other end.

Further, the physical properties, viscosity, and surface tension of the ERBS fuels were well bracketed by Jet A and DF-2. The density of the ERBS fuels is only slightly greater than that of DF-2, and the variation of density with temperature appears to correlate well with standard hydrocarbon relationships. Structural data, involving the composition of the ERBS fuels (Ref 6), were used to compute the latent heat of vaporization and molecular weight of the three ERBS fuels and the resulting values correlated well with those computed using the methods of Ref 2 and 4. Measured vapor pressures of the ERBS fuels (Ref 6) were bracketed by values of the vapor pressure for Jet A and DF-2.

One of the most important thermodynamic properties of a liquid fuel is its specific heat. An analysis of liquid droplet heating and evaporation reveals that the specific heat variation with temperature is one of the major controlling parameters in proper prediction of these rates. When a liquid spray is injected into hot combustion gases, the initial rate of evaporation is low, and most of the energy transferred to the drop from its surroundings is used in heating up the drop. As the liquid temperature rises, the vapor concentration at the drop's surface increases, and a larger proportion of the heat transferred to the drop is used to supply the latent heat of vaporization. Eventually the drop may attain its wet bulb temperature, and from then on, the rate of evaporation will remain nearly constant at its maximum value.

If, however, the liquid fuel's specific heat variation with temperature dramatically increases the value of specific heat, the rate at which the liquid temperature rises is slow enough to impede the evaporation rate of the droplet. Application of the methods of Ref 2 and 4 to compute the specific heat of the ERBS fuels failed to correlate with the measured values as recorded in Ref 6. This lack of correlation was initially responsible for the belief that the ERBS thermodynamic fuel properties could not be calculated by standard hydrocarbon correlations. Further investigation of the ERBS specific heat values reported in Ref 6 indicated, however, that their variations with temperature increased at a rate 2.5 to 5.5 times that of the specific heat variation with temperature of Jet A. Thus, at typical hydrocarbon wet-bulb temperatures of 288 to 316°C (550 to 600°F), the extrapolated ERBS specific heat values of Ref 6 were more than twice that of Jet A (or other hydrocarbon fuels). This value of the ERBS specific heat was high enough to cause the droplet evaporation rate to be negligibly low. (The evaporation rate dependence on temperature is not linear as the vapor pressure is an exponential function of temperature.) In fact, a combustion analysis of the ERBS fuels using the measured value of specific heat variation with temperature indicated that the combustor flow field would not sustain a flame at normal operating conditions.

Private communication between Gary Seng of the NASA Lewis Research Center fuel labs and R. D. Sutton resulted in a resolution of the problem. Calibration of the Ref 6 instrument used to measure the specific heat value of the ERBS fuels indicated that a significant error had been present during the measurements. Removal of this error resulted in specific heat values for the ERBS fuels that

correlated well with those computed using the methods of Ref 1 through 5. The enthalpy of the liquid fuels was obtained by integrating specific heat with respect to the thermochemical reference standard state of 298°K (77°F) and adding the enthalpy of formation of the liquid at this standard state.

No measured data exist for the thermodynamic or physical properties of the ERBS fuels in their vapor state. However, since the liquid properties of the ERBS fuels correlated well with standard liquid hydrocarbon correlations, the vapor properties of the ERBS fuel were computed using standard vapor hydrocarbon correlations.

Both the liquid and vapor properties of Jet A, ERBS 12.8, 12.3, 11.8, and DF-2 are presented in graphical form as a function of temperature in Appendix A. The correlations used to obtain the variation of the individual properties with temperature are also listed. Properties for JP-4 are not presented because the properties of Jet A and DF-2 effectively bracket most of the properties of the ERBS fuels.

1.3 COMPUTER ANALYSIS MODEL--STAC-I

Prediction techniques must be established for accurately estimating, for any given combustor, the impact of any change in fuel specification on hardware durability and the key aspects of combustion performance. A complicating factor in the attainment of this goal is that the effect of a change in fuel properties is not constant for all combustors but varies between one combustor and another, due to differences in operating conditions and differences in design. For example, the effect of an increase in carbon/hydrogen ratio on liner wall temperature is much greater for combustors featuring fuel-rich primary zones than for combustors in which the primary zone is fuel-weak. This is because with rich primary zones most of the heat transferred to the liner wall is by radiation, which is proportional to ϵT_g^4. Thus, liner wall temperature is dependent on the flame emissivity, ϵ, which, in turn, is dependent on the C/H ratio of the fuel. With fuel-weak primary zones, however, most of the heat transferred to the liner wall is by forced convection. Here the dominant term is the gas temperature, T_g, which is fairly insensitive to changes in C/H ratio. In consequence, quite large changes in C/H ratio produce only a slight effect on liner wall temperature.

Another complicating factor is that the various properties and characteristics of petroleum fuels are so closely interrelated that it is virtually impossible to change any one property without affecting many others.

The objective of this program is to advance combustion technology, relative to small gas turbine engines, through an analytical study evaluating the impact of broad property fuels on the performance, emissions, and durability of conventional, modified conventional, and advanced combustor systems. In recognition of this objective and because of the complicating factors, the use of empirical correlations to assess all aspects of such an impact was considered to be unsatisfactory. Empirical correlations to assess the effects of fuel composition on various gas turbine combustors are useful when experimental data are available. An excellent example of such use of empirical correlations is the work of Lefebvre (Ref 9). However, satisfactory correlation of the data to physical phenomena requires the adjustment of constants within the derived empirical expressions. These constants are, in general, specific to

the set of data being analyzed (i.e., the fuels, combustors, performance, emissions, and durability factors that comprise the data set) and, in most cases, specific to the individual combustor being analyzed. The variation in the values of the constants obtained from different combustor types virtually prohibits the extrapolation of predicting fuel effects on the performance, emissions, and durability of future combustor designs.

As this study is concerned primarily with analytically evaluating the impact of fuel effects on future combustors (for which no experimental data exist), a generalized computer model was specifically developed to determine the necessary size, configuration, and durability of combustors required to meet performance and emission standards while operating over a wide range of fuels. The model was used to assess concept trade offs relating to each of four combustor candidates selected from the eight initial concepts. The initial selection process, semi-quantitative in nature, is described in the following section. The formulation of the computer model and its application to the four final concept combustors are discussed in Sections III and IV of this report.

The quasi-two-dimensional (2-D) streamtube analysis in combustors, version I (STAC-I), code was designed to bridge the gap between nonrealistic, perfectly stirred global reactor concepts and full three-dimensional (3-D) codes that emphasize detailed aerodynamics and are better utilized to define the flow field within and required modifications to existing combustors. For example, STAC-I can analyze and evaluate a proposed new combustor design with respect to size, predicted performance, and emissions in approximately 5 to 10 min. This same evaluation would require up to 2 hr or more of computer time if one of the 3-D codes were used.

II. COMBUSTOR CONCEPTS

Eight candidate combustors were initially selected for the Allison Model 250-C30 gas turbine engine. Four of these concepts were analyzed with the combustor model, STAC-1, to assess their tolerance to broad property fuels.

The purpose of this section is to discuss the selection of the four combustor concepts that were considered to have sufficient merit to warrant further analysis. The eight preliminary combustor concepts consisted of the baseline production Model 250-C30 combustor, three concepts that were simple modifications to the baseline combustor, and four advanced combustor concepts. A list of these eight combustor concepts appears in Table III.

Table III.
Eight preliminary combustor concepts selected for Model 250-C30.

Concept Number	Classification	Concept Name/Description
1	Baseline	Production Model 250-C30
2	Baseline mod	Short precnamber
3	Baseline mod	Lean prechamber
4	Baseline mod	Piloted prechamber
5	Advanced design	Reverse flow
6	Advanced design	Annular primary
7	Advanced design	Variable geometry air addition
8	Advanced design	Staged fuel

2.1 DISCUSSION OF PRELIMINARY CONCEPTS

Each combustor concept was defined through the preliminary design phase to determine general sizing, basic dimensions, hole sizes, and airflow distributions. An aerodynamic analysis was performed on the baseline combustor to define individual airflows entering the combustor liner. The remaining seven concepts adjusted individual airflows by area ratios. A semi-quantitative stoichiometry zonal analysis was defined for each concept to permit fuel/air ratios and equivalence ratios to be computed for each internal zone (e.g., primary, intermediate, dilution, recirculation, etc). All of these analyses were performed assuming the combustors were burning a typical JP-4 fuel. Effects due to fuel property variations were computed by STAC-1 for the final four combustor concepts.

2.1.1 Concept 1--Baseline Model 250-C30 Combustor

The production combustor system for the current Allison Model 250-C30 engine is a single can-type combustor that directly feeds the first-stage turbine vane annulus. Components in the combustor system are identified in Figure 5. The can combustor is a prechamber type design that has been developed at Allison and has demonstrated exceptional combustion stability against lean

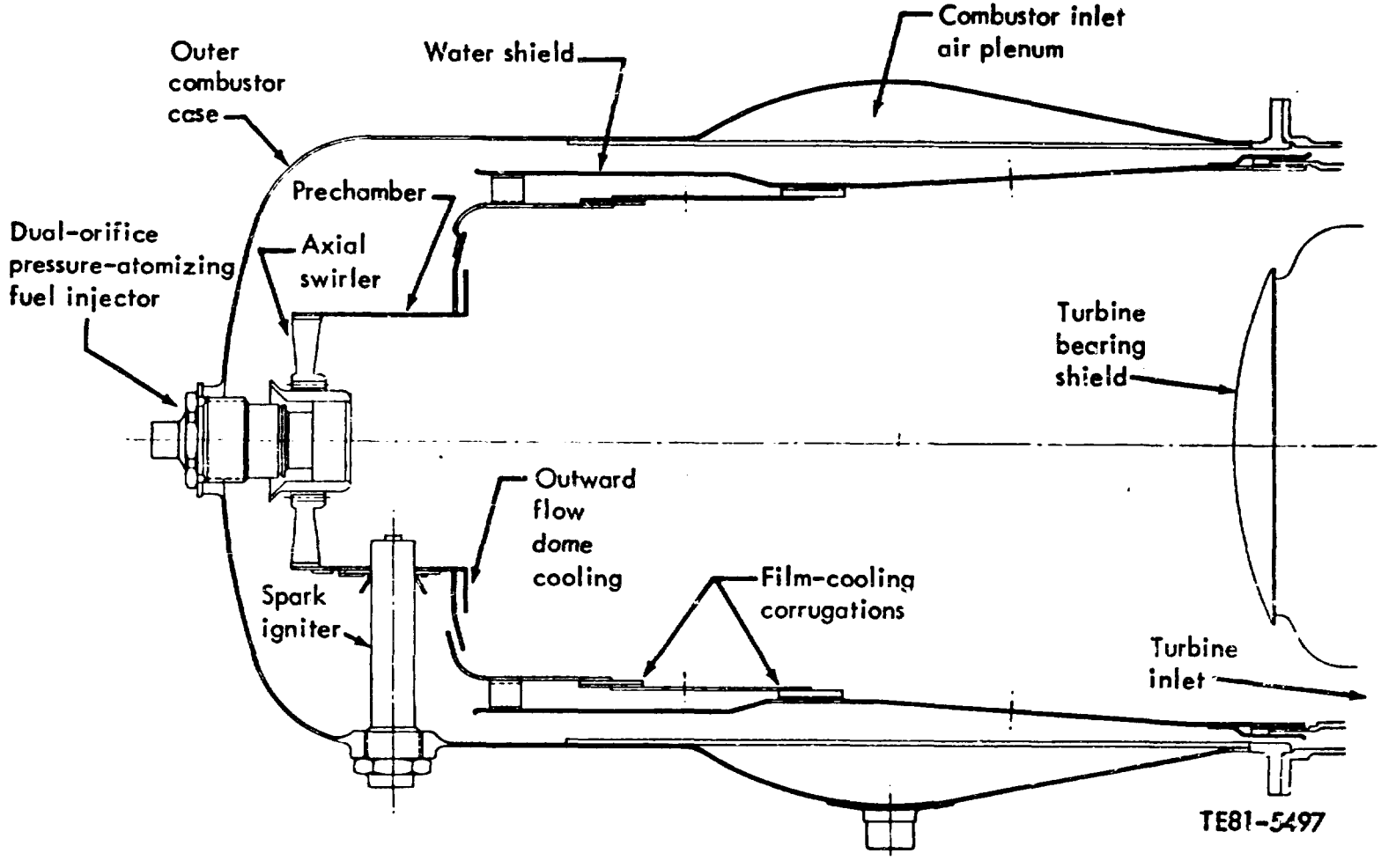

Figure 5. Combustor concept No. 1 production Model 250-C30.

blowout and engine water ingestion. The prechamber functions as a fuel/air premixing region that then supplies the swirl-stabilized, abrupt-expansion primary zone in the combustor liner. The production fuel nozzle is a dual-orifice, pressure-atomizing injector. The fuel nozzle and the axial swirler comprise the entrance area of the prechamber.

The combustion liner is cooled by two film-cooling baffles in the primary zone dome and by two film-cooling corrugations along the liner barrel. Ignition is accomplished with two surface-gap spark igniters located 90 deg apart at the bottom of the prechamber. A water shield covering both the primary air-addition holes and the two liner film-cooling corrugations is also used to improve the tolerance to engine water ingestion.

Aerodynamic mass flow distributions were predicted using the aerodynamic air distribution design model, CJ-2D, for the baseline combustor at each of the seven steady-state operating conditions. Differences in flow distributions among the operating conditions were negligible, so the maximum power flow distribution shown in Figure 6 was used for all operating conditions.

With the flow distributions defined, the stoichiometry zones for the baseline combustor were determined as illustrated in Figure 7. From a combustion design standpoint, the zones of fundamental interest are the prechamber,

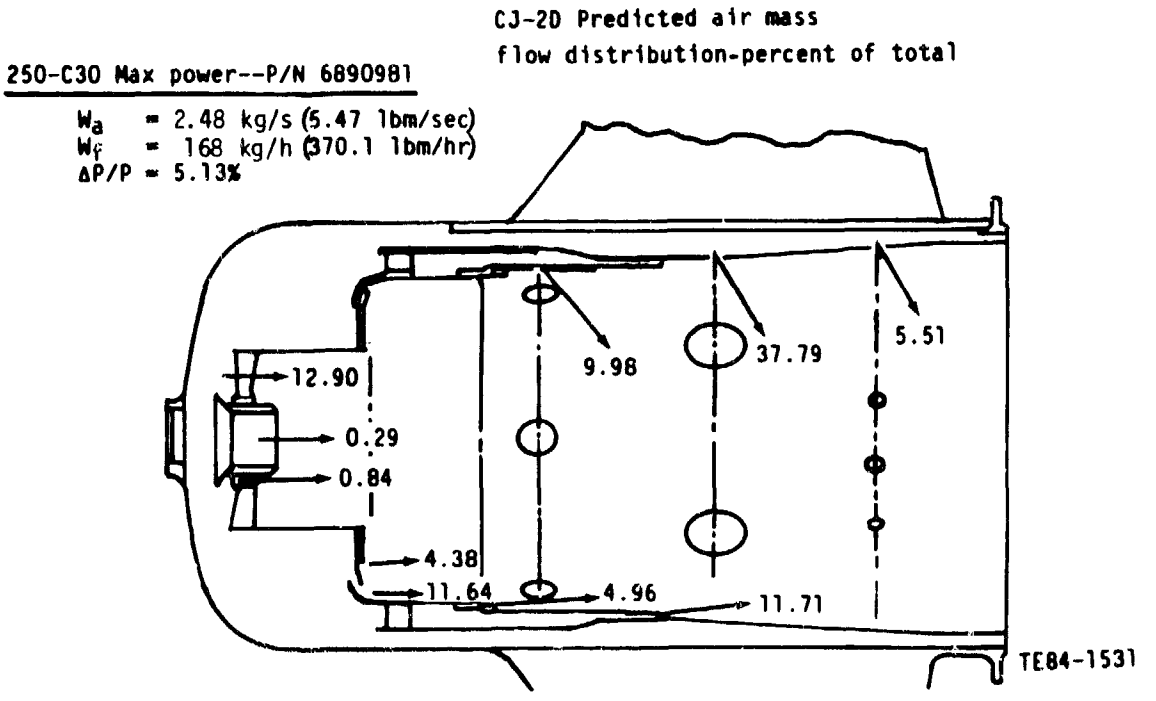

Figure 6. Baseline Model 250-C30 aerodynamic analysis flow distribution.

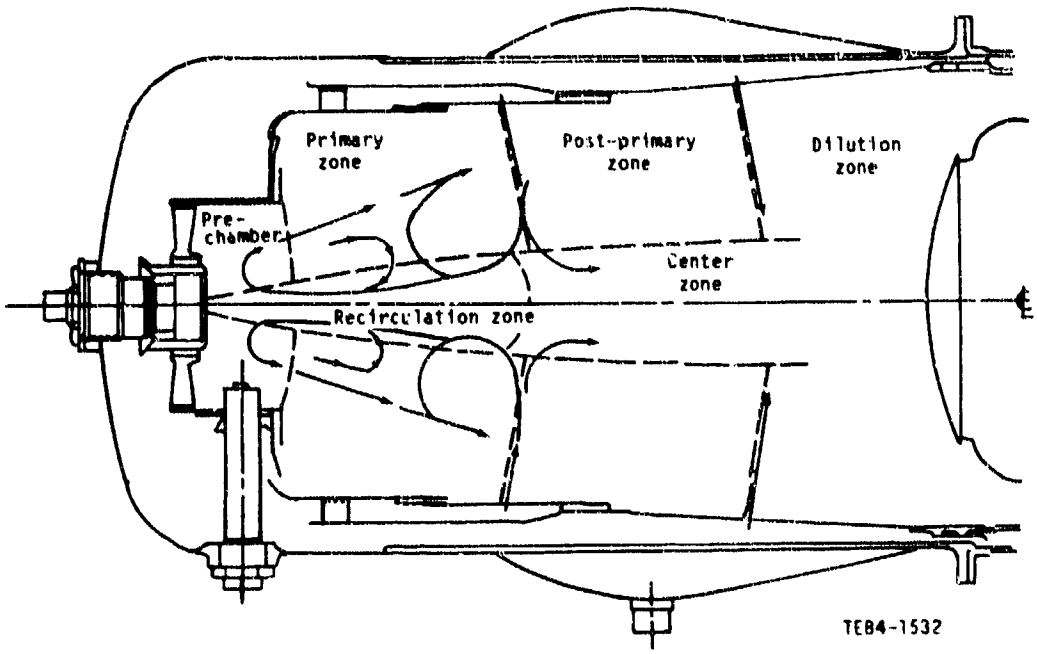

Figure 7. Definition of stoichiometry zones for baseline Model 250-C30 combustor.

primary, post-primary (intermediate), and center zones. Stoichiometries for each of these zones were defined based on a semi-analytical/empirical flow analysis employing past experience with other combustion systems.

The average equivalence ratio, ϕ, in each combustor zone is

$$\phi = \frac{W_f}{W_a}/(f/a_s)$$

where

W_a = fraction of the air in that zone
W_f = fractional expression of the fuel in that zone as compared with the overall fuel rate or, proportionately, the overall fuel/air ratio (f/a_o)
f/a_s = stoichiometric ($\phi = 1$) fuel/air ratio for the fuel being burned

Using this definition, air and fuel flow proportions were defined for each zone. From these definitions the average zone equivalence ratios were computed. In the following analysis, simplifying assumptions have been made. Only one, thin, hollow spray cone is assumed to flow from the fuel injector. This spray cone mass is "initially presumed" to flow through the prechamber and primary zone without loss of mass to the plane of the primary jets. There a certain percentage of the spray cone mass is entrained by the primary jets. This entrainment is denoted as primary hole blockage (PHB) and is computed in the following manner. The diameter of the thin spray cone at the primary jet

plane is assumed to be equivalent to the combustor diameter at this plane. Since the spray cone is considered to be thin, the proportion of the spray cone mass entrained by the primary jets is taken as the linear ratio of the number of primary jet holes times their diameter to the perimeter of the combustor at this plane. That is, the entrainment, or PHB, is:

$$PHB = \frac{\text{Number of primary jet holes x diameter hole}}{\Pi \text{ x diameter combustor}}$$

Of this entrained spray mass, half is assumed to recirculate and enter the primary zone. The remaining half of the entrained spray mass flows downstream into the center zone. This same proportion applies to the primary jet flow; half is assumed to recirculate into the primary zone and the other half flows into the center zone. Simple bookkeeping now indicates that, of the spray cone mass, (1 - PHB) of it is available for reaction in the prechamber and (1 - PHB + PHB/2) = (1 - PHB/2) is available for reaction in the primary zone and post primary zone. These results occur, of course, due to the initial assumption that the proportion of the total spray entrained by the primary jets is based on 100% of the spray available just prior to entrainment. In light of the other assumptions, an iteration on the amount of the spray cone mass available at the primary jet plane is not warranted.

In the analysis that follows, the equivalence ratio of the recirculation zone and the center zone are assumed to be the same. The recirculated combustion products shown in Figure 7 are not considered. Further, no pilot spray (as from an actual dual orifice injector) is considered. A portion of this spray flow, if it were present, would enter the recirculation zone and, in combination with the entering portion of the primary jet air and recirculated combustion products, increase the equivalence ratio of the recirculation zone and enhance both ignition and lean-blowout characteristics of the combustor. Finally, the concept of a center zone downstream of the recirculation zone, and into which half of the primary jet flows, is simply an artifice to permit the computation of the approximate equivalence ratio of the prechamber and primary zones. As each of the combustor candidates was analyzed and ranked using the same approximations, errors incurred through lack of detailed flow field information were thereby greatly diminished. Thus, the analysis and ranking procedure described in the following is considered quite valid. A full, detailed flow analysis of the final four selected combustor candidates was performed using STAC-I (see Sections III and IV) and, in general, tended to confirm the order of ranking

The following are the airflow and fuel flow definitions for the baseline combustor; f( ) in the following equations represents the fraction of the total airflow.

1. Prechamber

$$W_a(1) = f(\text{swirler}) + f(\text{ferrule}) + f(\text{fuel nozzle})$$
$$= 0.1290 + 0.0084 + 0.0029$$
$$= 0.1403$$

$$W_f(1) = (1 - \text{primary hole blockage}) * f/a_o$$
$$= (1 - 6 * 0.563/(\Pi*5.696)) * 0.0188$$
$$= (1 - 0.1888) * 0.0188$$
$$= 0.0153$$

Example calculations presented for $W_f(1)$ and ϕ (1) in the following were performed for the maximum power operating condition (e.g., $f/a_o = 0.0188$):

$$\phi (1) = W_f(1)/(W_a(1) * f/a_s)$$
$$= 0.0153/(0.1403 * 0.067920)$$
$$= 1.6005$$

Values used in these equations are given in the upper portion of Table IV. The lower portion of this table shows the zonal airflow, fuel flow, and equivalence ratios for each of the seven steady-state operating conditions. Note that the film-cooling from the corrugations is not assumed to mix into any of the zones analyzed:

2. Primary zone

$$W_a(2) = W_a(1) + 1/2* f(\text{primary}) + 1/4 * f(\text{dome cooling})$$
$$W_f(2) = (1 - 1/2 * \text{primary hole blockage}) * f/a_o$$

3. Post-primary zone

$$W_a(3) = W_a(1) + 1/2 * f(\text{primary}) + 1/2 * f(\text{dome cooling})$$
$$W_f(3) = W_f(2)$$

4. Center zone

$$W_a(4) = 1/2 * f(\text{primary})$$
$$W_f(4) = 1/2 * \text{primary hole blockage} * f/a_o$$

Using the numerical results from Table IV, the combustor prechamber and primary zones have the following average equivalence ratios (neglecting pilot flow):

	Prechamber	Primary zone
Takeoff	1.60	1.09
Ground idle	0.86	0.58

Thus, when the fuel rate in the baseline combustor drops to very low levels, as at idle, the prechamber retains an adequately rich fuel/air mixture that, when coupled with the recirculation zone (fueled with pilot spray flow) created by the swirl flow field and abrupt expansion flame stabilization, results in a very stable pilot region. It is this stability feature of the prechamber that allows it to behave as a premixing region at high power levels when the fuel carries into the primary zone or as a pilot region when the fuel rates are low and combustion occurs in the prechamber.

Table IV.

Zonal analysis results for baseline Model 250-C30 combustor operating on Jet A fuel.

DESCRIPTION OF FUEL

CONSTITUENTS	CARBON	HYDROGEN	OXYGEN	NITROGEN	SULFUR
WEIGHT FRACT	85.903000	14.097000	0.0	0.0	0.0
MOLAR FRACT	33.936304	66.163712	0.0	0.0	0.0
C1 BASE MOLE	1.000000	1.955404	0.0	0.0	0.0

HYDROGEN/CARBON WEIGHT RATIO = 0.164104
FUEL MOLECULE C1 BASE WEIGHT = 13.962048
FUEL STOICHIOMETRIC FUEL/AIR = 0.067920

NORMALIZATION OF FLOW FRACTIONS

0.12900	0.00290	0.00840	0.04380	0.11640	0.04960	0.09990	0.11710
0.37790	0.05510						

COMBUSTOR INTERNAL DIAMETERS

2.9360	0.0	0.0	0.0	0.0	5.4860	5.6960	5.9760
6.0436	6.3750	6.4700	5.1400				

NUMBER OF HOLES PER LOCATION

0.	0.	0.	0.	0.	0.	6.	0.
6.	12.						

DIA OF AIR HOLES AT EACH AXIAL LOCATION

0.0	0.0	0.0	0.0	0.0	0.0	0.56300	0.0
0.07000	0.25000						

TAKEOFF CONCEPT 1, BASELINE

REGION	WA	WF	PHI
PRECHAMBER	0.14030	0.01525	1.60046
CENTER	0.04990	0.00177	0.52356
PRIMARY	0.23025	0.01703	1.09969
POST-PRIMARY	0.27030	0.01703	0.92738

CRUISE @ 145 KN CONCEPT 1, BASELINE

REGION	WA	WF	PHI
PRECHAMBER	0.14030	0.01412	1.48127
CENTER	0.04990	0.00164	0.48457
PRIMARY	0.23025	0.01576	1.00751
POST-PRIMARY	0.27030	0.01576	0.85832

HOVER CONCEPT 1, BASELINE

REGION	WA	WF	PHI
PRECHAMBER	0.14030	0.01347	1.41317
CENTER	0.04990	0.00157	0.46229
PRIMARY	0.23025	0.01503	0.96129
POST-PRIMARY	0.27030	0.01503	0.81895

AIR TAXI CONCEPT I, BASELINE

REGION	WA	WF	PHI
PRECHAMBER	0.14030	0.01225	1.28547
CENTER	0.04990	0.00143	0.42052
PRIMARY	0.23025	0.01367	0.87442
POST-PRIMARY	0.27030	0.01367	0.74436

DESCENT CONCEPT 1, BASELINE

REGION	WA	WF	PHI
PRECHAMBER	0.14030	0.01095	1.14926
CENTER	0.04990	0.00127	0.37596
PRIMARY	0.23025	0.01223	0.78177
POST-PRIMARY	0.27030	0.01223	0.66594

FLIGHT IDLE CONCEPT 1, BASELINE

REGION	WA	WF	PHI
PRECHAMBER	0.14030	0.00884	0.92792
CENTER	0.04990	0.00103	0.30355
PRIMARY	0.23025	0.00987	0.63121
POST-PRIMARY	0.27030	0.00987	0.53768

GROUND IDLE CONCEPT 1, BASELINE

REGION	WA	WF	PHI
PRECHAMBER	0.14030	0.00819	0.85989
CENTER	0.04990	0.00095	0.28128
PRIMARY	0.23025	0.00915	0.58439
POST-PRIMARY	0.27030	0.00915	0.49822

2.1.2 Concept 2--Short Prechamber Combustor

The short prechamber combustor, shown in Figure 8, is very similar to the baseline. The distinguishing features are as follows:

- o slightly reduced prechamber length
- o increased prechamber swirl
- o airblast fuel injection
- o advanced cooling (Lamilloy®*)

The prechamber length reduction combined with increased prechamber swirl will provide more stable performance by avoiding prechamber wall fuel wetting, which is sometimes experienced on the baseline combustor and can cause unde sirable performance variations. The short prechamber will therefore be used on all of the remaining prechamber configurations.

The airblast fuel injector will provide reduced fuel droplet size and improved fuel dispersion into the combustion air. This improved fuel/air integration will exist at all operating conditions. The airblast fuel injector is therefore a fundamental improvement that will be used on all of the remaining configurations, whether or not they retain a prechamber.

The Lamilloy advanced cooling scheme will be used in the short prechamber design to overcome two shortcomings in the baseline combustor. First, exhaust emissions (CO, UHC, and smoke) would be reduced since Lamilloy does not quench and directly transport to the turbine incompletely oxidized components near the liner wall as does the film cooling system on the baseline combustor. By keeping these components in the reacting environment, they should continue to react to completion, resulting in significant lowering of exhaust pollutants. Second, the Lamilloy cooling system does not interfere with the primary zone aerodynamic recirculation pattern as does the aft flowing dome film-cooling system on the baseline combustor. This improvement in primary zone recirculation should improve lean blowout stability and low power combustion efficiency.

Zonal analysis definitions for the short prechamber combustor were identical to the baseline combustor, with adjustments made in flow distributions to account for differences in fuel nozzle and cooling flows. The equivalence ratios for the short prechamber were the following (again in the absence of a simplex pilot combined with the airblast main injector):

	Prechamber	Primary zone
Takeoff	1.49	1.04
Ground idle	0.80	0.56

The short prechamber design appears to be an excellent candidate combustor that incorporates some simple improvements to an already good combustor and should produce a low-emission, fuel tolerant, stable combustor system.

*Lamilloy is a registered trademark of General Motors Corporation.

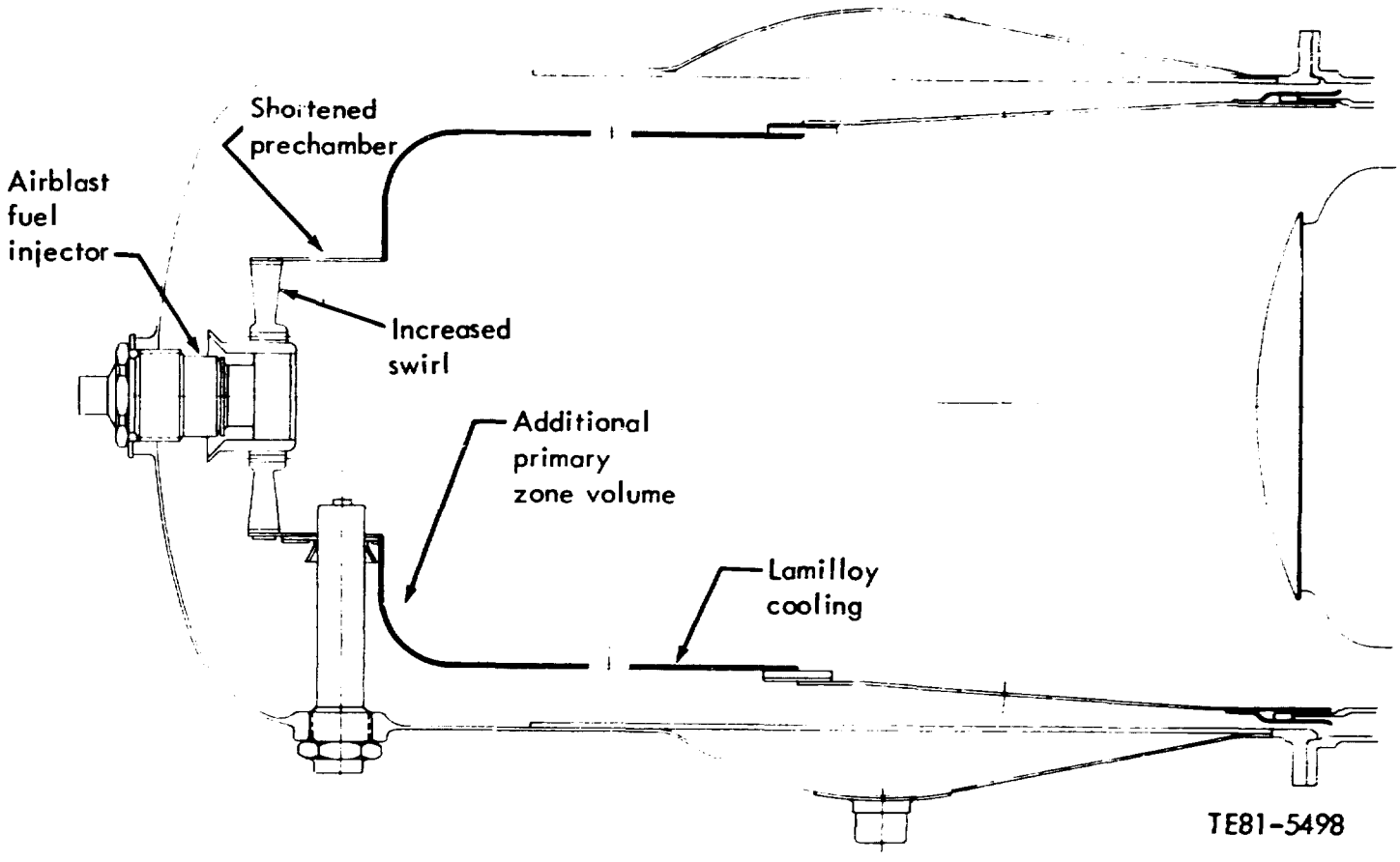

Figure 8. Combustor concept No. 2- short prechamber.

2.1.3 Concept 3--Lean Prechamber Combustor

This modified baseline concept is shown in Figure 9. This concept is similar to the short prechamber design, but additional air is introduced into the prechamber by means of a radial inflow swirler to achieve a leaner prechamber equivalence ratio. This will result in improved smoke control with the low hydrogen broad specification fuels. Operation of this type combustor on other experimental programs demonstrated excellent mixing efficiency and performance potential at the design point with airblast fuel injection and radial and axial air entry swirlers.

Zonal analysis definitions for air and fuel remained the same as for the baseline combustor, again with the air distributions adjusted to produce a leaner primary zone. Equivalence ratios for the lean prechamber were the following (again in the absence of a pilot flow):

	Prechamber	Primary zone
Takeoff	1.07	0.93
Ground Idle	0.57	0.50

Because the primary zone is leaner to reduce smoke and NO_x emissions, the range of satisfactory performance at low power and the range of lean blowout stability is somewhat compromised. Thus, this design may not perform as well overall as the short prechamber (Concept 2), which maintained the higher zonal stoichiometries.

2.1.4 Concept 4--Piloted Prechamber Combustor

This modified baseline concept is shown in Figure 10. The principal design objective of this concept is to accomplish improved prechamber piloting with a single centerpoint fuel injector. As illustrated, the pilot stage is fueled by a narrow spray-angle pilot tip. The pilot fuel spray engages a small amount of air entering the prechamber through a conventional axial swirler. The pilot zone flame stabilization is improved over conventional prechambers by the prechamber wall divergence, which sets up recirculation and flame stabilization in the swirling flow field.

The main zone is fueled by a very wide spray angle airblast atomizer. The main zone fuel is deposited on the prechamber walls by the wide fuel spray angle and the prechamber swirling flow field. Subsequently, the main zone fuel is airblast atomized from this surface into the main combustion zone by the main zone swirling air. This "wall film" fueling method has provided outstanding performance in several Allison advanced combustor programs. This arrangement ensures that the pilot zone is <u>not</u> overfueled by the main zone fuel. In effect, the piloted prechamber combustor is a staged combustor with the fueling simplicity of a single zone combustor. The staged combustion allows good idle and ignition performance from the pilot combustion zone. The main combustion zone also achieves excellent performance because this zone may be sized for lean conditions for low smoke, uncompromised by ignition and low power requirements, that are met in the pilot combustion zone.

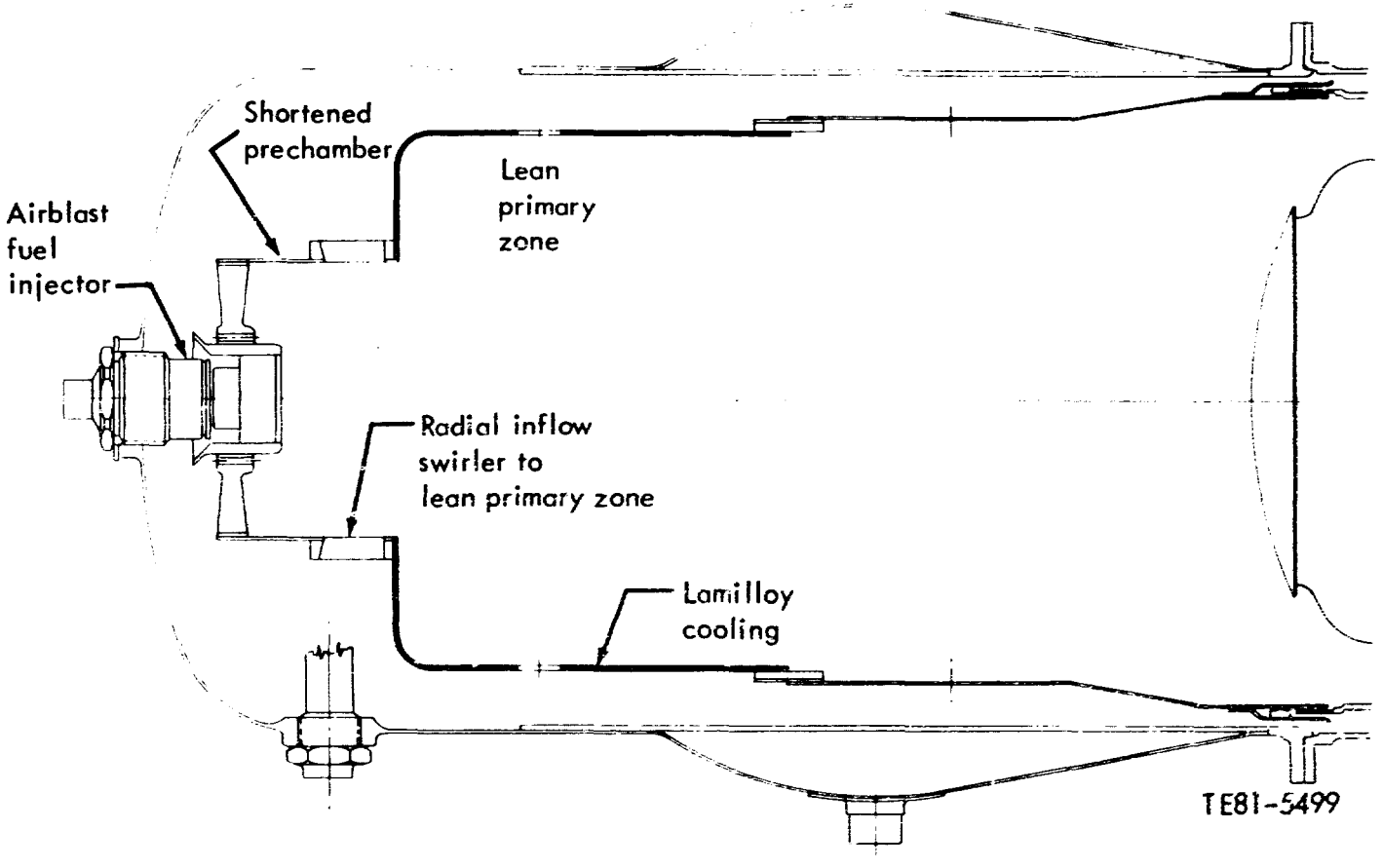

Figure 9. Combustor concept No. 3 - lean prechamber.

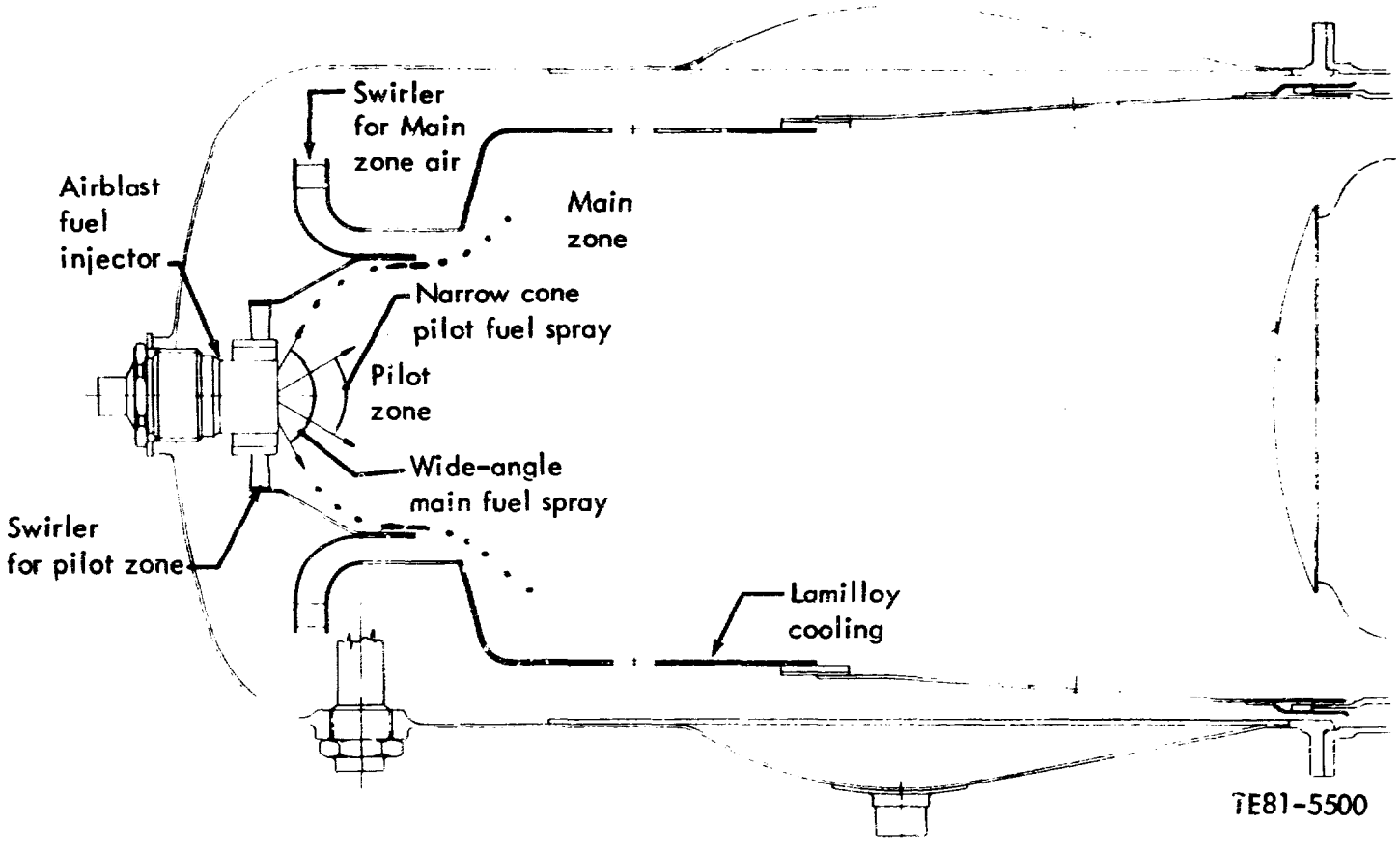

Figure 10. Combustor concept No. 4 piloted prechamber.

The main stage can achieve additional performance gains from fuel preheating and prevaporization resulting from the elevated pilot-side temperatures. The staged combustion characteristics of the piloted prechamber combustor in conjunction with its mechanical simplicity represents a definite combustor technology advancement.

The success of the piloted prechamber depends on the successful design and integration of the multiple orifice fuel nozzle. Initial designs of the fuel system used a two (or dual) orifice fuel injector--one orifice for the pilot and one orifice for the main flow. For good stoichiometry conditions at high power the main zone should operate at equivalence ratios of one or less. If both main and pilot nozzles operated at idle, then the main nozzle received insufficient fuel rates for stable operation. If the pilot orifice flowed all of the idle fuel with the main nozzle off, then at high power the pilot was overly rich creating excess smoke and NO_x. Thus, the solution evolved to a three orifice or triplex fuel nozzle incorporating idle, low, and high power. To control the local stoichiometries, the nozzle requires a valving system that directs fuel to the proper orifices as a function of power level or fuel pressure level.

The desired fuel nozzle operation is shown in Table V for various operating conditions.

Table V.
Fuel nozzle operation.

	Fuel nozzle orifice		
	Pilot	Low power	High power
Start	On	On	Off
Idle	On	On	Off
Descent	On	Off	On
Cruise	On	Off	On
Takeoff	On	Off	On

The pilot orifice flows as soon as pressure is applied to the nozzle and continues to flow at all conditions. The low-power (idle) orifice is sized in conjunction with the pilot nozzle to flow enough fuel to operate the engine at either ground or flight idle conditions (32 or 38 kg/h [70 or 84 lb/hr]). Above idle fuel rates (pressures) the low-power nozzle shuts off as the high power nozzle opens. This occurs in such a manner that there are no flow decreases with increasing fuel pressure. By the time the descent fuel flow level is reached (89 kg/h [197 lb/hr]), the low-power orifice is off and the high-power orifice is on. At this and all higher fuel flows only the pilot and high-power orifices flow fuel. The pilot and low-power orifices constitute the piloted, narrow-angle fuel spray, thus effectively being a dual orifice pilot whose secondary opens and then closes as fuel pressure increases. The high-power (main) orifice is the wide angle spray orifice that supplies the main primary zone. The fuel nozzle orifice schedules, for all three orifice flows, are presented in Figure 11.

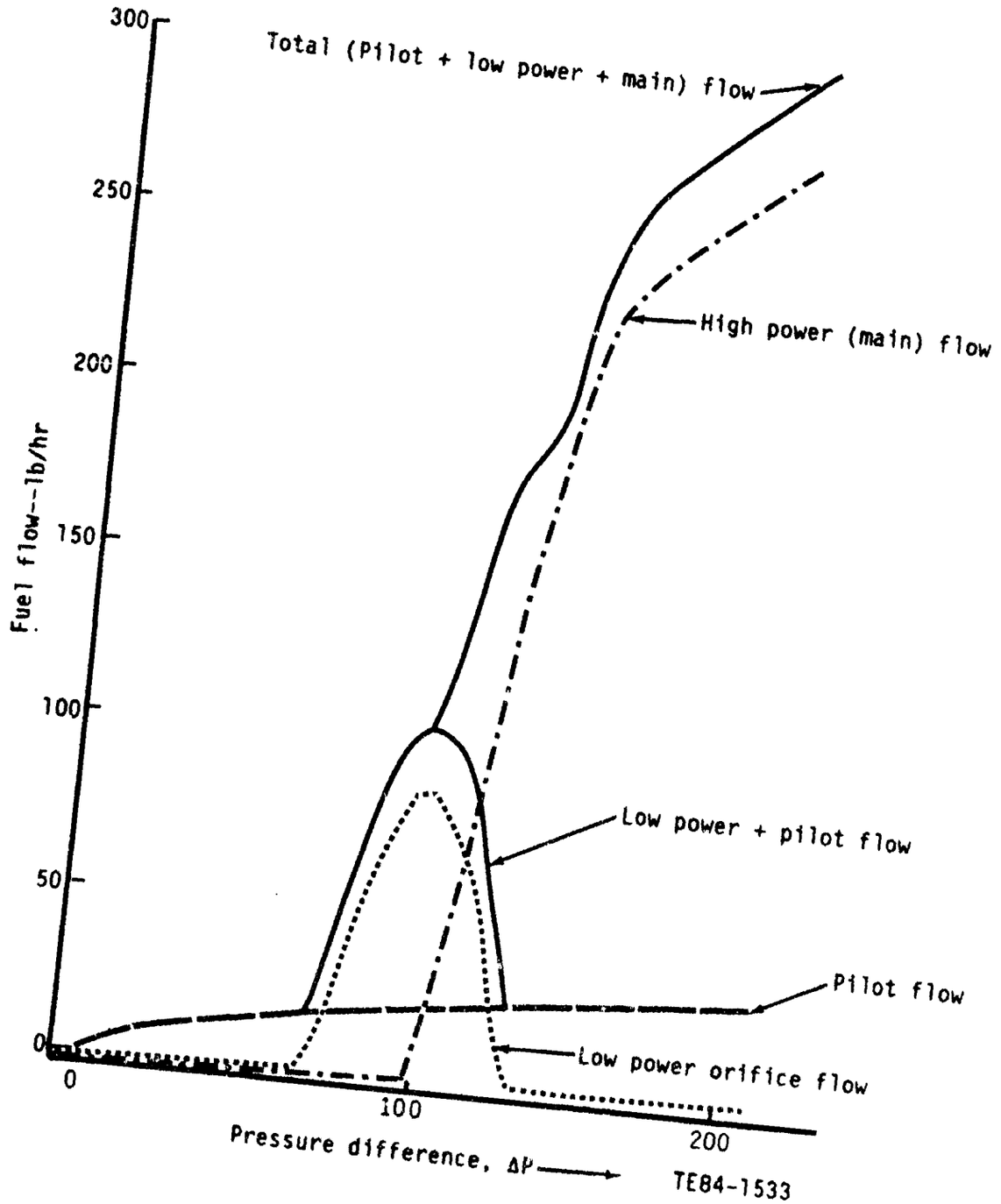

Figure 11. Fuel nozzle orifice schedules for triple orifice fuel nozzle required for piloted prechamber combustor.

The average zonal equivalence ratios for the piloted prechamber combustor using the special triplex fuel nozzle described are the following:

	Prechamber	Pilot	Main primary
Takeoff	2.32*	0.79	0.99
Ground Idle	1.20	1.23	0

*due to the presence of the largely unreacting main nozzle wall-filming flow

The prechamber in this case is the dome of the piloted section accounting for airflows from the fuel nozzle and adjacent axial swirler and the total injector fuel flow.

New internal zones and air and fuel proportions were established for this piloted prechamber design to be more representative of the expected internal flow patterns. The center zone becomes a true pilot zone operating independently from the main zone. As described, both the piloted and main zones are expected to operate relatively lean at high power. With all of the fuel constrained to the pilot region at low power, the combustor should exhibit high stability and have good lean-blowout characteristics.

2.1.5 Concept 5--Reverse Flow Primary Combustor

This design, depicted in Figure 12, employs a primary-zone film cooling air flow reversal. In this technique, the primary zone cooling air is also utilized as combustion air. Additional combustion air is supplied by the air-blast fuel injector, the dome swirler, and the primary jet air holes. This design concept is a fundamental improvement in cooling air management. Cooling air is generally bad for most combustion aspects because the reactions are quenched in the cooling air layer, thereby promoting CO, hydrocarbons, soot, and smoke. By reversing the cooling flow direction, these unburned products are returned to the combustion zone where the reactions can be completed, and the advanced cooling technique (Lamilloy) used on the other concepts is not required.

The reverse flow combustor concept is in production on the Allison Model 501-K industrial engine. This engine has met the stringent air pollution and smoke requirements that accompany a wide range of fuel usage in industrial gas turbines.

The excellent performance potential of the reverse flow combustor concept for the Model 250-C30 engine is based on results achieved in the NASA program Pollution Reduction Technology Program, Turboprop Engine -Phase I, Ref 10. Especially noteworthy is the low smoke No. of approximately 7, obtained over the entire engine operating range.

The internal stoichiometry of the reverse flow combustor should be improved over the baseline combustor. The equivalence ratios entering the combustor, comprised of the fuel nozzle and swirler air plus the fuel itself, are high as

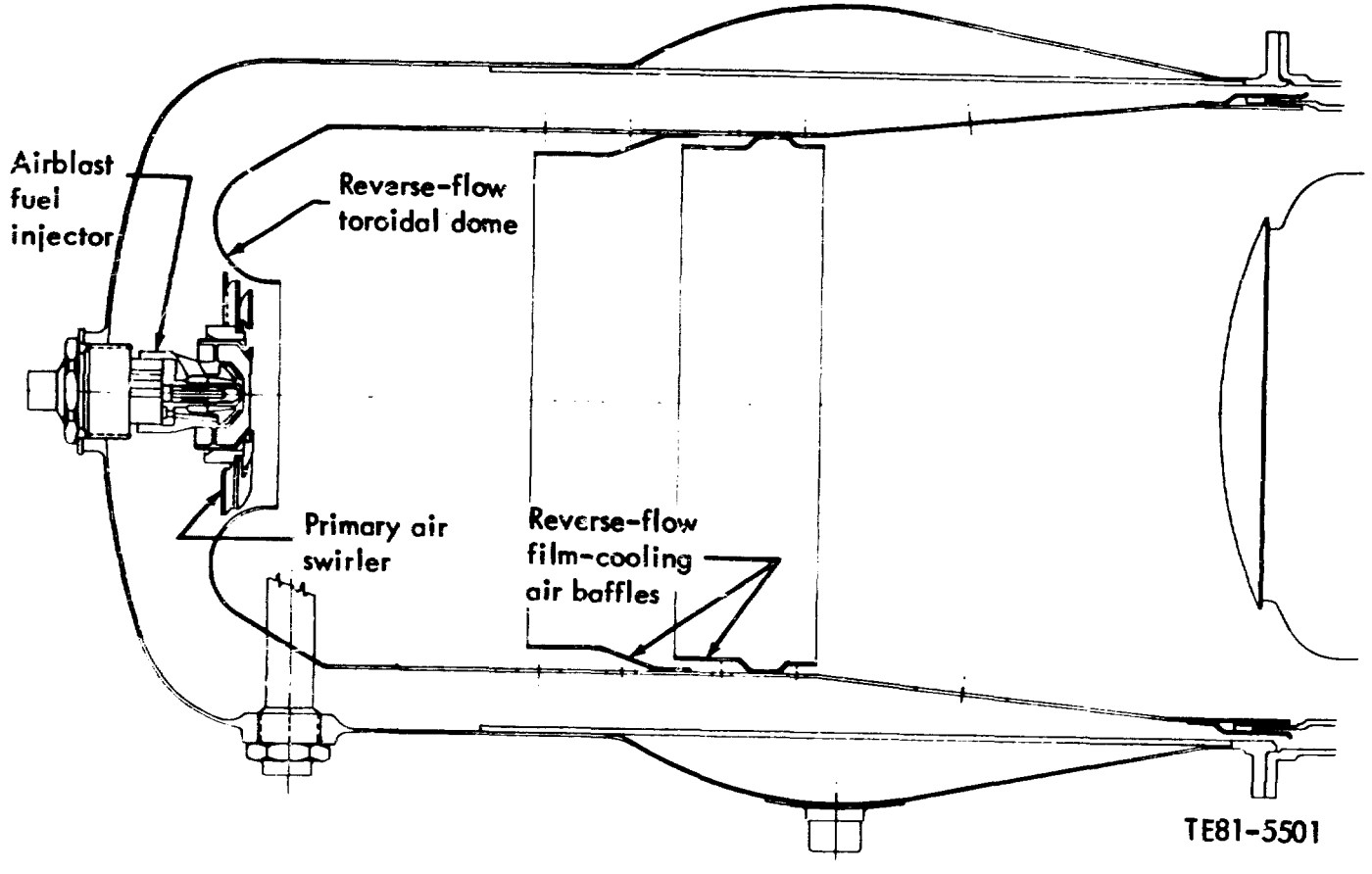

Figure 12. Combustor concept No. 5 reverse flow.

shown, as is the center zone (more properly, the recirculation zone), which should provide for greater LBO stability. These calculations do not include a simplex pilot flow.

	Fuel nozzle/swirler	Primary zone
Takeoff	2.52	1.10
Ground idle	1.36	0.59

2.1.6 Concept 6--Annular Primary Zone Combustor

This new design concept is presented in Figure 13. An annular combustor primary zone is employed in place of the current can-type primary zone. Airblast fuel injection is also employed. The airblast swirl air is supplemented by primary jet holes. The annular combustor concept has fuel injection from many points so that the mixing scale is greatly reduced compared with a single fuel nozzle can. These factors allow improved fuel/air mixing compared with the baseline can-type combustor. As a result, improved smoke control may be expected with this concept. The more uniform primary zone should produce a more uniform exhaust temperature profile when compared with a single fuel nozzle can such as the baseline combustor.

The negative aspects of this design are the increased liner surface/volume ratio, which requires additional air for cooling, and the problems associated with the increase in the number of fuel nozzles--from one in the baseline combustor to six for this annular primary zone design. The maximum engine fuel flow of 167.8 kg/h (370 lb/hr) is easily handled by the single fuel nozzle in the baseline combustor as is the idle fuel rate of 31.8 kg/h (70 lb/hr). The six fuel nozzles in this annular primary zone concept will each inject one-sixth of the total fuel flow: 28 kg/h (61.7 lb/hr) at takeoff and 5.3 kg/h (11.7 lb/hr) at ground idle. Therefore, the orifices in these low flow nozzles will be about 40% of the diameters in the single-nozzle combustor. Plugging of these fuel nozzles, thus can become more of a problem unless additional fuel filtering is added to the system. The lower fuel flow rates per nozzle can also result in longer residence times in the combustor inlet environment and become a problem for fuels having low thermal stability.

Because of the high surface/volume ratio in the primary zone of the liner, Lamilloy cooling is considered mandatory for this type of combustor. Cooling of this annular primary zone concept, even with the use of Lamilloy, will require 30% of the total airflow compared with the Lamilloy cooling-air flow rate requirement of 14% for Concept 2, the short prechamber.

Internal stoichiometries for Concept 6 are quite similar to the baseline combustor, again a simplex pilot fuel flow has been neglected.

	Fuel nozzle/swirler	Primary zone
Takeoff	1.84	1.07
Ground idle	0.95	0.57

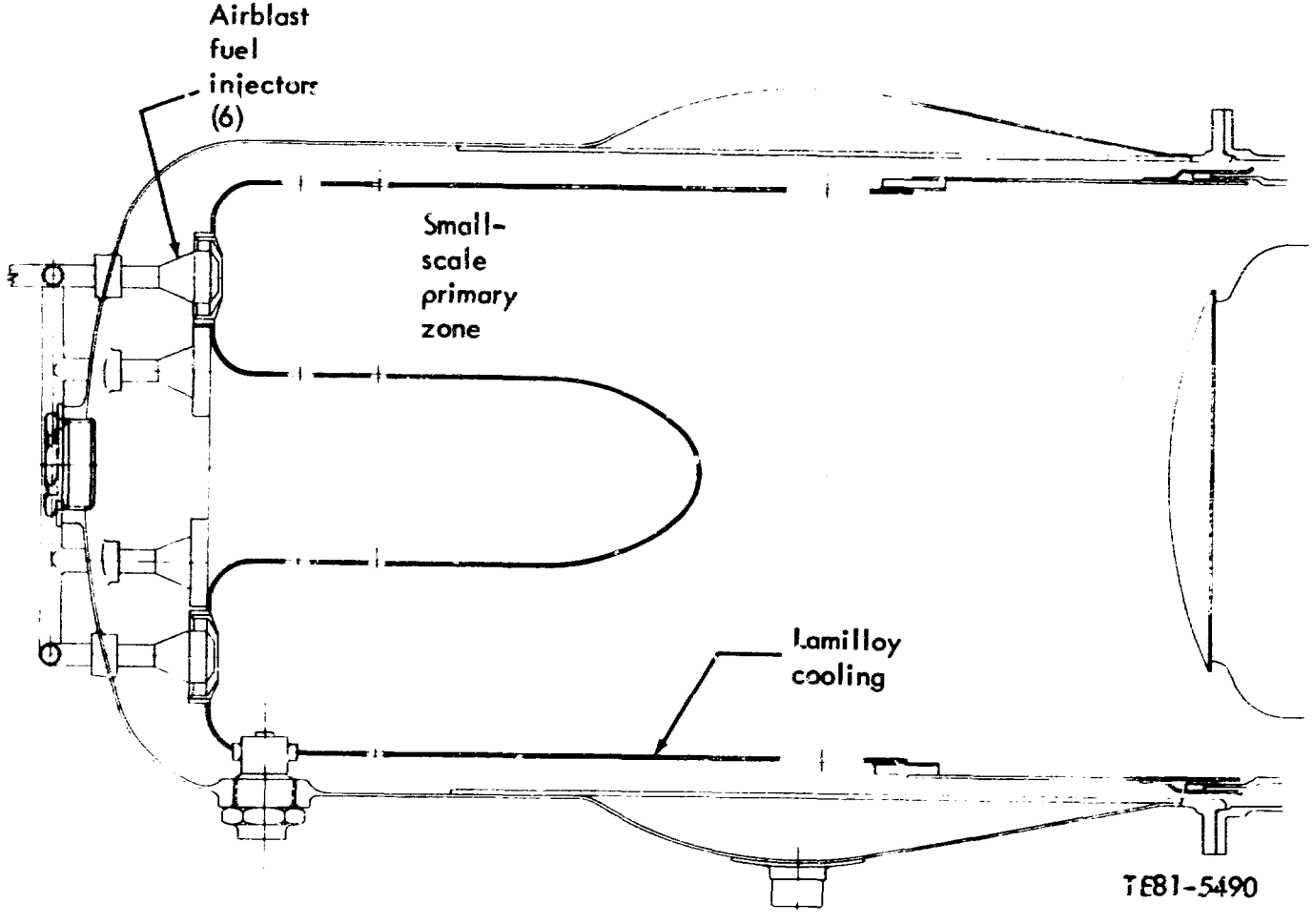

Figure 13. Combustor concept No. 7 annular.

A considerable degree of complexity is associated with the combustor in this concept. This may well be in excess of the needs required for proper combustion of the types of fuels being considered in this study.

2.1.7 Concept 7--Variable Geometry Combustor

This new design concept is shown in Figure 14. This concept is similar to the baseline design, but additional air is used in the prechamber to attain a lean zone in this area for improved smoke control with the low hydrogen broad specification fuels. The additional air is added by means of a radial inflow swirler in the prechamber. Variable geometry on the dilution holes and radial inflow swirlers is employed to accomplish primary zone airflow changes, thereby achieving optimum performance over the complete combustor operating range. The variable geometry system provides a small amount of combustion zone airflow at low power and ignition conditions. At high power, a large combustion zone airflow is employed to control smoke.

The variable geometry combustion air control can provide essentially optimum performance at all operating conditions. However, the increased complexity of this concept is less attractive for engine application. It is very likely that the program goals can be met with less complex combustors. The performance potential of the variable geometry combustor concept is similar, but superior, to the lean prechamber combustor concept previously discussed.

Allison has had 12 years of experience with various forms of variable geometry on automotive gas turbine engines where the variable geometry air staging was used to control engine exhaust emissions. Additional experience has been accumulated on aircraft gas turbine engine programs. A variable geometry combustor was rig tested on the NASA program Pollution Reduction Technology Program, Turboprop Engine--Phase I (Ref 10). Also an Allison Model 250-C20B gas turbine engine (predecessor to the Model 250-C30) was tested with a variable geometry combustor during the Army AMRDL contract Low-Emissions Combustor Demonstration, 1976 (Ref 11). On the engine used in this program the variable geometry was two position for low- (starting/idle) and high-power (cruise/takeoff) optimization. Actuation was pneumatic and was triggered by a speed switch on the engine. The engine was successfully operated on a dynamometer test stand from idle to takeoff power.

Internal stoichiometries for the variable geometry combustor employ an equivalence ratio range of about 2.5 to 1. The simplex pilot fuel flow (which has been neglected) would further increase this equivalence ratio range.

	Prechamber	Primary zone
Takeoff	0.73* - 2.04**	0.68* - 1.48**
Ground idle	0.39* - 1.09**	0.36* - 0.80**

*radial swirler in prechamber fully open
**radial swirler in prechamber fully closed

From these equivalence ratios, the prechamber can be maintained at near constant equivalence ratios of 1.0 for the prechamber and 0.80 for the primary zone. Thus near optimum stoichiometry can be maintained at any operating condition

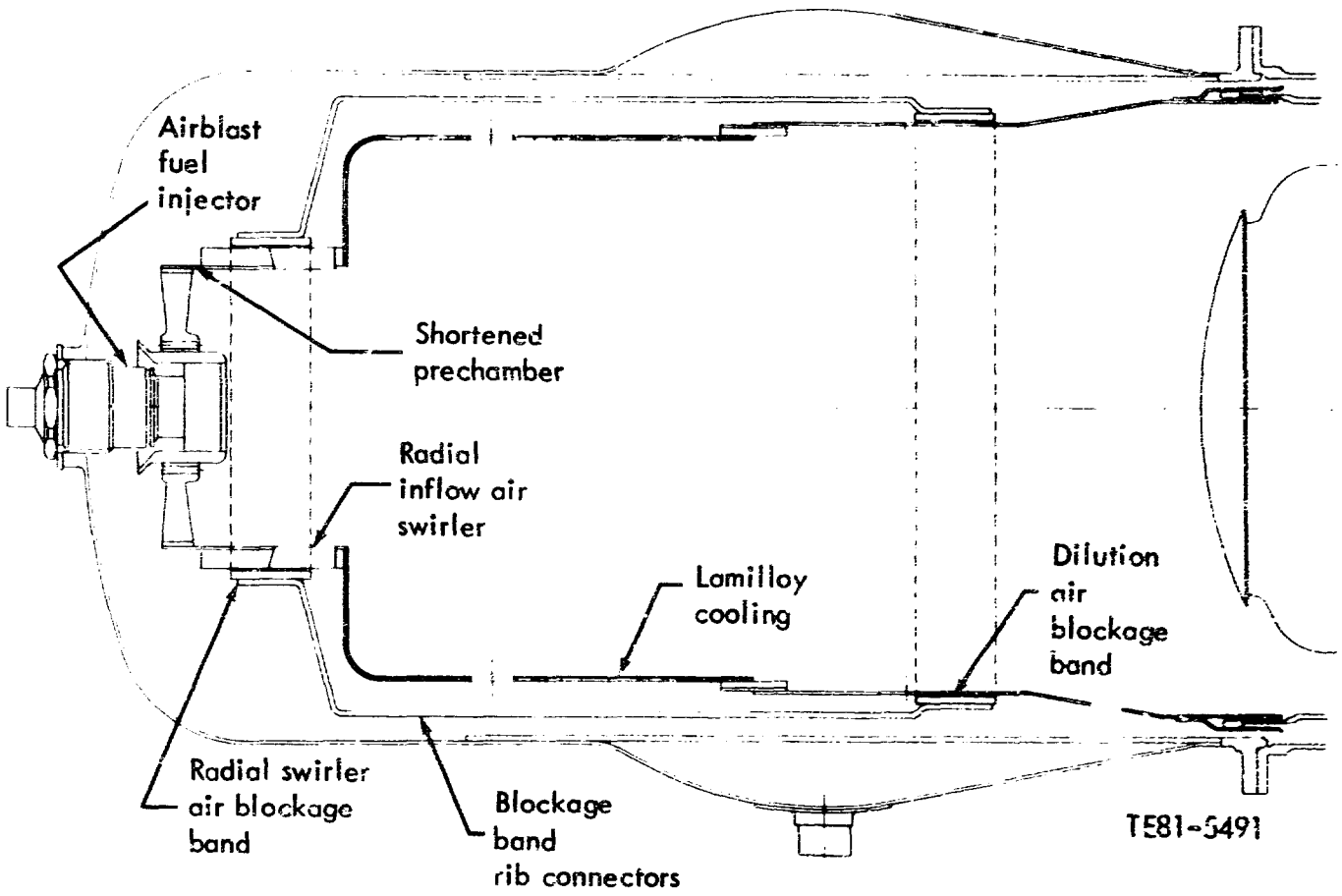

Figure 14. Combustor concept No. 7- variable geometry.

This concept adds control and mechanical complexity but does not compromise the fuel system in any manner. Thus for the broad property fuels that will be studied, this design should prove to be beneficial.

2.1.8 Concept 8--Staged Fuel Combustor

This new design concept is shown in Figure 15. The concept employs discretely fueled prechamber and main combustion zones. The prechamber combustion zone has low airflow to achieve near-stoichiometric conditions at low power for good low power and ignition performance. The main combustion zone has additional airflow to accomplish low-smoke operation at high power conditions. The prechamber combustion zone employs airblast fuel injection with conventional swirl and jet stabilization, accomplished with a short length arrangement. The main combustion zone employs airblast fuel injection and swirl stabilization in several swirl modules.

The staged combustor concept is very similar to the staged fuel combustor developed and tested on the Allison/NASA program "Pollution Reduction Technology Program, Turboprop Engine--Phase I" (Ref 10).

This staged-fuel concept is a more refined version of the Concept 4-piloted prechamber combustor. In this staged fuel design the prechamber and main combustion chambers are separately designed and fueled with their own special fuel systems. Therefore, the fuel distribution, complexity, and stability problems discussed for the annular primary combustor (Concept 6) are as much or even more of a problem with this design.

For proper operation (as was done in Concept 4) the main fuel nozzles operate (flow fuel) only at engine conditions above flight idle or above engine fuel rates of 45.36 kg/h (100 lb/hr). Therefore the main fuel nozzles (of which there are six) must either be purged or cooled during periods when they are not flowing fuel to avoid coking and fouling of the fuel system. Small orifice sizes and low flow rates for each nozzle would continue to be problem areas.

Performance and emission signatures for this combustor concept should be as good as or better than any other concept. The internal stoichiometries favor this excellent performance expectation, which has been proved in experimental tests on other staged combustor systems. The expected equivalence ratios for this combustor are given in the following (again neglecting a simplex pilot fuel flow):

	Prechamber	Main primary zone
Takeoff	0.87	1.01
Ground Idle	2.41	0

The sophistication of this design is probably not warranted for the change in fuel properties and the improvements beyond the baseline combustor needed for successful operation on the proposed fuels. Ultra-low smoke or emissions are certainly possible for this concept, but those are not the overriding priorities for this program.

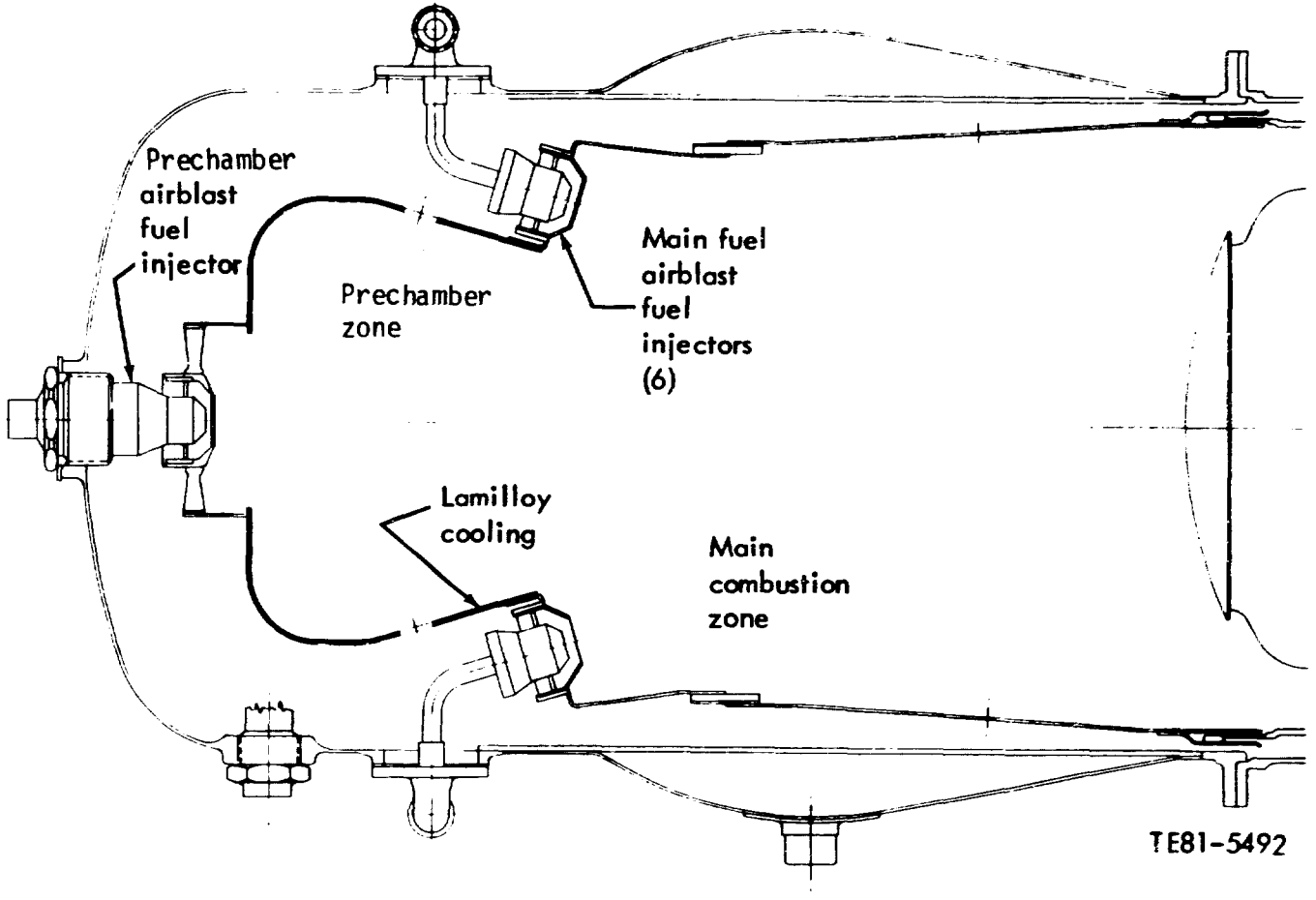

Figure 15. Combustor concept No. 8--staged fuel.

2.2 CONCEPT EVALUATION AND SELECTION

The selection of the four combustor concepts for further detailed computer analysis were made objectively on the basis of the merits of each of the eight combustor concept candidates. Toward this end, a concept ranking system that considered all of the combustor system factors deemed important to the success of this fuel property effects program was devised.

Five major classification areas for evaluation of the combustor concepts were determined: fuel system, performance, emissions, system effects, and development. A total of 17 concept selection criteria were assembled under these five classifications as shown in Table VI. The fuel system category was used to assess the potential effects of broad-property fuels on the candidate combustor concept. The performance category consisted of operational combustor characteristics that may be influenced by changes in fuel properties. The emissions category assessed the relative performance of each combustor concept with regard to the exhaust pollutants that it may produce. The systems effect

---

Table VI.
Task I concept selection criteria for Model 250-C30 combustor system.

Classification	Criteria	Maximum score
Fuel system		
	Complexity	8
	Fuel tolerance	8
Performance		
	Altitude/ground starting (relight)	8
	LBO stability	8
	Idle efficiency	8
	Exit temperature pattern	8
Emissions		
	Smoke	8
	NO_x	8
	CO and UHC	4
System effects		
	Liner durability	8
	Liner complexity	4
	Cost	8
	Weight	4
	Controls	4
	Reliability	8
	Maintainability	8
Development		
	Time/cost	8
	Total	120

category encompassed those aspects of combustion design and operation from a systems viewpoint for the combustor hardware itself and the interaction of the combustor on the rest of the engine. Finally the development of the combustor was included to aid in selecting the concepts from a cost and time effectiveness viewpoint with regard to what may be required to bring each concept to full production for the Model 250-C30 engine.

Once the selection criteria were determined, it was clear that some criteria were of more importance than others, so a simple numerical weighting system was chosen as shown in the right columns in Table VI (labeled maximum score). Since eight concepts were being evaluated, a maximum score of eight was selected for the major selection criteria.

Minor or lesser important selection criteria were given a maximum score of half value or four.

At this point in the selection process the preliminary designs of each of the eight candidate combustor concepts were finalized to aid in better defining the mechanical hardware (fuel nozzles, manifolds, actuators, cooling scheme, etc) and the internal zonal aerodynamic distributions such as those presented for the baseline combustor (e.g., Figures 6 and 7 and Table IV). Air and fuel distributions were determined for each combustor concept and the internal combustion stoichiometries were computed for all steady-state operating conditions. Zonal equivalence ratios for each combustor concept at takeoff and ground idle operating conditions for JP-4 fuel are presented in Table VII. Airflows were adjusted to give satisfactory compromise operation at both takeoff and idle. Again, except for Concept 4, these zonal equivalence ratios do not include the beneficial effects of a simplex pilot, particularly in combination with an airblast injector. Such a combination acts to increase the

Table VII.
Combustor zonal stoichiometries as equivalence ratios
JP-4 fuel.

	1 Base	2 Short	3 Lean	4 Pilot	5 Rev	6 Annul	7 VG	8 Staged
Takeoff								
Prechamber	1.60	1.49	1.07	2.32*	2.52*	1.84*	0.73-2.04	0.87
Recirculation/ Center	0.52	0.40	0.52	0.79	0.57	0.55	0.52	0.62
Main primary	1.09	1.04	0.93	0.99	1.10	1.07	0.68-1.48	1.01
Ground idle								
Prechamber	0.86	0.80	0.57	1.20*	1.36*	0.95*	0.39-1.09	2.41
Recirculation/ Center	0.28	0.22	0.28	1.23	0.31	0.29	0.28	1.72
Main primary	0.58	0.56	0.50	0.0	0.59	0.57	0.36-0.80	0.0

*at swirler/fuel nozzle exit plane

equivalence ratio in the recirculation/center zones, where needed, enhancing the performance characteristics of each of the combustors. This is particularly true with regard to starting, LBO stability, and idle efficiency. Pilot fuel flow affects were considered when the final four combustor concepts were analyzed using STAC-I.

2.3 FINAL COMBUSTOR CONCEPTS

Each of the eight preliminary combustor concepts were primarily designed to define air distributions, fuel placement, local stoichiometries, and hardware complexity. Each combustor concept was subdivided into several combustion zones and then evaluated over the engine operating range to assess zonal stoichiometries, noting any overly lean or rich conditions. Also a 17-category concept selection criteria list encompassing five general areas of classification was prepared to allow for the scoring of each combustor concept in a relative sense.

The rating/scoring system used for the combustor concepts was the "higher-is-better" system where each concept was rated at each of the selection criteria. Scoring was based on past experience, supportive test data, and the stoichiometric calculations resulting from the aerodynamic zonal analyses. Scores were restricted to whole numbers and duplicate scores were allowed. The final scores for each of the combustor concepts at each selection criterion are presented in Table VIII. Individual scores appear in the upper portion of the table, subtotals are shown for each classification category, and final percentages are given at the bottom.

The scores ranged from 73 to 96, which represents 81%-80% of the maximum possible. No combustor concept was outstanding in each of the five categories, and when one concept excelled in a particular area, it usually was lacking in other areas. Thus each combustor concept showed compromise in its design, which is reflected in the narrow range of the total scores.

The final scoring and ranking of the eight combustor concepts are summarized in Table IX.

In the five classification areas, some conclusions resulted that are not evident from the total scores or the rankings.

- Fuel System--The baseline combustor utilizes a single dual-orifice pressure atomizing fuel nozzle. Therefore, the annular primary (6) and the staged fuel (8) concepts may be less tolerant to alternate fuel types. Fuels which have lower thermal stability than Jet A will present problems in these combustor concepts because of the longer residence time of the fuel in the hot environment within the combustor outer case.

- Performance--It is expected that the lean prechamber (3) will fare worst in this category, particularly in the areas of starting, LBO stability, and idle performance. Those combustors exhibiting superior overall performance are the piloted prechamber (4), variable geometry (7), and staged fuel (8). These concepts have the ability to optimize performance at both low and high power independently. The other concepts must compromise their low and high power performance.

Table VIII.
Final scoring of Task I combustor concepts.

Concept Number		1	2	3	4	5	6	7	8
Fuel system									
	Complexity	8	8	8	5	8	5	6	3
	Tolerance	7	7	7	6	7	4	7	3
Performance									
	Altitude/ground start	6	5	4	8	5	4	7	8
	LBO stability	7	6	4	8	5	3	8	8
	Idle efficiency	4	4	2	7	4	3	7	7
	Exit pattern	4	5	5	4	5	7	5	5
Emissions									
	Smoke	3	5	5	6	7	6	6	6
	NO_x	5	5	7	7	6	6	7	8
	CO and UHC	2	2	1	3	3	3	4	3
System effect									
	Durability	5	7	8	7	7	7	6	6
	Complexity	4	4	3	2	4	2	2	1
	Cost	7	6	6	5	7	4	5	4
	Weight	3	4	3	3	3	3	2	2
	Controls	4	4	4	4	4	3	2	3
	Reliability	6	7	7	5	7	5	5	5
	Maintain	7	7	7	5	7	4	4	4
Development									
	Time/cost	8	7	7	4	7	4	4	4
Fuel system	Subtotal	15	15	15	11	15	9	13	6
Performance	Subtotal	21	20	15	27	19	17	27	28
Emissions	Subtotal	10	12	13	16	16	15	17	17
System effect	Subtotal	36	39	38	32	39	28	26	25
Development	Subtotal	8	7	7	4	7	4	4	4
Total score (max - 120)		90.0	93.0	88.0	90.0	96.0	73.0	87.0	80.0
Percent of max score		75.0	77.5	73.3	75.0	80.0	60.8	72.5	66.7
Percent of baseline		100.0	103.3	97.8	100.0	106.7	81.1	96.7	88.9

Table IX.
Final scoring and ranking of the eight combustor concepts.

Combustor Concept Number	1	2	3	4	5	6	7	8
Name	Base	Short	Lean	Pilot	Rev	Annul	VG	Staged
Total Scores (120 max)	90	93	88	90	96	73	87	80
Ranking	-	2	4	3	1	7	5	6
Final Selection	+	+		+	+		+	

- o Emissions--All of the concepts are expected to produce lower exhaust emissions than the baseline combustor due to the use of airblast atomization fuel nozzles and to improved wall cooling, which requires less total air and will consequently quench less of the unoxidized compounds along the walls. As was the case in the performance category, concepts 4, 7, and 8 should excel in the emissions category since these concepts will not need to compromise their operation between low and high power conditions.

- o System Effect--The criteria in this category all give preference to those concepts that are simple and straightforward in design. Combustors 2, 3, and 5 each are expected to perform as a system as well as, if not better than, the baseline combustor. Combustors 4, 6, 7, and 8 are more complex in design and as a consequence their overall system ranking with respect to durability, simplicity, low weight, reliability, and maintainability is not as high as those of the other combustors.

- o Development--With an eye on the relatively near term, the simpler combustor designs, deviating less from current experience, are the more desirable designs for this program. The more complex designs will require more development time and cost.

It is, therefore, recommended that the annular primary (6) and the staged fuel (8) combustor concepts be dropped from further consideration in this program due to their substantially increased complexity and expected reduced tolerance to broad-property fuels. The other concepts have a sufficiently high expectation of success that the higher levels of advanced technology inherent in these two designs are not warranted.

Also, the lean prechamber design (3) should be combined with the variable geometry air staged (7) concept as the high power or lean setting on the variable geometry combustor resulted in very nearly the same configuration.

The reverse-flow design (5) has demonstrated excellent performance in Allison Model 501-K industrial engines and indicated a high potential for this study. Because of the reverse-flow aerodynamics, this concept could not be analyzed with the computer model and was dropped from further analysis.

Thus, the four concepts evaluated for fuel tolerance with the computer model are shown in Table X.

Table X.
Concepts evaluated for fuel tolerance with the computer model.

Concept Number	Classification	Concept Name/Description
1	Baseline	Production Model 250-C30
2	Baseline mod	Short prechamber
4	Baseline mod	Piloted prechamber
7	Advanced design	Variable geometry air addition

III. COMPUTER ANALYSIS MODEL--STAC-I

3.1 GENERAL FORMULATION

STAC-I is a quasi-2-D model essentially composed of streamtubes (zones) of flowing air, unburned spray, and combustion products surrounding a central recirculating zone (CTRZ), shown in Figure 16. The number of external streamtubes (zones) may vary from one (the simplest case) to five or more. The size of the CTRZ is determined by COSMIC, Allison's existing, axisymmetric gas phase elliptic flow code. The amount of mass recirculating (recirculated combustion products, air from the primary jets and/or airblast injectors, and fuel) within the CTRZ is computed internally within STAC-I. Essentially, this is accomplished by performing an energy balance on the amount of mass leaving the CTRZ and that with which it mixes in the external streamtubes.

Mass enters the CTRZ near its downstream boundary from the primary jet air and from recirculated combustion gases from each streamtube. Fuel and additional air (when present) enter from the upstream injector boundary. Fuel entry into the CTRZ is usually determined by specifying that the ratio of fuel/fresh air within the CTRZ is stoichiometric. The proportion of primary jet air entering the CTRZ is not allowed to exceed more than 1/3 of that entering the liner (based on comparisons with 3-D analysis). Additional mass requirements are supplied by the recirculated combustion products. This latter amount of mass can be substantial and the resulting equivalence ratio within the CTRZ is normally not stoichiometric. The volume, and hence residence time of the mass within the CTRZ, is computed, and a chemically kinetic limited, uniform CTRZ temperature is determined. This high-temperature recirculated mass exits from the upstream portion of the CTRZ and mixes with the air and fuel flowing in the adjacent streamtubes. An energy balance on those computational cells into which the CTRZ mass flows must result in mixed gas/fuel unreacted temperatures sufficient to sustain ignition. This is required to avoid having a cold, nonreacting solution propagate throughout the flow field when a combustion solution is desired. The subsequent reacted gas temperatures in each streamtube are determined by fuel vaporization and chemical kinetics, and if a nonreacting solution results, the program reestimates predicted higher mixed gas/fuel unreacted temperatures, which in turn increases the amount of mass recirculated. In effect, the CTRZ acts as an ignition source for the surrounding streamtube flow, and on a quasi-2-D basis the CTRZ appears to well represent the actual physical processes occurring within the combustor.

The proportion of air from axial and/or radial swirlers to each of the surrounding streamtubes is determined by COSMIC, while the proportion of the fuel spray to each streamtube is determined through radial patternation of the fuel nozzle. Cooling air (shown as zone 3 in Figure 16) can be assigned its own streamtube. Conversely, if detailed spray patternation is not available, the flow field is usually described by one external streamtube and the model considers the flow to be swirling about the radius of gyration of the flow field. The proportion of air and fuel initially assigned to each streamtube remains invariant. Mixing between streamtubes is not allowed, rather the area assigned to each streamtube varies in proportion to the gas phase evolution (continuity requirements) within the streamtube. External mixing of the recirculating combustion products from each streamtube to and from the CTRZ and of tne primary, dilution, and trim air jets to the streamtubes is, of course, allowed. Recirculating combustion products are withdrawn from the streamtubes in a region just prior to entry of the primary air jet. The air jets' penetration

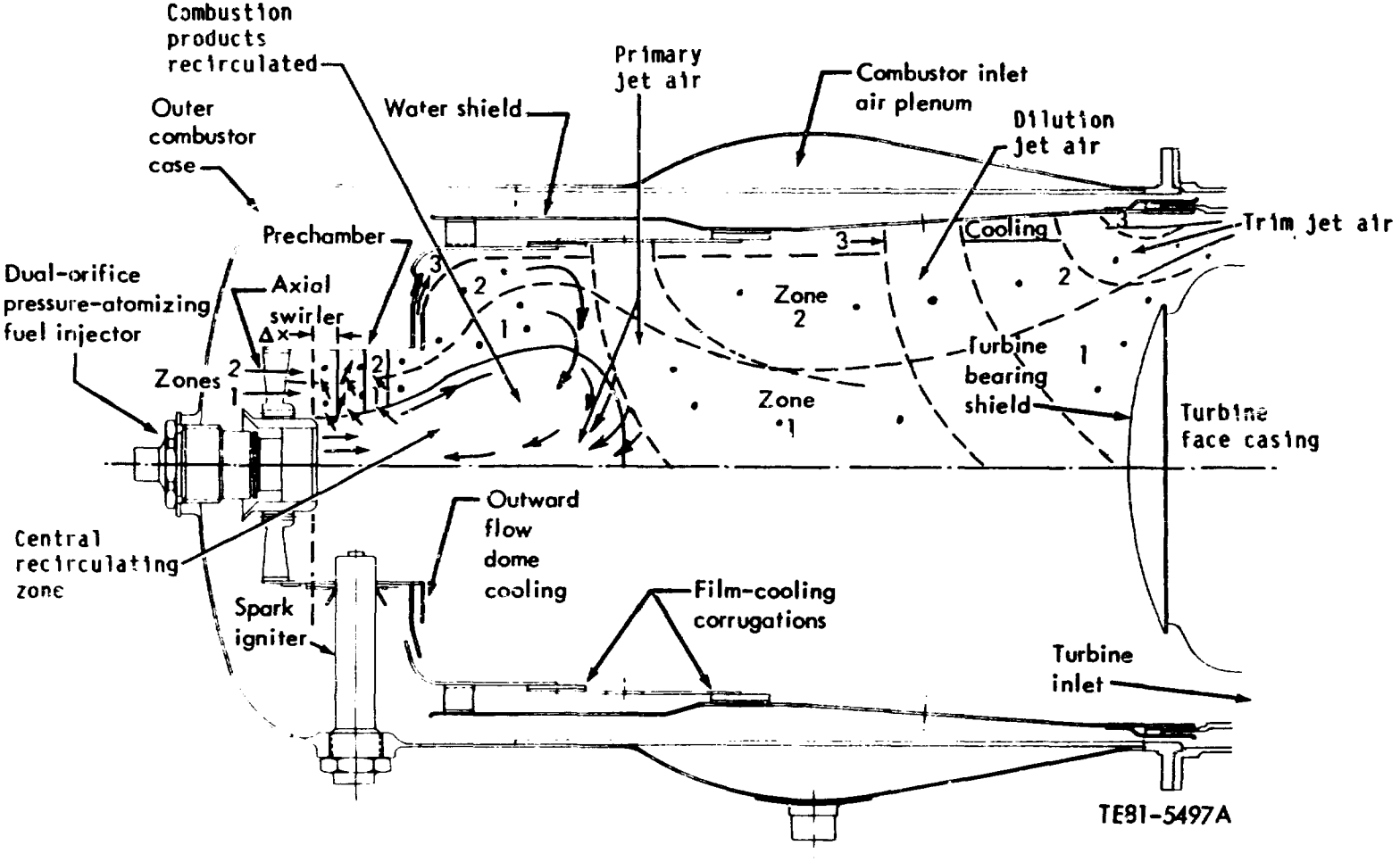

Figure 16. STAC-1 representation of flow field within a baseline Model 250-C30.

and mixing rates were equated to expressions describing the centerline temperature "decay" rate of the jets (Ref 12) and have been subsequently modified through comparisons with 3-D aerodynamic analyses. Provision for jet collisions has been incorporated. Film-cooling air in the single-streamtube mode is mixed into the streamtube by input specification, usually linear in nature.

The spray and gas phase conservation equations in the streamtubes are fully coupled, and while the model treats radial swirlers (in the single-streamtube mode), jet mixing, and film cooling in a semi-analytical/empirical manner, the physical and chemical aspects of the reacting flow are treated in great detail. The model includes real fuel and combustion gas properties, effects of injector type on atomization and drop-size distributions, detailed droplet dynamics, and multistep chemical kinetics.

As the model is quasi-2-D, a marching technique is employed to describe the droplet drag, heating, vaporization, and subsequent chemically kinetic controlled combustion yielding the gas phase combustion products. Since the properties of the recirculated combustion products to a large extent determine the properties of the CTRZ gas (which in turn establish the initial mixed gas conditions within the streamtubes), an iterative marching analysis from the injector to the primary jet plane is employed until the computed temperature of the CTRZ converges to within 0.09°C (0.05°F). After this convergence has occurred the remainder of the combustor is analyzed.

The model has broad application to both can and annular combustions; the streamtubes are circumferentially uniform but may take any shape as only an area specification is required to solve the axial spray and gas phase conservation equations. An approximation is necessary only when droplet and gas phase angular momentum and radial pressure gradient are computed in a sector portion of an annular combustor. To eliminate the 3-D profile of the swirl velocities, an equivalent hydraulic diameter of the sector is used to compute swirl moment arms in the angular momentum equations. This does not alter that portion of the program that computes jet penetrations based on sector height and axial flow field considerations.

3.1.1 Real Fuel Properties

Currently, properties of eight different fuels have been assembled, curve fitted, and coded. These include both the liquid and vapor transport and thermodynamic properties of fuels ranging in characterization from JP-4 to DF-2 and ERBS 11.8. Specific properties correlated to temperature (Appendix A) include the following:

- liquid droplet
  - molal mass
  - density
  - specific heat
  - enthalpy (including enthalpy of formation)
  - vapor pressure
  - heat of vaporization
  - themal conductivity
  - absolute and kinematic viscosity
  - surface tension

- o droplet vapor
  - o molal mass
  - o specific heat
  - o enthalpy (including enthalpy of formation)
  - o thermal conductivity
  - o entropy (including entropy of formation)
  - o absolute viscosity

3.1.2 Combustion Gas and Droplet Film Properties

The detailed droplet dynamics model developed for use in STAC-I requires knowledge of the mixed droplet vapor and combustion gas properties at the droplet film temperature. This temperature is computed from the addition of 2/3 of the droplet temperature and 1/3 of the combustion gas temperature and has been found to best correlate experimental data obtained under convective conditions (Ref 13). The film mixture properties are obtained by combining drop vapor and combustion gas properties at the film temperature using the 1/3 rule of Sparrow and Gregg (Ref 13). Using this rule, the film fuel and combustion gas mole fractions are determined in a manner similar to the one used to determine film temperature. Film thermodynamic properties can then be directly computed; however, the computation of the film transport properties (viscosity, thermal conductivity, and the multicomponent diffusion coefficient for the fuel vapor) is considerably more complicated (Ref 14). Specific combustion gas and mixed film properties computed as a function of temperature and pressure include the following:

- o combustion gas
  - o specific heat, composition
  - o molal mass
  - o thermal conductivity
  - o absolute viscosity
- o droplet film
  - o composition of film mixture
  - o molal mass
  - o density
  - o specific heat
  - o thermal conductivity
  - o absolute viscosity
  - o vapor multicomponent diffusion coefficient

3.1.3 Effects of Injector Type on Spray Formation

The model uses the transport and thermodynamic properties of the liquid fuel combined with detailed geometric descriptions of simplex, dual orifice, various types of airblast injectors, and empirical correlations (Ref 5) to predict the injected Sauter mean diameters (SMD) of each spray cone. Each fuel spray cone is further characterized by a 10-drop group initial drop-size distribution about the SMD. The spray drop-size distribution utilized is that of Rossin-Rammler.

3.1.4 Improved Droplet Dynamics and Chemical Kinetics Submodels

The improved droplet drag, heating, and vaporization submodel is based on work originally performed for the Space Shuttle Main Engine development (Ref 15).

The submodel has been updated to include multicomponent hydrocarbon fuel composition and uses drag coefficients, at the lower Reynolds numbers (< 200), more representative of the flow field within gas turbines (Ref 16). The submodel employs the real fuel properties described earlier and recognizes that when a liquid spray is injected into hot combusting gases, the initial rate of evaporation is low and most of the energy transferred to the drop from its surroundings is used in heating up the drop. As the liquid temperature rises, the vapor concentration at the drop's surface increases and a larger proportion of the heat transferred to the drop is used to supply the latent heat of vaporization. Eventually the drop may attain its wet-bulb temperature, and from then on the rate of evaporation remains nearly constant at its maximum value.

These effects are well illustrated in Figure 17, which presents GTAC-I predictions of Jet-A spray droplet diameter and temperature variations with axial length. The resulting flow field in these computations is representative of that within a Model 250-C30 baseline configuration combustor operating at the maximum power condition. The predicted injected spray distribution simulates a dual orifice pressurized atomizer injector having both a pilot and main nozzle flow. The injected spray for both nozzle flows was characterized by a 10-drop group initial drop size distribution about the SMD of each flow, as previously described. Selected values of drop diameter and temperatures for both the pilot and main spray flows are shown in the figure. The values are representative of the smallest (1), mean (4), and largest (10) initial drop group size for each spray. The mean value (4) depicted has nearly the same diameter as the injected SMD. Despite the length of the Model 250-C30 the largest droplet not completely vaporized at the combustor exit plane is 33 microns in diameter. However, because this droplet represents $(33/201)^3$ of 1/10 of the injected main spray mass flow, only 0.35% of the total flowing spray mass has not been evaporated. Nevertheless, predictions such as these can aid designers in the selection of injector types and indicate the combustor size required for complete combustion.

The entire set of conservation equations for the spray field, and the coupled gas phase conservation equations of mass and axial and angular momentum, were solved using an optimal solution algorithm for these hydrodynamic equations, all of which are interrelated by weakly linked source terms. The remaining species and enthalpy conservation equations must then be solved, point by point, for simultaneous determination of all the local thermochemical variables, species mass fractions, and temperature (T). However, the species and enthalpy (thermochemical) equations have strongly linked, nonlinear source terms, particularly under fuel-rich conditions, and form a set of highly "stiff differential equations." The solution of these equations requires an optimal algorithm different from that used in solving the hydrodynamic equations. Convergence problems were first encountered in attempting to attain a correct Arrhenius type solution that yielded accurate and consistent values of the species mass fractions when the oxygen concentration was near zero (fuel rich). This problem was resolved by using an updated version of CREK (Ref 17) to solve the thermochemical conservation equations.

The new field values of species mass fractions, temperature, and mass density, obtained from the equation of state, are then used to redetermine the hydrodynamic solutions. This superiteration between hydrodynamic and thermo-chemical fields is repeated until pointwise (at each node) convergence on temperature

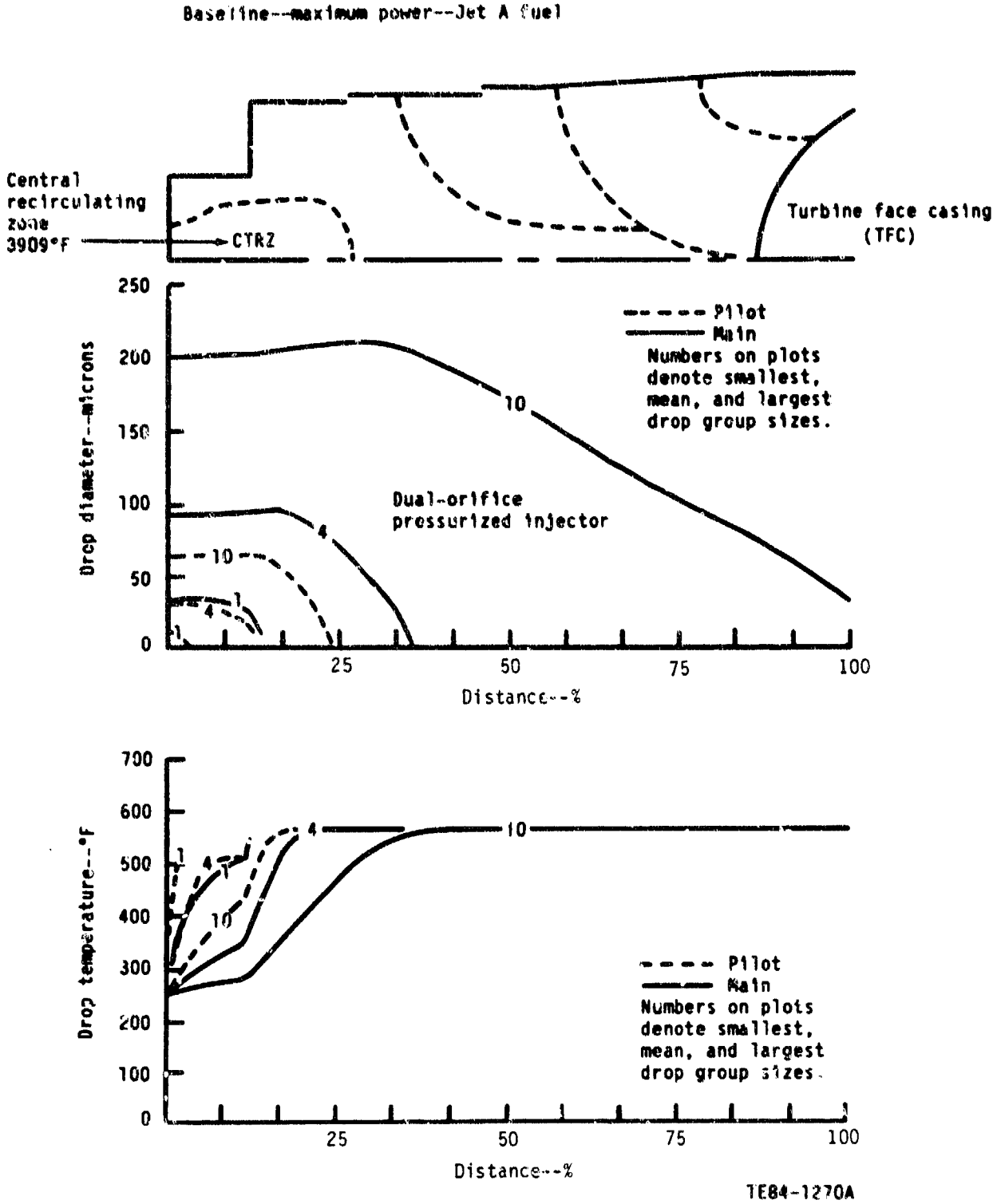

Figure 17. Spray droplet diameter and temperature variations with axial length, STAC-I predictions for flow field of the Model 250-C30 baseline configuration combustor-maximum power operating conditions, Jet A fuel.

is achieved. The chemical source term in each species conservation equation is calculated in this procedure at the mean local temperature. The optimal algorithm for the thermochemical equations (with strongly linked, nonlinear source terms) and the optimal algorithm for the hydrodynamic equations (with weakly linked source terms) combine to provide a rapidly converging code when CREK's new asymptotic estimate approach is used. CREK is one of four available codes capable of both accurately predicting the resulting species and reaching a converged solution under high temperature, fuel rich exothermic conditions (Ref 18).

A version of CREK, employing a single-global decomposition mechanism of the fuel to H_2 and CO and full kinetics thereafter, was successfully developed and incorporated into STAC-1. The code solves for 15 species using 17 step chemistry as illustrated in Table XI. Jet A is used in the example but any of the other hydrocarbon fuels (with appropriate kinetic rate adjustments) could be represented similarly.

Table XI.
Chemical kinetic mechanism.

1	Jet A	+	O_2			$\longrightarrow$	CO	+	H_2		
2	CO	+	OH			$\longrightarrow$	CO_2	+	H		
3	CO_2		+		M	$\longrightarrow$	CO	+	O	+	M
4	H	+	OH			$\longrightarrow$	H_2	+	O		
5	H_2O		+		M	$\longrightarrow$	OH	+	H	+	M
6	H	+	HO_2			$\longrightarrow$	OH	+	OH		
7	OH	+	H_2			$\longrightarrow$	H	+	H_2O		
8	H	+	O	+	M	$\longrightarrow$	OH		+		M
9	OH	+	O			$\longrightarrow$	H	+	O_2		
10	H	+	O_2	+	M	$\longrightarrow$	HO_2		+		M
11	OH	+	OH			$\longrightarrow$	H_2O	+	O		
12	OH	+	N			$\longrightarrow$	H	+	NO		
13	H	+	N_2O			$\longrightarrow$	OH	+	N_2		
14	N	+	NO			$\longrightarrow$	N_2	+	O		
15	N	+	O_2			$\longrightarrow$	NO	+	O		
16	N_2O	+	O			$\longrightarrow$	NO	+	NO		
17	N_2O		+		M	$\longrightarrow$	N_2	+	O	+	M

Chemical species--15

Jet A	CO	CO_2	H	H_2	H_2O	HO_2	N
NO	NO_2	N_2	N_2O	O	OH	O_2	

The resulting gas phase flow-field temperature and combustion efficiency (corresponding to the conditions specified for the results previously shown in Figure 17) as a function of axial combustor length as predicted by STAC-I are illustrated in Figure 18.

The emission indices (EI) for NO_x, CO, and UHC as a function of axial combustor length at the maximum power condition are presented in Figure 19. Normally, the values of the overall combustion efficiency and emission indices are stated at the exit plane of the combustor where the combustion reaction has either gone to completion or has been quenched. Combustion efficiency and emission indices, presented as a function of combustor length in Figures 18 and 19, are of interest only in that they show how these respective parameters vary as functions of the degree of reaction within the combustor along its length. The values of the combustion efficiency and emission indices at the combustor exit are those that represent the actual efficiency produced by and emissions exiting from the combustor.

The Jet A performance efficiency and emissions were checked against 250-C30 baseline engine data at maximum power and ground idle operating conditions and showed good correlation. Comparisons are listed in Table XII.

Table XII.
Jet A performance at max power and ground idle Model 250-C30 baseline configuration.

	Measured	Predicted
Max power		
UHC--EI	0.2	0.26
CO--EI	7	4.99
NO_x--EI	9	13.3
Efficiency--%	99+	99.8
Ground idle		
UHC--EI	100-150	70.2
CO--EI	100-150	100.3
NO_x--EI	1	0.88
Efficiency--%	91	90.6

These comparisons were considered sufficient to verify the use of the detailed droplet dynamics and CREK chemistry submodels in STAC-I. The comparisons were also sufficient to verify STAC-I's overall use as an initial design code.

Both the axial variation of the combustor residence times of representative Jet A spray droplets and the total and gas phase equivalence ratios at the maximum power condition are presented in Figure 20. The residence time for the mean injected diameter of the main nozzle flow droplets is nearly three milliseconds, while that of the largest droplet is nearly seven milliseconds.

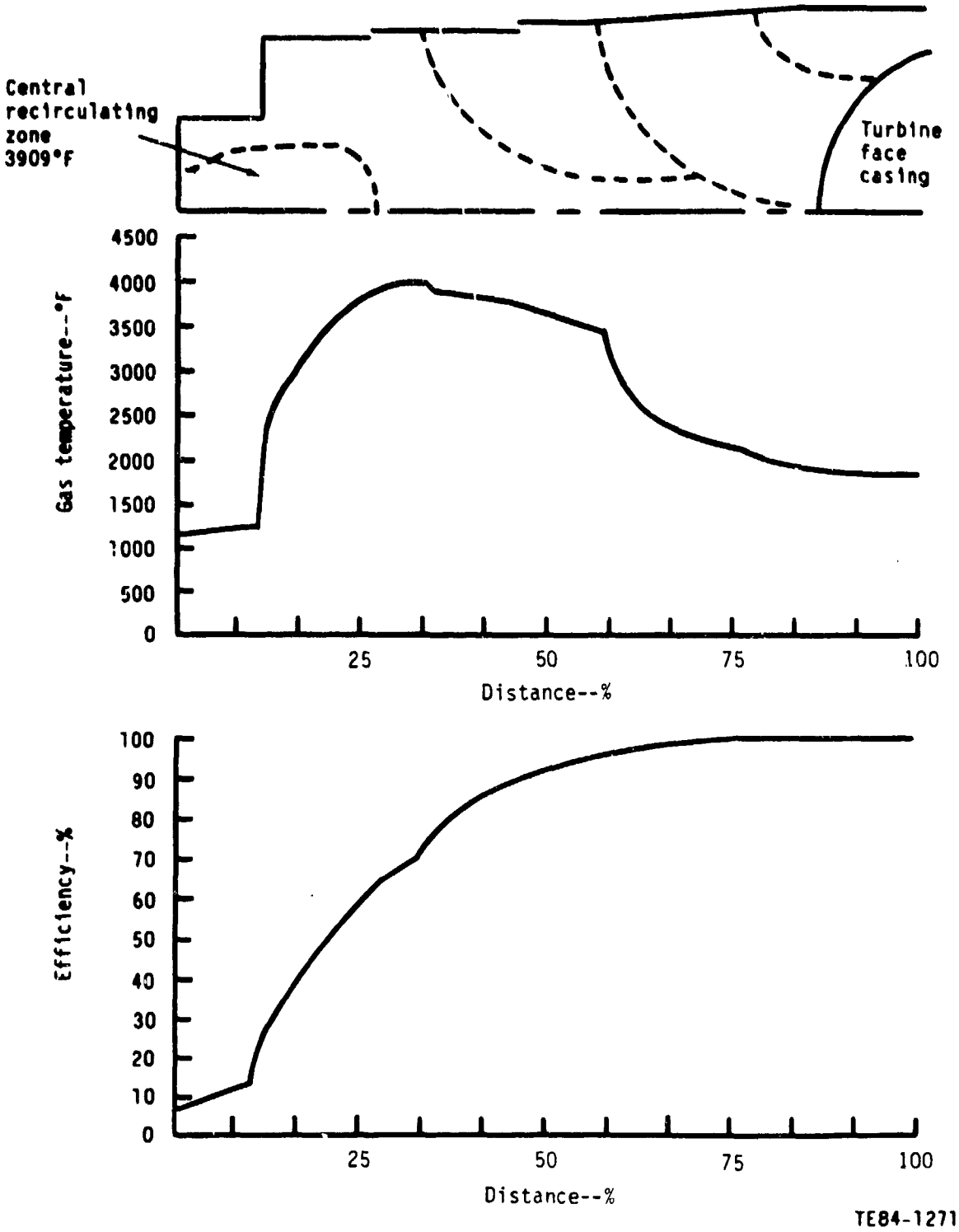

Figure 18. Gas phase temperature and overall combustion efficiency variation with axial length--STAC-I prediction for flow field conditions of Figure 17.

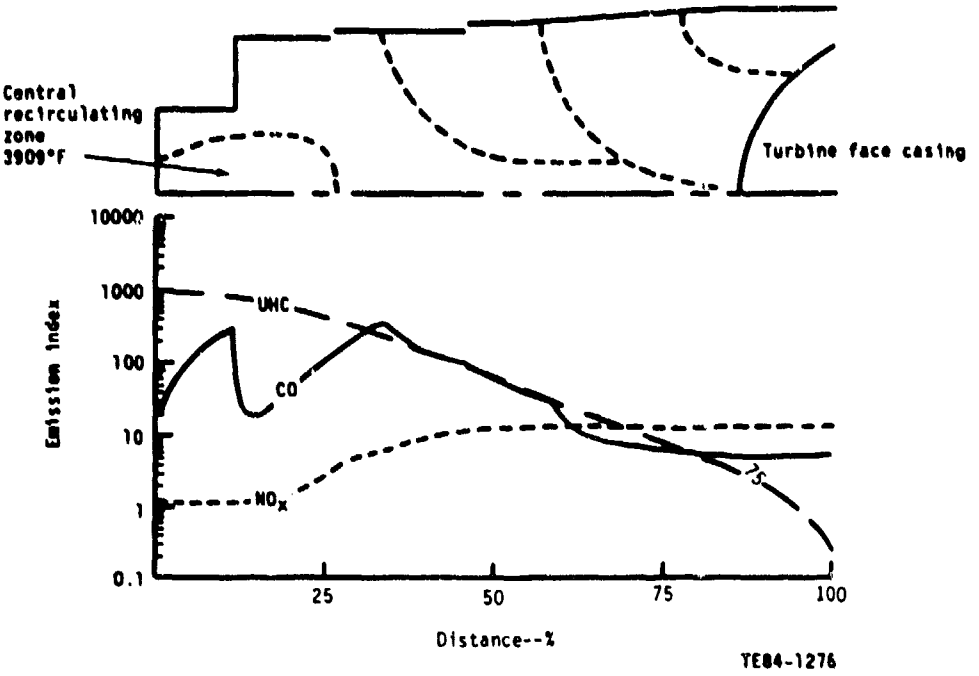

Figure 19. Emission index for NO_x, CO, and UHC, variation with axial length--STAC-I predictions for flow field conditions of Figure 17.

The total equivalence ratio includes the liquid spray, while the gas phase equivalence ratio is based solely on the vaporized (and partially or completely reacted) spray. It is interesting to note that the gas phase equivalence ratio is nearly stoichiometric at the plane of the primary jets. This is an indication that the 250-C30 design has evolved into a very stable and high performance combustor at the maximum power operating condition. The equivalence ratio of the central recirculating zone (CTRZ) is also nearly stoichometric and the temperature within it is 2154°C (3909°F). This high temperature is due to a portion of the spray nozzle flows being injected into the CTRZ and indicates good combustion stability, lean-blowout, and ignition characteristics.

Representative Jet A spray droplet and combustion gas axial and tangential (swirl) velocity variations with combustor length are presented in Figure 21. The pilot flow, by design, produces small droplets by employing a high pressure drop across the tip of the simplex pilot nozzle. This results in high initial velocities for the pilot spray, usually exceeding the combustion gas velocity. Because the pilot spray droplets are so small, they rapidly approach the gas velocity as they vaporize. One to two micron droplets follow the gas flow field exactly, but after attaining that size they vaporize within less than 0.127 cm (0.05 in.). The main nozzle spray droplets (from this dual orifice injector) are injected at velocities closer to the initial gas velocity; but because of their larger size and decreased velocity relative to the gas flow, the drag force has a smaller effect on these droplets. The axial velocity of the largest droplet (10) of the main spray flow is nearly unaffected by the gas flow field until the droplet has sufficiently vaporized so

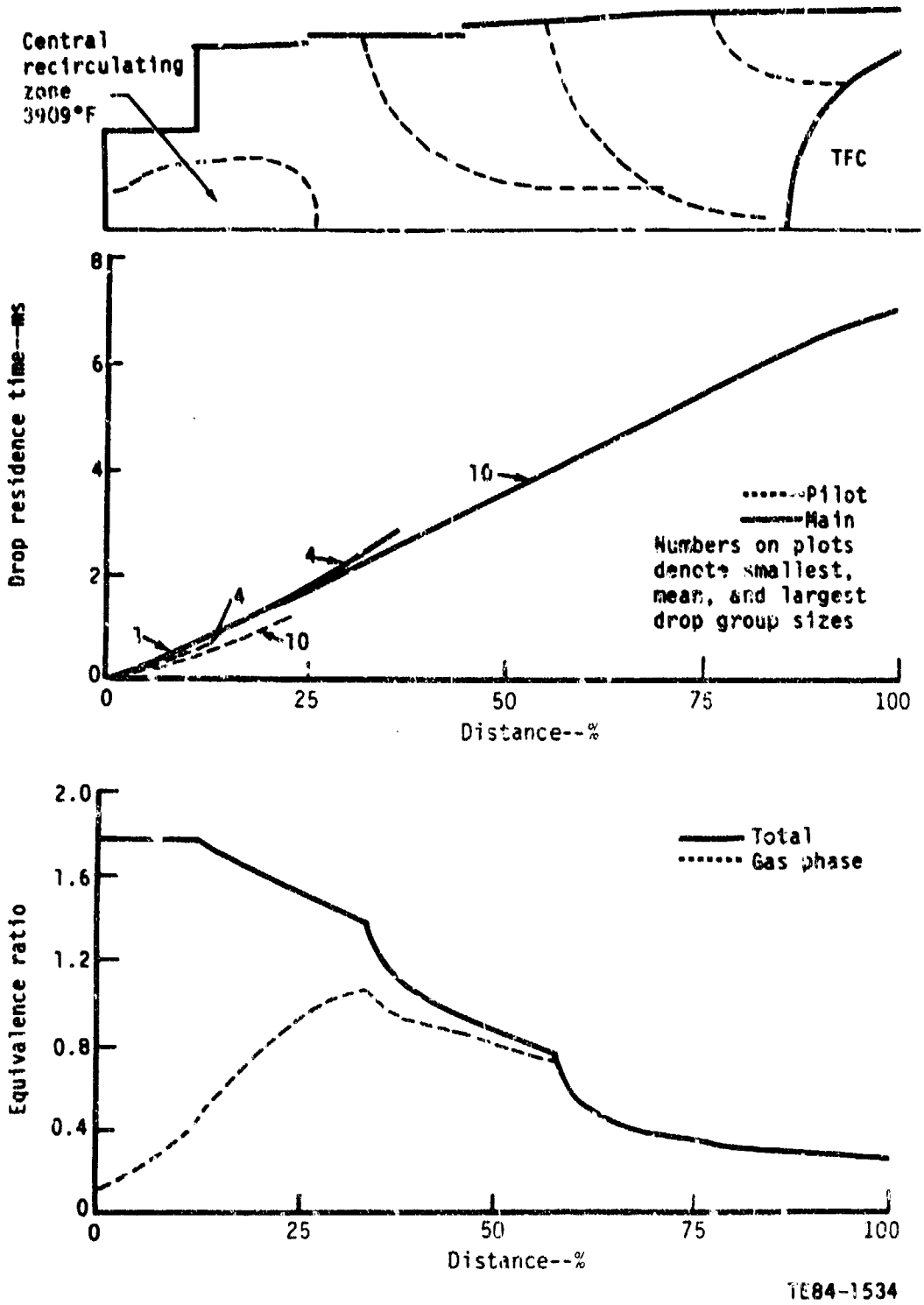

Figure 20. Spray droplet residence time and total gas phase equivalence ratio variation with axial length--STAC-1 predictions for flow field conditions of Figure 17.

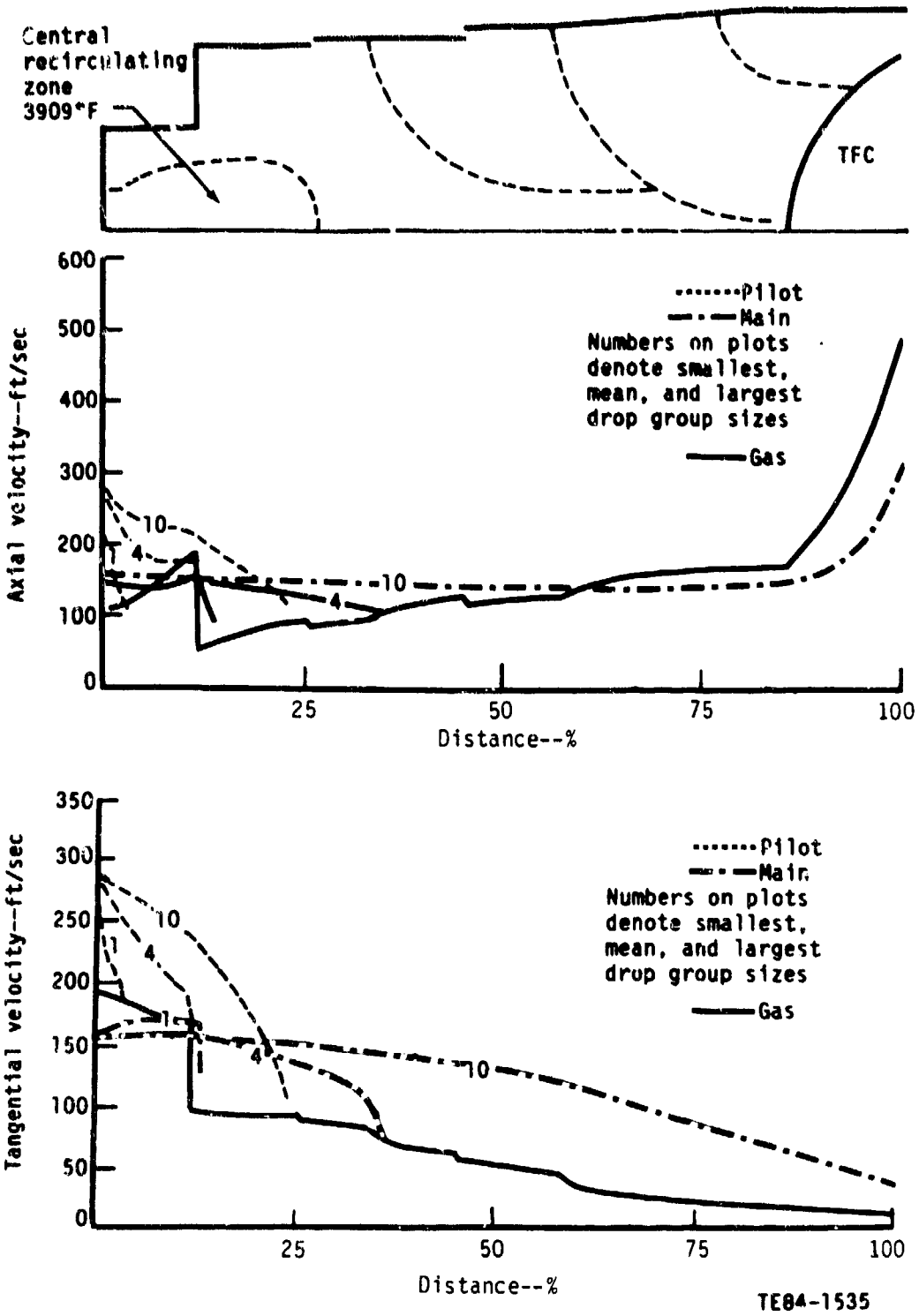

Figure 21. Spray droplet and combustion gas axial and tangential (swirl) velocity variations with axial length-STAC-1 predictions for flow field conditions of Figure 17.

its remaining mass (Figure 17) is quite small. At this point, 25.4 cm (10 in.) down the combustor, the drag force (which is also increasing due to increased axial gas velocity) now has an appreciable effect on the droplets' trajectory.

As power is decreased, the injected velocity difference between the pilot and main nozzle fuel spray flows is increased. For example, at ground idle the pilot nozzle spray has a velocity of nearly 46/meter/sec (150 ft/sec), while that of the main nozzle spray is only 4.6 meter/sec (15 ft/sec). These results are for dual orifice injectors. When hybrid airblast injectors (airblast with simplex pilot) are used, which is the case for the three remaining candidate combustors, the difference between the injected velocities of the pilot nozzle and the main filming nozzle fuel spray flow is larger at nearly all operating conditions. This is due to the fact that the film velocity from the main nozzle ranges from about 2 to 30 m/sec (6 to 100 ft/sec) depending on the power level and combustor type. Small droplets in the fuel film are rapidly accelerated by the airblast air velocity. However, particularly at lower power levels, a smaller pilot nozzle spray droplet often travels further downstream before being totally vaporized than a larger, slower moving main nozzle spray droplet. Proper interpretation of graphical results requires the consideration of the large difference in the pilot and main nozzle injected droplet velocities. This phenomenon also occurs when dual orifice injectors are used. Graphical presentations for Jet A and DF-2 in Appendix B, similar to those in Figures 17, 18, 19, and 20, reflect this phenomenon.

3.2 APPLICATION OF THE COMPUTER ANALYSIS (STAC-I) TO THE FOUR FINAL COMBUSTOR CONCEPTS

Each of the four final combustor candidates was analyzed using STAC-I. The analysis was performed for the takeoff, cruise, air taxi, descent, and ground idle conditions listed in Table I. These power conditions were sufficient to represent the entire operating cycle of the Model 250-C30 combustor. The reacting flow fields within each of the four combustors, resulting from the combustion of five different fuels--Jet A, ERBS 12.8, ERBS 12.3, ERBS 11.8, and DF-2--were predicted by STAC-I for each of the different power levels. Overall airflow rates (Table I) to the individual combustors at similar power settings remained unchanged. Fuel flow rates were varied by the ratio of the lower heating value of each fuel to that of JP-4 so that, when used in an engine, power output would remain unchanged. Fuel injection temperature for the 250-C30 combustor also remains nearly unchanged, 121°C (250°F), with power level. This fuel injection temperature was assumed to apply for all fuels at all operating conditions, regardless of combustor concept.

Burner inlet pressures and temperatures at each power level also retained their values as presented in Table I. In addition to the use of different fuels, the major changes in the analysis occurred due to consideration of the different geometries and the airflow management (around the liner) of each of the four individual combustors. In total, more than 100 separate cases were analyzed using STAC-I, as some of the initial model checkout analyses were performed using JP-4 and JP-5 fuels.

3.2.1 Computation of the Size of the Central Recirculation Zone

Additionally, Allison's 2-D axisymmetric elliptic flow code, COSMIC, was used to obtain the size of the CTRZ. For the baseline (dual-orifice injector) case, COSMIC was employed to determine the size of the CTRZ at each of the five power levels being considered. (A sample case for the maximum power condition is presented in Figure 91 in Appendix B.) COSMIC uses a weighted average of single-step chemistry and a two-equation (k-ε type) turbulent mixing expression to determine both the rate at which fuel is consumed and the resulting, reacting flow field within the combustor. Because of COSMIC's axial symmetric nature, the effect of primary, dilution, and trim jets on the flow field cannot be analyzed (as these are three-dimensional effects). Further, the fuel within COSMIC is assumed to enter in a premixed, prevaporized state, so the model is insensitive to fuel type. Nevertheless, COSMIC's use to approximate the size of the CTRZ is sufficient for the analysis being considered. The size of the CTRZ is less important than the amount of mass within it, and this latter term is computed internally within STAC-I as previously described.

Application of the COSMIC code to analyze the recirculating flow fields within the three airblast-injected combustors resulted in little change in size of the individual combustors CTRZs over their entire operating power range. Consequently, for these combustors, the size of their CTRZ at maximum power, as shown in Figures 92, 93, and 94, respectively, in Appendix B, was used to represent their CTRZ size at all power levels. The CTRZ size differs, of course, for each individual combustor. The CRTZ size used in the variable geometry combustor concept represents an exception to this application of COSMIC. The descent and ground idle operating conditions employed variable geometry settings that resulted in full closure of the radial swirler. The flow field at these conditions is similar to that within the short prechamber combustor. Consequently the short prechamber CTRZ size was used to represent the volume of the CTRZ within the variable geometry combustor at low power levels.

3.2.2 Combustor Geometric Conditions-Liner Airflow Management Effects

The different operating characteristics of each combustor is best illustrated by describing the air mass management (flow distribution) around each of the liners similar to that presented in Figure 6 for the baseline configuration. These air mass distributions were input directly to STAC-I, along with the individual geometries of each combustor. Total fuel flow rates for each fuel at the different operating conditions were determined by employing the ratio of the lower heating value of the fuel to that of JP-4 and multiplying by the JP-4 total fuel flow rate listed in Table I. Both the dual orifice and (hybrid) airblast injectors employ a simplex pilot nozzle. The geometry and operating characteristics of this pilot nozzle remained invariant for all of the combustor configurations. Flow rates to, and tip delta pressure across, the simplex pilot were taken to be the same as that calculated for the baseline configuration at each of the various power levels for each of the fuels. This was done to aid proper ignition characteristics and lean-blowout operation at and below the idle power condition (the Model 250-C30 baseline configuration has excellent combustion stability) of each of the combustor candidates and to eliminate additional, unnecessary variability among the combustors when comparing results from the STAC-I analyses. The geometric conditions of interest and the airflow management around the liner (in percent of total air mass flow) of each combustor candidate are presented in Table XIII. Where possible, geometric conditions were kept as similar as possible to facilitate comparisons among the combustors.

Table XIII.
Combustor geometric conditions and liner airflow management (% of total air mass flow).

Parameter	Baseline	Combustor: Short prechamber	Piloted prechamber	Variable geometry
HUBID--in.	0.945	0.945	0.945	0.945
HUBOD--in.	1.173	1.173	1.173	1.173
ASLHUB--in.	1.550	1.550	1.550	1.550
ASLTIP--in.	2.872	2.872	2.282	2.872
SWLAAS--deg	70	76.45	70	78.315
PCID--in.	2.936	2.936	2.282	2.936
RRS--in.	--	--	--	1.468
SWLARS--deg	--	--	--	55
DSLHUB--in.	--	--	3.0	--
DSLTIP--in.	--	--	3.438	--
SWLADS--deg	--	--	70	--
DIJETP--in.	5.68	5.68	5.68	5.68
WDOTAS--%	13.74	8.39	6.0	5.38
WDOTAF--%	0.29	5.64	5.93	5.64
WDOTRS--%	--	--	--	0*-20**
WDOTDS--%	--	--	5.74	--
WDOTFC (1)--%	4.38	--	--	--
WDOTFC (2)--%	11.64	--	--	--
WDOTNL--%	--	3.57	3.57	3.57
WDOTSL--%	--	10.42	10.42	10.42
WDOTFC (3)--%	4.96	--	--	--
WDOTPJ--%	9.98	16.97	9.98	9.98
WDOTFC (4)--%	11.71	11.71	11.71	11.71
WDOTSJ--%	37.79	37.79	41.14	27.79**-47.79*
WDOTDJ--%	5.51	5.51	5.51	5.51

*Radial swirler fully closed
**Radial swirler fully open

HUBID = Hub internal diameter, houses the fuel injector--in.
HUBOD = Hub outer diameter, forms the inner portion of the external streamtube flow--in.
ASLHUB = Inlet axial swirler inner diameter or hub--differs from the HUBOD due to metal thickness--in.
ASLTIP = Inlet axial swirler tip diameter, differs from the pre chamber internal diameter due to metal thickness--assumed same as PCID for piloted prechamber--in.
SWLAAS = Inlet axial swirler swirl angle as measured from the centerline of the combustor--deg
PCID = Prechamber internal diameter surrounding axial swirler- in.
RRS = Radius of radial swirler entrance--half of prechamber internal diameter--in.

Table XIII. (cont)

SWLARS	=	Radial swirler swirl angle as measured from a diametric line through the prechamber centerline--deg
DSLHUB	=	Downstream axial swirler hub inner diameter--in.
DSLTIP	=	Downstream axial swirler tip outer diameter--in.
SWLADS	=	Downstream axial swirler swirl angle as measured from the centerline of the combustor--deg
DIJETP	=	Internal diameter of the combustor liner at the plane of the primary jet--in.
WDOTAS	=	Percentage of total airflow through the inlet axial swirler
WDOTAF	=	Percentage of total airflow through the fuel injector
WDOTRS	=	Percentage of total airflow through the radial swirler (variable geometry concept only)
WDOTDS	=	Percentage of total airflow through the downstream axial swirler (piloted prechamber concept only)
WDOTFC (1)	=	Percentage of total airflow through the first film cooling slot (baseline concept only)
WDOTFC (2)	=	Percentage of total airflow through the second film cooling slot (baseline concept only)
WDOTNL	=	Percentage of total airflow through the Lamilloy forming the normal walls of the combustor liner inner diameter sudden expansion from the prechamber diameter (all concepts except baseline)
WDOTSL	=	Percentage of total airflow through the Lamilloy forming the side walls of the combustor liner following the sudden expansion (all concepts except baseline)
WDOTFC (3)	=	Percentage of total airflow through the third film cooling slot (baseline concept only)
WDOTPJ	=	Percentage of total airflow through the primary jet holes (all concepts)
WDOTFC (4)	=	Percentage of total airflow through the fourth film cooling slot (Though denoted fourth, this is the only film cooling slot on the modified and/or advanced combustor concepts. The number designation is for generalized usage in STAC-1, all concepts)
WDOTSJ	=	Percentage of total airflow through the secondary jet holes, all concepts. (Secondary usage here is equivalent to the more common designation of dilution jet holes.)
WDOTDJ	=	Percentage of total airflow through the dilution jet holes, all concepts. (Dilution usage here is equivalent to the more common designation of trim jet holes.)

That portion of the combustor housing the fuel spray injector (dual orifice or hybrid airblast) is denoted as the hub. An axial air swirler surrounds the hub, the outside of which forms the initial diameter of the prechamber. The hub inner dimension (HUBID), which contains the fuel spray injector, and the hub outer dimension (HUBOD), which forms the inner portion of the external streamtube flow, were held constant for all of the combustor configurations. The prechamber initial diameter differed only for combustor concept No. 4--the piloted prechamber. Similarly, the dimensions of the main filming nozzle of the airblast injectors were held constant for all combustor concepts. The cone angles for the pilot and main nozzle spray flows of the baseline, short prechamber and variable geometry combustor concepts are both 90 deg, while those of the piloted prechamber are 60 deg and 110 deg, respectively. The cone angle of the piloted prechamber's airblast start nozzle, which was used in place of its main nozzle at idle conditions, is also 60 deg.

The Sauter mean diameter (SMD) for the pilot spray fuel flow for each combustor concept is identical when compared at each operating condition. The SMD differs for fuel type but is the same for each fuel. SMDs for the main nozzle fuel flow differ with combustor concept even though the airblast injector main nozzle dimensions are identical. Because of the air management around each liner, different amounts of air pass through that portion of the airblast nozzle that atomizes the fuel film. Despite having identical burner inlet pressures, the air management around the liner affects the liner annulus pressure, and, hence, the available pressure difference through the airblast injector. Lower pressure differentials produce lower air velocities which, in an airblast injector, have a detrimental effect on the quality of the spray produced.

3.2.3 Summary--STAC-I Combustor Analysis

Summaries of the predicted results from STAC-I, which determined the flow field within the individual combustors for each fuel type undergoing reaction at the various operating conditions, are presented in Tables XIV, XV, XVI, and XVII. The results presented in these tables clearly indicate that for these combustor concepts most of the predicted effects of using broad-property fuels such as ERBS 12.8, 12.3, and 11.8 are effectively bracketed at each operating condition by the results obtained when Jet A and DF-2 are considered to be the turbine combustor fuel. The major exception to this statement is the level of NO_x emission of the ERBS fuels as compared with those from DF-2. Under some operating conditions within the various combustor concepts the NO_x emission levels from DF-2 exceeds that from the ERBS fuels and at times even that from Jet A. This is primarily a result of the time-temperature history of the DF-2 droplets as they travel through the combustor and are exposed to the hot combustion gases. A comparison of Figures 107 to 109 and 110 to 112 illustrates this phenomenon.

Because of these and other effects, the predicted Jet A and DF-2 maximum power and ground idle flow fields within each combustor concept are graphically depicted in Figures 95 through 124, and 131 through 148 in Appendix B. These figures show droplet diameter and temperature, overall and gas phase equivalence ratio, gas temperature, percent combustion efficiency, and emission indices, as a function of combustor length. These graphic presentations are useful in understanding the results presented in Tables XIV through XVII and in the Analytical Results and Comparisons section.

Table XIV.
Summary STAC-I baseline combustor predicted results.

	Jet-A	ERBS-12.8	ERBS-12.3	ERBS-11.8	RF-2
MAX POWER					
SMD, pilot	28.5	33.9	34.1	34.1	36.9
SMD, main	89.0	105.9	106.5	106.5	115.0
Percent efficiency	99.8	97.9	97.7	97.7	94.6
UHC emission index	0.26	16.5	17.8	17.4	46.3
CO emission index	4.99	18.8	21.1	22.3	33.2
NOx emission index	13.3	4.57	4.52	4.77	2.20
MAX POWER (Jet-A SMD's)					
SMD, pilot	28.5	28.5	28.5	28.5	28.5
SMD, main	89.0	89.0	89.0	89.0	89.0
Percent efficiency	99.8	99.5	99.5	99.5	99.2
UHC emission index	0.26	2.03	2.21	2.22	4.64
CO emission index	4.99	8.38	8.98	9.31	10.6
NOx emission index	13.3	10.8	11.0	11.2	8.90
CRUISE					
SMD, pilot	29.7	35.3	35.5	35.5	38.5
SMD, main	94.0	108.3	108.9	109.0	117.6
Percent efficiency	99.6	96.8	96.5	96.5	92.1
UHC emission index	1.39	24.0	25.5	24.8	62.3
CO emission index	3.51	33.9	38.9	41.5	68.3
NOx emission index	9.09	2.37	2.33	2.41	1.52
AIR TAXI					
SMD, pilot	32.7	38.9	39.1	39.1	42.4
SMD, main	96.0	114.2	114.9	115.0	124.2
Percent efficiency	98.5	91.5	90.9	90.9	81.9
UHC emission index	7.39	51.1	53.4	52.2	116.5
CO emission index	31.6	140.4	154.1	157.1	273.8
NOx emission index	2.69	1.32	1.32	1.32	1.23
DESCENT					
SMD, pilot	34.4	40.9	41.1	41.1	44.5
SMD, main	101.5	120.7	121.4	121.5	131.1
Percent efficiency	96.0	85.1	84.5	84.5	74.7
UHC emission index	19.8	87.4	90.5	88.7	171.1
CO emission index	87.6	257.0	267.8	268.9	347.1
NOx emission index	1.61	1.10	1.11	1.10	1.13
GROUND IDLE					
SMD, pilot	46.5	47.9	48.1	48.1	52.1
SMD, main	131.9	157.0	157.9	158.0	170.6
Percent efficiency	90.6	84.1	84.0	84.0	79.3
UHC emission index	70.2	128.6	129.3	128.0	173.9
CO emission index	100.3	124.9	127.9	130.4	138.7
NOx emission index	0.88	0.71	0.73	0.71	0.79

Table XV.

Summary STAC-I short prechamber combustor predicted results.

	Jet-A	ERBS-12.8	ERBS-12.3	ERBS-11.8	DF-2
MAX POWER					
SMD, pilot	28.5	33.9	34.1	34.2	36.9
SMD, main	36.6	41.2	42.3	43.3	45.2
SMD, downstream swirler	17.5	19.5	20.1	20.6	21.4
Percent efficiency	99.9	99.9	99.9	99.9	99.9
UHC emission index	0.00	0.00	0.00	0.00	0.00
CO emission index	0.11	0.12	0.12	0.12	0.12
NOx emission index	10.0	9.02	9.18	9.11	9.36
MAX POWER (Jet-A SMD's)					
SMD, pilot	28.5	28.5	28.5	28.5	28.5
SMD, main	36.6	36.6	36.6	36.6	36.6
SMD, downstream swirler	17.5	17.5	17.5	17.5	17.5
Percent efficiency	99.9	99.9	99.9	99.9	99.9
UHC emission index	0.00	0.00	0.00	0.00	0.00
CO emission index	0.11	0.12	0.12	0.12	0.12
NOx emission index	11.1	9.14	9.35	9.30	9.37
CRUISE					
SMD, pilot	29.8	35.4	35.6	35.5	38.5
SMD, main	37.2	41.8	43.0	43.9	45.9
SMD, downstream swirler	17.8	19.8	20.4	21.0	21.8
Percent efficiency	100.0	100.0	100.0	100.0	100.0
UHC emission index	0.00	0.00	0.00	0.00	0.00
CO emission index	0.10	0.11	0.11	0.11	0.10
NOx emission index	6.48	5.77	5.83	5.79	5.66
AIR TAXI					
SMD, pilot	32.7	38.9	39.2	39.1	42.4
SMD, main	39.7	44.4	45.7	46.7	48.8
SMD, downstream swirler	19.0	21.1	21.8	22.4	23.2
Percent efficiency	100.0	100.0	100.0	100.0	100.0
UHC emission index	0.00	0.00	0.00	0.00	0.00
CO emission index	0.06	0.06	0.07	0.07	0.06
NOx emission index	2.15	1.94	1.94	1.92	1.88
DESCENT					
SMD, pilot	34.4	40.9	41.1	41.1	44.5
SMD, main	42.1	47.1	48.4	49.6	51.8
SMD, downstream swirler	20.2	22.5	23.2	23.8	24.7
Percent efficiency	100.0	100.0	100.0	100.0	100.0
UHC emission index	0.00	0.00	0.00	0.00	0.00
CO emission index	0.02	0.03	0.03	0.03	0.04
NOx emission index	0.93	0.83	0.83	0.82	0.81
GROUND IDLE					
SMD, pilot	40.3	47.9	48.2	48.2	52.2
SMD, starter	68.9	76.1	78.5	80.5	83.8
Percent efficiency	99.7	98.8	98.6	98.5	97.5
UHC emission index	1.19	4.90	5.88	6.53	13.5
CO emission index	3.91	29.7	32.6	34.1	49.8
NOx emission index	0.08	0.06	0.06	0.06	0.05

Table XVI.
Summary STAC-I piloted prechamber combustor predicted results.

	Jet-A	ERBS-12.8	ERBS-12.3	ERB3-11.8	BF-2
MAX POWER					
SMD, pilot	28.5	35.9	34.1	34.1	36.9
SMD, main	48.1	53.8	55.4	56.8	59.1
Percent efficiency	100.0	100.0	100.0	100.0	99.9
UHC emission index	0.00	0.00	0.00	0.00	0.06
CO emission index	0.06	0.19	0.38	0.64	3.05
NOx emission index	3.36	2.87	2.88	2.83	2.89
MAX POWER (Jet-A SMD's)					
SMD, pilot	28.5	28.5	28.5	28.5	28.5
SMD, main	48.1	48.1	48.1	48.1	48.1
Percent efficiency	100.0	100.0	100.0	100.0	100.0
UHC emission index	0.00	0.00	0.00	0.00	0.00
CO emission index	0.06	0.07	0.07	1.44	0.05
NOx emission index	3.36	3.02	3.03	3.06	3.22
CRUISE					
SMD, pilot	29.7	35.4	35.6	35.5	38.5
SMD, main	48.9	54.5	56.2	57.6	59.9
Percent efficiency	100.0	100.0	100.0	99.9	99.8
UHC emission index	0.00	0.00	0.00	0.00	0.68
CO emission index	0.05	0.49	1.00	1.56	5.59
NOx emission index	2.72	2.43	2.46	2.42	2.56
AIR TAXI					
SMD, pilot	32.8	38.9	39.2	39.2	42.4
SMD, main	52.1	58.1	59.8	61.3	63.8
Percent efficiency	100.0	99.9	99.8	99.7	99.2
UHC emission index	0.00	0.00	0.01	0.18	3.13
CO emission index	0.17	4.67	7.69	10.3	19.0
NOx emission index	2.19	1.95	1.97	1.94	2.06
DESCENT					
SMD, pilot	34.4	40.9	41.2	41.1	44.6
SMD, main	39.7	44.4	45.7	46.7	48.8
Percent efficiency	99.9	100.0	99.9	99.9	99.9
UHC emission index	0.00	0.00	0.00	0.00	0.00
CO emission index	0.04	0.48	0.05	0.05	0.48
NOx emission index	7.33	6.81	6.99	6.93	7.67
GROUND IDLE					
SMD, pilot	40.3	47.9	48.2	48.2	52.2
SMD, main	64.7	71.5	73.7	75.6	78.7
Percent efficiency	99.9	99.7	99.6	99.5	99.1
UHC emission index	0.08	1.33	1.76	2.11	4.47
CO emission index	1.74	8.07	9.48	10.3	19.6
NOx emission index	0.60	0.47	0.47	0.47	0.48

Table XVII.

Summary STAC-I variable geometry combustor predicted results.

	Jet-A	ERBS-12.8	ERBS-12.3	ERBS-11.8	DF-2
MAX POWER					
SMD, pilot	28.5	33.9	34.1	34.1	36.9
SMD, main	39.6	44.4	45.7	46.8	48.8
Percent efficiency	99.9	99.9	99.9	99.9	99.9
UHC emission index	0.00	0.00	0.00	0.00	0.00
CO emission index	0.10	0.11	0.11	0.11	0.10
NOx emission index	11.1	10.5	10.9	10.8	13.3
MAX POWER (Jet-A SMD's)					
SMD, pilot	28.5	28.5	28.5	28.5	28.3
SMD, main	39.6	39.6	39.6	39.6	39.6
Percent efficiency	99.9	99.9	99.9	99.9	99.9
UHC emission index	0.00	0.00	0.00	0.00	0.00
CO emission index	0.10	0.11	0.11	0.11	0.10
NOx emission index	11.3	9.90	10.1	9.96	11.6
CRUISE					
SMD, pilot	29.7	35.3	35.5	35.5	38.5
SMD, main	40.2	45.1	46.3	47.4	49.5
Percent efficiency	99.9	99.9	99.9	99.9	99.9
UHC emission index	0.00	0.00	0.00	0.00	0.00
CO emission index	0.09	0.09	0.09	0.10	0.09
NOx emission index	11.0	10.3	10.6	10.5	11.3
AIR TAXI					
SMD, pilot	32.7	38.9	39.1	39.1	42.4
SMD, main	42.8	47.9	49.2	50.4	52.6
Percent efficiency	100.0	100.0	100.0	100.0	100.0
UHC emission index	0.00	0.00	0.00	0.00	0.00
CO emission index	0.05	0.06	0.06	0.07	0.21
NOx emission index	6.06	5.15	5.14	5.05	4.71
DESCENT					
SMD, pilot	34.4	40.9	41.1	41.1	44.5
SMD, main	45.4	50.7	52.2	53.4	55.7
Percent efficiency	100.0	100.0	100.0	100.0	99.9
UHC emission index	0.00	0.00	0.00	0.00	0.00
CO emission index	0.02	0.12	0.31	0.62	3.22
NOx emission index	2.81	2.34	2.33	2.28	2.19
GROUND IDLE					
SMD, pilot	40.3	47.9	48.2	48.1	52.2
SMD, main	74.0	81.6	84.2	86.4	89.9
Percent efficiency	99.8	99.3	99.2	99.1	98.6
UHC emission index	0.70	2.56	2.98	3.31	6.23
CO emission index	5.28	19.8	21.4	22.6	31.0
NOx emission index	0.13	0.11	0.11	0.11	0.10

Appendix B also contains the Jet A and DF-2 graphical presentations for the variable geometry combustor concept descent operating condition, Figures 125 through 130. As indicated in Table XVII, this descent operating condition was analyzed assuming the radial swirler to be fully closed. This assumption resulted in a considerable increase in the predicted prechamber and primary zone stoichiometry (equivalence ratio) and in the gas temperature in these regions, producing an excessive amount of NO_x emission. This operating condition should have been analyzed with an intermediate variable geometry setting producing more favorable equivalence ratios and lower NO_x emissions than were predicted. Unfortunately, this anomaly was not detected until the final report was in progress and, thus, this data point is not representative of the true flexibility of the variable geometry combustor concept. Nevertheless, this anomaly does indicate the ability of STAC-I to predict both favorable and unfavorable variable geometry positional settings as a function of power level for this combustor concept.

The figures showing the piloted prechamber concept, 137 through 148 presented in Appendix B, are also useful in understanding the predicted results (Table XVI and Section IV) from this combustor. Spray from the piloted prechamber's main filming fuel nozzle is unique in that it is deposited on the initial portion of the prechamber walls, refilms, and is then subsequently reatomized by the high velocity air exiting from the downstream axial air swirler. Heating and vaporization of this spray flow is not considered prior to the wall refilming process. Drag forces on this spray are considered, however, to allow proper prediction of the trajectory of the droplets, the film velocity, and the subsequent reatomization process.

Axial locations of the important characteristics of each combustor concept are also depicted in Figures 95 through 148 in Appendix B.

Finally, the results presented in Tables XIV through XVII clearly indicate that any deteriorated performance characteristic of the ERBS fuels and DF-2, as compared with Jet A, are primarily due to the physical properties of the fuels as they affect atomization. This is particularly true for the baseline combustor. The maximum power operating conditions were recomputed for each combustor concept and each fuel type using the same SMDs as those predicted for Jet A. The deteriorated baseline combustor performance of the ERBS fuels and DF-2, Table XIV, was restored to nearly the level attained when Jet A was used as the fuel. The thermodynamic properties of the fuels, therefore, have little effect on performance; however, the physical properties, viscosity, surface tension, and liquid density, as they affect the atomization process, also determine the level of performance.

As expected, those combustors that employ airblast atomization are less sensitive to the properties of alternate fuel type, and performance deterioration can be nearly negligible (Tables XV through XVII).

IV. ANALYTICAL RESULTS AND COMPARISON

Graphical presentations of the summaries of STAC-I predicted results for the flow fields of each combustor, as listed in Tables XIV through XVII, are used in this section to evaluate the relative merit regarding fuel type tolerance of each combustor concept. This is accomplished through the use of cross plotting to determine the relationships of the pilot and main SMD, combustion efficiency, and emission indices to power level and fuel type for each combustor concept. The relationships of these same parameters to power level and combustor concept for each fuel type is then determined and these latter relationships are a direct indication of the sensitivity (or tolerance) of each combustor concept to the fuel type undergoing reaction within it. Combined with considerations of such items as ignition limits, lean-blowout stability, smoke, combustor durability, and pattern factor an analytically determined ranking of the combustor candidates with regard to fuel type tolerance is possible.

4.1 BASELINE COMBUSTOR

The baseline combustor depicted in Figure 5 was determined to have the following zonal stoichiometries (as equivalence ratios), Table VII:

Takeoff
Prechamber ϕ = 1.60
Main primary ϕ = 1.09

Ground idle
Prechamber ϕ = 0.86
Main primary ϕ = 0.58

The assumptions employed in the analysis (performed in Section II) would associate the prechamber equivalence ratio with the overall fuel spray available, while the main primary zone equivalence ratio would be considered to be that of the reacted portion of the spray. This latter term is also denoted as the gas phase equivalence ratio. These equivalence ratios may be directly compared with those computed by STAC-I. The assumptions employed in the analysis of Section II produce little difference in predicted equivalence ratios for JP-4 or Jet A fuels. STAC-I computed takeoff and ground idle equivalence ratios for Jet A fuel usage in the baseline combustor are presented in Figures 96 and 101 in Appendix B.

Takeoff--STAC-I
Prechamber exit overall ϕ = 1.77
Main primary jet plane gas phase ϕ = 1.07

Ground idle--STAC-I
Prechamber exit overall ϕ = 0.82
Main primary jet plane gas phase ϕ = 0.53

The takeoff and ground idle equivalence ratios computed by the two methods exhibit excellent agreement. The flow computations from STAC-I are more detailed and exact than the simplistic assumptions used in Section II. Nevertheless, the agreement is sufficient to validate the approach used in Section II to accomplish the initial ranking of the combustors.

The relationships of the pilot and main nozzle fuel spray SMDs to combustor power level and fuel type are presented in Figures 22 and 23. These spray nozzles are simplex (combined to form a dual orifice) and are quite sensitive to fuel properties. The SMDs decrease with power level (higher nozzle ΔP) and with use of fuels having low viscosity and surface tension. SMDs for the ERBS fuels are bracketed by those for Jet A and DF-2 fuels. Since increased combustion efficiency and decreased unburned hydrocarbon (UHC) and carbon monoxide (CO) emissions are usually inversely proportional to the SMD, the results presented in Figures 24, 25, and 26 are, with one exception, those expected. The single exception is the ground idle power level CO emissions level for the ERBS and DF-2 fuels. Normally CO emissions continue to increase with decreasing power level in the same manner as the unburned hydrocarbon emissions. Figures 104, 105, and 106 (Appendix B) indicate that the gas phase reaction within the baseline combustor flow field at the ground idle power level ceases in the latter third of the combustor. This is normally the location during which CO is formed due to added oxygen from the dilution jets, but not further oxidized to CO_2 because of the low gas temperatures at these decreased power levels. The ground idle power level for the ERBS and DF-2 fuels appears to be an extreme case where the temperature in the final third of the combustor is so low that the reaction of the fuel to form CO is nearly nonexistent. The lack of increase of the combustion efficiency in this region, while a significant quantity of spray still remains, confirms this observation.

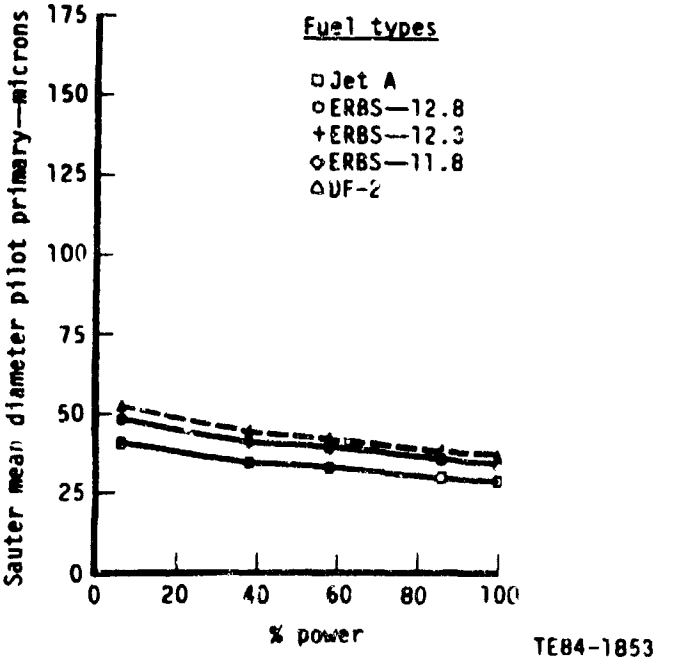

Figure 22. Pilot nozzle Sauter mean diameter as a function of power level and fuel type- baseline combustor.

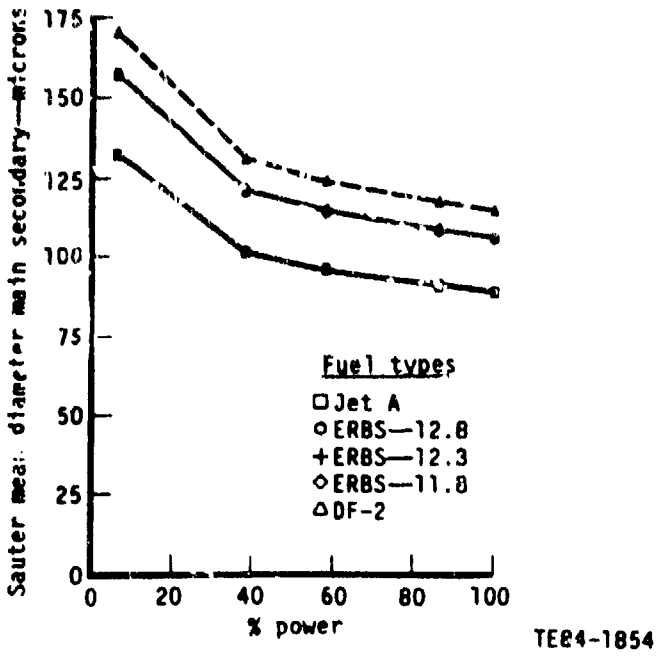

Figure 23. Main nozzle Sauter mean diameter as a function of power level and fuel type--baseline combustor.

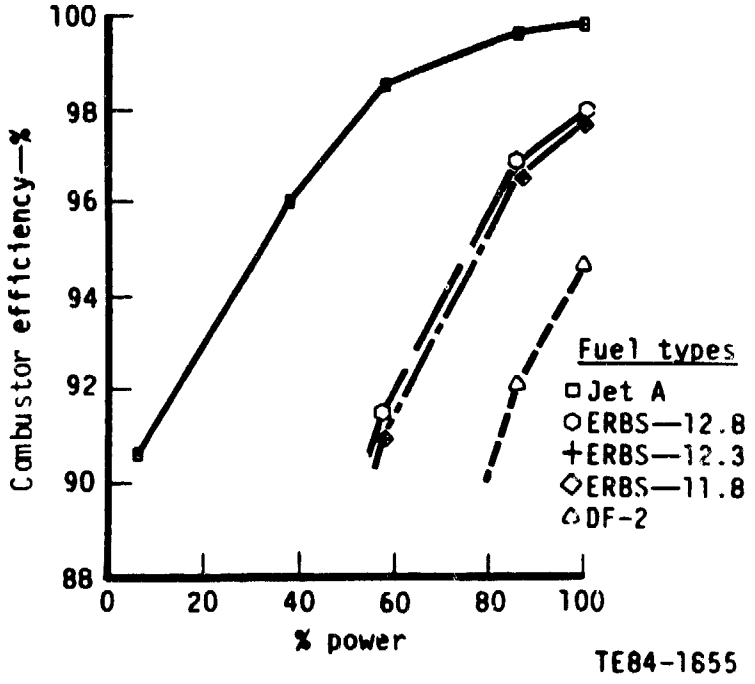

Figure 24. Combustion efficiency as function of power level and fuel type--baseline combustor.

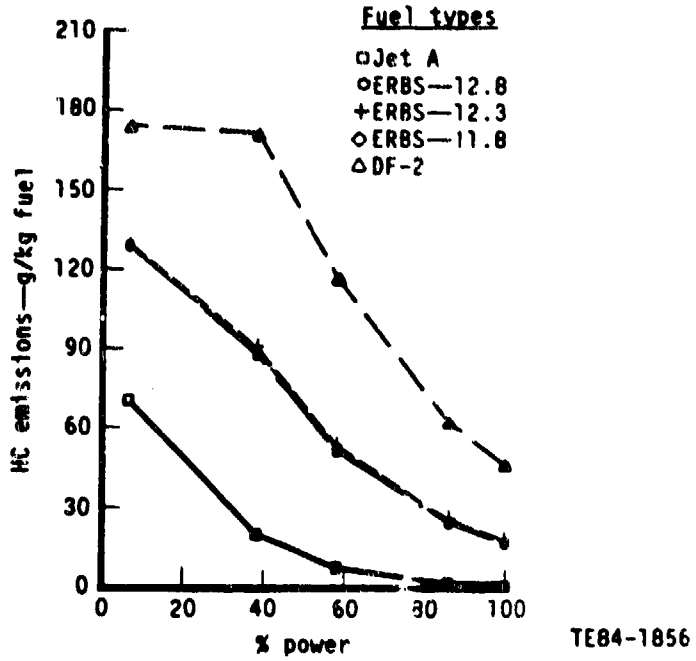

Figure 25. Unburned hydrocarbon emission as a function of power level and fuel type--baseline combustor.

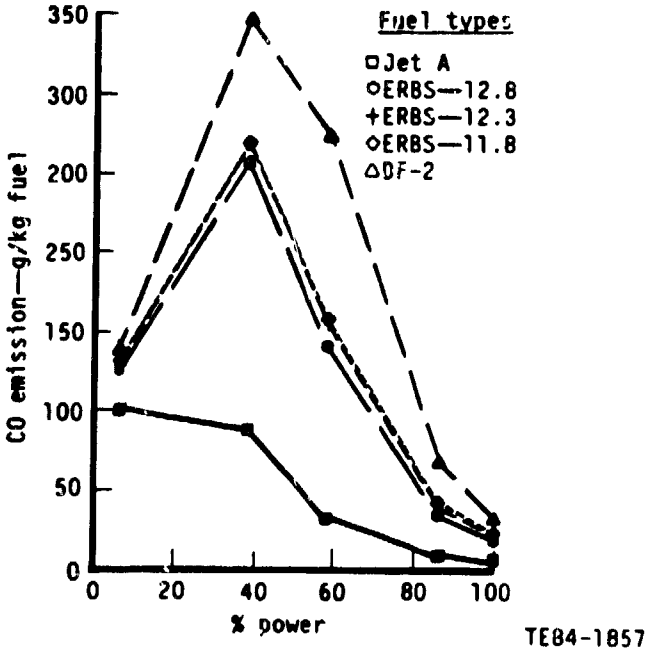

Figure 26. Carbon monoxide emission as a function of power level and fuel type--baseline combustor.

The emission levels of NO_x as a function of power level and fuel type are presented in Figure 27. NO_x emissions for the baseline combustor increase both with power level and with the use of fuels that atomize to smaller SMDs producing more rapid vaporization and higher gas temperatures.

4.2 SHORT PRECHAMBER COMBUSTOR

The short prechamber combustor, Figure 8, was determined, similar to the baseline combustor, to have the following zonal equivalence ratios, Table VII:

Takeoff
Prechamber ϕ = 1.49
Main primary ϕ = 1.04

Ground idle
Prechamber ϕ = 0.80
Main primary ϕ = 0.56

Again, these equivalence ratios may be directly compared with those computed by STAC-I in Figures 108 and 114 (Appendix B).

Takeoff--STAC-I
Prechamber exit overall ϕ = 1.42
Main primary jet plane gas phase ϕ = 0.93

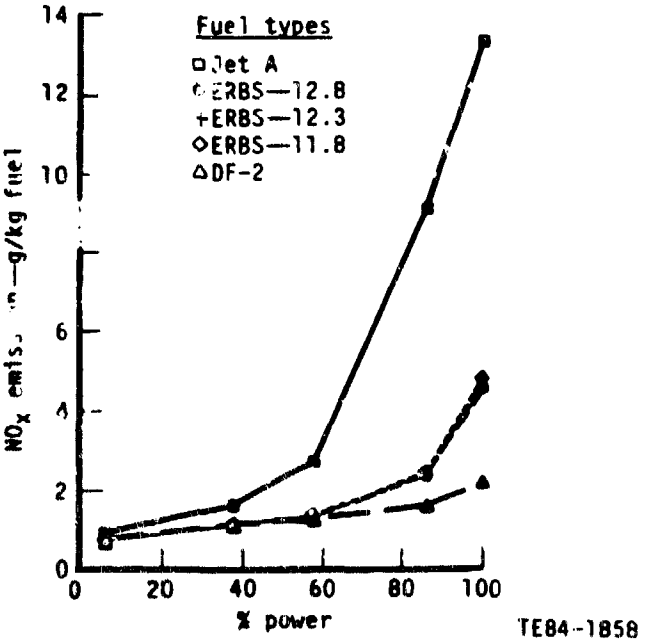

Figure 27. Nitric oxide emission as a function of power level and fuel type--baseline combustor.

Ground idle--STAC-I
Prechamber exit overall ϕ = 0.62
Main primary jet plane gas phase ϕ = 0.48

The agreement between the methods is, again, very satisfactory. The lower ground idle prechamber exit overall ϕ predicted by STAC-I is due to considerable recirculation of primary jet air and combustor products into the prechamber. This resulted in an equivalence ratio of 0.675 for the CTRZ (that of the CTRZ for the baseline combustor at ground idle was 0.964). However, this region within the short prechamber is well stabilized due to the overall increased gas temperature resulting from the use of an airblast injector, as compared with the gas temperature at ground idle for the baseline combustor, Figure 102 (Appendix B).

The relationship of the pilot nozzle fuel spray SMD to combustor power level and fuel type as presented in Figure 28 is the same as for the baseline combustor. Indeed this is true of the piloted prechamber and variable geometry combustors as well and will not be the subject of further discussion. The relationship of the main nozzle fuel spray SMDs, as shown in Figure 29, to power level and fuel type reflects the use of an airblast injector. These drop sizes, though exhibiting the same trend with fuel physical properties as the dual orifice injector, are less sensitive to fuel type and are also less than one-half the size of those droplets produced by the baseline dual orifice main nozzle injector. The SMDs decrease with power level reflecting the beneficial effect of increased air density and enhanced momentum exchange between the fuel film and airblast injector airflow.

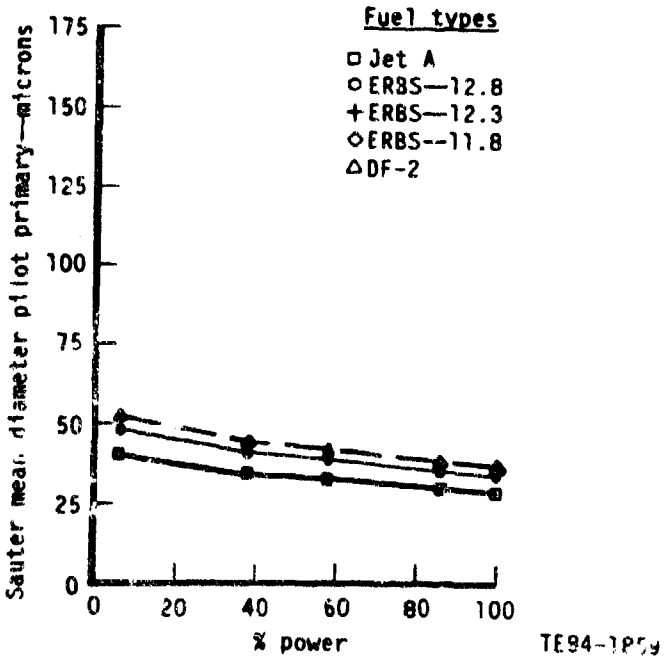

Figure 28. Pilot nozzle Sauter mean diameter as a function of power level and fuel type--short prechamber combustor.

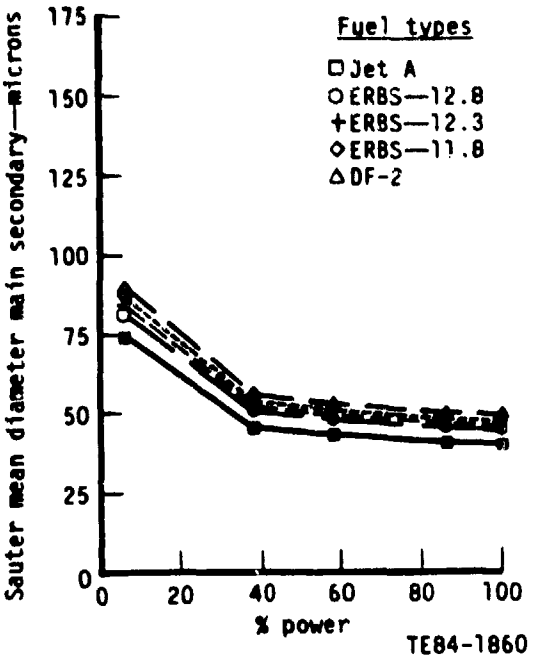

Figure 29. Main nozzle Sauter mean diameter as a function of power level and fuel type--short prechamber combustor.

The combustion efficiency and UHC and CO emission levels presented in Figures 30-32 follow the expected trend. The combustion efficiency is increased for all fuel types. The NO_x emission index presented in Figure 33 exhibits a reversal in fuel property effect at the higher power levels. DF-2 produces a very slight increase in the quantity of NO_x emitted compared with that produced by Jet A fuel usage. Figures 107 through 112 (Appendix B) indicate that this reflects a slightly increased DF-2 combustion gas temperature in the post primary zone due to the presence of DF-2 spray in this region.

4.3 PILOTED PRECHAMBER COMBUSTOR

The piloted prechamber combustor, shown in Figure 10, was determined, similar to the baseline combustor, to have the following zonal equivalence ratios, Table VII:

Takeoff
Prechamber ϕ = 2.32 (swirler/fuel nozzle-exit plane)
Main primary ϕ = 0.99

Ground idle
Prechamber ϕ = 1.20 (swirler/fuel nozzle exit plane)
Main Primary ϕ = 0
*Starter primary ϕ = 1.23

*Corresponds to absence of main nozzle fuel spray--called recirculation/center zone in Table VII.

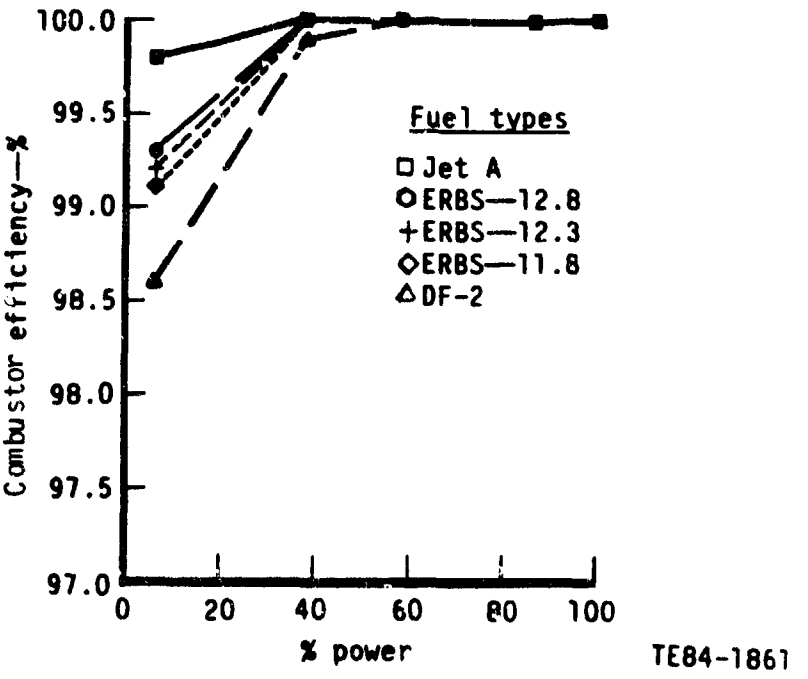

Figure 30. Combustion efficiency as a function of power level and fuel type--short prechamber combustor.

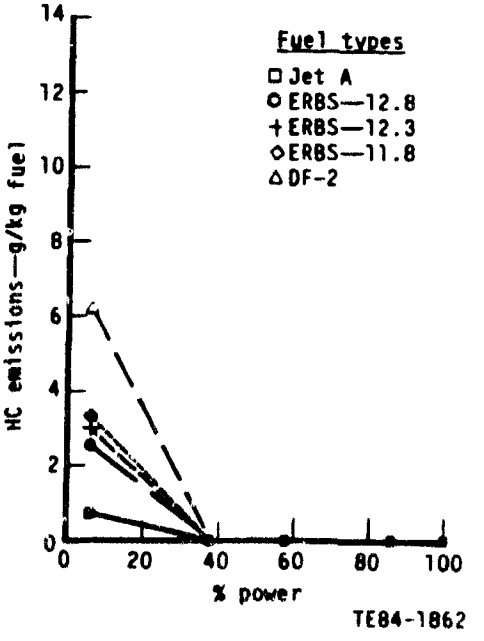

Figure 31. Unburned hydrocarbon emission as a function of power level and fuel type--short prechamber combustor.

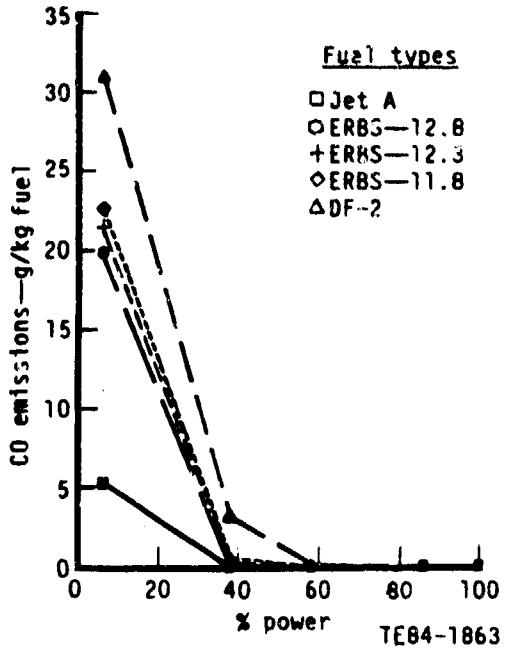

Figure 32. Carbon monoxide emission as a function of power level and fuel type--short prechamber combustor.

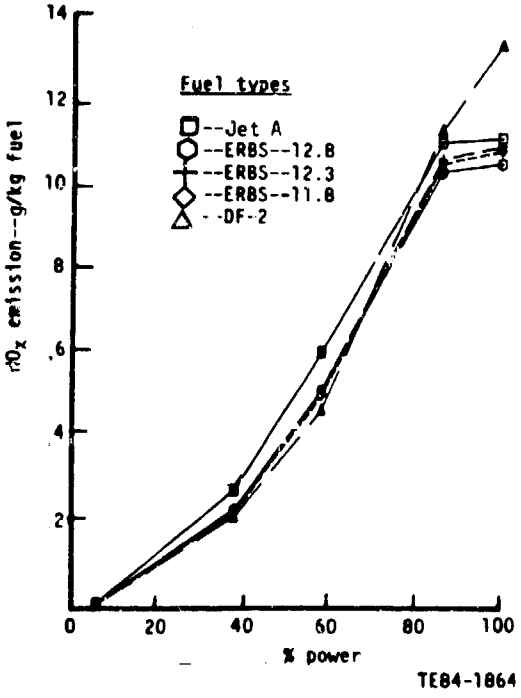

Figure 33. Nitric oxide emission as a function of power level and fuel type--short prechamber combustor.

Again, these equivalence ratios may be directly compared with those computed by STAC-I in Figures 138 and 144 (Appendix B).

Takeoff--STAC-I
Prechamber swirler/fuel nozzle exit plane overall $\phi = 2.5^{+}$
Main primary jet plane gas phase $\phi = 0.91$

Ground idle--STAC-I
Prechamber swirler/fuel nozzle exit plane overall $\phi = 0.8$
Starter primary/jet plane gas phase $\phi = 0.46$

The agreement between the methods at the takeoff power level is quite satisfactory. The lower ground idle prechamber swirler/fuel nozzle exit plane overall ϕ predicted by STAC-I is due to considerable pilot and starter nozzle fuel spray injection into the CTRZ and to considerable recirculation of primary jet air and combustion products into the CTRZ and, hence, the prechamber. This resulted in an equivalence ratio of 0.685 for the CTRZ. This region within the piloted prechamber, however, is well stabilized for the same reason as is this region within the short prechamber combustor. The starter primary zone equivalence ratio, as calculated by the technique used in Section II, based the equivalence ratio on only the air within the central region. The value computed by STAC-I includes the downstream swirler air as this air would rapidly mix with the prechamber flow. An equivalent STAC-I computation would take the total available spray flow at the axial location just prior to entrance of the downstream axial swirler air and divide this value (0.63 from Figure 144) by the ratio of the prechamber airflow to that including the downstream axial swirler flow (11.93/17.67 from Table XIII); the resulting equivalence ratio is then 0.93. This value is in better agreement with but still lower than the 1.23 calculated from Section II. The difference is due to considerable recirculation into and from the CTRZ.

The pilot nozzle SMD is shown as a function of power level and fuel type in Figure 34. The relationship of the main nozzle fuel spray SMDs, as presented in Figure 35, to power level and fuel type again reflects the use of airblast injection. The trends are the same as those for the short prechamber, but the SMDs are considerably smaller, except at the idle power level, due to secondary reatomization of the main spray flow.

The combustion efficiency, unburned hydrocarbon, and carbon monoxide emission levels in Figures 36 through 38 follow the expected trend. The piloted prechamber is slightly more sensitive to fuel type at the ground idle condition because the starter flow does not reatomize and the addition of the downstream swirler air trends to reduce the combustion gas temperature. This increases the UHC and CO emissions while decreasing the combustion efficiency. The effect is more evident for the ERBS and DF-2 fuels. The NO_x emission index, depicted in Figure 39, follows the normal trend of increasing with increasing power level (i.e., increased gas temperature within the combustor). DF-2 fuel usage produces slightly more NO_x emission than the ERBS fuels due to increased spray reaction in the post primary zone.

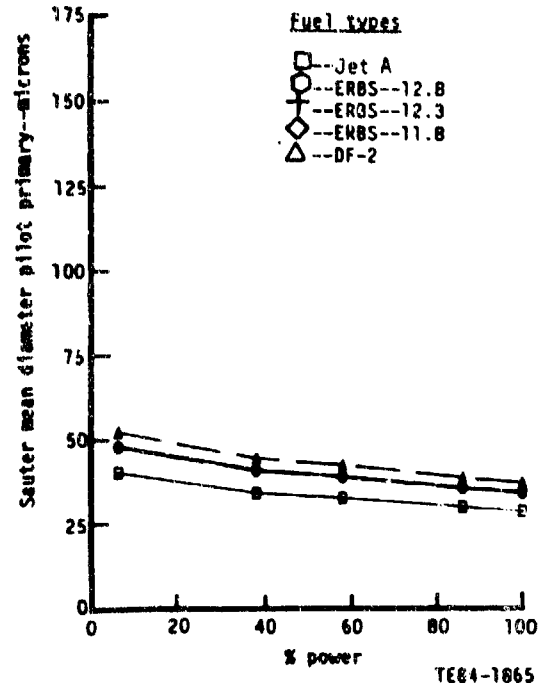

Figure 34. Pilot nozzle Sauter mean diameter as a function of power level and fuel type--piloted combustor.

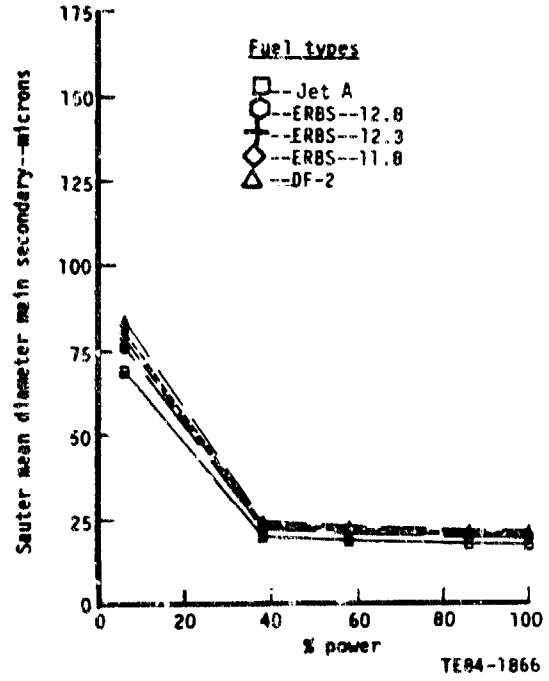

Figure 35. Main nozzle Sauter mean diameter as a function of power level and fuel type--piloted combustor.

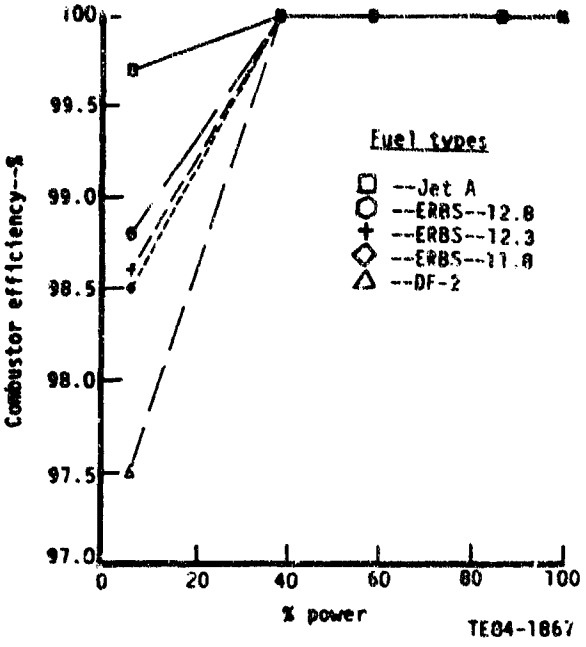

Figure 36. Combustion efficiency as a function of power level and fuel type--piloted combustor.

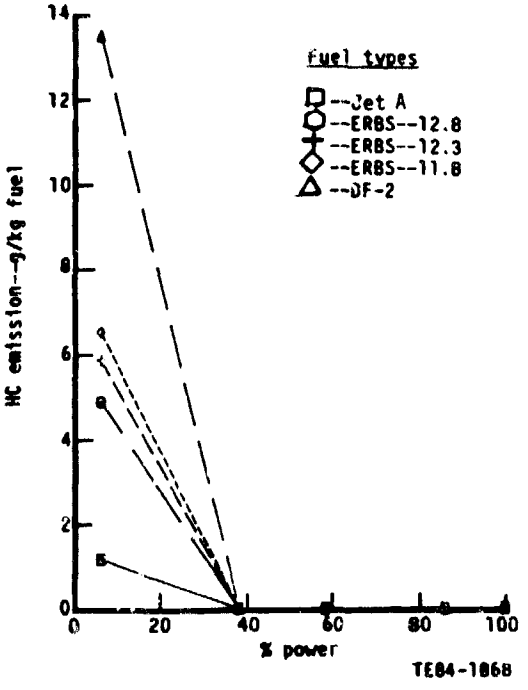

Figure 37. Unburned hydrocarbon emission as a function of power level and fuel type--piloted combustor.

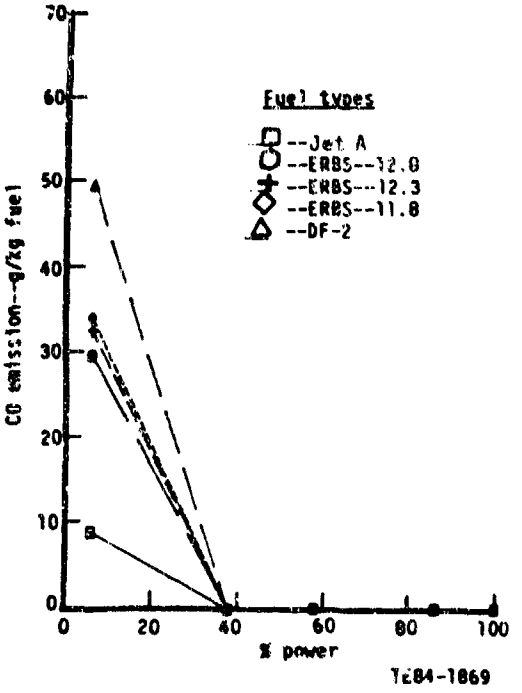

Figure 38. Carbon monoxide emission as a function of power level and fuel type--piloted combustor.

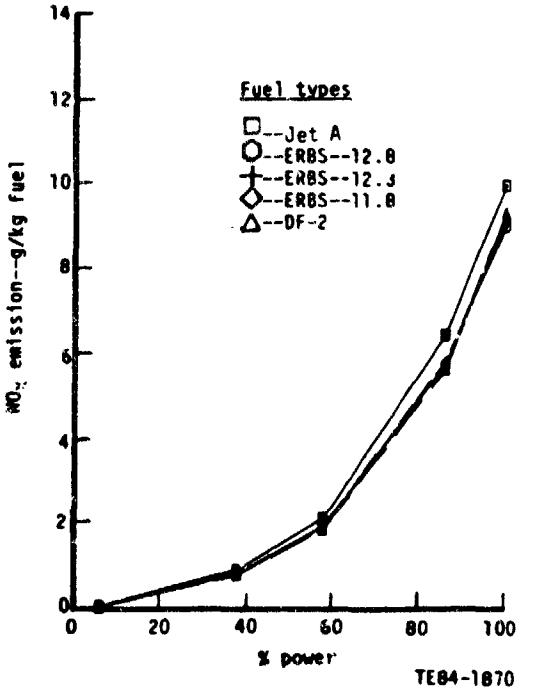

Figure 39. Nitric oxide emission as a function of power level and fuel type--piloted combustor.

4.4 VARIABLE GEOMETRY COMBUSTOR

The variable geometry combustor, Figure 14, was determined to have the following zonal equivalence ratios, Table VII:

Takeoff
Prechamber ϕ = 0.73
Main primary ϕ = 0.68

Ground idle
Prechamber ϕ = 1.09
Main primary ϕ = 0.80

These equivalence ratios may be directly compared with those computed by STAC-I in Figures 120 and 132 (Appendix B).

Takeoff--STAC-I
Prechamber exit overall ϕ = 0.82
Main primary jet plane gas phase ϕ = 0.65

Ground idle--STAC-I
Prechamber exit overall ϕ = 0.875
Main primary jet plane gas phase ϕ = 0.60

The agreement between the methods at the takeoff power level is excellent. The STAC-I predicted equivalence ratios at ground idle are somewhat lower than those calculated using the method of Section II. This again reflects considerable recirculation into and from the CTRZ; the resulting equivalence ratio in the CTRZ at ground idle is 0.82.

Pilot nozzle SMD as a function of power level and fuel type is shown in Figure 40. The relationship of the main nozzle fuel spray SMDs, as presented in Figure 41, to power level and fuel type reflects both the use of airblast injection and the beneficial effects of variable geometry. Closure of the radial swirler with decreasing power levels permits a nearly constant primary zone temperature to be achieved at all operating conditions. The available combustor front end delta pressure at low power results in excellent airblast atomization of the fuel film. This produced the lowest SMD at that power level among the combustors analyzed.

The combustion efficiency, unburned hydrocarbon, carbon monoxide, and nitric oxide emissions, Figures 42 through 45, follow the expected trends. The very low level of emissions and high combustion efficiency reflects the use of variable geometry. The descent power level predictions have been eliminated in these figures because they represented an anomaly in the prediction set. This particular power level should have been analyzed at an intermediate variable geometry setting, rather than with a fully closed radial swirler inlet.

4.5 PARAMETER RELATIONSHIP TO POWER LEVEL AND COMBUSTOR CONCEPT FOR EACH FUEL TYPE

The relationship of the pilot and main nozzle SMDs, combustion efficiency, and unburned hydrocarbon, carbon monoxide, and nitric oxide emission quantities to power level and combustor concept for each fuel type is a direct indication of

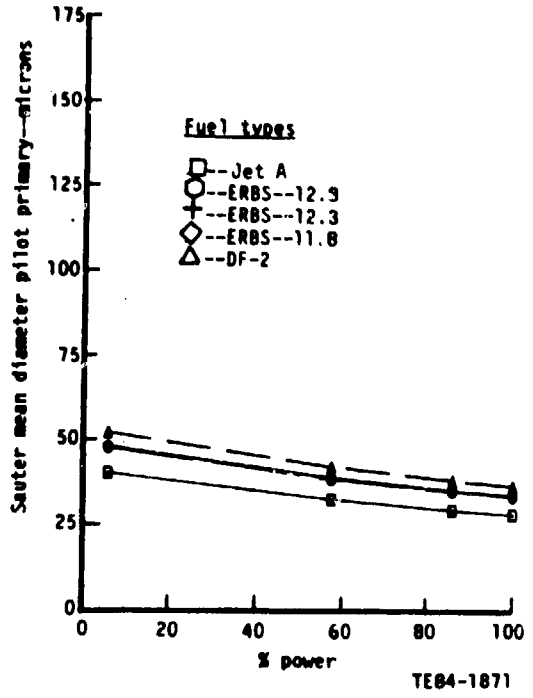

Figure 40. Pilot nozzle Sauter mean diameter as a function of power level and fuel type--variable geometry combustor.

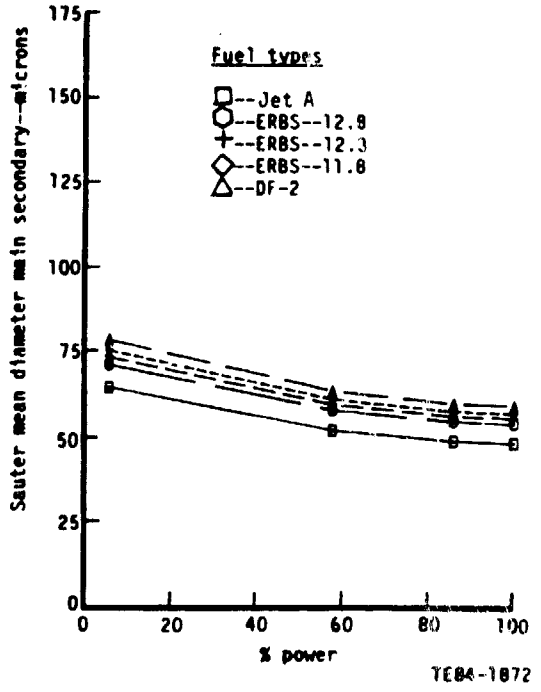

Figure 41. Main nozzle Sauter mean diameter as a function of power level and fuel type--variable geometry combustor.

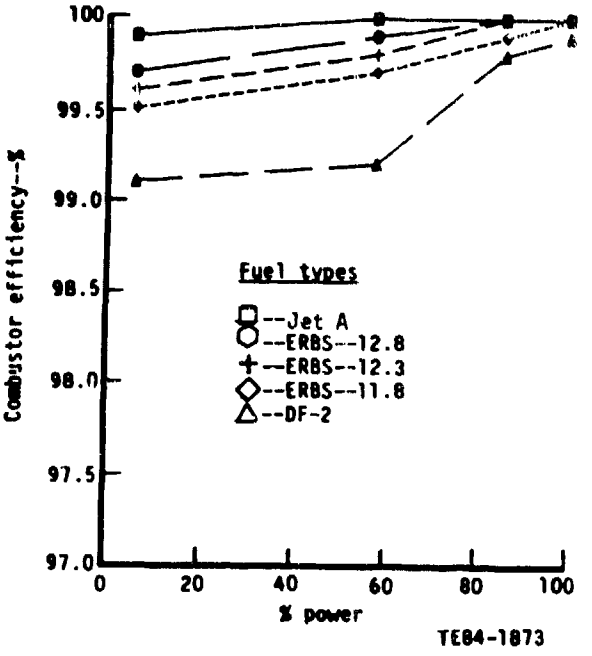

Figure 42. Combustion efficiency as a function of power level and fuel type--variable geometry combustor.

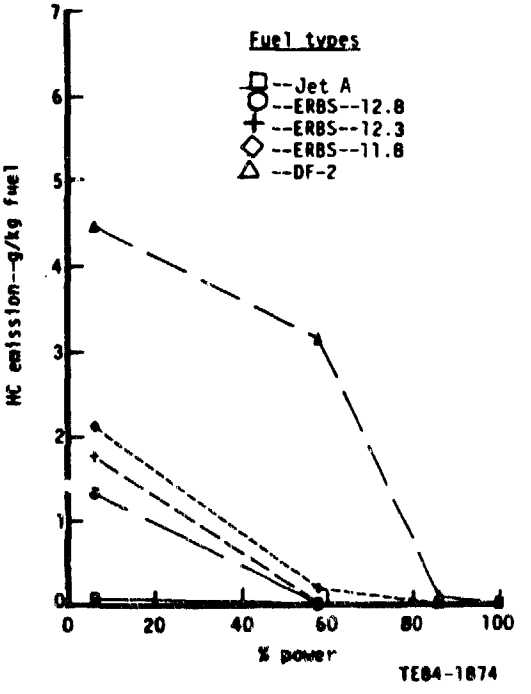

Figure 43. Unburned hydrocarbon emission as a function of power level and fuel type--variable geometry combustor.

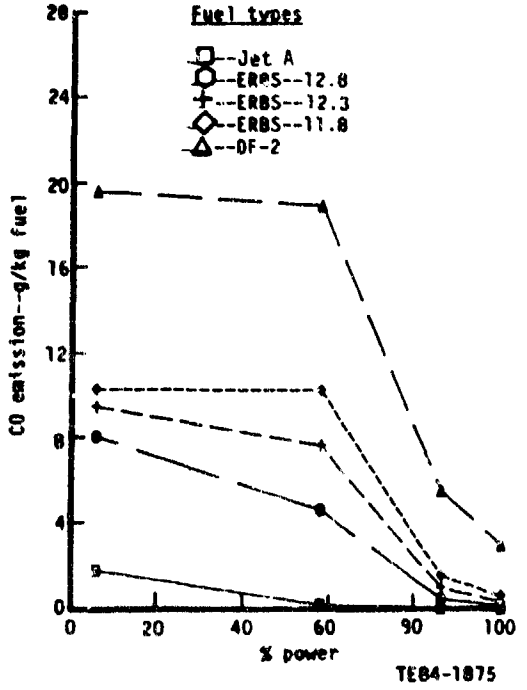

Figure 44. Carbon monoxide emission as a function of power level and fuel type--variable geometry combustor.

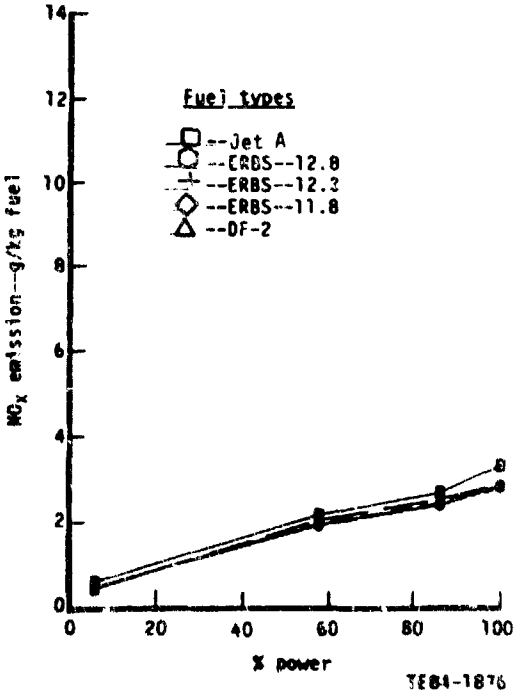

Figure 45. Nitric oxide emission as a function of power level and fuel type--variable geometry combustor.

the sensitivity (or tolerance) of each combustor concept to the fuel type undergoing reaction within it. The predicted effects of the broad-property fuels, ERBS 12.8, 12.3, and 11.8, have been shown to be effectively bracketed at each operating condition by the predicted results obtained when Jet A and DF-2 are considered to be the turbine combustor fuel. Consequently, the relationships of the parameters discussed to power level and combustor concept are presented for each fuel type in the fuel order Jet A, ERBS 12.8, ERBS 12.3, ERBS 11.8, and DF-2.

4.5.1 Pilot Nozzle Fuel Spray SMD

Pilot nozzle fuel spray variations with fuel type and power level are presented in Figures 46 through 50. Pilot nozzle fuel spray SMD is not a function of combustor concept because the geometry and pilot fuel flow through the simplex tip of the pilot nozzle was fixed for each fuel. This ensures the same pilot fuel flow rate (of each fuel) to each combustor at similar operating conditions. The resulting pilot nozzle fuel spray SMD, however, decreases with increased power level (larger delta pressure across the simplex tip) and increases with increasing fuel viscosity and surface tension. The SMDs for the ERBS fuels are nearly the same but are considerably larger than those for Jet A at similar operating conditions. DF-2 pilot fuel SMDs are the largest at all operating conditions.

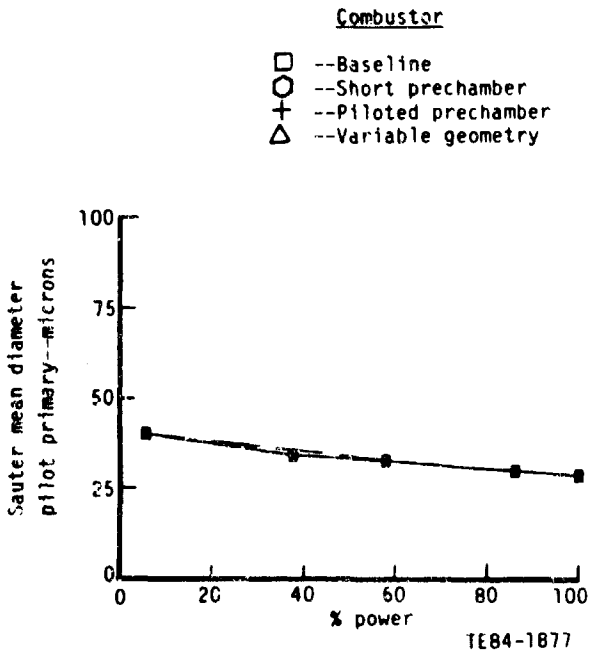

Figure 46. Pilot nozzle Sauter mean diameter as a function of power level and combustor type--Jet A fuel.

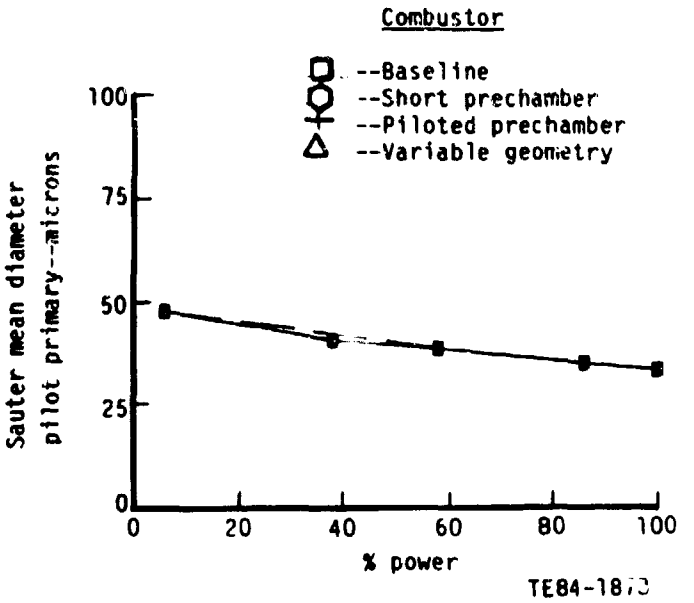

Figure 47. Pilot nozzle Sauter mean diameter as a function of power level and combustor type--ERBS 12.8 fuel.

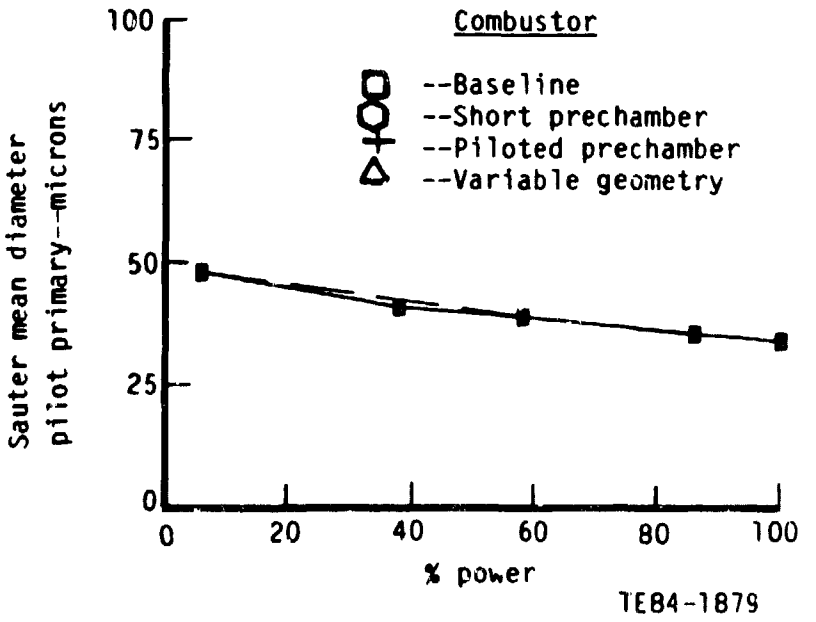

Figure 48. Pilot nozzle Sauter mean diameter as a function of power level and combustor type--ERBS 12.3 fuel.

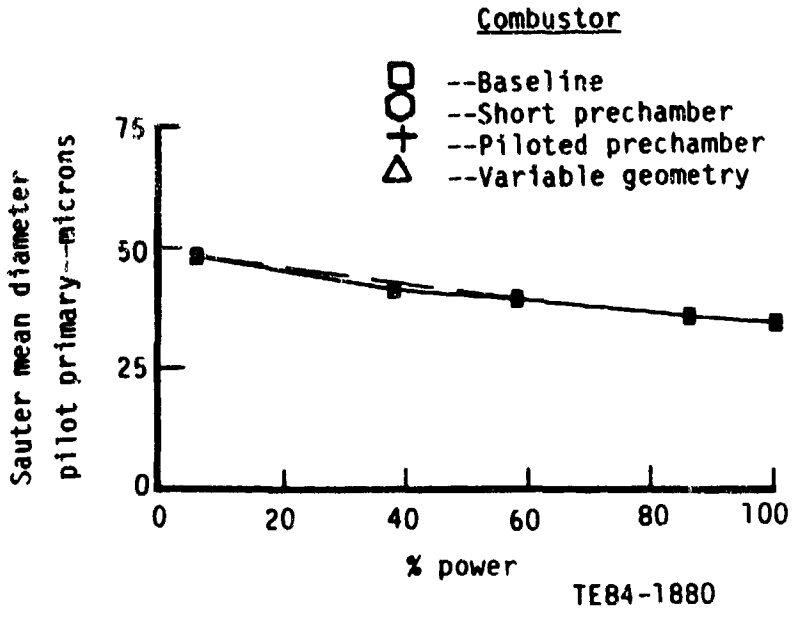

Figure 49. Pilot nozzle Sauter mean diameter as a function of power level and combustor type--ERBS 11.8 fuel.

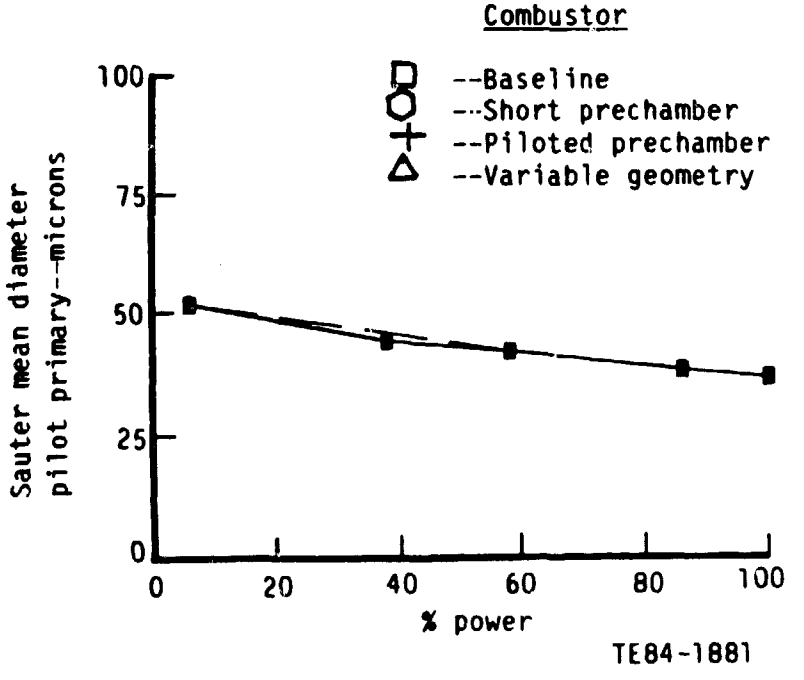

Figure 50. Pilot nozzle Sauter mean diameter as a function of power level and combustor type--DF-2 fuel.

4.5.2 Main Nozzle Fuel Spray SMD

Main nozzle fuel spray SMD variations with power level, fuel type, and combustor concept are presented in Figures 51 through 55. Although the main nozzle geometry was identical for all of the airblast injected combustors, SMD variation with combustor concept at similar operating conditions occurs due to differences in air management around the individual liner. This results in differences in the available delta pressure across the airblast fuel nozzle (and hence different airblast air velocities) and produces different SMDs for each of the airblast injected combustor concepts. The main nozzle SMD trend with power level is similar for all fuels. At all but the ground idle condition the smallest SMD was obtained using the piloted prechamber combustor (because of secondary reatomization) followed in order by the short prechamber, variable geometry, and baseline combustor. The large difference between the baseline combustor produced SMDs and those from the other combustor concepts reflect the change from dual orifice to airblast fuel injection. Further, the drop size variation between fuels was minimized using airblast injection concepts. At ground idle all of the airblast injected combustor concepts produced approximately the same SMD for each fuel. This drop size was approximately one half that produced by the dual orifice injector of the baseline combustor.

4.5.3 Combustion Efficiency

Combustion efficiency variations with power level, fuel type, and combustor concept are presented in Figures 56 through 60. The combustion efficiency at

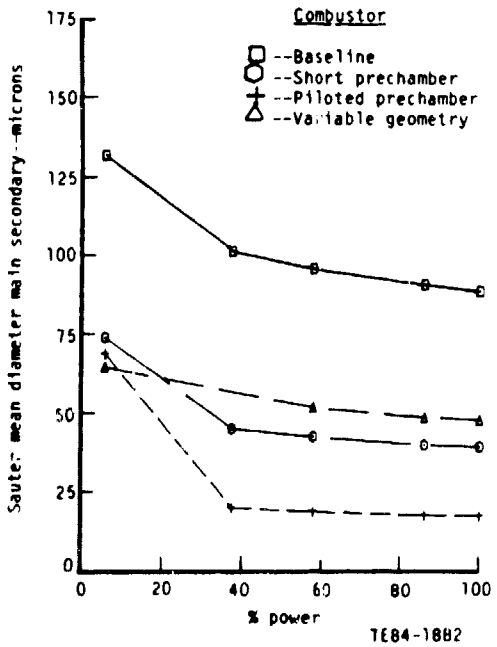

Figure 51. Main nozzle Sauter mean diameter as a function of power level and combustor type - Jet A fuel.

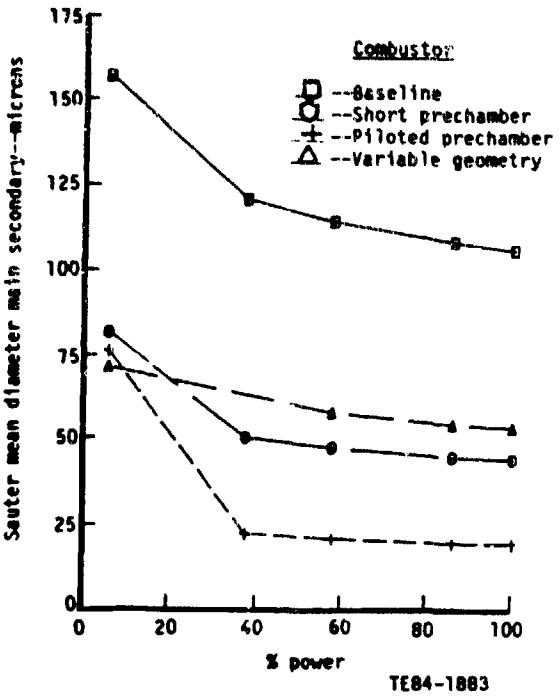

Figure 52. Main nozzle Sauter mean diameter as a function of power level and combustor type--ERBS 12.8 fuel.

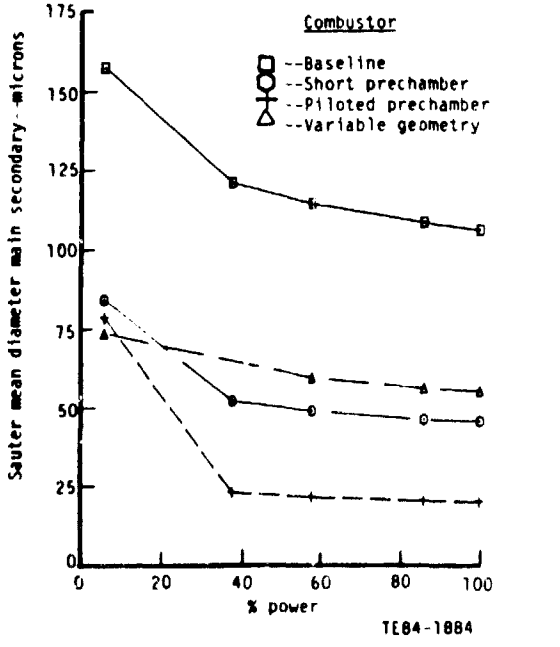

Figure 53. Main nozzle Sauter mean diameter as a function of power level and combustor type--ERBS 12.3 fuel.

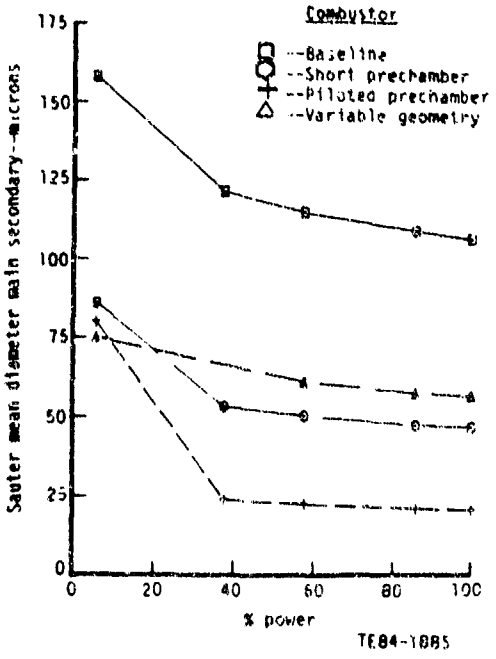

Figure 54. Main nozzle Sauter mean diameter as a function of power level and combustor type---ERBS 11.8 fuel.

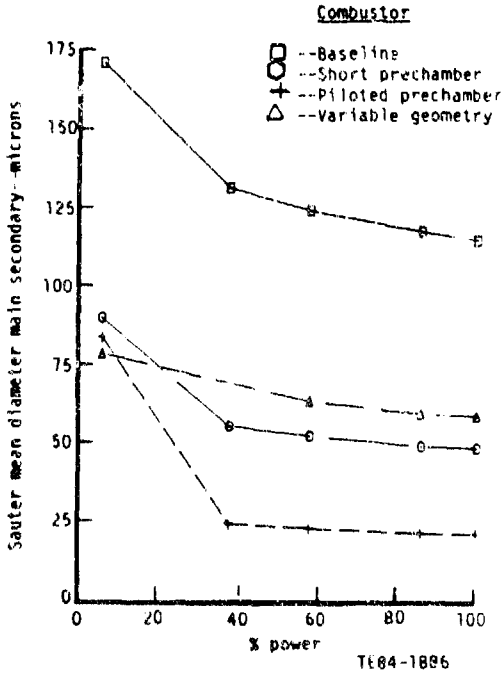

Figure 55. Main nozzle Sauter mean diameter as a function of power level and combustor type - DF-2 fuel.

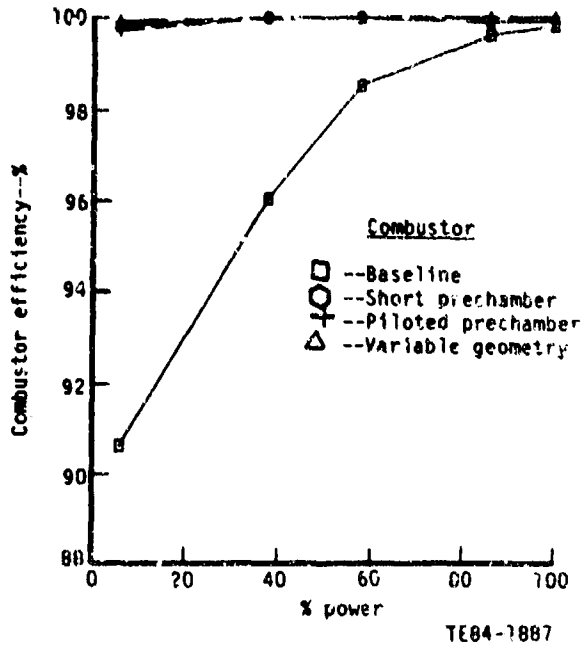

Figure 56. Combustion efficiency as a function of power level and combustor type--Jet A fuel.

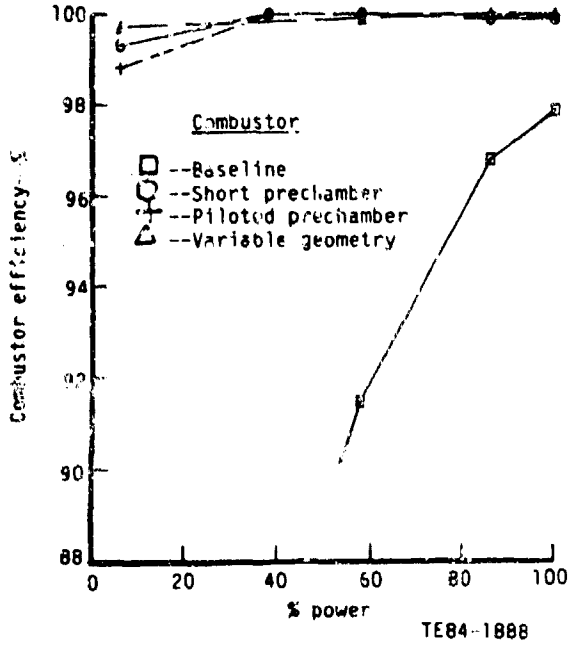

Figure 57. Combustion efficiency as a function of power level and combustor type--ERBS 12.8 fuel.

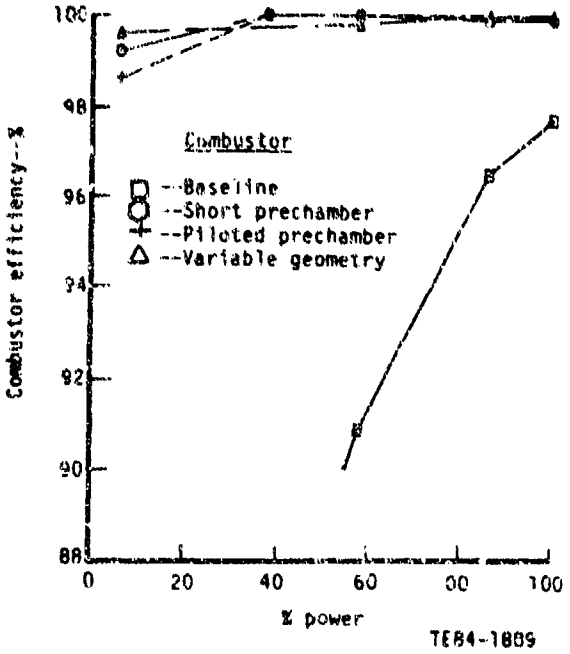

Figure 58. Combustion efficiency as a function of power level and combustor type--ERBS 12.3 fuel.

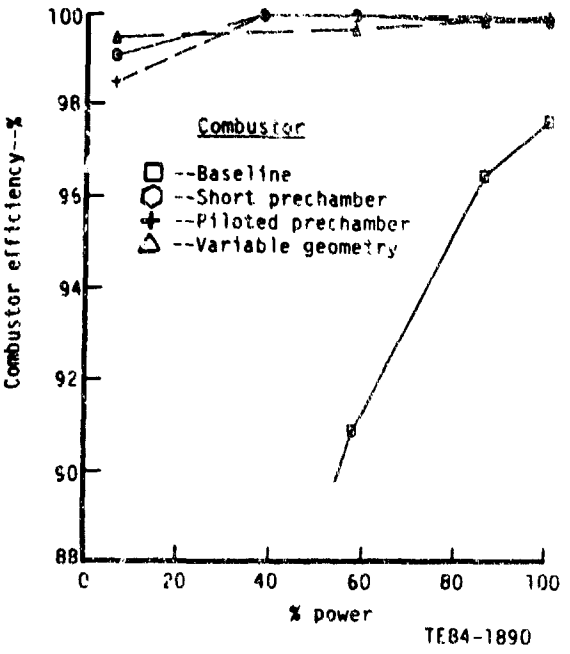

Figure 59. Combustion efficiency as a function of power level and combustor type--ERBS 11.8 fuel.

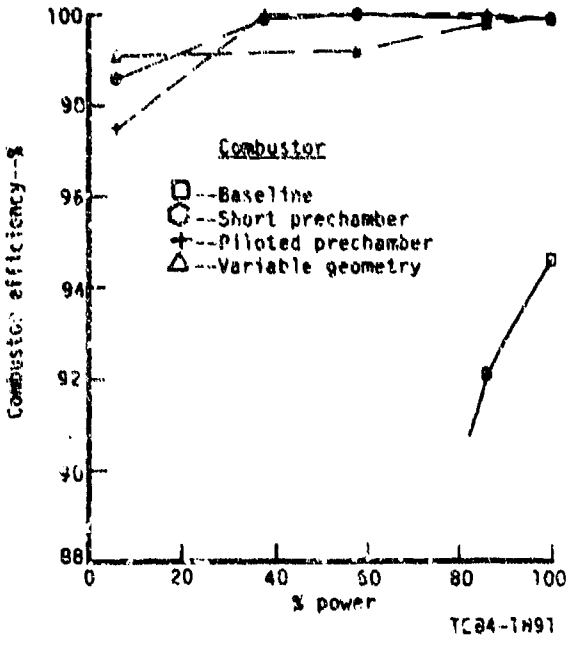

Figure 60. Combustion efficiency as a function of power level and combustor type--DF-2 fuel.

power levels above ground idle is essentially independent of combustor concept for those combustors with airblast injection. The usage of broad property fuels, such as the ERBS fuels, and more viscous fuels, such as DF-2, require airblast injection concepts to achieve acceptable performance efficiency even at increased power levels. Predicted ground idle combustion efficiency for the airblast-injected combustor concepts is increased, regardless of fuel type, when the variable geometry combustor concept is employed. The lowest combustion efficiency at this operating condition occurs when the piloted prechamber concept is used as the combustor. The ground idle combustion efficiency of the short prechamber concept falls between that of the variable geometry and piloted prechamber combustors. In actuality, the variable geometry combustor, with optimum radial swirler inlet adjustment for each fuel, would have the highest combustion efficiency throughout the power range. No attempt was made to analyze optimum radial swirler adjustments; however, the results presented in Figures 120 and 132 in Appendix B for fully open or closed radial swirler settings, respectively, indicate the capacity for this combustor to maintain a nearly constant primary zone temperature. The short prechamber and piloted prechamber combustors both have higher primary zone temperatures at takeoff and lower primary zone temperatures at ground idle as indicated in Figures 108, 114, 138, and 144 of Appendix B.

4.5.4 Unburned Hydrocarbon and Carbon Monoxide Emissions

An increase in engine power setting reduces the emission of unburned hydrocarbons, partly by improved fuel atomization, but mainly through the effects of higher inlet air pressure and temperature that together enhance chemical reaction rates in the primary combustion zone. Carbon monoxide is produced

mainly in the primary zone of a gas turbine combustor. If this zone is fuel rich, large amounts of CO will be formed due to lack of the oxygen needed to complete the reaction to CO_2. If the primary zone equivalence ratio is stoichiometric or moderately fuel-lean significant amounts of CO will be present due to the dissociation of CO_2. The resulting oxidation of this CO to CO_2 depends on the subsequent time-temperature history of the CO molecule within the combustor. The reaction of CO to CO_2 is one of nonequilibrium and is strongly dependent on chemical kinetics. Additional CO can be formed in downstream regions of the combustor at lower power levels if fuel vapor is present and reacting to form CO but further oxidation of the CO to CO_2 is impeded by low gas temperatures. In general, the emissions of UHC and CO parallel one another. Any factor that raises the level of CO emissions will tend to raise UHC emissions. Conversely, any combustor/nozzle modifications carried out for the reduction of CO will usually reduce the UHC emission also.

The variation of these emissions with power level, fuel type, and combustor concept is presented in Figures 61 through 70. The trends described are clearly evident. Unburned hydrocarbon emissions are nearly eliminated through the use of airblast injection concepts. Some minor levels of UHC emissions exist at the ground idle power level when ERBS (all 3 types) and DF-2 are used as the combustor fuel. Again, the difference between combustor concepts is nearly negligible but the variable geometry concept appears to be the most optimum combustor type followed by the short prechamber and piloted prechamber concepts.

Carbon monoxide emission at the lower power levels is somewhat more sensitive to fuel type. ERBS and DF-2 produce considerably more CO than Jet A when used as the combustor fuel. The ground idle level of CO emissions for the baseline combustor is an extreme case where the combustion efficiency has fallen so low that little CO is even produced. Again, airblast fuel injection is required to lower the CO emission to an acceptable level. Combustor concept is more important for CO emission control at the lower power levels than it was for UHC emissions. The ranking of the combustors with regard to CO emission control is the same as that for UHC emission control. This clearly reflects the time-temperature history of the CO produced within the different combustors as indicated in Figures 117, 118, 135, 136, 147, and 148 in Appendix B.

4.5.5 Nitric Oxide Emission

Both NO and N_2O are included in the term "nitric oxide emission." Oxides of nitrogen are produced by the oxidation of atmospheric nitrogen in high-temperature regions of the combustor. In contrast to CO and UHC emissions NO arises only in the hot regions of the combustor, and NO levels are highest at full power conditions. Only thermal NO is considered in this report and such NO formation is found to peak on the fuel-lean side of stoichiometric. This results as a consequence of the competition between fuel and nitrogen for the available oxygen. At equivalence ratios at or slightly above stoichiometric the combustor temperature is at a maximum, but the available oxygen is then all consumed preferentially by the fuel. Conversely, at equivalence ratios below about 0.8, the reduction in temperature is sufficient to override the effect of increasing free oxygen concentration, and NO levels begin to fall.

The optimum combustor would be one that achieves high combustion efficiency throughout its power range without producing the high primary zone

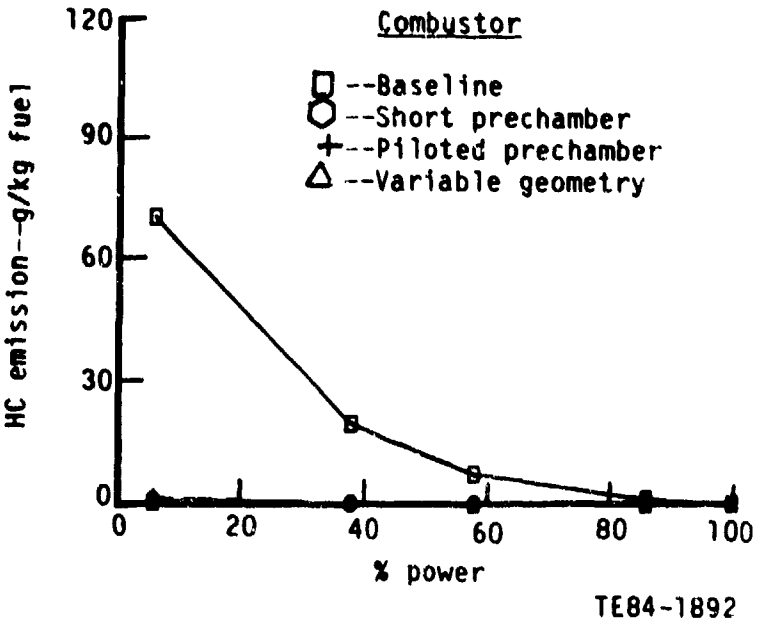

Figure 61. Unburned hydrocarbon emission as a function of power level and combustor type--Jet A fuel.

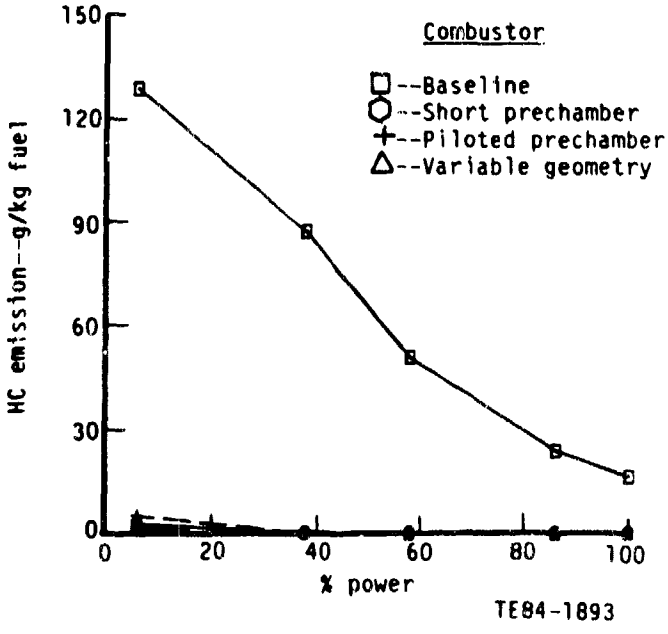

Figure 62. Unburned hydrocarbon emission as a function of power level and combustor type ERBS 12.8 fuel

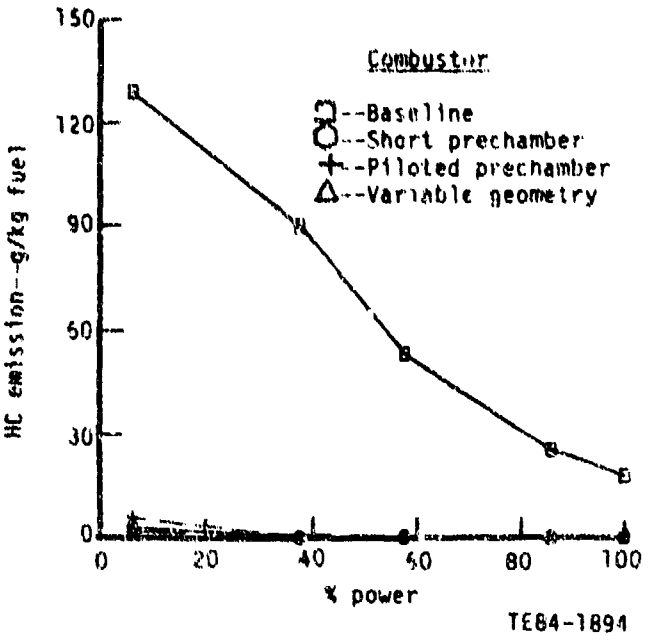

Figure 63. Unburned hydrocarbon emission as a function of power level and combustor type -ERBS 12.3 fuel.

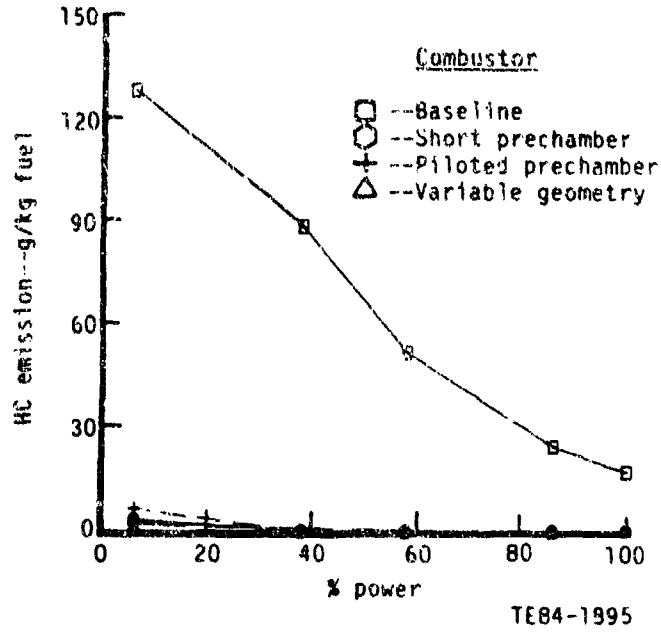

Figure 64. Unburned hydrocarbon emission as a function of power level and combustor type - ERBS 11 8 fuel.

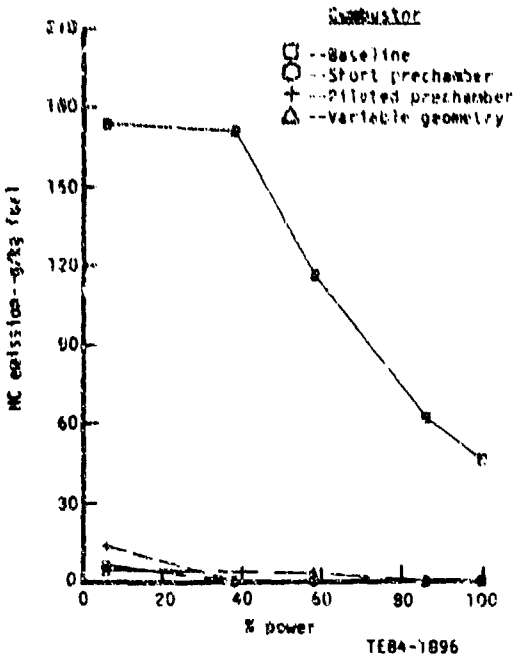

Figure 65. Unburned hydrocarbon emission as a function of power level and combustor type--DF-2 fuel.

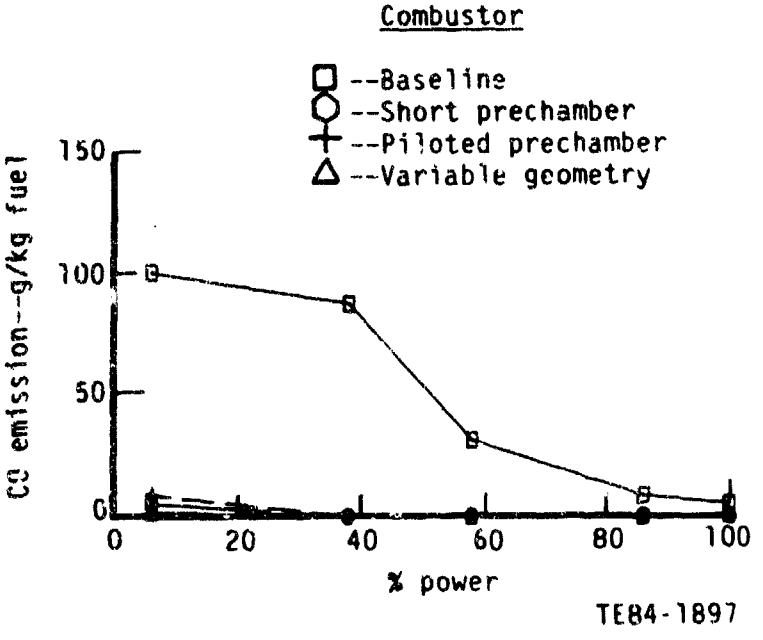

Figure 66. Carbon monoxide emission as a function of power level and combustor type--Jet A fuel.

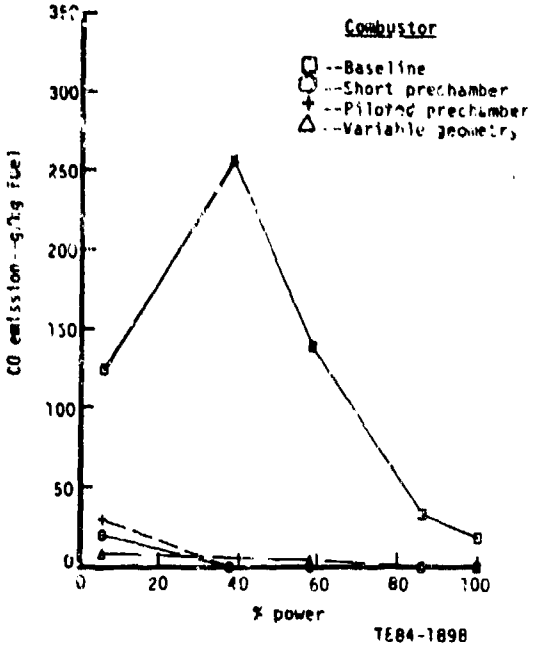

Figure 67. Carbon monoxide emission as a function of power level and combustor type--ERBS 12.8 fuel.

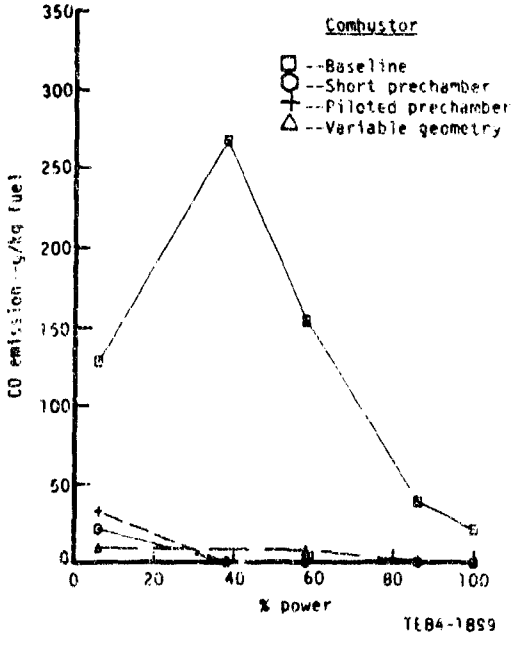

Figure 68. Carbon monoxide emission as a function of power level and combustor type- ERBS 12.3 fuel.

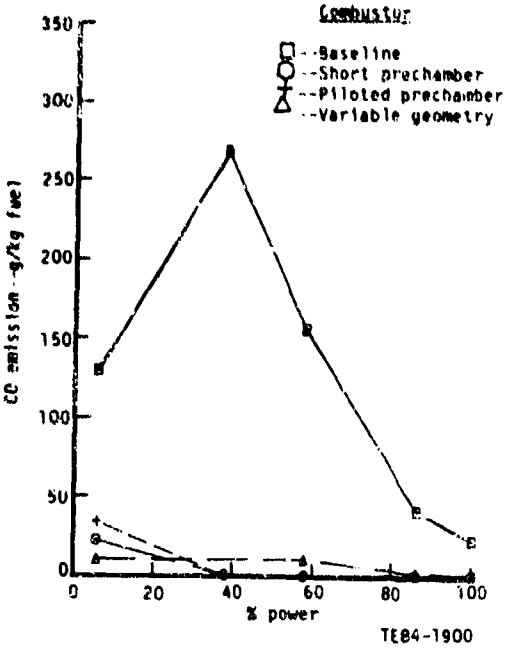

Figure 69. Carbon monoxide emission as a function of power level and combustor type--ERBS 11.8 fuel.

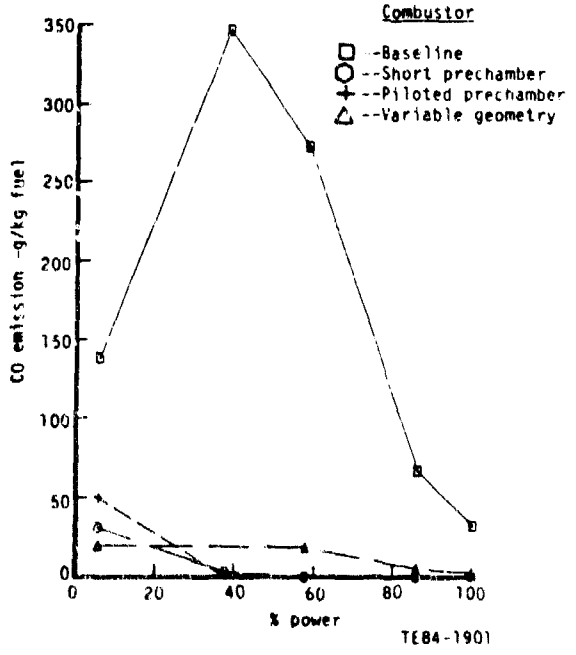

Figure 70. Carbon monoxide emission as a function of power level and combustor type DF-2 fuel.

temperatures that result in large quantities of NO formation. Once formed the dissociation of NO back to N_2 and O_2 is strongly temperature dependent; the rate of dissociation becomes virtually nonexistent as the temperature falls due to the quenching mechanism of the dilution jets.

The variation of NO emissions with power level, fuel type, and combustor concept are presented in Figures 71 through 75. The trend described previously is evident. Nitric oxide emissions are not necessarily reduced through the use of airblast injection, although such injection techniques can produce more uniform mixing and reduced overall flame temperatures. The quantity of NO formed and emitted is clearly more sensitive to power level and combustor concept than to fuel type. The amount of NO formed is dependent on the time temperature history within the combustor as indicated in Figures 111, 112, 123, 124, 141, and 142 in Appendix B. In this respect the variable geometry combustor exhibits optimum control of the primary zone temperature and produces the least NO. The short prechamber and piloted prechamber combustors both produce about 3 to 4 times the amount of NO as compared with that produced by the variable geometry combustor. Maximum levels of NO emission correspond to about 200 ppm. The low NO emission of the baseline combustor when ERBS and DF-2 are used as fuels reflects poor combustion efficiency, not favorable NO control.

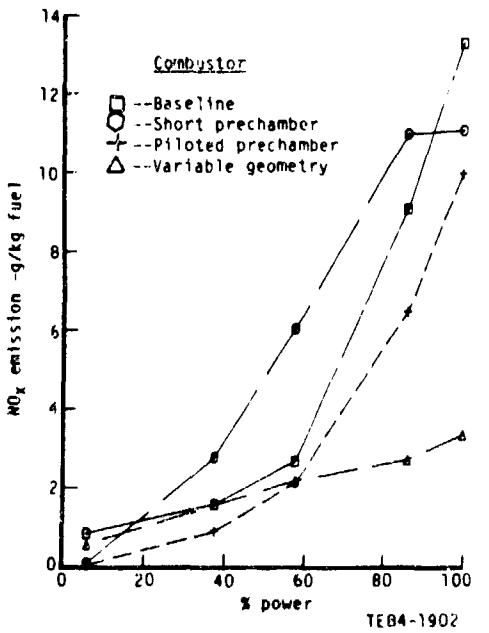

Figure 71. Nitric oxide emission as a function of power level and combustor type--Jet A fuel.

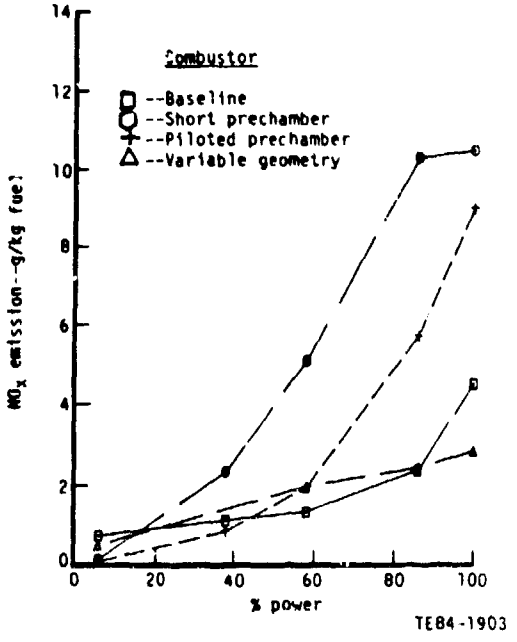

Figure 72. Nitric oxide emission as a function of power level and combustor type--ERBS 12.8 fuel.

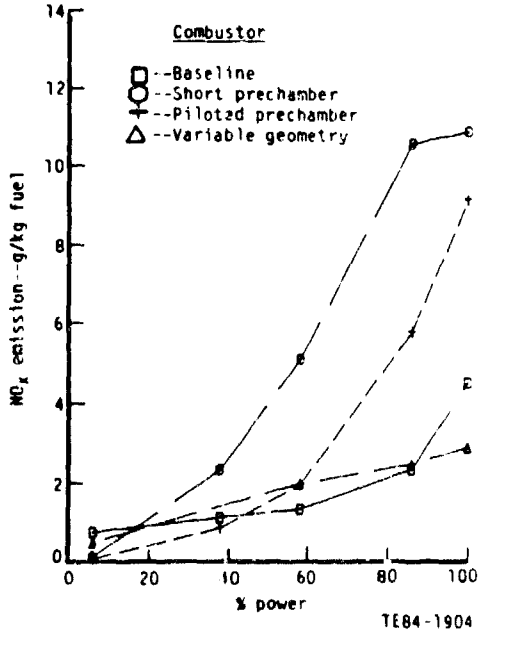

Figure 73. Nitric oxide emission as a function of power level and combustor type ERBS 12.3 fuel.

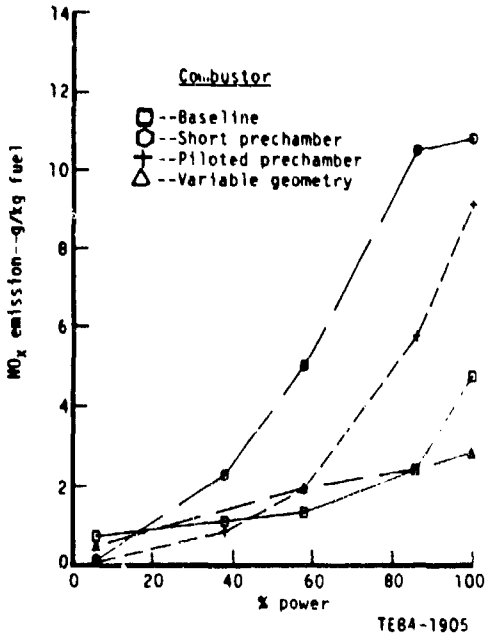

Figure 74. Nitric oxide emission as a function of power level and combustor type--ERBS 11.8 fuel.

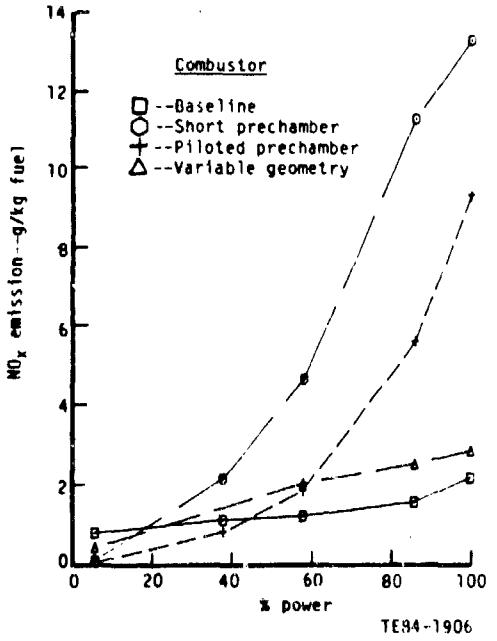

Figure 75. Nitric oxide emission as a function of power level and combustor type--DF-2 fuel.

4.6 SPECIFIC FUEL EFFECTS AS RELATED TO COMBUSTOR CONCEPT AND OPERATING CONDITION

The relationships of the pilot and main SMD, combustion efficiency, and emission indices (except that of smoke) to power level and combustor concept for each fuel type have been determined. These relationships, even though they reflect the tolerance of each combustor concept to the fuel type undergoing reaction within it, are not completely sufficient to permit an analytically determined ranking of the combustor candidates. Other specific fuel effects such as flash point, freezing point, thermal stability, lean-blowout stability, ignition limits, combustor durability, smoke, and pattern factor must also be considered. Some of these effects will be related to the combustor concept while others are physical or thermodynamic characteristics of the fuel type.

4.6.1 Physical and Thermodynamic Fuel Characteristics

Flash Point

The flash point temperature of the five fuels considered in this report are tabulated in Table XXIII of Appendix A. As expected, the flash point temperature for the ERBS blends decreases with increasing aromatic content. The flash point temperatures of Jet A and ERBS 12.8 are identical, ERBS 12.3 is 7°C (13°F) lower, and ERBS 11.8 is 12°C (22°F) lower than Jet A or ERBS 12.8. However, this decrease in flash point temperature, as exhibited by the ERBS blends, is not significantly different to indicate that the fire risks associated with the ERBS blends constitute an unknown, unacceptable hazard. Indeed, as discussed in Appendix A and Ref 19, it is "peculiar that one of the specification limits (flash point) which obviously influences [fuel] availability has so little relevancy in the real world."

Freezing Point

The freeze point temperatures of the ERBS blends are significantly higher than the freeze point temperature of Jet A (Table XXIII, Appendix A). As discussed in Appendix A and Ref 19, the freezing characteristics of the ERBS blends proposed by NASA (those presented in this report) represent extreme cases and could create a severe effect on the whole system of fuel handling.

Thermal Stability

The thermal stability of the five fuels considered in this point are also tabulated in Table XXIII of Appendix A. Fuel thermal stability, as explained in Appendix A, is represented by the JFTOT (ASTM D-3241) procedure. If the fuel is unstable, deposits will form on a heated [260°C (500°F)] tube over which the fuel is pumped. The fuel then flows through a test filter and is returned to its reservoir. Any particulates formed will lead to an increase in pressure drop across the filter. The amount of deposit on the tube can be rated by using a tube deposit rater (TDR) that operates on a light reflectance principle. A set standard is used as a criterion for passing the standard JFTOT test. In addition to the requirement on deposits, the ΔP value across the filter must not exceed 25 torr during the 2-1/2 hr test. By operating at temperatures other than 260°C (500°F), the temperature at which a fuel just fails either of the tests regarding tube deposit amount or filter ΔP may be determined. This temperature is referred to as the "breakpoint temperature" and is used to compare the thermal stability of fuels.

One of the more surprising results of this investigation was the discovery that the ERBS blends exhibited considerable thermal stability when subjected to the JFTOT procedure. Table XXIII indicates that the ERBS 12.8 and 12.3 blends actually exhibited more thermal stability than that of Jet A, while ERBS 11.8 is only slightly less stable, requiring a maximum fuel cooling of 9°C (16°F) to achieve similar thermal stability as Jet A.

In any event the fuel nozzle configurations of the final combustor concepts analyzed in this report would not involve thermal stability considerations. The fuel is rarely heated beyond 121°C to 149°C (250°F to 300°F) prior to actual injection into the combustor during any operating condition.

4.6.2 Lean-Blowout Stability

The poor mixing characteristics of typical pressure-swirl atomizers, such as that used in the baseline combustor, while creating potential performance problems at low power or on alternate fuels, have the advantage of allowing combustion to occur at air/fuel ratios well below the normal weak-extinction limit. Lean-blowout limits in excess of 1000 air/fuel ratio, based on overall combustor values of air and fuel flow rates, used to be commonplace (Ref 9). Poor atomization from typical pressure-swirl atomizers helped widen lean-blowout limits by producing locally fuel rich-rich zones in which the equivalence ratio was considerably above lean-blowout limits. However, the continuing trend toward improved fuel/air mixing prior to combustion (e.g., airblast atomizers and/or prechambers) to reduce the emission levels of NO_x and smoke has led to a narrowing of stability limits and to increasing concern over the attainment of satisfactory lean-blowout performance.

In the design of a gas turbine combustor, steps must be taken to ensure that combustion can be sustained over the entire range of engine operating conditions, including the transient states of rapid acceleration and deceleration. The stability performance of a combustor is usually expressed in the form of a stability plot that separates the regions of stable and unstable combustion. The usual plot has equivalence ratio, or fuel/air ratio, as the ordinate, and a loading parameter, such as air mass flow through the combustor, as the abscissa. The stability performance of an aircraft combustor is obtained by carrying out a series of flame extinction tests at constant, predetermined levels of air temperature and pressure. With the fuel flowing and the mixture ignited, the fuel flow is gradually reduced until flame extinction occurs. This set of conditions is known as a weak-extinction point.

Weak-extinction conditions can be found at airflows, pressures, and temperatures corresponding to various power levels, but those of most interest include ground-idle and altitude-start conditions. In general, the stability limits are, or can be, extended by the following (see Ref 5 and 9):

- o a reduction in the combustor-stream velocity (air mass flow rate)
- o an increase in the inlet temperature
- o an increase in the gas inlet pressure
- o a reduction in the turbulence intensity
- o any change in the equivalence ratio toward unity
- o an increase in the fuel volatility
- o finer atomization, i.e., reduction of the mean drop size
- o the mode of fuel injection
- o design of the primary zone

For homogeneous fuel/air mixtures flame blowout occurs when the rate of heat liberation in the primary zone becomes insufficient to heat the incoming fresh mixture up to the required reaction temperature. With heterogeneous mixtures, however, an additional factor is the time required for fuel evaporation. For fuel sprays of low volatility and large mean drop size this time is relatively long and is, often, the main factor limiting the overall rate of heat release.

For homogeneous mixtures it has been shown that the lean-blowout (LBO) fuel/air ratio (f/a) depends on the inlet air velocity, pressure, and temperature of the combustion zone (Ref 9), as shown in the following:

$$\text{f/a at lean blowout for homogeneous mixture} \propto \left[\frac{\dot{m}_A}{V_{PZ} P_3^n \exp(T_3/b)}\right]^x$$

where

$\dot{m}_A$ = the air mass flow rate within the combustor

V_{PZ} = volume corresponding to the primary combustion zone

P_3^n = inlet air pressure raised to exponent n

T_3 = inlet air temperature

b, x = constants determined by experimental data

If all of the fuel is not fully vaporized, then clearly the "effective" fuel/air ratio will be lower than the nominal value. However, if the fraction of fuel that is vaporized is known, or can be calculated, it can then be combined with the previous equation to yield the fuel/air ratio at lean blowout as follows:

$$\text{f/a at LBO with heterogeneous mixture} = \text{f/a at LBO with homogeneous mixture} \times f_f^{-1}$$

where f_f is the fraction of fuel that is vaporized within the primary combustor zone. Alternate fuels with reduced fuel fluidity and volatility can cause an increase in the fuel flow (hence f/a ratio) required to stabilize the flame within the combustor at any given operating condition.

Following Lefebvre (Ref 9), f_f can be related to the factors governing the rate of evaporation of a fuel spray, as follows:

$$f_f = \frac{8\rho_g V_{PZ} \lambda_{eff}}{f_{PZ} \dot{m}_A D_o^2}$$

where

ρ_g = the gas density

λ_{eff} = the effective evaporation constant, D_o^2/t_e

D_o = the spray SMD

f_{PZ} = the fraction of the total combustor air employed in primary zone combustion

t_e = the total time required to vaporize the fuel droplet

Substituting the relationship for f_f into the equation for $f/a_{LBO/heterogeneous}$, employing the equation of state to eliminate the gas density, as follows:

$$f/a \text{ at LBO with heterogeneous mixture} \propto \left[\frac{f_{PZ}}{V_{PZ}^{(1+x)}}\right] * \left[\frac{\dot{m}_A^{(1+x)}}{F_3^{(1+nx)} \exp\,(xT_3/b)}\right] * \left[\frac{D_o^2}{(\lambda_{eff})(LHV)}\right]$$

where the lower heating value (LHV) of the fuel has also been incorporated. This term arises from the assumption that for any given operating conditions the lean-blowout temperature is the same for all hydrocarbon fuel/air mixtures; this implies that fuels with a high gravimetric heat content should be capable of burning down to weaker fuel/air ratios than fuels having a lower heat content. Available experimental data do not allow the values of n and x to be determined with any degree of accuracy. It can be deduced that the exponents of V_{PZ} and $\dot{m}_A$ should be the same and that the pressure exponent should be somewhat higher by an amount depending on the effective reaction order. What experimental data exist regarding the lean-blowout fuel/air ratio suggest that the pressure exponent is about 30% larger than that of the air mass flow rate and, further, the temperature dependence corresponds to the following relationship:

$$f/a \text{ at LBO} \propto \left[\exp - (T_3/300)\right]$$

Thus, the simplest form in which the lean-blowout fuel/air ratio can be expressed that is consistent with experimental data is the following:

$$f/a \text{ at LBO with heterogeneous mixture} = \left[\frac{C' * f_{PZ}}{V_{PZ}}\right] * \left[\frac{\dot{m}_A}{P_3^{1.3} \exp\,(T_3/300)}\right] * \left[\frac{D_o^2}{\lambda\,\text{eff} * \text{LHV}}\right]$$

where C' is a constant whose value depends on the geometry and mixing characteristics of the combustion zone and is usually determined experimentally.

The first term on the right side of the equation is a function of combustor design. The second term represents the combustor operating conditions, and the third term embodies the relevant fuel-dependent properties. In practice, as the ratio of primary-zone volume to predilution volume tends to be fairly constant, the combustor predilution volume, V_c, is often substituted for V_{PZ}. If the operating conditions, P_3, T_3, and $\dot{m}_A$, are determined by the surrounding environment, then the lean-blowout fuel/air ratio of a given fuel relative to that of Jet A may be determined, for each combustor, by the following equation:

$$\text{BFA}_{(LBO)} = \frac{f/a \text{ LBO Fuel X}}{f/a \text{ LBO Jet A}} = \frac{D_R^2}{\lambda_r * \text{LHR}_r} = \frac{f_{f \text{ Jet A}}}{(f_{f_{\text{Fuel X}}}) * (\text{LHR}_r)}$$

where

$RFA_{(LBO)}$ = the relative lean-blowout fuel/air ratio of fuel x at P_3, T_3, and $\dot{m}_A$ compared with that of Jet A at the same conditions.
D_R = the Sauter mean diameter of the fuel relative to that of Jet A
LHR_r = the lower heating value of the fuel relative to that of Jet A
$\lambda_r = D_r^2 * (t_{Jet\ A}/t_{fuel})$
t = the total time required to evaporate the fuel droplet

Thus, the relative fuel/air ratio at the lean blowout limit can be determined as follows:

$$RFA_{(LBO)} = \frac{D_R^2}{\lambda_r * LHR_r} = \frac{f_{f\ Jet\ A}}{f_{f_{Fuel\ X}} * LHR_r} = \frac{t_{fuel}}{t_{Jet\ A} * LHR_r}$$

and either the fraction of the fuel vaporized within the primary zone or the SMD total evaporation (residence) time may be obtained from STAC-I at P_3, T_3, and $\dot{m}_A$.

Further, if the combustors are generically related as those in this study, then at P_3, T_3, and $\dot{m}_A$ the ratio C'/V_{PZ} may be considered, as a first approximation, to be a constant. This permits the relative fuel/air ratio at lean-blowout of one combustor to be directly compared with that of another combustor, providing the entering temperature, pressure, and airflow rates through the combustors are identical.

$$\frac{RFA_{(LBO)\ Combustor\ 1}}{RFA_{(LBO)\ Combustor\ 2}} = \frac{f_{PZ_1}}{f_{PZ_2}} * \frac{t_{fuel_1}}{t_{fuel_2}} * \frac{t_{Jet\ A_2}}{t_{Jet\ A_1}}$$

This appears to be an appropriate correlating expression as the relative fuel/air ratio at lean-blowout is known to increase with the use of airblast injection, and the fraction of the combustor air in the primary zone increases with the utilization of such injectors. The primary zone air fraction, f_{PZ}, can be estimated by summing the values of WDOTAS, WDOTAF, WDOTRS, WPOTDS, and up to 1/3 of WDOTPJ from Table XIII. However, more appropriate values of f_{PZ} were obtained from STAC-I computer printouts as a considerable amount of recirculated combustion gases are present in the primary zone at ground-idle and altitude-restart conditions. The difference in primary zone combustion gas temperatures among the combustors is reflected in the droplet SMD evaporation (residence) time.

Because this was the first attempt to extend analytical prediction capability with respect to the lean-blowout limit to include both fuel effects and combustor design, only the ground-idle condition has been computed. Altitude-restart analyses indicated that the available pressure differential across the liner was only 0.2 kPa (0.03 lb/in.^{2}, 0.83 in. of water). Under such conditions the single, large airblast injector of these concepts would not be effective and fuel flow to it would be rerouted to the pilot. The initial size of the droplets produced by the pressurized pilot nozzle of these hybrid injected combustors is independent of combustor type but dependent on fuel type, as shown in Figures 22, 28, 34, and 40. However, the subsequent temperature/

time history of the pilot spray evaporation does depend on combustor concept design. The combustors can be qualitatively ranked with respect to the lean-blowout limit at altitude restart conditions by reference to the ground-idle lean-blowout predicted limits.

The lean-blowout relative fuel/air ratio is proportional to either the fraction of the fuel evaporated in the primary zone or, equivalently, the evaporation time of the SMD of the droplet spray. Since the baseline combustor uses a dual orifice injector, while the other concepts use hybrid airblast injectors, it is appropriate to determine whether the pilot nozzle SMD or the main nozzle SMD is the better correlation parameter with respect to the fuel fraction evaporated in the primary zone. The spray from the main nozzle of the baseline's dual-orifice injector barely evaporates at ground-idle conditions, Figures 101, 104, Appendix B. It is not surprising, therefore, that the pilot nozzle SMD is the better correlating parameter for this combustor. Main nozzle spray from the airblast injectors of the other three combustor concepts undergoes considerably more evaporation at ground idle, Figures 113 and 116, Appendix B, for example. Both pilot and main-nozzle SMDs correlated fairly well with fuel fraction evaporated in the primary zone. The pilot SMD, however, was the better correlating parameter across the entire fuel type range. To eliminate confusion, the relative fuel/air ratio at lean-blowout has been correlated directly to fuel fraction evaporated within the primary zone region in Table XVIII.

Note that both idle and altitude lean-blowout and ignition operation with respect to fuel type could be improved by optimal redesign of the injection system. The object of this study, however, was to predict the effects of fuel type on several fixed candidate combustors and to rank those combustor candidates with respect to sensitivity to fuel type.

The dual-orifice injected baseline combustor exhibits more relative sensitivity to fuel type with respect to lean-blowout than do the airblast injected concepts. As expected, the variable geometry combustor exhibits the least relative lean-blowout sensitivity to fuel type. The relative lean-blowout sensitivity to fuel type of the piloted prechamber and short prechamber are both somewhat greater than that of the variable geometry concept and are quite similar. The rankings given do not compare the actual lean-blowout fuel/air ratios of each combustor. Rather the comparison is with respect to the individual combustor's sensitivity to fuel type as compared with its lean-blowout limit using Jet A as the fuel. The combustor concepts can be ranked relative to one another, and fuel type, through the following equation:

$$\frac{RFA_{(LBO)\ \text{Combustor 1}}}{RFA_{(LBO)\ \text{Combustor 2}}} = \frac{f_{PZ_1}}{f_{PZ_2}} * \frac{f_{f_{\text{Jet A}_1}}}{f_{f_{\text{Jet A}_2}}} * \frac{f_{f_{\text{fuel}_2}}}{f_{f_{\text{fuel}_1}}}$$

The lean-blowout stability characteristics of the combustors have been normalized with regard to fuel type in Table XIX. Of the airblast-injected combustor concepts only the variable geometry combustion has lean-blowout stability characteristics similar to that of the baseline combustor. Both the piloted and short prechamber combustors require considerably more fuel to

Table XVIII.
Relative fuel/air lean-blowout limits and relative fuel/air ignition limits-ground idle.

Baseline combustor

	Jet A	ERBS 12.8	DF-2
f_f	0.72	0.58	0.47
LHR_r	1.00	0.974	0.990
$RFA_{(LBO)}$	1.00	1.275	1.547
$f_{PZ\ air}$--%	17.68	17.74	17.71

Short prechamber

	Jet A	ERBS 12.8	DF-2
f_f	0.88	0.77	0.66
LHR_r	1.00	0.974	0.990
$RFA_{(LBO)}$	1.00	1.173	1.347
$f_{PZ\ air}$--%	39.36	40.63	40.81

Piloted prechamber

	Jet A	ERBS 12.8	DF-2
f_f	0.91	0.81	0.71
LHR_r	1.00	0.974	0.990
$RFA_{(LBO)}$	1.00	1.153	1.295
$f_{PZ\ air}$--%	34.56	35.36	35.73

Variable geometry

	Jet A	ERBS 12.8	DF-2
f_f	0.97	0.91	0.83
LHR_r	1.00	0.974	0.990
$RFA_{(LBO)}$	1.00	1.094	1.180
$f_{PZ\ air}$--%	21.98	22.28	22.31

Table XIX.

Normalized relative fuel/air lean-blowout limits and relative fuel/air ignition limits of combustor concept and fuel type-ground idle

2 ↓ \ 1 →		Baseline	Short prechamber	Piloted prechamber	Variable geometry
Baseline	Jet A	1.000	2.226	1.955	1.243
	ERBS 12.8	1.000	2.109	1.804	1.078
	DF-2	1.000	2.006	1.688	0.961
Short prechamber	Jet A	1.000	0.878		0.558
	ERBS 12.8	1.000	0.856		0.511
	DF-2	1.000	0.842		0.479
Piloted prechamber	Jet A		1.000	1.000	0.636
	ERBS 12.8		1.000	1.000	0.598
	DF-2		1.000	1.000	0.569
Variable geometry	Jet A			1.000	1.000
	ERBS 12.8			1.000	1.000
	DF-2			1.000	1.000

sustain combustion than does the baseline combustor. Clearly, with respect to design and actual fuel/air ratio required to sustain combustion, regardless of fuel type, the combustors may be ranked in the following order:

1. baseline
2. variable geometry
3. piloted prechamber
4. short prechamber

A considerable variation in lean-blowout stability occurs between the variable geometry and the remaining two airblast-injected combustor candidates.

The results were obtained using parameters that correlated with the mean droplet residence time of the pilot nozzle spray. This vindicates the choice of the hybrid airblast injector concept for these combustor designs (single, large airblast injector with simplex pilot). Altitude-restart conditions employ only pilot nozzle flow. This implies that the correlations developed for predicting the ground idle relative lean-blowout limits would apply equally well at altitude-restart conditions. The combustion stability characteristics of the combustors at altitude would be expected to be the same as at ground idle. Therefore, the relative ranking of the combustors with regard to lean-blowout stability should not change at conditions other than ground idle.

4.6.3 Ignition-Relight

Detailed experimental studies confirm practical experience in showing that ignition is enhanced by increases in pressure, temperature, and spark energy, and is impeded by increases in velocity and turbulence intensity. Ignition

performance is affected by fuel properties, particularly volatility as it affects evaporation rates, through the way in which they influence the concentration of fuel vapor in the immediate vicinity of the igniter plug. Surface tension and viscosity also are important in the way they affect the mean fuel droplet size. Much of the extra energy required to ignite a heterogeneous mixture is absorbed in the evaporation of fuel droplets, the actual amount depending on the distribution of the fuel throughout the primary zone and the quality of the atomization. In essence, what is done to enhance lean-blowout stability also enhances ignition. Ignition stability plots are similar to those for lean-blowout; the occurrence of ignition, however, requires a higher fuel/air ratio than would be necessary for combustion stability at the same operating conditions. Once the mixture is ignited, the fuel/air ratio may be reduced to just above the lean-limit while still maintaining combustion stability.

It is not surprising, therefore, that when recourse is made to relationships in which the key fuel properties are expressed in values relative to those of a baseline fuel--Jet A in this study, the approach leads to an equation that is nearly identical to that for the lean-blowout fuel/air ratio (Ref 9). The only difference is a higher pressure dependence $P_3^{1.5}$ for the lean-lightup fuel/air ratio versus $P_3^{1.3}$ for the lean-blowout fuel/air ratio. Again, if it is assumed that the combustors are generically related, and that at similar operating conditions, the ratio B/V_{PZ} may be considered to be a constant, the relative fuel/air ratio results for lean-lightup are identical to those for lean blowout. Thus, Tables XVIII and XIX, as indicated, may also be used to correlate ignition characteristics of the combustors and fuels.

4.6.4 Liner Wall Temperature

The liner may be regarded as a container of hot flowing gases surrounded by a casing in which air is flowing in the space between the liner and the casing. The liner is heated by radiation and convection from the hot combusting gases within it and is cooled by radiation to the outer casing and (primarily) by convection to the annulus air. The relative proportions of the hot side radiation and convection components depend on combustor design, operating conditions, and fuel type.

Increased liner wall temperatures can dramatically alter combustor life. The life of conventionally cooled combustor liners is generally limited by cracks in specific seam welds caused by low-cycle fatigue. Low-cycle fatigue results from cyclic expansion and contraction of the combustor liner during engine operation. Increased liner wall temperatures can increase the thermal gradient in critical areas of the combustor and cause higher stresses in seam welds and increased sensitivity to low-cycle fatigue. At high-power operating conditions the stress concentrations in the vicinity of seam welds can be well above the yield strength of the material causing plastic deformation with each cycle. Differences of as little as 11°C (6°F) increase in wall temperature have been reported to decrease combustor life by approximately 10%-30% depending on combustor design (Papers 4, 5, and 7 of Ref 19).

High power operating condition liner wall temperature effects due to fuel type appear to be fairly well characterized by fuel hydrogen content. As fuel

hydrogen content is reduced, soot formation is increased. Increased soot formation leads to higher flame emissivity within the combustor and increased smoke emissions at the combustor exit. Internal radiation from the hot gases depends on the temperatures and emissivities of the hot combustion gases and of the inner surface of the combustor liner. The liner temperature increases observed with reduced fuel hydrogen content are almost totally attributed to increased internal radiation, primarily due to increased flame emissivity. Internal radiation heat transfer can be reduced by reducing the emissivity or temperature of the combustion gases, by increasing the liner surface temperature (undesirable), or by reducing the liner absorptivity. Liner wall temperatures, then, can be reduced by reducing the emissivity of the combustion gas and/or a mechanical change enhancing the effectiveness of the wall cooling. Ceramic thermal barrier coatings have also been used in the inner surface of the liner wall to reduce metal temperatures.

Soot formation and increased flame radiation are closely related. Soot formation in the primary zone is determined to a large extent by combustor design, i.e., the stoichiometry and mixedness of the primary zone; however, fuel properties can play an important role. A number of authors have conducted a series of experimental combustor studies to determine which fuel properties, physical and chemical, are important to soot formation, and, hence, increased flame emissivity, in gas turbine combustors (Papers 5-8, Ref 19). Despite the apparent influence of hydrocarbon type (especially differences between 1-ring, 2-ring, and 3-ring aromatics), the effects of fuels tested to date appear to correlate most satisfactorily with hydrogen content. Hydrogen content and aromatic content appear to be of equal value as correlating parameters for increased flame radiation, while ring carbon appears to be a relatively poor correlating parameter. This suggests that the aromatic ring structure itself is not of great importance, and that aromatic content correlates the data well only because of the lower hydrogen content of the aromatic molecules (Paper 7 of Ref 19). This same study suggested that polycyclic aromatics such as tetralins and naphthalenes might not follow such a simple hydrogen correlation. Test evidence indicated that fuels containing significant amounts of polynuclear aromatics (> 5% by vol) can produce more soot than their hydrogen content would predict, but that the increase is dependent on the combustor design and operating conditions. Combustor design and operating condition can become of significant importance when burning ERBS blends that contain significant amounts (> 10% by vol) of naphthalenes. Alternatively, if reduced hydrogen content is desired, it may still be reasonable to restrict the amount of naphthalenes within the fuel.

No attempt was made to predict the liner wall temperature as a function of fuel type for the different combustors being considered in this report. Heat transfer models considering the effect of fuel composition, based on the simple methods of Kretschemer and Odgers (Ref 21), have been developed by those authors in Paper 8 of Ref 19 and by Lefebvre (Ref 9). In each case, the luminosity factor, L, an empirical correction to the flame emissivity, must be introduced to obtain reasonable agreement between experimental data on gas radiation and prediction. In the absence of experimental data a relationship for L has been developed that is related to fuel hydrogen content. But this relationship should only be applied to combustors in which the primary zone equivalence ratio is near unity and the flow field in that region has been established by a pressure fed atomizer.

The use of such a model yields results for standard type combustors that are in good agreement with the correlation obtained by Blazowski and Jackson (Ref 22 and 23) between hydrogen content and liner wall temperature for several engines. The predicted mean effects on wall temperatures in the recirculation zone are presented in Figure 76*. The effects are expressed in the dimensionless form used by Blazowski, where T_{LO} is the wall temperature resulting from using a fuel containing a standard amount of hydrogen (usually a hypothetical baseline fuel, H% = 14.5). The magnitude of the effects due to hydrogen content is most significant when the emissivity is low, such as at low pressures. The data shown in Figure 77 represent cruise conditions with combustor inlet temperatures ranging from 274°C (525°F) to 463°C (865°F). The shaded zone represents primary zone predictions for these cruise conditions. Again, good agreement between experimental data and predicted results, in terms of the Blazowski parameter, is attained for these standard type combustors.

Data for a more modern combustor, the F101, are plotted in Figure 78. The engine data points lie below the general scatter of the previous engines and also below the predicted values at the engine operating conditions. The F101 uses an airblast injected combustor and, as is the case for the airblast injected combustor candidates in this report, the primary zone established within the F101 combustor is leaner and more uniform compared with the primary zone produced by pressure fed atomizers. The emissivity of the combustion gas

*Figures 76, 77, and 78 are from Paper 8, Ref 19.

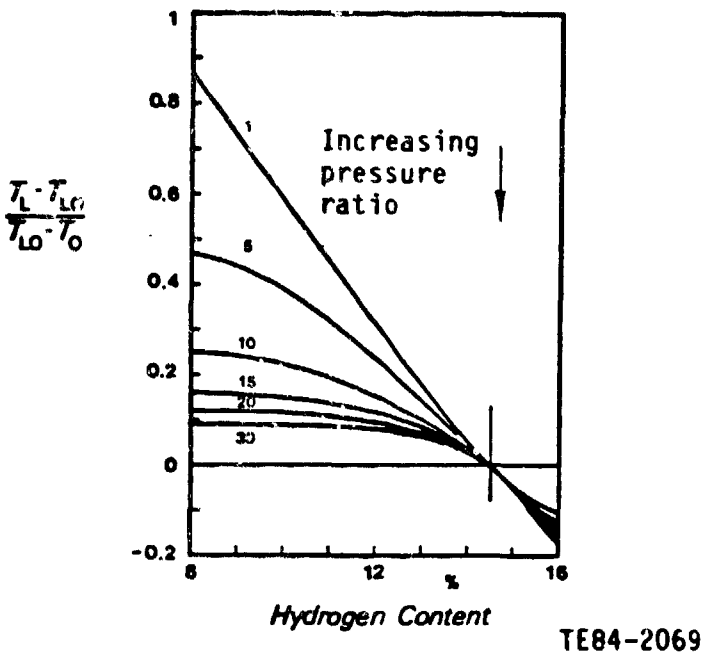

Figure 77. Predicted changes in combustor wall temperatures in the recirculation zone due to pressure ratio and fuel composition.

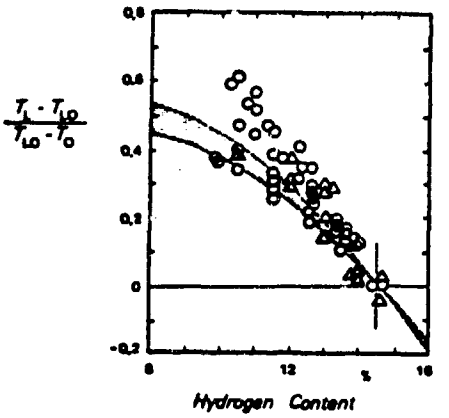

Triangles: J79
Circles: T56, J79, JT8D, CJ805, J57

Shaded zone: Primary zone predictions

TE84-2190

Figure 77. Effect of fuel composition on wall temperature.

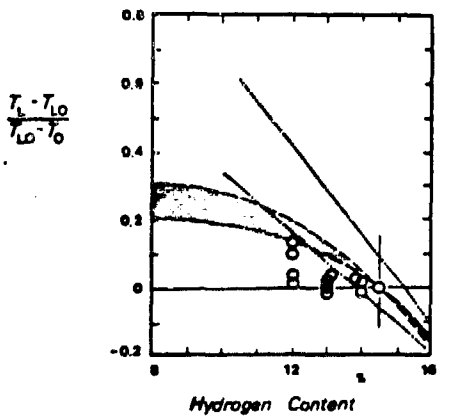

F101
Dotted lines are limits of units from Figure 77
Shaded zone: Primary zone predictions

TE84-2191

Figure 78. Effect of fuel composition on combustor wall temperatures.

has, consequently, been reduced through combustor design; soot formation in the primary zone has been reduced due to decreased stoichiometry and increased mixedness. The use of a model employing an empirical relation for the flame luminosity factor that does not consider combustor design and operating conditions should not be applied to more modern combustors. Additional work remains to generalize the relationships governing the flame luminosity factor, L, if it is to be retained as a generalized correlating parameter for determining liner wall temperatures.

The trends depicted in Figures 77 and 78 do, however, allow some generalizations concerning the sensitivity of the liner wall temperatures of the combustor candidates to fuel type. The increase in liner wall temperature for the three airblast injected combustors will be considerably less than that of the baseline combustor as the fuel hydrogen content is reduced Assuming that the fuel-air mixture within the primary zone of each of the airblast injected combustors is well mixed, the combustion gas emissivity (and, hence, total radiation) will then be proportional only to the combustion gas temperature. The predicted combustion gas temperatures at maximum power (Jet A and DF-2) for the individual combustors are presented in Figures 108, 111, 120, 123, 138, and 141 of Appendix B. The combustion gas temperature is lowest for the variable geometry combustor and increases with the use of the piloted prechamber and short prechamber combustors, respectively.

Further, even if the assumption were made that the liner wall temperature increase of these combustors followed the model prediction, a change of fuel from Jet A to ERBS 11.8 would cause a 38°C (100°F) change in combustor hot spot temperature. This calculation was based on an allowable hot spot temperature of 899°C (1650°F) on Jet A and no enhancement in liner cooling. The airblast-injected combustor liners are, however, fabricated from Lamilloy. The transpiration cooling effectiveness of this cooling technique has been shown to reduce the liner wall temperature by more than 38°C (100°F) on Jet A fuel. This computation was performed for the specified amount of cooling as presented in Table XIII. Consequently, no adverse liner temperature effects would be expected for any of these combustor candidates.

With respect to design and liner wall temperature sensitivity to fuel type. the combustors may be ranked in the following order as a function of their internal gas temperature and mixedness:

1. variable geometry
2. piloted prechamber
3. short prechamber
4. baseline

4.6.5 Smoke

Exhaust smoke is caused by the production of finely divided soot particles in fuel-rich regions of the flame and may be generated in any part of the combustion zone where mixing is inadequate. Most of the soot produced in the primary zone is consumed in the high temperature regions downstream. The rate of soot formation is governed by conditions within the primary zone, while the rate of soot consumption is determined by the post-primary and, in modern high temperature engines, the dilution zone also. The soot concentration observed in the exhaust gases is an indication of the dominance of one zone over the other.

Soot is not an equilibrium product of gas turbine combustion, and it is, to date, not possible to predict its rate of formation and final concentration from kinetic or thermodynamic data. The rate of soot formation tends to be governed more by the physical processes of atomization and fuel/air mixing than by kinetics.

Although a number of specific mechanistic models for soot formation have been proposed, the exact mechanism is not understood. It is generally believed that condensed ring aromatic hydrocarbons may produce soot through a different mechanism than do aliphatic hydrocarbons. Both types of hydrocarbons may produce soot through a fragmentation/polymerization route but aromatic hydrocarbons can also produce soot through a condensation of the aromatic rings into a graphitelike structure. This latter route is believed to be faster than the fragmentation/polymerization route so that during the fuel-rich combustion of a fuel blend composed of aromatics and aliphatics, the aromatic hydrocarbons would produce the major quantity of soot. Experimental data obtained by Blazowski (Ref 24) using various blends of iso-octane and toulene fuels were found to be consistent with this model. The results reported in Paper 7 of Ref 19 indicates that the actual mechanism is considerably more complicated for fuels containing appreciable amounts of polycyclic aromatics, such as tetralins and naphthalenes. These fuels, depending on combustor design and operating conditions, can produce more soot than their hydrogen content would predict.

Lefebvre (Ref 9) indicates that the controlling factors for soot formation and, hence, smoke from gas turbines have been determined to be fuel properties, combustion pressure and temperature, fuel/air ratio, atomization quality, and the mode of fuel injection.

The influence of fuel properties on smoke production are through the inducement of formation of local highly fuel-rich regions and the variable resistance to carbon formation as exhibited by different fuel types. Formation of fuel-rich regions is controlled by physical properties such as viscosity and volatility, which affect the mean drop size, penetration, and rate of evaporation of the fuel spray. The resistance to carbon formation relates to molecular structure, and the relationships of soot formation to hydrogen content, aromatics, polycyclic aromatics, etc, have already been discussed.

Problems of soot and smoke are always more severe at high pressures. The reasons for this derive both from chemical effects and physical factors, which affect spray characteristics and the distribution of fuel/air within the soot-generating regions of the flame. Increased pressure extends the limits of flammability, so that soot is produced in regions that, at lower pressures, would be too rich to burn. An increase in pressure also accelerates chemical reaction rates, so that combustion is initiated earlier and a larger proportion of the fuel is burned in fuel-rich regions adjacent to the spray. Increased pressure primarily affects spray characteristics from pressure fed atomizers, tending to reduce spray penetration and concentrating the fuel in soot-forming regions just downstream of the nozzle. An additional adverse effect of an increase in pressure is a reduction in the cone angle of the spray. This increases soot formation both by increasing the mean drop size and, again, raising the fuel concentration in soot-forming regions close to the spray nozzle. The production of soot from airblast atomizers is less dependent on

pressure because the atomized spray from such injectors is always airborne. The distribution of the spray droplets throughout the combustion zone is dictated by the liner airflow pattern, which is not as susceptible to changes in pressure.

The effect of changes in combustor inlet temperature on soot formation is not entirely clear. Changes in this parameter influence many variables that relate to the soot formation process. On the other hand an increase in combustor outlet temperature reduces smoke by extending the soot oxidation region further downstream into the dilution zone where additional oxygen exists.

Because soot is formed only in fuel-rich regions of the combustors, soot and smoke can be eliminated by limiting the local equivalence ratio in the primary zone to around 1.3. The superior performance of airblast atomizers with respect to low soot formation is due both to better atomization and to the thorough fuel/air mixing incurred in the atomization process prior to combustion. This effectively eliminates fuel-rich pockets from the combustion zone.

Lefebvre also attempted in Ref 9 to develop a generalized correlation for the soot formation and oxidation processes. The difference between the two would allow prediction of the combustor outlet soot concentration. This value can then be related to smoke number. The expressions for the correlations involve pressure, airflow rate, primary zone fuel/air ratio, temperature, and air fraction, post-primary zone fuel/air ratio and temperature, and fuel aromatic or hydrogen content. Although the correlations predicted the influence of combustor operating conditions on smoke output, and demonstrated that soot concentrations rise with increase in aromatic content of the fuel, they also showed that the extent of this increase varied from one combustor to another in a manner that cannot be predicted a priori. The correlations offered no guidance on the likely smoke emissions to be anticipated from any new type of combustor. Lefebvre concluded that the correlations failed to take into account one or more processes important to soot formation. One obvious omission is a term to describe the degree of mixing of fuel and air (such as from an airblast injector) prior to combustion.

Following Lefebvre's conclusion (Ref 9) that little improvement in the prediction of smoke emission can be expected until more quantitative information is available on the influences of fuel/air preparation and fuel chemistry on soot formation, no attempt was made to predict the soot emission index (or smoke number) as a function of fuel type for the different combustors being considered in this report. However, as soot formation and flame radiation are interrelated, as described in the previous section, the trends summarized in that section can be expected to apply for smoke emission levels also. Thus, the smoke number of the exhaust from the three airblast injected combustors will be considerably less than that from the baseline combustor as the fuel hydrogen content is reduced. With respect to design and soot formation sensitivity to fuel type, the combustors can again be ranked as a function of their internal gas temperature and mixedness. This order is the same as that found for liner wall temperature sensitivity.

4.6.6 Pattern Factor

One of the most important and difficult problems in the design and development of gas turbine combustion chambers is achieving a satisfactory and consistent

distribution of temperature in the exhaust gases discharging into the turbine. It is generally accepted that a satisfactory temperature profile is dependent on adequate penetration of the dilution jets in the combustor and the presence of the proper number of such jets to form sufficient localized mixing regions. However, the manner in which the total dilution hole area is utilized in terms of number and size of holes is still largely a matter of experience.

If only the final mixing process is considered, the temperature and composition of an elemental volume of gas is affected in a complicated manner by the dimensions, geometry, and pressure drop of the liner, the size, shape, and discharge coefficients of the liner holes, the airflow distribution to various zones of the chamber, and the temperature distribution of the hot gases entering the dilution zone. For any given combustor, the latter is strongly influenced by fuel spray characteristics such as drop size, cone angle, and penetration. These control the pattern of burning and, hence, the distribution of temperature in the primary-zone efflux (Ref 9). The mode of fuel/air preparation, therefore, can be of paramount importance in determining the effectiveness of subsequent dilution zone mixing and the resulting temperature profile of the gases entering the turbine.

The most important temperature parameters are those that affect the power output of the engine and the life and durability of the downstream hot sections. The temperature parameter best reflecting the overall engine performance is the burner outlet, or alternatively, the turbine inlet temperature, T_4, which is the mass flow weighted mean of the combustor exit temperature. Since the nozzle guide vanes are fixed relative to the combustor, they must be designed to withstand the maximum temperature measured in a burner outlet temperature survey, or traverse. The parameter of most relevance to nozzle guide vane design is the overall temperature distribution factor, which highlights this maximum temperature. It is defined as

$$\text{Pattern Factor} = \frac{T_{max}-T_4}{T_4-T_3}$$

where

T_{max} = the maximum recorded temperature in the exhaust gas survey
T_3 = the mean inlet air temperature
T_4 = the mean exit temperature of the combustion gases

The pattern factor (PF) depends at least on liner length, which controls the time and distance available for mixing, and the pressure drop across the liner, which governs the penetration of the dilution jets and their rate of mixing with the products of combustion. Lefebvre (Ref 4), from an analysis of experimental data on tubular combustors, developed the following correlation for pattern factor:

$$PF = \frac{T_{max}-T_4}{T_4-T_3} = 1-\exp\left[-Q * \frac{\Delta P_L}{q_{ref}} * \frac{L_L-L_e}{D_L}\right]^{-1}$$

where

$\frac{\Delta P_L}{q_{ref}}$ = the liner pressure loss factor
L_L = the total liner length
D_L = the liner diameter
L_e = the liner length required to evaporate the fuel spray
Q = a constant of proportionality for the liner type

Lefebvre used correlating parameters to estimate L_e and found that Q is a slowly varying function of tubular (can) combustor type. For the purposes of this report L_e will be computed directly from the results of STAC-I. Paper 5 of Ref 19 found that trends obtained in pattern factor variations with fuel properties correlated with a vaporization index of the fuel in which the 90% recovery temperature of the fuel was used in determining the relative droplet size and mass-transfer number. Processes within the combustor that would tend to influence droplet size, penetration, and vaporization, all of which subsequently impact the pattern factor, were considered more dependent on the final stages of droplet life than on the initial stages.

Lefebvre, on the other hand, used a correlating parameter (for L_e) that involves the length to vaporize the Sauter mean diameter of the main spray flow. These approaches are not entirely inconsistent. STAC-I results indicate that at the lengths required to vaporize the SMD of the main spray at maximum power (Figures 95, 98, 107, 110, 119, 122, 137, and 140 in Appendix B), 80% to 85% of the total spray mass evaporated, regardless of fuel type or combustor concept.

Following the type of procedure used in determining relative lean-blowout and ignition limits, the combustors can be considered to be generically related such that Q can be assumed, as a first approximation, to be little different for the various combustor concepts considered in this report. Using known values for the liner pressure loss factor, L_L [304.8 mm (12 in.)], D_L [151.38 mm (5.960 in.)], and L_e from the appropriate combustion chamber, the relative pattern factor of one combustor can be directly compared with that of another using the same or different fuel type. A value of Q was determined and held constant during the comparisons. The pattern factor for the baseline combustor using Jet A is known to be 0.23, which when combined with the equations for the pattern factor utilizing a liner pressure loss factor of 21.1, and L_e equal to 109 mm (4.3 in.) (Figure 95, Appendix B), yielded a value of 0.140 for Q.

Thus

$$PF = 1 - \frac{1}{\exp\left[\frac{q_{ref}}{Q} * D_L * \frac{1}{\Delta P_L * (L_L - L_e)}\right]}$$

$$= 1 - \frac{1}{\exp\left[6.569 * \frac{1}{\Delta P_L * (L_L - L_e)}\right]}$$

and the relative pattern factor (RPF) can be computed as

$$RPF\ \frac{\text{combustor 1 or fuel 1}}{\text{combustor 2 or fuel 2}} = \frac{1 - \dfrac{1}{\exp\left[6.569 * \dfrac{1}{\Delta P_L * (L_L - L_e)}\right]_1}}{1 - \dfrac{1}{\exp\left[6.569 * \dfrac{1}{\Delta P_L * (L_L - L_e)}\right]_2}}$$

Smaller values of the pattern factor, or relative pattern factor, reflect more uniformity in the exhaust gases. The relative pattern factors as a function of fuel type and combustor concept are tabulated in Tables XX and XXI.

The dual orifice injected baseline combustor exhibits more relative sensitivity to fuel type with respect to pattern factor than do the airblast injected concepts. Obviously, the pattern factor improves with increasing engine power level due to the reduction in droplet evaporation time and, hence, L_e. This phenomenon is verified by actual engine data (Ref 9). However, decreasing power levels, down to about 35% of maximum power, do not necessarily result in operating conditions where the evaporation time constitutes a significant proportion of the total residence time. For the airblast-injected combustor concepts the evaporation time is not a significant fraction of the total combustor residence time, regardless of fuel type, for power levels above 35% of maximum. The length required for vaporization, L_e, does not substantially differ with power except at idle conditions. There the evaporation time does constitute a significant portion of the total residence time, and a strong effect of combustor concepts and fuel type on pattern factor can be expected.

The influence of fuel type on pattern factor is manifested through the effects of mean drop size (viscosity and surface tension effects) and the rate of droplet evaporation (volatility as correlated to fuel normal boiling temperature, as an example). Over the range of fuels examined the effect of fuel type on pattern factor is relatively small, at least for the airblast-injected concepts at the higher power levels. The high power conditions are where pattern factor is most important to engine durability, and fortunately at these conditions, variation in fuel type has a nearly negligible effect. The combustor concepts can be ranked relative to one another, and fuel type, as tabulated in Table XXI.

All of the airblast injected combustor concepts have a lower pattern factor than the baseline combustor. This decrease is more pronounced as the fuel type is varied with increasing viscosity (Jet A to DF-2) reflecting the sensitivity of the dual-orifice pressurized atomizers to increasing fuel viscosity. The short prechamber and piloted prechamber exhibit the lowest predicted pattern factor. The sensitivity of these two combustors with respect to both pattern factor magnitude and variation with fuel type is nearly identical. The variable geometry combustor exhibits the same relative insensitivity of pattern factor to fuel type but the magnitude of the pattern factor is predicted to be slightly larger. Physically, this is partly due to the decreased liner pressure drop predicted for the variable geometry combustor at maximum power. However, the correlating equation for predicting the pattern factor

Table XX.

Relative pattern factor as a function of fuel type at maximum power.

Baseline combustor

	Jet A	ERBS 12.8	DF-2
L_e--in.	4.3	5.8	7.2
L_L-L_e--in.	7.7	6.2	4.8
ΔP_L--lb/in.^{2}	3.255	3.255	3.255
PF	0.230	0.277	0.342
RPF	1.0	1.205	1.489

Short prechamber

	Jet A	ERBS 12.8	DF-2
L_e--in.	0.8	1.2	1.5
L_L-L_e--in.	11.2	10.8	10.5
ΔP_L--lb/in.^{2}	3.248	3.248	3.248
PF	0.158	0.171	0.176
RPF	1.0	1.082	1.112

Piloted prechamber

	Jet A	ERBS 12.8	DF-2
L_e--in.	2.2	2.3	2.4
L_L-L_e--in.	9.8	9.7	9.6
ΔP_L--lb/in.^{2}	3.658	3.658	3.658
PF	0.167	0.169	0.170
RPF	1.0	1.009	1.019

Variable geometry

	Jet A	ERBS 12.8	DF-2
L_e--in.	1.0	1.5	2.2
L_L-L_e--in.	11.0	10.5	9.8
ΔP_L--lb/in.^{2}	2.304	2.304	2.304
PF	0.228	0.237	0.252
RPF	1.0	1.041	1.106

Table XXI.

Normalized relative pattern factor as a function of both combustor concept and fuel type at maximum power.

2↓ \ 1→		Baseline	Short prechamber	Piloted prechamber	Variable geometry
Baseline	Jet A	1.000	0.687	0.726	0.991
	ERBS 12.8	1.000	0.617	0.610	0.856
	DF-2	1.000	0.515	0.497	0.737
Short prechamber	Jet A	1.000	1.057	1.443	
	ERBS 12.8	1.000	0.988	1.386	
	DF-2	1.000	0.966	1.432	
Piloted prechamber	Jet A		1.000	1.365	
	ERBS 12.8		1.000	1.403	
	DF-2		1.000	1.482	
Variable geometry	Jet A			1.000	
	ERBS 12.8			1.000	
	DF-2			1.000	

may not be entirely applicable to variable geometry combustors in which 30% or more of the entire airflow enters forward of the primary zone. In such cases the uniformity of the primary-zone efflux may be more important than liner dilution zone pressure drop or liner length. The pattern factor of this combustor may be as good as that predicted for the other two airblast-injected concepts.

With respect to design and predicted pattern factor, regardless of fuel type, the combustors may be ranked in the following order:

1. piloted prechamber
2. short prechamber
3. variable geometry
4. baseline

No clear-cut distinction exists between the first two combustor concepts; both have equally good pattern factors. The variable geometry combustor is predicted to have a slightly poorer pattern factor compared with the former two combustors, but the pattern factor for this combustor is still highly acceptable (< 0.255 for DF-2 fuel). And because of some doubt as to the applicability of the correlating equation for pattern factor to the variable geometry combustor, it may rank as well as the first two combustors. The baseline combustor is clearly inferior compared with the airblast injected combustor concepts, particularly with respect to pattern factor sensitivity to fuel type.

V. REVIEW OF RESULTS AND CONCLUSIONS

5.1 GENERAL FUEL-COMBUSTOR INTERACTION EFFECTS

Analysis of the processes occurring within gas turbine combustor indicates that although the impact of fuel type on combustion performance and liner durability is usually small in comparison with the effects of combustor concept, liner geometry, and combustor operating conditions, it is nevertheless of sufficient magnitude to warrant serious consideration. Essentially the most important factors governing liner durability and combustion performance are combustor concept (liner size, liner pressure drop, fuel-air injection mode), and combustor operating conditions. Fuel effects tend to play a secondary role, particularly for advanced combustor concepts. However, in modern engines the combustor must perform satisfactorily for long periods at extreme conditions even on current fuels. Any factor, however, secondary, that creates a more adverse combustor environment, can have a large, disproportionate effect on combustion performance and liner durability.

In general fuel property effects on various combustor concepts can be classified as chemical or physical in nature. Predictions from STAC-I and correlations indicate that fuel chemistry, as delineated primarily by hydrogen content, has a significant effect on flame radiation, liner wall temperature, and smoke emissions.

Fuel physical properties that govern atomization quality and evaporation rates are predicted to affect ignition characteristics, lean-blowout limits, combustion efficiency, unburned hydrocarbon, and carbon monoxide emissions. Just as these parameters, and nitric oxide emissions, are predicted to be nearly unaffected by fuel chemistry, flame radiation, liner wall temperature, smoke emissions, and even nitric oxide emission are predicted to be sensible independent of physical properties. Nitric oxide emission is important only at high power levels and neither fuel chemical nor fuel physical properties have significant effects on NO_x formation in this regime. Nitric oxide formation is predicted to be dependent primarily on the combustion gas temperature and available oxygen concentration.

Fuel chemistry also is predicted to have no direct influence on pattern factor. Physical properties affect the pattern factor at low power through decreased evaporation of the spray. The importance of the effects of this physical property diminish with engine power becoming very small at the highest power setting where the effect of pattern factor on engine life is most significant.

Finally, STAC-I predicted results clearly indicate that any deteriorated performance characteristics of the ERBS fuels and DF-2, as compared with Jet A, are primarily due to the physical properties of the fuels as they affect atomization. This is particularly true for the dual orifice injected baseline combustor. The maximum power operating conditions were recalculated for each combustor concept and each fuel type using the same SMDs as those predicted for Jet A. The deteriorated baseline combustor performance of the ERBS fuels and DF-2 was restored to nearly the level attained when Jet A was used as the fuel. The thermodynamic properties of the fuels, therefore, have little effect on performance; however, the physical properties, viscosity, surface tension, and liquid density, as they affect the atomization process, also determine the level of performance.

As expected, the remaining combustor candidates which employ hybrid airblast atomization are predicted to be less sensitive to the properties of alternate fuel type, and performance deterioration can be nearly negligible.

5.2 GENERAL FUEL EFFECTS

Some of the physical and thermodynamic fuel properties can be characteristics solely of the fuel type. Among such phenomena are flash point, freezing point, and thermal stability.

5.2.1 Flash Point

The flash point temperatures of Jet A and ERBS 12.8 are identical, ERBS 12.3 is 7°C (13°F) lower, while ERBS 11.8 is 12°C (22°F) lower than Jet A. This decrease in flash point temperature, as exhibited by the ERBS blends, is not significantly different to indicate that the fire risks associated with the ERBS blends constitute an unknown, unacceptable hazard.

5.2.2 Freezing Point

The freezing characteristics of the ERBS blends proposed by NASA represent extreme cases and could create a severe effect on the whole system of fuel handling.

5.2.3 Thermal Stability

The ERBS blends exhibited considerable thermal stability when subjected to the JFTOT procedure. The ERBS 12.8 and 12.3 blends actually exhibited more thermal stability than that of Jet A, while ERBS 11.8 was only slightly less stable, requiring a maximum fuel cooling of 9°C (16°F) to achieve similar thermal stability as that of Jet A fuel.

5.3 PARAMETER VARIATION AND SPECIFIC FUEL EFFECTS AS RELATED TO COMBUSTOR CONCEPT AND OPERATING CONDITION

The four final combustor candidates selected for detailed analysis in this study included: the current production, dual-orifice injected baseline 250-C30 combustor, two baseline modifications, a short prechamber and a piloted prechamber combustor, representing a second level of technology, and a fourth combustor, with variable geometry, that reflected a third or higher level of technology. These latter three combustors were all hybrid airblast injected (airblast with simplex pilot).

It should be kept in mind that individual combustor concept operation with respect to fuel type could have been improved by optimal redesign of the injection system. The object of this study, however, was to predict the effects of fuel type on several fixed candidate combustors and to rank those combustor candidates with respect to their sensitivity to fuel type. Consequently, the dual-orifice injector in the baseline combustor was identical to that in a 250-C30 engine and remained unchanged as fuel type was varied. The airblast atomizers for the remaining three combustor candidates were designed to give good performance on Jet A and their geometry was then "standardized." Subsequent predicted assessment of the atomization characteristics of these airblast injectors, using broad-specification fuels, is a direct indication of the tolerance of the injector/combustor concept to fuel type usage.

5.3.1 Pilot Nozzle Fuel Spray SMD

Pilot nozzle fuel spray SMD was not a function of combustor concept because the geometry and pilot fuel flow through the simplex tip of the pilot nozzle was fixed for each fuel. The resulting pilot nozzle fuel spray SMD decreased with increasing power level (larger ΔP across the simplex tip) and increased with increasing fuel viscosity and surface tension. The SMDs for the ERBS fuel were predicted to be approximately 19% larger than those for Jet A. Pilot nozzles were added to the airblast injectors to enhance their ignition and lean-blowout stability characteristics.

5.3.2 Main Nozzle Fuel Spray SMD

At all but the ground idle condition the smallest, predicted SMD was obtained using the piloted prechamber combustor (because of its use of secondary re-atomization) followed in order by the short prechamber, variable geometry, and baseline combustors. The large difference between the predicted baseline combustor produced SMDs and those from the other combustors reflects the change from dual orifice to airblast fuel injection. Further, the predicted drop size variation between fuels was minimized using airblast injection concepts.

5.3.3 Combustion Efficiency

The combustion efficiency increases with increasing inlet pressure and temperature (particularly as they affect the combustion gas temperature), combustor volume, and with decreasing airflow rate (both of the latter trends increase droplet residence time). Combustion efficiency is primarily affected by physical properties as they govern the mean drop size and spray evaporation rate. Consequently, the predicted combustion efficiency at power levels above ground idle is essentially independent of combustor concept for those combustors with airblast injection. The usage of broad-property fuels, such as the ERBS blends, require airblast injection concepts to achieve predicted, acceptable performance efficiency even at increased power levels. Regardless of fuel type, the variable geometry combustor, with optimized radial swirler inlet adjustments, would have the highest predicted combustion efficiency throughout the power range, followed closely by the short prechamber and piloted prechamber concepts. The predicted difference in combustion efficiency above ground idle is, however, nearly negligible among the three combustors. The combustion efficiency of the baseline combustor using the broad-property fuels is predicted to be so low that it is an unacceptable candidate.

5.3.4 Unburned Hydrocarbon and Carbon Monoxide Emissions

In general, the emissions of UHC and CO parallel one another. The resulting oxidation of UHC to water and CO (or CO_2) and the further oxidation of CO to CO_2 depends on the subsequent time-temperature history of the molecules within the combustor.

Predicted unburned hydrocarbon emissions are nearly eliminated through the use of airblast injection concepts. Some minor predicted levels of UHC emissions exist at the ground idle power level when the ERBS blends are used as the combustor fuel. Again, the predicted difference between the airblast injected combustor concepts is nearly negligible but the variable geometry concept appears to be the most optimum combustor type closely followed by the short and piloted prechamber concepts.

CO production is larger at the lower power levels where an appreciable portion of the total residence time in the combustion zone is occupied by the evaporation process. The influence of the fuel physical properties become important as they control the mean drop size, the spray evaporation rate, and the time-temperature evolution of the combustion gas temperature that controls the subsequent chemical-kinetic rate of oxidation of CO to CO_2. CO emission from the ERBS blends is predicted to be considerably greater than that produced when Jet A is used as the combustor fuel at these power levels. Again, airblast fuel injection is required to lower the CO emission to an acceptable level. Combustor concept is more important for CO emission control at the lower power levels than it was for UHC emissions. The ranking of the combustors with regard to CO emission control is predicted to be the same as that for UHC emission control. This clearly reflects the increased low-power combustion gas temperature produced by the variable geometry combustor.

5.3.5 Nitric Oxide Emission

The quantity of NO formed and emitted is predicted to be more sensitive to power level and combustor concept than to fuel type. The optimum combustor would be one that achieves high combustion efficiency throughout its power range without producing the high primary zone temperatures that result in large quantities of NO formation. In this respect the variable geometry combustor exhibits optimum predicted control of the primary zone temperature and produces the least NO. The short prechamber and piloted prechamber combustors are both predicted to produce 3-4 times the amount of NO as compared with that produced by the variable geometry combustor.

5.3.6 Lean-Blowout Stability and Ignition

In general, both the stability and ignition limits are, or can be, extended by an increase in inlet pressure and temperature, and reduction in the air mass loading and turbulent intensity. The latter effect local changes in the equivalence ratio and any change in equivalence ratio toward unity enhances lean-blowout stability and ignition.

Lean-blowout stability and ignition characteristics are very dependent on the fuel physical properties that control fuel volatility and atomization. Fuel sprays of low volatility and large mean droplet size have relatively long times required for fuel evaporation and this time is often the main factor limiting the overall rate of heat release. Consequently, the mode of fuel injection and design of the primary zone (increased size, equivalence ratio) are of prime importance in determining lean blowout stability and ignition characteristics.

The fraction of the fuel vaporized within the primary combustor zone can be combined with a correlation for the lean-blowout (ignition) fuel/air ratio for homogeneous mixtures to determine the fuel/air ratio at lean-blowout (ignition) for heterogeneous mixtures. Alternate fuels with reduced fuel fluidity and volatility can cause an increase in the fuel flow (hence fuel/air ratio) required to ignite the mixture or stabilize the flame within the combustor at any given operating condition.

The final expression for lean-blow stability or ignition contains terms that involve both the fraction of the total combustor air employed in primary-zone combustion and the fraction of the fuel vaporized within the same zone. These

parameters can be directly predicted by STAC-I. This permits the relative fuel/air ratio at ignition or lean-blowout of one combustor to be directly compared with that of another combustor at similar inlet conditions.

The relative fuel/air ratio at ignition and lean-blowout generally increases with the use of airblast injection as the fraction of the combustor air in the primary zone increases with the utilization of such injectors, decreasing the equivalence ratio. Offsetting this is the finer atomization of airblast injectors, which increases the fuel fraction evaporated in the primary combustion zone volume (increasing the equivalence ratio). Terms representing these effects are in inverse proportion to each other in the correlation as they should be.

If comparisons are first computed with respect to the individual combustor's sensitivity to fuel type as compared with its ignition or lean-blowout limits using Jet A as the fuel, the dual orifice injected baseline combustor exhibits more relative sensitivity to fuel type than do the airblast injected concepts. As expected, the variable geometry combustor exhibits the least relative sensitivity to fuel type, while that of the piloted prechamber and short prechamber combustors are quite similar in nature and are both more sensitive to fuel type than the variable geometry concept.

The rankings given do not compare the actual ignition and lean-blowout fuel/air ratios of each combustor. The combustor concepts can be ranked relative to one another, and fuel type, using the newly developed correlation equation. When this is done, only the variable geometry combustor of the airblast injected combustor concepts has ignition and lean-blowout stability characteristics similar to that of the baseline combustor. Both the piloted and short pre chamber combustors require more fuel to ignite and sustain combustion. With respect to design and actual fuel/air ratio required to sustain combustion, regardless of fuel type, the combustors may be ranked in the following order: baseline, variable geometry, piloted prechamber, and short prechamber. The baseline and variable geometry combustors were quite similar and considerably better with respect to ignition and lean-blowout stability than the remaining two airblast injected combustor candidates.

5.3.7 Liner Wall Temperature and Smoke

High power operating condition liner wall temperature effects due to fuel type appear to be fairly well characterized by increasing inlet temperature and pressure and fuel hydrogen content. As pressure is increased and fuel hydrogen content is reduced, soot formation is increased. Increased soot formation leads to higher flame emissivity within the combustor and increased smoke emissions at the combustor exit. Internal radiation from the hot gases depends on the temperatures and emissivities of the hot combustion gases (hence, the dependence on inlet gas temperature). The liner temperature increases observed with reduced fuel hydrogen content are almost totally attributed to the increased internal radiation, primarily due to the increased flame emissivity

Because of the high temperature involved at high power operation, fuel physical properties have little or no effect on liner wall temperature. Liner wall temperatures can be reduced by either reducing the emissivity of the combustion gas and/or a mechanical change enhancing the effectiveness of the wall cooling.

Soot formation and increased flame radiation are closely related. Soot formation in the primary zone is to a large extent determined by combustor design, i.e., the stoichiometry and mixedness of the primary zone; however, fuel chemical properties may play an important role. Polycyclic aromatics such as tetralins and naphthalenes might not follow a simple hydrogen correlation. There is evidence indicating that fuels containing significant amounts of polynuclear aromatics (>5%) can produce more soot than their hydrogen content would predict; however, the increase is dependent on the combustor design and operating conditions.

No attempt was made to predict the liner wall temperature as a function of fuel type for the different combustors being considered in this report. Heat transfer models considering the effect of fuel composition have been developed, but the luminosity factor, L, an empirical correction to the flame emissivity, must be introduced to relate predictions to fuel hydrogen content. However, this relationship should only be applied to combustors in which the primary zone equivalence ratio is near unity and the flow field in that region has been established by a pressure fed atomizer.

The predictions from the model do, however, allow some generalizations concerning the sensitivity of the liner wall temperatures of the combustor candidates to fuel type. The increase in liner wall temperature for the three airblast injected combustors is predicted to be considerably less than that of the baseline combustor as the fuel hydrogen content is reduced. Assuming that the fuel-air mixture within the primary zone of each of the airblast injected combustors is well mixed, the combustion gas emissivity (and, hence, total radiation) will then be proportional only to the combustion gas temperature. The combustion gas temperature is lowest for the variable geometry combustor and increases with the use of the piloted prechamber and short prechamber combustors, respectively.

Further, the airblast injected combustor liners are fabricated from Lamilloy. The transpiration cooling effectiveness of this cooling technique has been shown to reduce liner wall temperatures significantly. Consequently, no adverse liner temperature effects would be expected for any of these combustor candidates.

With respect to design and liner wall temperature sensitivity to fuel type, the combustors may be ranked in the following order as a function of their internal gas temperature and mixedness: variable geometry, piloted prechamber, short prechamber, and baseline. Little difference would be expected in the liner wall temperatures of the piloted and short prechamber combustors.

Formations of fuel-rich regions are controlled by fuel physical properties such as viscosity and volatility, which affect the mean drop size, penetration, and rate of evaporation of the fuel spray. The resistance to carbon formation relates (chemically) to molecular structure and the relationship of soot formation to hydrogen content, aromatics, and polycyclic aromatics, etc.

Because soot is formed only in fuel-rich regions of the combustors, smoke can be eliminated by limiting the local equivalence ratio in the primary zone. The superior performance of airblast atomizers with respect to low soot formation is due primarily to thorough fuel-air mixing incurred in the atomization process prior to combustion. This effectively eliminates fuel-rich pockets from the combustion zone.

Little improvement in the prediction of smoke emissions can be expected until more quantitative information is available on the influences of fuel-air preparation and fuel chemistry on soot formation. Consequently, no attempt was made to predict the soot emission index (or smoke number) as a function of fuel type for the different combustors being considered in this report. However, as soot formation and flame radiation are interrelated, the trends summarized with respect to liner wall temperature can be expected to apply for smoke emission levels also. Thus, the smoke number of the exhaust from the three airblast injected combustors will be considerably less than that from the baseline combustor as fuel hydrogen content is reduced. With respect to design and soot formation sensitivity to fuel type, the combustors can again be ranked as a function of their internal gas temperature and mixedness. This order is predicted to be the same as that found for liner wall temperature sensitivity.

5.3.8 Pattern Factor

The downstream hot section of a gas turbine engine must be designed to withstand the maximum temperature measured in a burner outlet temperature survey, or traverse. The most relevant parameter is the overall temperature distribution factor, which highlights this maximum temperature. It is denoted as the pattern factor.

The pattern factor depends at least on liner length, which controls the time and distance available for mixing, and the pressure drop across the liner, which governs the penetration of the dilution jets and their rate of mixing with the products of combustion (i.e., the smoothing of the temperature distribution of the hot gases entering the dilution zone). For any given combustor, the latter is strongly influenced by fuel spray characteristics such as drop size, cone angle, and penetration, as these control the pattern of burning and, hence, the distribution of temperature in the primary-zone efflux. The mode of fuel/air preparation can therefore be of paramount importance in determining the effectiveness of subsequent dilution zone mixing and the resulting temperature profile of the gases entering the turbine.

Correlations to determine the pattern factor have been developed that depend on the liner pressure loss factor and the "equivalent" liner length (that beyond the length required for fuel spray evaporation) divided by the liner diameter. The "equivalent" liner length has been "computed" in several different ways. Some investigators found that trends obtained in pattern factor variations with fuel properties correlated with the final stages of droplet life times, i.e., parameters based on the 90% recovery temperature. Others used a correlating parameter that involves the length to vaporize the Sauter mean diameter of the main spray flow. These approaches are not entirely inconsistent. STAC-1 results indicate that, at the lengths required to vaporize the SMD of the main spray at maximum power, 80-85% of the total spray mass has evaporated, regardless of fuel type or combustor concept.

Following the type of procedure used in determining relative lean blowout and ignition limits, the relative pattern factor of one combustor can be directly compared with that of another using the same or a different fuel type. The dual orifice injected baseline combustor exhibits more relative sensitivity to fuel type with respect to pattern factor than do the airblast injected concepts. Obviously, the pattern factor improves with increasing engine power

level due to the reduction in liner length required for droplet evaporation. For the airblast injected combustor concepts the evaporation time is not a significant fraction of the total combustor residence time, regardless of fuel type, for power levels above 35% of maximum. The length required for vaporization does not substantially differ with power except at idle conditions. There the evaporation time does constitute a significant portion of the total residence time, and a strong effect of combustor concepts and fuel type on pattern factor can be expected.

Over the range of fuels examined the effect of fuel type on pattern factor is relatively small, at least for the airblast injected concepts at the higher power levels. It is at the high power conditions where pattern factor is most important to engine durability and, fortunately at these conditions, variation in fuel type has a nearly negligible effect. All of the airblast injected combustor concepts have a lower pattern factor than the baseline combustor. This decrease is more pronounced as the fuel type is varied with increasing viscosity reflecting the sensitivity of the dual-orifice pressurized atomizers to increasing fuel viscosity. The short prechamber and piloted prechamber exhibit the lowest predicted pattern factor. The sensitivity of these two combustors with respect to both pattern factor magnitude and variation with fuel type is nearly identical. The variable geometry combustor exhibits the same relative insensitivity of pattern factor to fuel type, but the magnitude of the pattern factor is predicted to be slightly larger.

With respect to design and predicted pattern factor, regardless of fuel type, the combustors may be ranked in the following order: piloted prechamber, short prechamber, variable geometry, and finally the baseline concept. There is no clear-cut distinction between the first two combustor concepts; both have equally good pattern factors. The variable geometry combustor is predicted to have a slightly poorer pattern factor compared with the former two combustors, but the pattern factor for this combustor is still highly acceptable.

5.4 SUMMARY OF COMBUSTOR CONCEPT RANKING ORDER

Four combustor concept candidates have been analyzed by STAC-I (or combinations of STAC-I results and correlations) and ranked relative to one another with respect to fuel type sensitivity, according to their predicted combustion efficiency, emissions, ignition and lean-blowout characteristics, liner wall temperature and durability, and pattern factor.

With respect to combustion efficiency, unburned hydrocarbon, and carbon monoxide emissions, the relative ranking order of the combustors was unchanged:

- o variable geometry
- o short prechamber
- o piloted prechamber
- o baseline

The airblast injected combustors were clearly superior to the baseline combustor and their overall performance was nearly identical.

Both the baseline and variable geometry combustors exhibited better predicted ignition and lean-blowout stability characteristics than either the piloted or

short prechamber combustors. The latter two combustors were predicted to have similar ignition and lean-blowout fuel/air ratios, but both of these combustors required considerably higher fuel/air ratios to ignite and sustain combustion.

Combustor concept ranking with respect to liner wall temperature effects, nitric oxide, and smoke emissions were predicted to be a function of the individual combustor's internal combustion gas temperature. The ranking of the combustors is, therefore, in inverse order of their combustion gas temperature:

- o variable geometry
- o piloted prechamber
- o short prechamber
- o baseline

Liner wall temperature effects as a function of fuel type, would be minimized for the airblast injected concepts since they are to be constructed of Lamilloy, which provides enhanced cooling effectiveness. Soot emission (smoke) is expected to be low for these three combustors, again due to their use of airblast injection. The variable geometry combustor exhibited a clear advantage in regard to decreased nitric oxide emission.

The predicted pattern factor of all three airblast injected combustor concepts was superior to that of the baseline combustor, reflecting the increased spray evaporation rate for all fuel types. Predicted pattern factor differences between the piloted and short prechamber concepts was very small, followed closely by the variable geometry combustor. The baseline combustor was predicted to exhibit considerable sensitivity to fuel type.

On an overall basis, without regard to cost or operating complexity, the analyses would rank the combustors in the following order:

- o variable geometry
- o piloted prechamber
- o short prechamber
- o baseline

The piloted prechamber combustor exhibited a clear, but admittedly small, advantage with respect to ignition and lean-blowout stability, and nitric oxide emission compared with the short prechamber combustor.

When cost and/or operating complexity is included in the analysis, the order of ranking would change as follows:

- o short prechamber
- o piloted prechamber
- o variable geometry
- o baseline

The short prechamber concept represents a very simple modification to the baseline combustor, while the variable geometry would require extensive controls for fuel flow and airflow rate scheduling.

VI. RECOMMENDATIONS

1. Freeze point characteristics can create severe effects on the whole system of fuel handling. Future wide-cut blends should retain freezing point characteristics similar to Jet A to eliminate the need for airborne fuel tank heaters.

2. At least one or two of the final airblast injected combustor candidate concepts (short and/or piloted prechamber) should be constructed and a test program initiated to evaluate and verify the predictions resulting from the STAC-I computer code. The code has the potential to predict combustor performance efficiency, emissions, ignition and lean-blowout characteristics, and pattern factor as a function of combustor concept, operating condition, and fuel type.

REFERENCES

1. Barnett, H. C., and Hibbard, R. R., Properties of Aircraft Fuels, NASA Technical Note 3276, Lewis Flight Propulsion Laboratory, Cleveland, Ohio, August 1956.
2. Fuels and Fuel Systems, Coordinating Research Council Aviation Handbook, NAVAIR 06-5-504, May 1967.
3. Handbook of Aviation Fuel Properties, CRC Report No. 530, Coordinating Research Council, Inc, Atlanta, Georgia, 1983.
4. Maxwell, J. B., Data Book on Hydrocarbons, Ninth Printing, Robert E. Krieger Publishing Co, Malabar, Florida, 1977.
5. Lefebvre, A. H., Gas Turbine Combustion, McGraw-Hill Series in Energy, Combustion, and Environment, Hemisphere Publishing Corp, Washington, D.C., 1983.
   (Additional fuel formulas by the same author are published in "Fundamentals of Gas Turbine Combustion," Short Course, Fundamentals of Gas Turbine Combustion, School of Mechanical Engineering, Purdue University, Lafayette, Indiana, 1982.)
6. Hodgson, F. N., "Characterization of Blended CRDS Fuels from NASA," Report No. 81-7, Monsanto Research Corporation, Dayton Laboratory, Dayton, Ohio, March 1981.
7. Reider, S. B., Vogel, R. E., and Weaver, W. E., "Effect of Fuel Composition on Navy T56 Aircraft Engine Hot Section Components," NAPC-PE-89C, Final Report, November 1983.
8. Riddlebaugh, S. M., and Norgren, C. T., "Effect of Broad Properties Fuel on Injector Performance in a Reverse Flow Combustor," NASA-TM-83013, also AIAA Paper presented at the 21st Aerospace Sciences Conference, Reno, Nevada, January 1983.
9. Lefebvre, A. H., "Fuel Effects on Gas Turbine Combustion," AFWAL-TR-83-2004, January 1983.
10. Anderson, R. D., Herman, A. S., Tomlinson, J. G., Vaught, J. M., and Verdow, A. J., "Pollution Reduction Technology Program, Turboprop Engines--Phase 1," NASA CR-135040, March 1976.
11. Troth, D. L., "Low-Emissions Combustor Demonstration," USAAMRDL-TR-76-29, March 1977.
12. References used in determining the mixing rate expressions include:
    Norster, E. R., "Jet Penetration and Mixing Studies," Report PD/JP1 and JP2, College of Aeronautics, Cranfield, England, 1964.
    Holdeman, J. D., Walker, R. E., and Kors, D. L., "Mixing of Multiple Dilution Jets with a Hot Primary Airstream for Gas Turbine Combustors," AIAA Paper 73-1249, Las Vegas, Nevada, 1973 (also NASA TM X-71426).
    Walker, R. E., and Kors, D. L., "Multiple Jet Study," Final Report, NASA CR 121217, 1973.
    Walker, R. E., and Eberhardt, R. G., "Multiple Jet Study Data Correlations," NASA CR-134795, 1975.
    Holdeman, J. D., and Walker, R. E., "Mixing of a Row of Jets with a Confined Cross-flow," AIAA Journal, Vol 15, No. 2, February 1977, pp 243-249.
13. Hubbard, G. L., Denny, V. E., and Mills, A. F., International Journal of Heat and Mass Transfer, Vol 16, pp 1003-1008, 1973. (These authors were verifying the work of Sparrow, E. M., and Gregg, J. L., Trans. ASME, Vol 80, pp 879-886, 1958.)
14. Reid, R. C., Sherwood, T. K., and Prausnitz, J. M., The Properties of Gases and Liquids, 3rd edition, McGraw-Hill, New York, 1977.

15. Sutton, R. D., Schuman, M. D., and Chadwick, W. D., "Operating Manual for Coaxial Injection Combustion Model, Final Report--Space Shuttle Main Engine Development," NASB-29664, April 1974; also published as a JANNAF Standardized Performance Evaluation Procedure, CPIA, John Hopkins University, 1975.
16. Onuma, Y., and Ogasawara, M., "Studies on the Structure of a Spray Combustion Flame," Fifteenth Symposium (International) on Combustion, 1974.
17. Pratt, D. T., "CREK--A Computer Program for Calculation of Combustion, Reaction Equilibrium, and Kinetics in Laminar or Turbulent Flow," Revised for Allison Gas Turbine Operations. August 1983.
18. Radhakrishnan, K., "A Comparison of the Efficiency of Numerical Methods for Integrating Chemical Kinetic Rate Equations," NASA Technical Memorandum 83590, NASA Lewis Research Center, Cleveland, Ohio, February 1984.
19. "Combustion Problems in Turbine Engines," AGARD Conference Proceedings, No. 353, Propulsion and Energetics Panel, 62nd Symposium, Cesme, Turkey, October 1983.
Paper 1. Gardner, L., and Whyte, R. B., "Aviation Fuel Specification Requirements--Their Significance and Future Trends."
Paper 4. Dodds, W. J., "Combustor Technology for Broadened-Properties Fuels."
Paper 5. Moisier, S. A., "Fuel Effects on Gas Turbine Combustion Systems."
Paper 6. Sampath, S., and Gratton, M., "Fuel Character Effects on Performance of Small Gas Turbine Combustion Systems."
Paper 7. Moses, C. A., "U.S. Army Alternative Gas Turbine Fuels Research: MERADCOM."
Paper 8. Odgers, J., and Kretschmer, D., "The Effects of Fuel Composition upon Heat Transfer in Gas Turbine Combustors."
20. Gordon, S., and McBride, B. J., "Computer Program for Calculations of Complex Chemical Equilibrium Compositions, Rocket Performance, Incident and Reflected Shocks, and Chapman-Jouguet Detonations," NASA SP-273, NASA Lewis Research Center, Cleveland, Ohio, 1971.
21. Kretschmer, D., and Odgers, J., "A Simple Method for the Prediction of Wall Temperatures in Gas Turbines," ASME Paper No. 78-GT-90, Gas Turbine Conference and Products Show, London, England, April 1978.
22. Blazowski, W. S., "Combustion Considerations for Future Jet Fuels," Sixteenth Symposium (International) on Combustion, The Combustion Institute, pp 1631-1638, 1977.
23. Jackson, T. A., "Fuel Character Effects on the J79 and F101 Engine Combustion Systems," Symposium on Aircraft Research and Technology for Future Fuels, NASA-Lewis Research Center, Cleveland, Ohio, 1980.
24. Blazowski, W. S., "Dependence of Soot Production on Fuel Blend Characteristics and Combustion Conditions," Journal of Engineering Power, Vol 102, pp 403-408, April 1980.

APPENDIX A

PHYSICAL AND THERMODYNAMIC PROPERTIES AND CORRELATION EQUATIONS OF LIQUID AND VAPOR JET A, ERBS 12.8, ERBS 12.3, ERBS 11.8, AND DF-2 FUELS

FUEL CHARACTERIZATION RESULTS

The characterization results (not including distillation data that appear in Figure 4 in the main text) of the ERBS blends used in this study are presented in Table XXII. Some of these results are also presented in summary form in Table II in the main text.

Comparisons of certain critical properties of the ERBS blends and those of Jet A and DF-2 are presented in Table XXIII.

As expected, the flash point and freezing point both decrease with increasing aromatic content. The 12°C (22°F) maximum decrease in flash point, as represented by ERBS 11.8 compared with Jet A, is not significantly different to indicate that the fire risks associated with the ERBS blends constitute an unknown, unacceptable hazard. Indeed, the flash points for the other ERBS fuels 12.8 and 12.3, are not very different from that of Jet A. Further, as stated by the authors of Paper 1, Ref 19, in real operating conditions "there must be tropical airports where fuels are continually being handled above their flash points. Only the strict airfield fuel handling rules, where all fuels--kerosine, wide-cut, and gasoline--are treated as flammable, minimize the dangers involved. . . .it does seem peculiar that one of the specification limits which obviously influences availability has so little relevancy in the real world."

These same authors are much more concerned with the freezing characteristics of the fuel blends. They believe the ERBS fuels proposed by NASA (as presented in this report) represent extreme cases and would have such a severe effect on the whole system of fuel handling, etc, that it would require redesign of the airframe to allow fuel heating, and drastic changes to the combustor/engine to overcome problems caused by the high aromatic content and high viscosity.

The authors of this report disagree regarding the extent of the severity of potential problems within the combustor caused by increased fuel aromatic content and liquid viscosity. Changes to the injection processes and liner cooling techniques (as evidenced in the short prechamber, piloted prechamber, and variable geometry concepts) appear to alleviate those problems. However, the concerns with the freezing characteristics of the ERBS blends appear real. These concerns should probably be given more consideration than combustor requirements when official fuel property specifications are established. It will be simpler and less expensive to modify the combustor to meet future fuel specifications than it will be to modify most other engine/airframe systems.

One of the more surprising results of this investigation was the discovery that the ERBS blends exhibited considerable thermal stability when subjected to the JFTOT (ASTM D 3241) procedure. The JFTOT procedure pumps the fuel from a reservoir through an annulus surrounding a small, electrically heated, aluminum tube that raises the fuel to the desired test temperature. The fuel is then pumped through a test filter and back to the upper portion of the fuel reservoir. If the fuel is unstable, deposits will form on the heated tube, and any particulates formed will lead to an increase in pressure drop across the

Table XXII.
ERBS fuel, ERBS fuel blends, and blending stock characterization results.

Characterization results (not including distillation data)

Property classification	Property	12.8% H ERBS-3	ERBS-3 12.3% H blend	ERBS-3 11.8% H blend	Blending stock	Test method
Appearance	*Saybolt color	Below -16	Below -16	Below -16	Below -16	ASTM D-156
composition	Hydrogen--wt %	12.85	12.30	11.78	10.26	ASTM D-3701
	Carbon--wt %	86.36	87.52	87.46	89.32	Microcombustion
	Sulfur--wt %	0.062	0.051	0.058	0.088	S specific WDXRF
	*Sulfur, Mercaptan--wt %	0.0003	0.0003	0.0004	0.0003	ASTM D-1219
	Nitrogen, ppm by wt	43	48	60	77	ASTM D-3431
	Aromatics--vol % - FIA, HPLC	28.8, 26.5	39.6, 37.7	49.6, 47.3	83.4, 80.1	ASTM D-1319
	Saturates--vol % - FIA, HPLC	71.8, 73.5	60.8, 62.3	50.2, 52.7	17.7, 19.9	and
	Olefins--vol % - FIA, HPLC	0.7, < 0.3	0.5, < 0.3	0.7, < 0.3	0.8, < 0.3	HPLC
	Naphthalenes--vol % (wt %)	11.76 (13.97)	13.41 (15.72)	14.74 (17.06)	20.51 (22.89)	ASTM D-1840
Volatility	Flash point--°C (°F)	60 (140)	53 (127)	48 (118)	36 (96)	ASTM D-56
	Flash point--°C (°F)	79 (174)	69 (156)	64 (148)	56 (133)	ASTM D-92
	*Vapor pressure--21°C, mm Hg	12.5	8.0	14.5	18.0	Ref 3
	Gravity, API--15°C	36.6	34.3	32.3	26.4	ASTM D-287
	Gravity, specific (15°/15°C)	0.8418	0.8532	0.8639	0.8961	ASTM D-1298
	Distillation temperature	See Figure 4		See Figure 4		ASTM D-86
Fluidity	Freezing point--°C (°F)	-26 (-15)	-25 (-13)	-24 (-11)	-22 (-8)	ASTM D-2386
	Setа point fr. pt. detector:					
	Endpoint--°C (°F)	-35.0 (-31.0)	-37.3 (-35.1)	-35.7 (-32.3)	-33.5 (-28.3)	Freezing point
	Visual melt--°C (°F)	-30.3 (-22.5)	-25.8 (-14.4)	-33.5 (-28.3)	-26.5 (-15.7)	Detector
	Viscosity- cS, -23°C (-10°F)	9.2	7.9	7.0	4.6	ASTM D-445
	Viscosity--cS -20°C (-4°F)	8.19	6.92	6.04	4.63	
	Viscosity--cS 0°C (32°F)	4.29	3.67	3.20	2.65	
	Viscosity--cS 40°C (104°F)	1.79	1.63	1.51	1.29	
Combustion	Net heat of combustion--kJ/kg (Btu/lb)	42,020 (18,100)	41,640 (17,940)	41,200 (17,750)	40,230 (17,330)	ASTM D-2382
	Smoke point	14	11	9	5	ASTM D-1322
	Luminometer No.	27	20	13	3	ASTM D-1740
Stability	JFTOT, breakpoint--°C (°F)	277 (531)	276 (530)	266 (511)	253 (499)	ASTM D-3241
contaminants	*Existent gum--mg/100 mL	2.0	1.6	2.0	1.8	ASTM D-381
	*Particulates--mg/L	2.5	0.5	2.1	2.3	ASTM D-2276
	*Water reaction vol change--mL	0.0	0.0	0.0	0.5	ASTM D-1094
	*Water reaction interface rating	2	1	1	a	ASTM D-1094
Additives	Antioxidant--24.0 mg/L	75% min 2,6-ditertiary-butyl phenol plus 25% max tertiary and tritertiary butyl phenols				
Other	*Surface tension--dynes/cm, 21°C	27.7	28.3	28.6	30.0	Capillary rise
	Ramsbottom C on 10% residue	0.11	0.095	0.092	0.14	ASTM D-524
	Refractive index--27°C	1.4700	1.4782	1.4866	1.5118	ASTM D-1218

Table XXIII.
Selected characterization results for Jet A, the ERBS blends, and DF-2 fuels.

Property	Jet A	ERBS 12.8	ERBS 12.3	ERBS 11.8	DF-2
Flash point--°C(°F)	60 (140)	60 (140)	53 (127)	48 (118)	73 (163)
Specific gravity 16/16°C (60/60°F)	0.808	0.842	0.853	0.864	0.840
Freezing point--°C (°F)	-46 (-50)	-26 (-15)	-25 (-14)	-24 (-11)	-3 (+26)
Net heat of combustion-- MJ/kg (Btu/lbm)	43.2 (18,576)	42.1 (18,100)	41.7 (17,940)	41.3 (17,750)	42.8 (18,393)
Thermal stability JFTOT, breakpoint temperature--°C(°F)	275 (527)	277 (531)	277 (530)	266 (511)	221 (430)

filter. The standard JFTOT procedure specifies the flow rate of the aerated fuel, predetermined by a set nitrogen gas pressure, over the heated tube (260°C) for 2 1/2 hr.

The amount of deposit on the tube can be rated either visually, or by using a tube deposit rater (TDR) that operates on a light reflective principle. Although the visual rating is the method currently called for by ASTM D-3241, the TDR is frequently used in fuels research, and its scale ranges from 0-50. A value of 12-13 is generally used as an equivalent criterion for passing the standard JFTOT test. In addition to the requirement on deposits the ΔP value across the filter must not exceed 25 torr by the end of the 2 1/2-hr test. By operating the JFTOT at temperatures other than 260°C, the temperature at which a fuel just fails either of the described tests may be determined. This temperature is referred to as the breakpoint temperature and is used to compare the thermal stability of fuels.

The results tabulated in Table XXIII indicate that the ERBS 12.8 and 12.3 blends actually exhibited more thermal stability than that exhibited by Jet A. ERBS 11.8 is only slightly less stable, requiring maximum fuel cooling of 9°C (16°F) to achieve the same thermal stability as Jet A.

The fuel nozzle configurations of the final combustor concepts analyzed in this study do not involve thermal stability considerations. The fuel is rarely heated beyond 121°C to 149°C (250°F to 300°F) prior to injection into the combustor.

FUEL PHYSICAL AND THERMODYNAMIC PROPERTIES

Molal Mass and Chemical Formula

The molal mass of the more common hydrocarbons can be computed using the techniques of Ref 1 to 5. Generally, the American Petroleum Institute (API) gravity correlates well with molal mass, as follows:

$$\hat{M} = \frac{A}{(API)^B}$$

where

$$API = \frac{141.5}{\text{Specific gravity}} - 131.5$$

Published data (Ref 1-5) regarding the actual molal mass of JP-4, JP-5, Jet A/JP-8, and DF-2 permitted the following satisfactory correlation to be obtained:

$$\hat{M} = \frac{11,216}{(API)^{1.119076}}$$

Fuel	$\hat{M}$
JP-4	125
JP-5	169
Jet A/JP-8	164
DF-2	198

The correlation cannot be used to obtain the molal mass for high aromatic concentrate fuels such as the ERBS blends. The molal mass of these fuels was obtained using structural data from Ref 6. Alternatively, the characterization factor technique of Ref 2 yielded very nearly the same result. The ERBS fuel blends exhibit unusual behavior in that their molal mass decreases as their specific gravity increases (decreasing API).

ERBS fuel blends	$\hat{M}$ avg
12.8	175
12.3	174
11.8	172

The equivalent chemical formula of each fuel may be computed assuming the fuel is composed of only hydrogen and carbon, and the hydrogen/carbon ratio and molal mass are known.

Fuel	Chemical formula
JP-4	$C_{8.8985}\ H_{17.9750}$
JP-5	$C_{12.1301}\ H_{23.1199}$
Jet A/JP-8	$C_{11.7678}\ H_{22.4764}$
ERBS 12.8	$C_{12.6948}\ H_{22.3428}$
ERBS 12.3	$C_{12.7059}\ H_{21.2188}$
ERBS 11.8	$C_{12.6342}\ H_{20.0884}$
DF-2	$C_{14.3005}\ H_{26.0269}$

The ERBS fuel blends are both lower and upper bounded by Jet A and DF-2 with respect to carbon content and upper bounded by both fuels with respect to hydrogen content. The ERBS fuels formulae reflect their lowered H/C ratio

(higher aromatic content). The chemical formulae given were used to represent the chemical kinetic single-step global decomposition mechanism of the fuel to CO and H_2.

Fuel Liquid Density

The liquid density of each of the fuels was correlated using an equation, suggested by Ref 5, which is considered to be quite accurate at the increased temperatures encountered in combustion systems. The accuracy of this equation has been verified through comparison with experimental data, and the close agreement between predicted and experimental values is retained until the temperature of the fuel approaches its critical value. At the critical temperature the density predicted for the fuel becomes that of the fuel vapor.

In this and all other correlations, the fuel is treated as a well-stirred, heated homogeneous liquid. Distillation of the more volatile components is not allowed, so that the dependent variable being correlated is a function of the entire liquid constituency, temperature, and, by inference, pressure. This concept of correlation does not violate application to droplet heating and vaporization within spray combustion (gas turbine) systems. Indeed, the normal ASTM D-86 derived distillation curves do not represent equilibrium values nor are they intended to do so. At small relative Reynolds numbers (35-40) vaporizing droplets undergo intense internal recirculation; droplet internal temperature (and constituent and density) gradients cease to exist and the droplet vaporizes as if it were composed of a homogeneous fluid. Mean droplet lifetime within a gas turbine combustor is on the order of 3-5 milliseconds, and within this short time span, homogeneous vaporization is a valid approximation (Ref 15).

The liquid density was correlated by the following equation and is presented graphically as a function of temperature in Figure 79.

$$RLJN(TJS2K, JF) = RHOF(JF) * (1.0 - (1.8 * CEX(JF) * (TJS2K - 288.6)) - 0.09 * ((TJS2K - 288.6)/(TCRK(JF) - 288.6))^2) \quad (1)$$

where

RLJN = density of liquid--lbm/ft^3
TJS2K = temperature of liquid--K
JF = fuel type--see information that follows
RHOF = density of liquid at 15°C
CEX = coefficient of expansion of liquid
TCRK = critical temperature of liquid--K

The critical temperatures were calculated using the methods of Ref 4.

JF	1	2	3	4	5
Fuel	Jet A	ERBS 12.8	ERBS 12.3	ERBS 11.8	DF-2
RHOF	50.44177	52.5518	53.2635	53.9315	52.4395
CEX	0.000510	0.000462	0.000453	0.000440	0.000467
TCRK	671.0 K	697.1 K	697.4 K	696.0 K	722.3 K

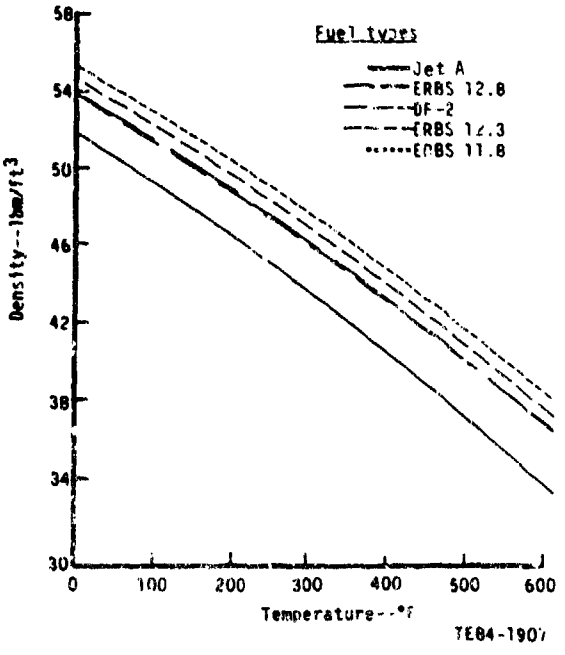

Figure 79. Liquid density as a function of temperature.

Conversion to kg/m^3 is accomplished by multiplying the first equation (or RLJN) by 16.01847.

Liquid Specific Heat

The liquid specific heat was correlated by the following equation, which is a modified and more accurate form of that presented in Ref 1 and 5, and is also presented graphically as a function of temperature in Figure 80.

```
CPLJN (TJS2K, JF) = ((0.758 + 0.0033 * TJS2K)/
SQRT ((2.0 * RHOF (JF) + RLJN (T2S2K, JF))                    (2)
* 0.01601847/3.0) * 0.2388459
```

where

CPLJN = the liquid specific heat--Btu/lbm-°F

and the other symbols have the same meaning and units as used in Equation 1.

Conversion to kJ/kg-K is accomplished by multiplying Equation 2 (or CPLJN) by 4.1868 (inverse of 0.2388459).

Liquid Specific Enthalpy

The liquid specific enthalpy is the integral of the liquid specific heat (Equation 2) referenced to 25°C plus the enthalpy of formation (for each fuel) at this standard reference state (25°C). In the integration the contribution

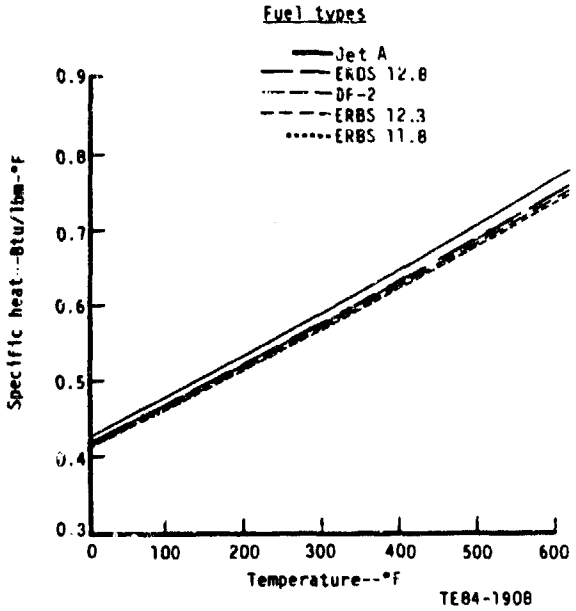

Figure 80. Liquid specific heat as a function of temperature.

from the square root term in Equation 2, which contains only the density variation, is treated as an averaged constant. The liquid specific enthalpy is presented graphically as a function of temperature in Figure 81.

$$HJN\ (TJS2K,\ JF) = ([0.758 * (TJS2K - 298.15) + 0.00165 * ((TJS2K)^2 - 88{,}893.0)]/SQRT\ (\{2.0 * RHOF(JF) + RLJN\ (298.15 + (TJS2K - 298.15)/2.0,\ JF)\} * 0.01601847/3.0)) * 0.429926 + DELHFO\ (JF) \quad (3)$$

where

HJN = the liquid specific thermochemical enthalpy referenced to 25°C--Btu/lbm

DELHFO (JF) = the liquid enthalpy of formation for each fuel at 25°C--Btu/lbm

Values of DELHFO for each fuel are tabulated as follows:

JF	1	2	3	4	5
Fuel	Jet A	ERBS 12.8	ERBS 12.3	ERBS 11.8	DF-2
DELHFO	-702.312	-823.693	-767.176	-762.280	-673.476

Conversion to kJ/kg is accomplished by multiplying Equation 3 (or HJN) by 2.32600 (inverse of 0.4299226).

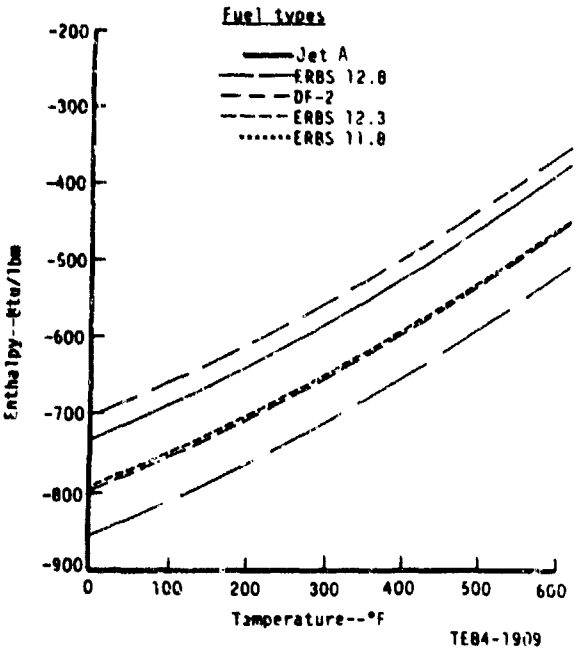

Figure 81. Liquid enthalpy as a function of temperature.

Vapor Pressure

The vapor pressure was correlated by an equation developed in Ref 5. While the values predicted by the equation do not represent an exact reproduction of the "true equilibrium vapor pressure" variation with temperature, the equation, expressed as a modified form of the Clausius-Clapeyron relationship, represents a best fit between true vapor pressure, fuel temperature, and vaporization data as measured through the use of porous spheres. The predicted vapor pressure and the true vapor pressure dependence on temperature agree exactly at atmospheric pressure and at the critical pressure. The vapor pressure is presented graphically as a function of temperature in Figures 82 and 83.

$$PVJN(TJS2K, JF) = EXP(APV(JF) - BPV(JF)/(TJS2K-43.0)) * 0.1450378 \quad (4)$$

where

PVJN = the vapor pressure in $lb/in.^2$ absolute

APV and BPV are constants based on analysis of the experimental data of vapor pressure available in the literature. Values for different fuels are tabulated in the following:

JF	1	2	3	4	5
Fuel	Jet A	ERBS 12.8	ERBS 12.3	ERBS 11.8	DF-2
APV	15.0723	15.2720	15.2971	15.6028	15.52954
BPV	4620.67	4943.29	4922.89	5008.91	5383.59

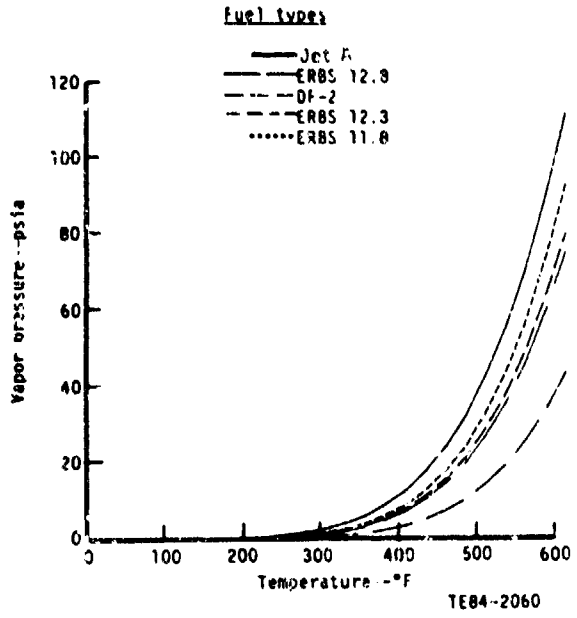

Figure 82. Vapor pressure as a function of temperature.

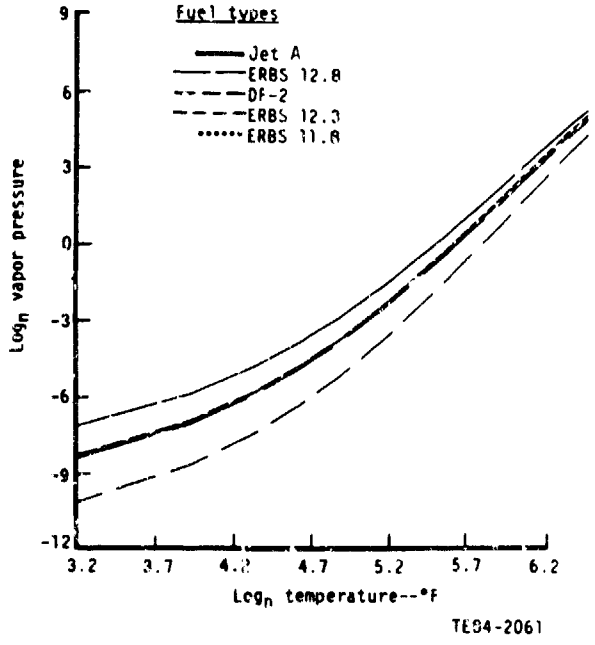

Figure 83. Log_n-log_n plot--vapor pressure as a function of temperature.

Conversion to kPa is accomplished by multiplying Equation 4 (or PVJN) by 6.894757 (inverse of 0.1450378).

Latent Heat of Vaporization

The latent heat of vaporization at the fuel atmospheric normal boiling temperature was determined by standard type correlation equations for the normal hydrocarbons and from structural data (Ref 6) for the ERBS blends.

The latent heat of vaporization (LTBN) at TBN (the fuel normal boiling temperature at 1 atm) for the normal hydrocarbons was determined by the following equation:

$$LTBN = A(JF) + B(JF) * Ln_{10} (\hat{M}) \quad (5)$$

where

A and B = constants determined by comparison to experimental values for LTBN.

The latent heat of vaporization for the ERBS blends at 25°C was determined from structural data, and the LTBN was then computed using the correlation equation recommended by Ref 5. This same correlation equation was used to determine the latent heat of vaporization as a function of temperature for all the fuels. The latent heat of vaporization as a function of temperature is presented graphically in Figure 84

$$DLHVJN (TJS2K, JF) = LTBN (JF) * [(TCRK (JF) - TJS2K) / (TCRK (JF) - TBN (JF))]^{0.38} * 0.4299226 \quad (6)$$

where

DLHVJN = the latent heat of vaporization at the temperature TJS2K--Btu/lbm
LTBN = the latent heat of vaporization at the fuel atmospheric normal boiling temperature, TBN--kJ/kg
TBN = the fuel normal boiling temperature at 1 atmosphere pressure--K, as determined by the methods of Maxwell, Ref 4

Values of A, B, TBN, and LTBN are as listed in the following:

JF	1	2	3	4	5
Fuel	Jet A	ERBS 12.8	ERBS 12.3	ERBS 11.8	DF-2
A	721.837	---	---	---	721.837
B	-203.3556	---	---	---	-203.3556
TBN--K	485.0	507.0	504.0	499.0	536.0
LTBN - kJ/kg	271.0	258.0	262.0	266.0	254.0

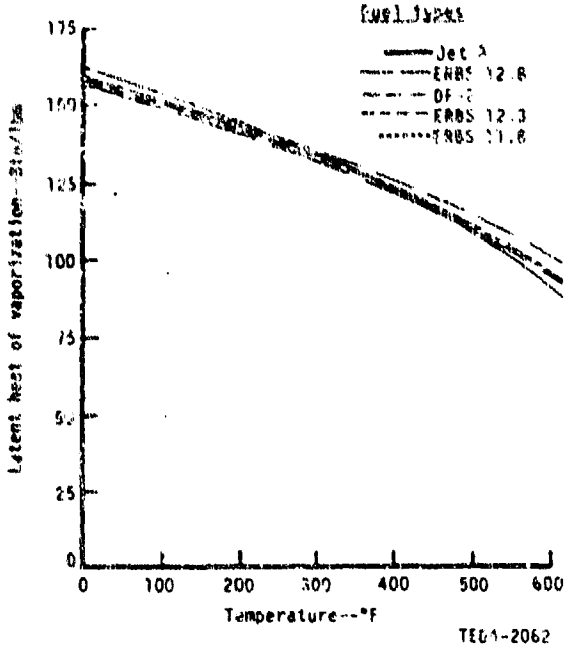

Figure 84. Latent heat of vaporization as a function of temperature.

Conversion to kJ/kg is accomplished by multiplying Equation 6 (or DLHVJN) by 2.32600 (inverse of 0.4299226).

Liquid Kinematic and Absolute Viscosity

The liquid absolute viscosity appears in the Reynolds number and drop size correlations used in combustion modeling. However, almost all experimental data related to viscosity are reported in terms of the kinematic viscosity. Thus, the liquid kinematic viscosity was correlated by the following equation (Ref 1) and then multiplied by the fuel density to yield the absolute viscosity. The final results are presented graphically as a function of temperatures in Figures 85 and 86.

Kinematic viscosity, KMUL

$$KMUL(TJS2K, JF) = [EXP(EXP(AMUK(JF) * Ln_n(TJS2K) + BMUK(JF))) - CMUK(JF)] * 0.000001$$

where

KMUL = the kinematic viscosity in m^2/sec
AMUK, BMUK, CMUK = constants determined by comparison with experimental values of the kinematic viscosity and tabulated in the following:

Absolute viscosity, MULJN

$$MULJN(TJS2K, JF) = (KMUL(T2S2K, JF) * RLJN(TJS2, JF) * 16.01847) * 0.0208855 \quad (7)$$

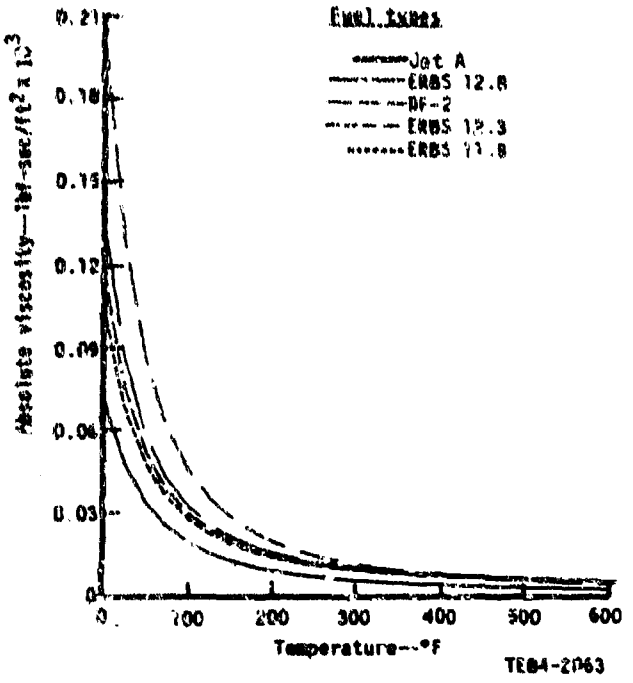

Figure 85. Liquid absolute viscosity as a function of temperature.

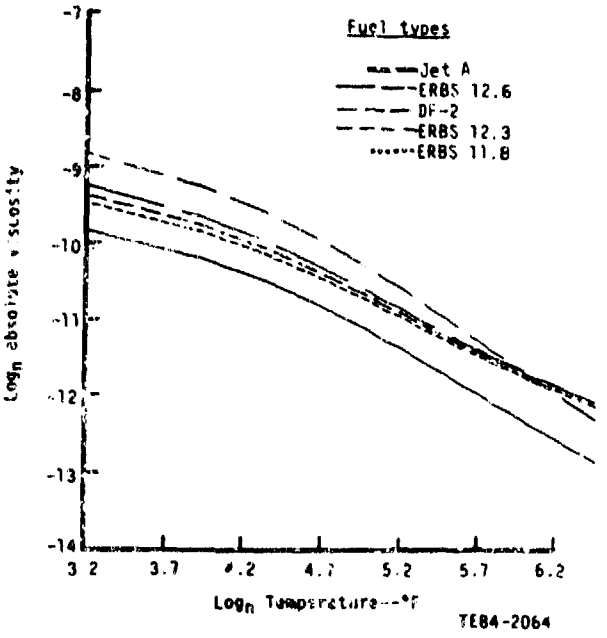

Figure 86. Log$_n$-log$_n$ plot--liquid absolute viscosity as a function of temperature.

where

MULJN = the absolute viscosity in lbf-sec/ft^2

JF	1	2	3	4	5
Fuel	Jet A	ERBS 12.8	ERBS 12.3	ERBS 11.8	DF-2
AMUK	-4.21621	-4.26859	-4.28084	-4.23908	-3.60526
BMUK	23.83556	24.40040	24.39413	24.10158	20.89333
CMUK	0.823940	0.8268811	0.830850	0.857279	0.7800

Conversion to N-s/m^2 is accomplished by multiplying Equation 7 (or MULJN) by 47.8803 (inverse of 0.0208855).

Liquid Surface Tension

The liquid surface tension, used primarily in correlations determining droplet mean diameters as produced by various injector types, was determined by the following equations in which the constants were determined by comparison with experimental data. Experimental surface tension data for the normal hydrocarbons can be found in Ref 1-5, while those for the ERBS blends are tabulated as a function of temperature in Ref 6. The final results for surface tension are presented graphically as a function of temperature in Figure 87. Note that the units are retained in N/m since all correlations for obtaining mean droplet sizes use SI units.

First the API gravity is determined.

```
API(JF) = 141.5/(0.01601847 * RHOF(JF)) - 131.5
```

The term 0.01601847 * RHOF(JF) is 0.001 * RHOF(JF) in kg/m^3. At 15°C the approximate density of water is 1000 kg/m^3; the term in the denominator of the equation for API is the specific gravity.

The surface tension is then calculated by the following equation:

```
SURTJN(TJS2K, JF) = [ASURT(JF) - BSURT(JF)
* API(JF) - CSURT(JF) * (TJS2K-290.0)] * 0.001                    (8)
```

where

SURTJN = the surface tension, Newton/meter
API = the "API" gravity as defined previously
ASURT, BSURT and CSURT = constants determined by comparison with experimental values of the surface tension and tabulated in the following:

JF	1	2	3	4	5
Fuel	Jet A	ERBS 12.8	ERBS 12.3	ERBS 11.8	DF-2
ASURT	30.129	40.5	40.5	40.5	40.5
BSURT	0.1424	0.3381	0.3444	0.3570	0.3020
CSURT	0.07916	0.097965	0.093609	0.088422	0.07916

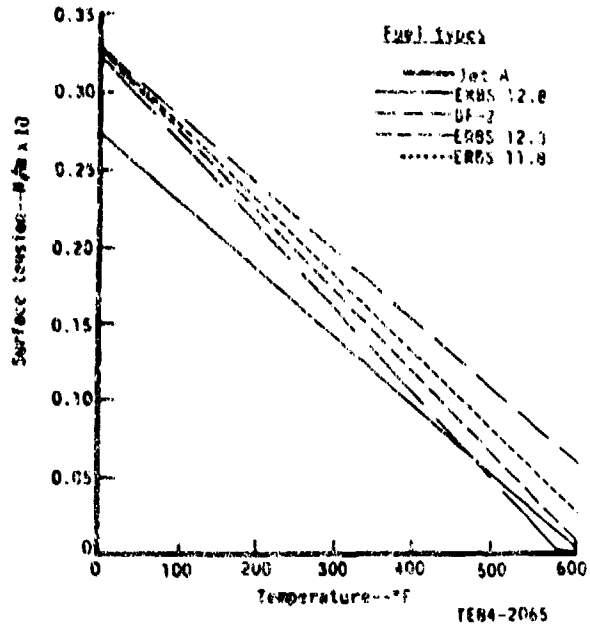

Figure 87. Surface tension as a function of temperature.

Conversion to lbf/ft is accomplished by multiplying Equation 8 (or SURTJN) by 0.068522.

Fuel Vapor Specific Heat

The fuel vapor specific heat is one of the most important variables determining the rate of vaporization of a fuel droplet. Within combustion models that consider spray evaporation and combustion, the fuel vapor specific heat is usually determined at the so-called droplet film temperature, TFJ. The droplet film temperatures may be defined in a number of ways; but experimental data obtained under convective conditions appear to correlate well when TFJ is defined as the addition of 2/3 of the droplet temperature and 1/3 of the combustion gas temperature. That is,

```
TFJ = (2 * TJS2 + T2)/3.0
```

where

TFJ = the film temperature--°R
TJS2 = the droplet temperature--°R
T2 = the combustion gas temperature--°R

Degrees in Rankine are used as this is the basic temperature unit in STAC-1. Further, all gas phase species considered in STAC-I express the thermodynamic functions, specific heat, enthalpy, and entropy as functions of temperature in the form of least squares coefficients following the technique used by Gordon and McBride (Ref 20):

$$C_p = \frac{R_u}{\hat{M}} \left(Z_1 + \frac{Z_2 * T°R}{1.8} + \frac{Z_3 * (T°R)^2}{3.24} + \ldots\ldots\right) \qquad (9a)$$

where

C_p = Btu/lbm-°R
R_u = 8tu/lbm-mole °R = 1.98586
$\hat{M}$ = the molal mass of the fuel
Z = the least square coefficients

When the specific heat of the vapor is being considered, the temperature becomes TFJ in °R.

The vapor specific heat of the fuels was correlated using an equation suggested by Ref 5. This equation is considerably more accurate than a better known equation proposed by Maxwell, Ref 4.

$$\text{CPVFJN(TFJ, JF)} = [(0.363 + 0.000467 * TFJ/1.8) * (5.0 - 0.01601847 * \text{RHOF(JF)})] * 0.2388459 = (0.433505309 - 0.001388818 * \text{RHOF(JF)}) \qquad (9b)$$
$$+ ((0.000309836 - 0.000000993 * \text{RHOF(JF)}) * TFJ)$$

By direct comparison to Equation 9a

$$Z_1 = \frac{\hat{M}(JF)}{1.98586} (0.433505309 - 0.001388818 * \text{RHOF(JF)}) \qquad (9c)$$

$$Z_2 = \frac{1.8 * \hat{M}(JF)}{1.98586} (0.000309836 - 0.000000993 * \text{RHOF(JF)})$$

Z_3 , Z_4, and Z_5 = 0

Equation 9b for CPVFJN is presented graphically in Figure 88 as a function of temperature. As indicated in the figure, there is little difference in the value for the vapor specific heat for the fuels being considered. Conversion from Btu/lbm-°F to kJ/kg-K is accomplished by multiplying Equation 9b (or CPVFJN) by 4.1868 (inverse of 0.2388459).

Fuel Vapor Enthalpy and Entropy

Fuel vapor enthalpy is important in those fuel rich regions of the combustor where sufficient quantities of unreacted fuel vapor exist and contribute to both the constituent mix and energy of the gas phase flow. The vapor enthalpy is expressed in a similar manner as the vapor specific heat. In fact, the vapor enthalpy is simply the integral of the expression for the vapor specific heat referenced to the standard state (25°C) plus the vapor enthalpy of formation at this standard state.

Following Gordon and McBride (Ref 20), the vapor enthalpy in the gas phase is expressed as

$$\text{HVAPG (T2, JF)} = \frac{1.98586}{\hat{M}(JF)} \left(Z_1 * T °R + \frac{Z_2 * (T°R)^2}{3.6} + 1.8 * Z_6\right) \qquad (10a)$$

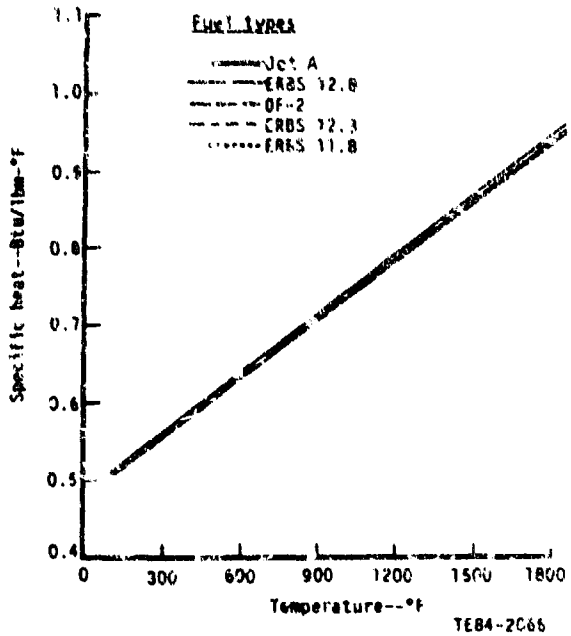

Figure 88. Vapor specific heat as a function of temperature

Since Z_3, Z_4, and Z_5 are equal to zero, Z_6 represents the terms arising from reference of the enthalpy to the standard state If the integration of the vapor specific heat equation is performed, this latter term, Z_6, can be expressed as follows:

$$Z_6 = - (Z_1 * 293.15) - (Z_2 * 44,446.71) + \frac{M(JF)}{3.574548} * DELHFV(JF) \qquad (10b)$$

where DELHFV(JF) is the enthalpy of formation of the vapor at 25°C and differs from the enthalpy of formation of the liquid (DELHFO at 25°C) by the addition of the standard state enthalpy of vaporization.

The entropy of the fuel vapor is important only as it affects the calculations of the species concentrations and temperature if an equilibrium reaction state is assumed. The fuel vapor entropy enters the computation relating to the minimization of the Gibb's function. As the concentration of fuel vapor is virtually zero in the reacted equilibrium state, the contribution of the fuel vapor entropy to the computations involved is nearly negligible. Nevertheless, the entropy of the fuels referenced to the standard state was again computed following Gordon and McBride (Ref 20). The entropy can be expressed as follows:

$$\frac{SVAPG(T2, JF)}{R_u} = Z_1 * Ln_n {}^{T2}/_{T^\circ} + Z_2*(T2-T^\circ) + S_f^{T^\circ}/R_u \qquad (11a)$$

where

T2 = the gas temperature-K
T° = the standard state temperature--25°C (298.15 K)
$S_f^{T^{\circ}}$ = the entropy of formation of the fuel at the standard state
R_u = the universal gas constant

The entropy of the fuel vapor can be expressed in canonical form as follows (Ref 20, with Z_3, Z_4, Z_5 all equal zero):

$$\frac{SVAFG(T2, JF)}{R_u} = Z_1 * Ln_n T2 + Z_2 * T2 + Z_7 \qquad (11b)$$

the coefficient Z_7 is then, by inspection,

$$Z_7 = S_f^{T^{\circ}}/R_u - Z_1 * Ln_n T^{\circ} - Z_2 * T^{\circ}$$

where

R_u = 8314.41 J/kg-K
T° = 298.15 K (25°C)

$S_f^{T^{\circ}}$ was computed by comparison to pure hydrocarbon fuels having similar structure to Jet A, the ERBS blends, and DF-2.

Jet A and the ERBS blends were compared with 1-Dodecene while DF-2 was compared with 1-Dodecane. Typical values for $S_f^{T^{\circ}}$ for Jet A and the ERBS blends were 607.1 kJ/kg-mole-K while that for DF-2 was 595.01 kJ/kg-mole-K.

Fuel Vapor Thermal Conductivity

The fuel vapor thermal conductivity is similar in importance to the fuel vapor specific heat as one of the variables determining the rate of vaporization of a fuel droplet. The fuel vapor thermal conductivity is usually determined at the film temperature, TFJ. The vapor thermal conductivity of the fuels was correlated using the following equation suggested by Ref 5. First, an exponential term involving the film temperature in K is evaluated.

$$EXPN(TFJK, JF) = 2.0 - 0.0372 * (TFJK/TBN(JF))^2 \qquad (12a)$$

where

TFJK = the film temperature in K

then

$$KVFJN(TFJK, JF) = [(13.2 - 0.0313 * (TBN(JF)-273)) * (TFJK/273) ** EXPN(TFJK, JF)] * 0.000001 * 0.1605028 \qquad (12b)$$

where

KVFJN = the fuel vapor thermal conductivity at the droplet film temperature--Btu/ft-sec-°R

Equation 12b for KVFJN is presented graphically in Figure 89 as a function of temperature. Conversion from Btu/ft-sec-°R to kJ/m-sec-K is accomplished by multiplying Equation 12b (or KVFJN) by 6.230421 (inverse of 0.1605028).

Fuel Vapor Absolute Viscosity

The fuel vapor absolute viscosity affects droplet vaporization through the film Reynolds or Prandtl number contributions in Nusselt and Sherwood numbers for heat and mass transfer, respectively. The fuel vapor absolute viscosity does not appear by itself in such correlations but is always combined (in a very rigorous and complex manner) with the combustion gas absolute viscosity to form the true film absolute vircosity. The fuel vapor absolute viscosity was correlated using the following equation suggested by Ref 5:

$$MUVFJN(TFJK, JF) = [AMUV(JF) * (TFJK)^{2.5}/ (BMUV(JF) + CMUV(JF) * TFJK + (TFJK)^2)] * 0.000001 * 0.0208855 \quad (13)$$

where

MUVFJN = the fuel vapor absolute viscosity at the film temperature, TFJK in K. The viscosity has the units lbf-sec/ft^2.
AMUV, BMUV, and CMUV = constants determined by comparison with experimental values of the vapor absolute viscosity and are tabulated in the following:

JF	1	2	3	4	5
Fuel	Jet A	ERBS 12.8	ERBS 12.3	ERBS 11.8	DF-2
AMUV	0.741367	0.741367	0.741367	0.741367	0.533305
BMUV	226,180	226,180	226,180	226,180	398,407.8
CMUV	-206.996	-206.996	-206.996	-206.996	-704.042

No experimental data for fuel vapor absolute viscosity were available for the ERBS blends. Because of their similarity to Jet A, they were assumed to have the same vapor absolute viscosity as Jet A. Equation 13 for MUVFJN is presented graphically in Figure 90, as a function of temperature. The assumption of equating the vapor absolute viscosity of the ERBS blends to that of Jet A appears valid as little variation in this parameter occurs even when DF-2 is considered to be the turbine fuel. Conversion from lbf-sec/ft^2 to N-s/m^2 is accomplished by multiplying Equation 13 (or MUVFJN) by 47.8803 (inverse of 0.0208855).

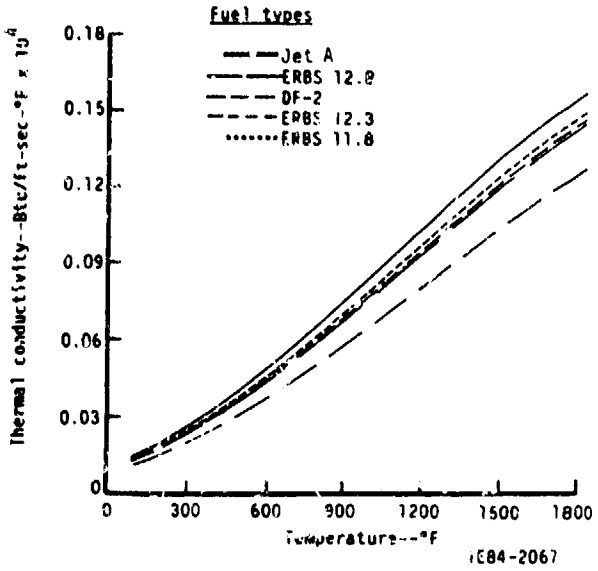

Figure 89. Vapor thermal conductivity as a function of temperature.

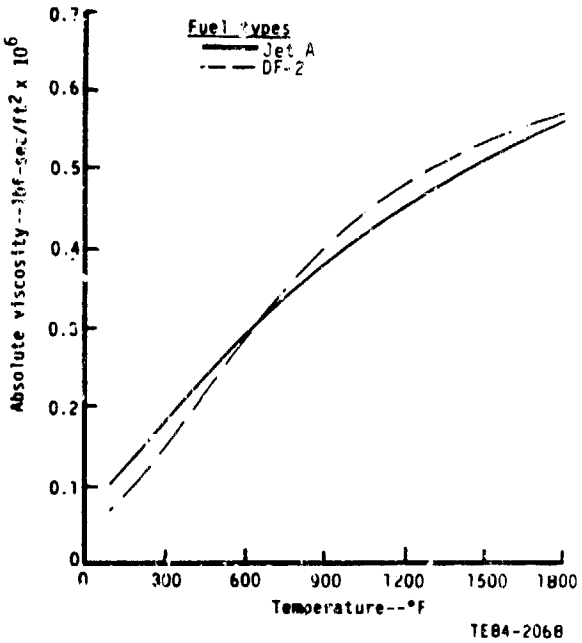

Figure 90. Vapor absolute viscosity as a function of temperature.

APPENDIX B

COMBUSTOR FLOW FIELD GRAPHIC PRESENTATIONS

CENTRAL RECIRCULATION ZONE

The volumetric size of the individual combustor's central recirculation zone (CTRZ) was determined by Allison's axisymmetric streamline analysis, COSMIC, at the maximum power operating condition. The results of this streamline analysis, for the final four combustor concepts, are presented in Figures 91 through 94.

MAXIMUM POWER AND GROUND IDLE OPERATING CONDITION COMBUSTOR FLOW FIELD PRESENTATIONS

Graphic presentations of the STAC-I predicted flow fields within the four combustor concepts operating at maximum power and ground idle conditions on Jet A and DF-2 fuels are presented in Figures 95 through 124 and Figures 131 through 148. The order of the graphical presentations with respect to combustor concept is: baseline, short prechamber, variable geometry, and piloted prechamber combustors.

DESCENT POWER OPERATING CONDITION VARIABLE GEOMETRY COMBUSTOR FLOW FIELD PRESENTATIONS

Graphic presentation of the STAC-I predicted flow field within the variable geometry combustor concept operating at the descent power condition on Jet A and DF-2 fuels are presented in Figures 125 through 130.

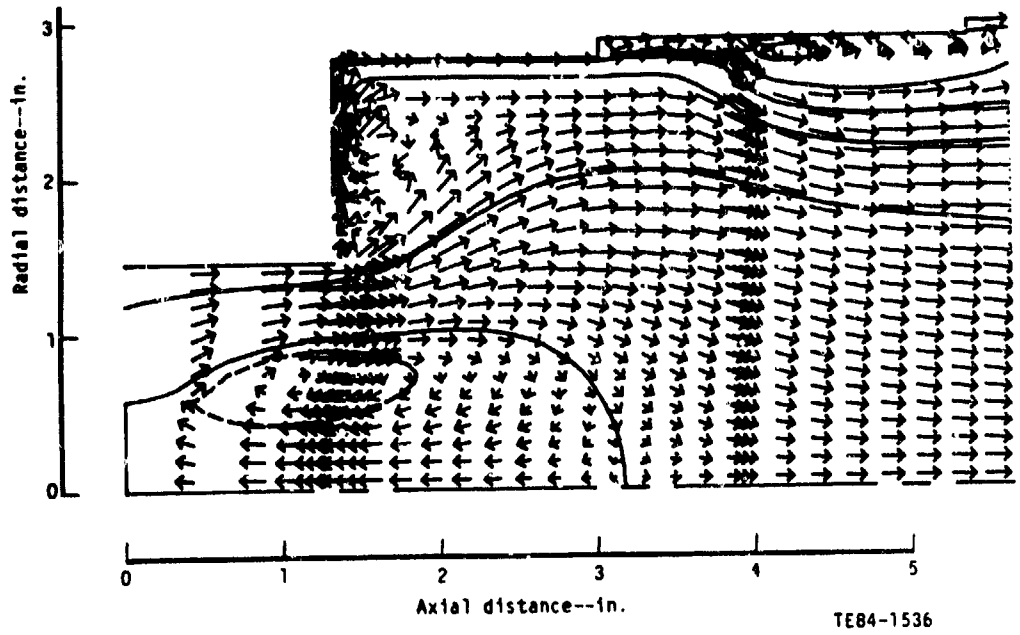

Figure 91. Concept 1--baseline Model 250-C30 liner--maximum power flow streamlines.

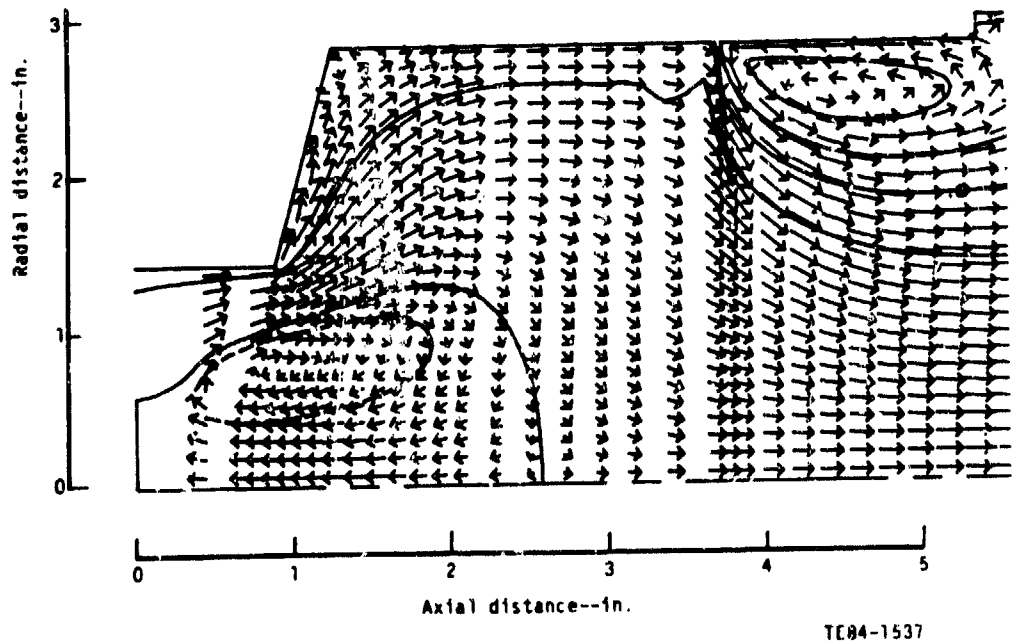

Figure 92. Concept 2--short prechamber 250-C30 liner--maximum power flow streamlines.

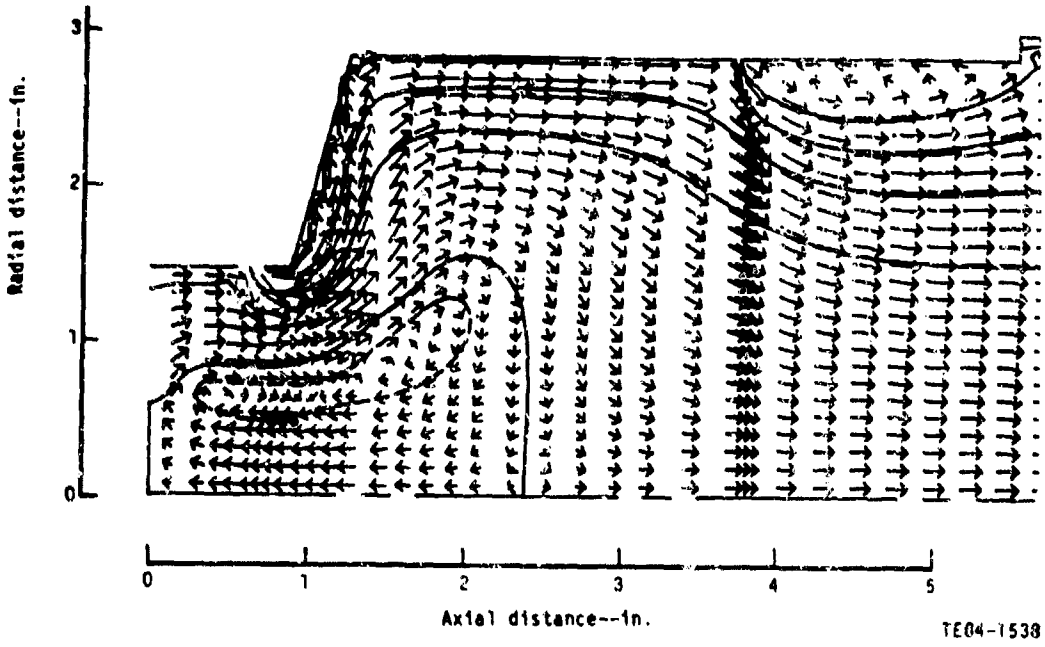

Figure 93. Concept 3--variable geometry Model 250-C30 liner--maximum power flow streamlines.

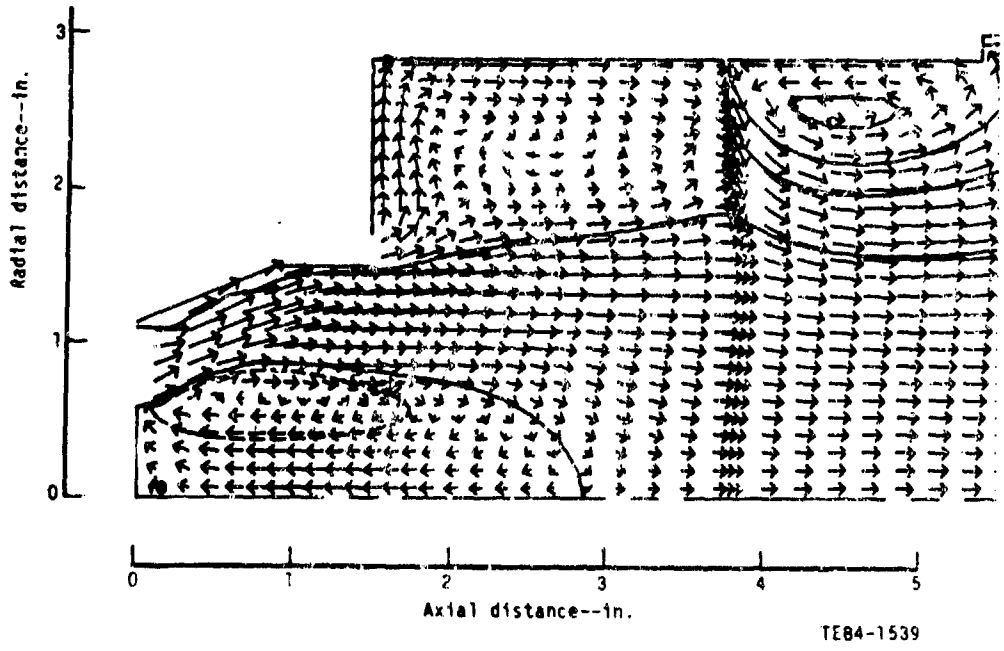

Figure 94. Concept 4--pilot prechamber Model 250-C30 liner--maximum power flow streamlines.

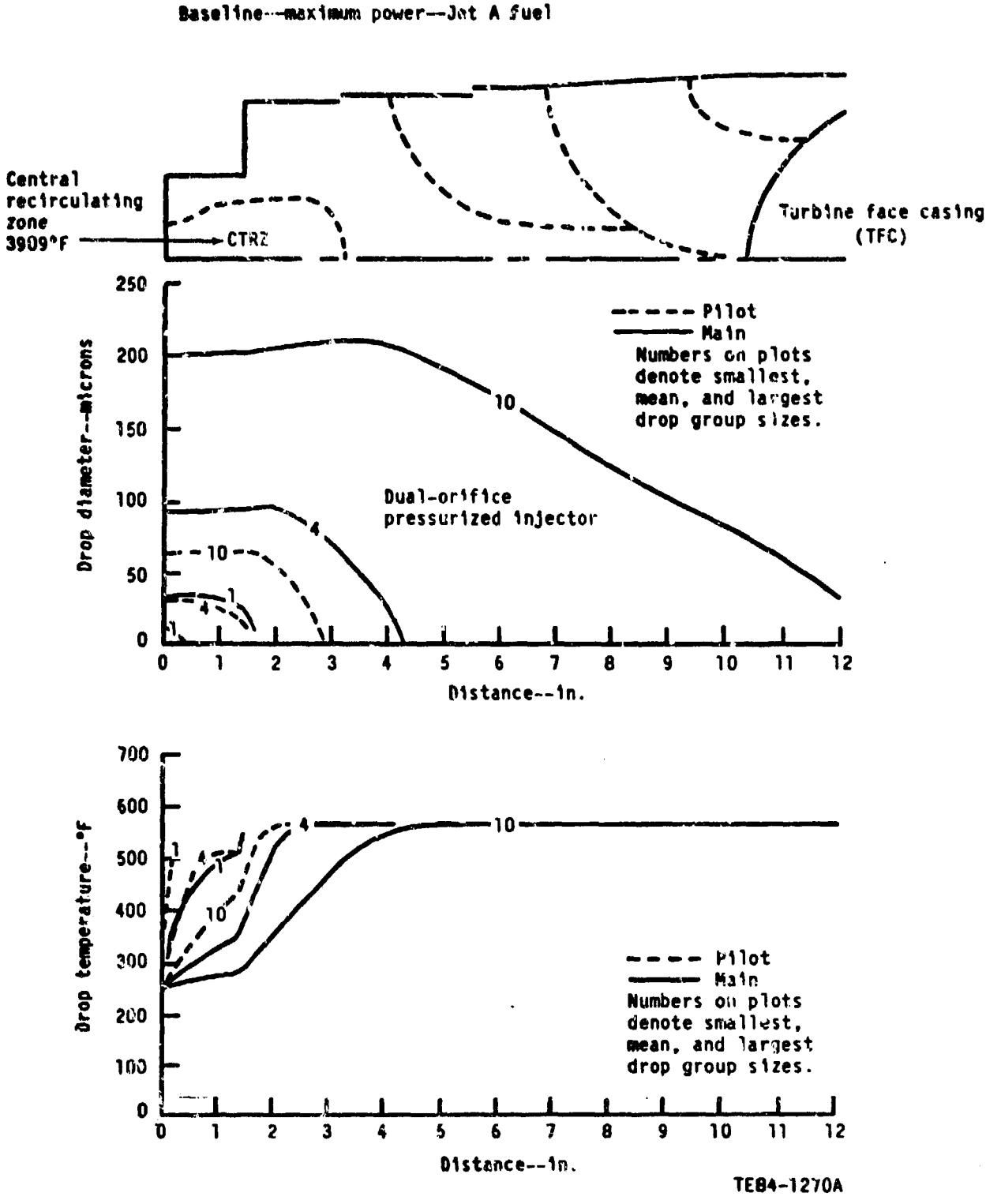

Figure 95. Baseline--maximum power with Jet A fuel.

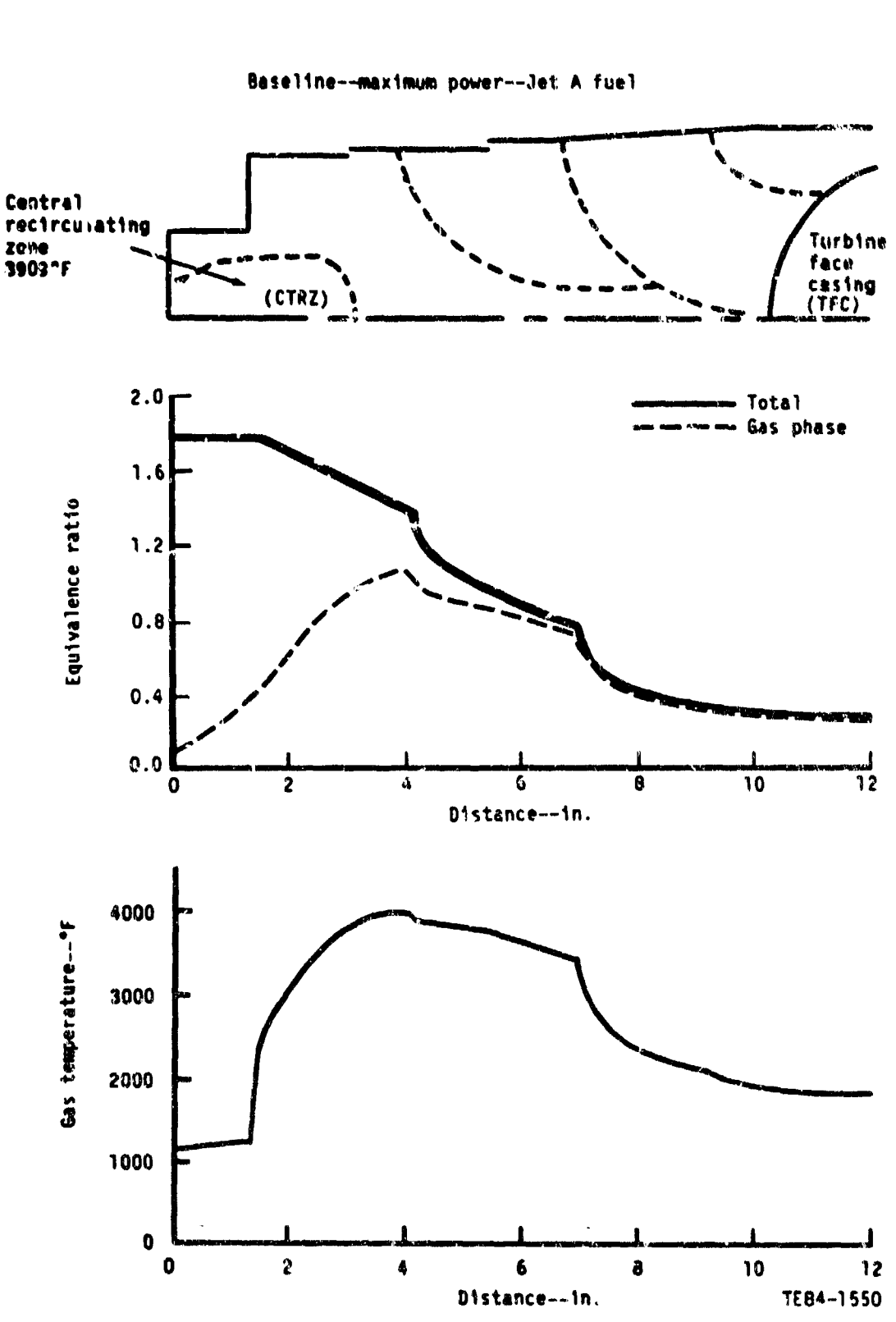

Figure 96. Baseline--maximum power with Jet A fuel.

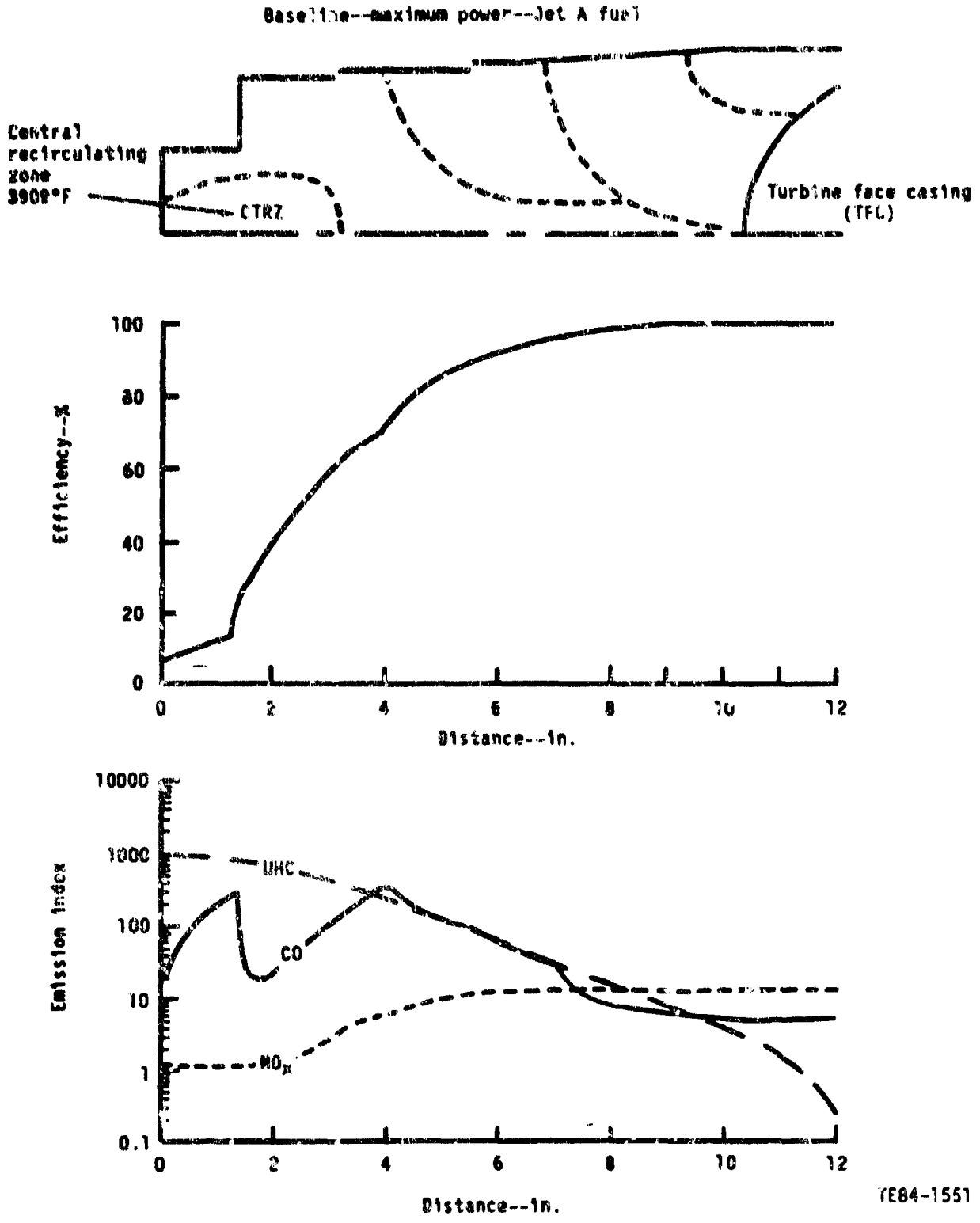

Figure 97. Baseline--maximum power with Jet A fuel.

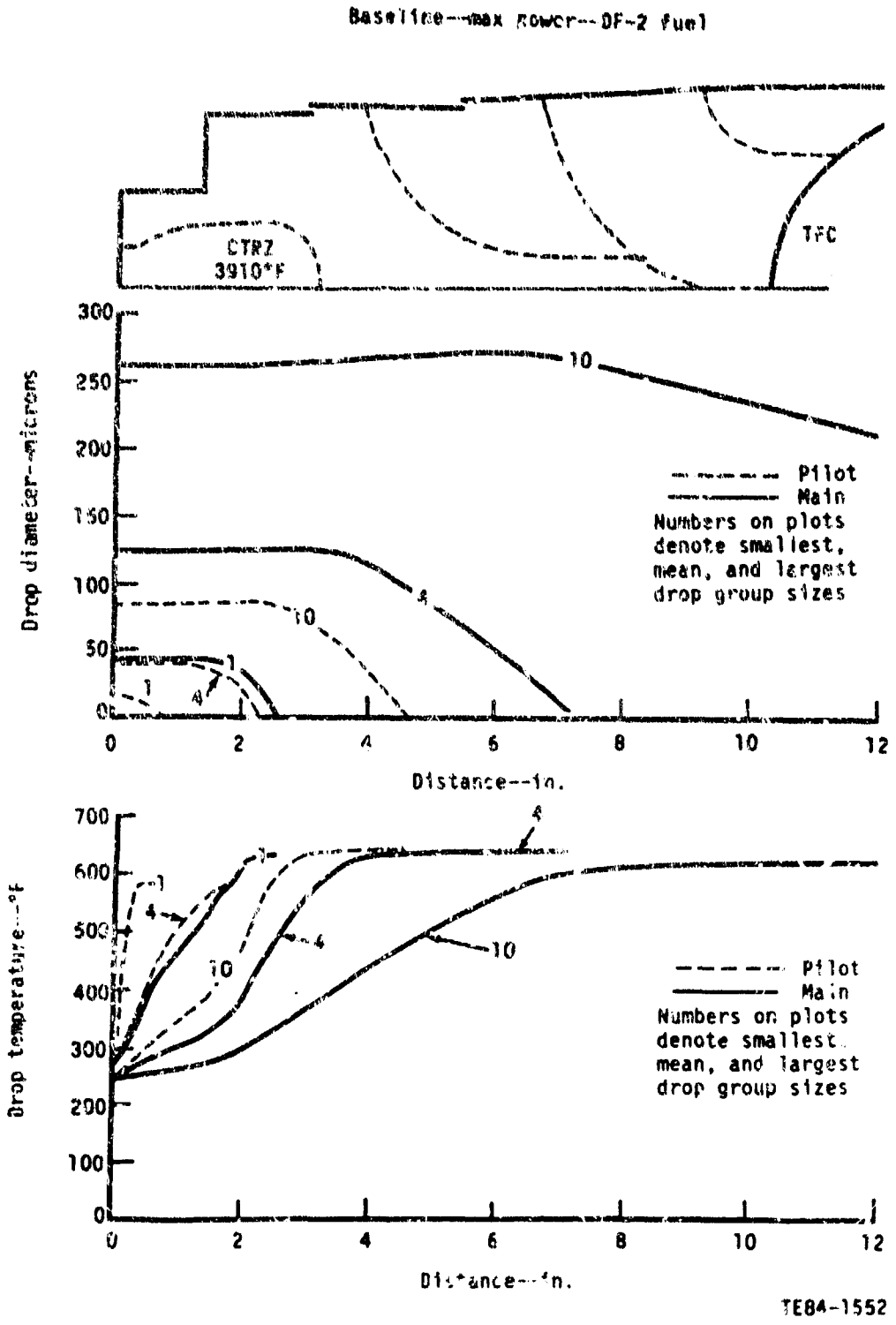

Figure 98. Baseline--maximum power with DF-2 fuel.

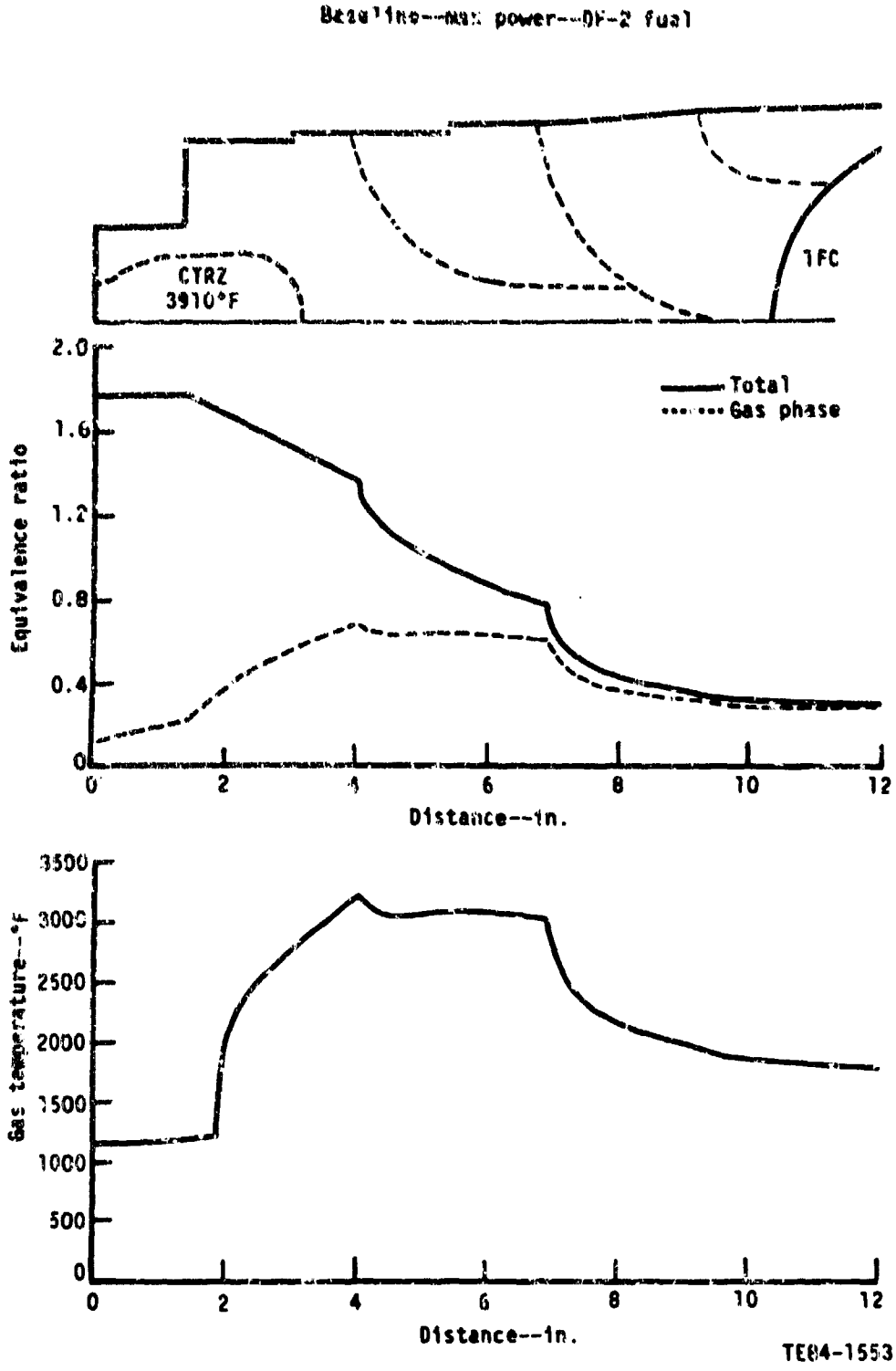

Figure 99. Baseline--maximum power with DF-2 fuel.

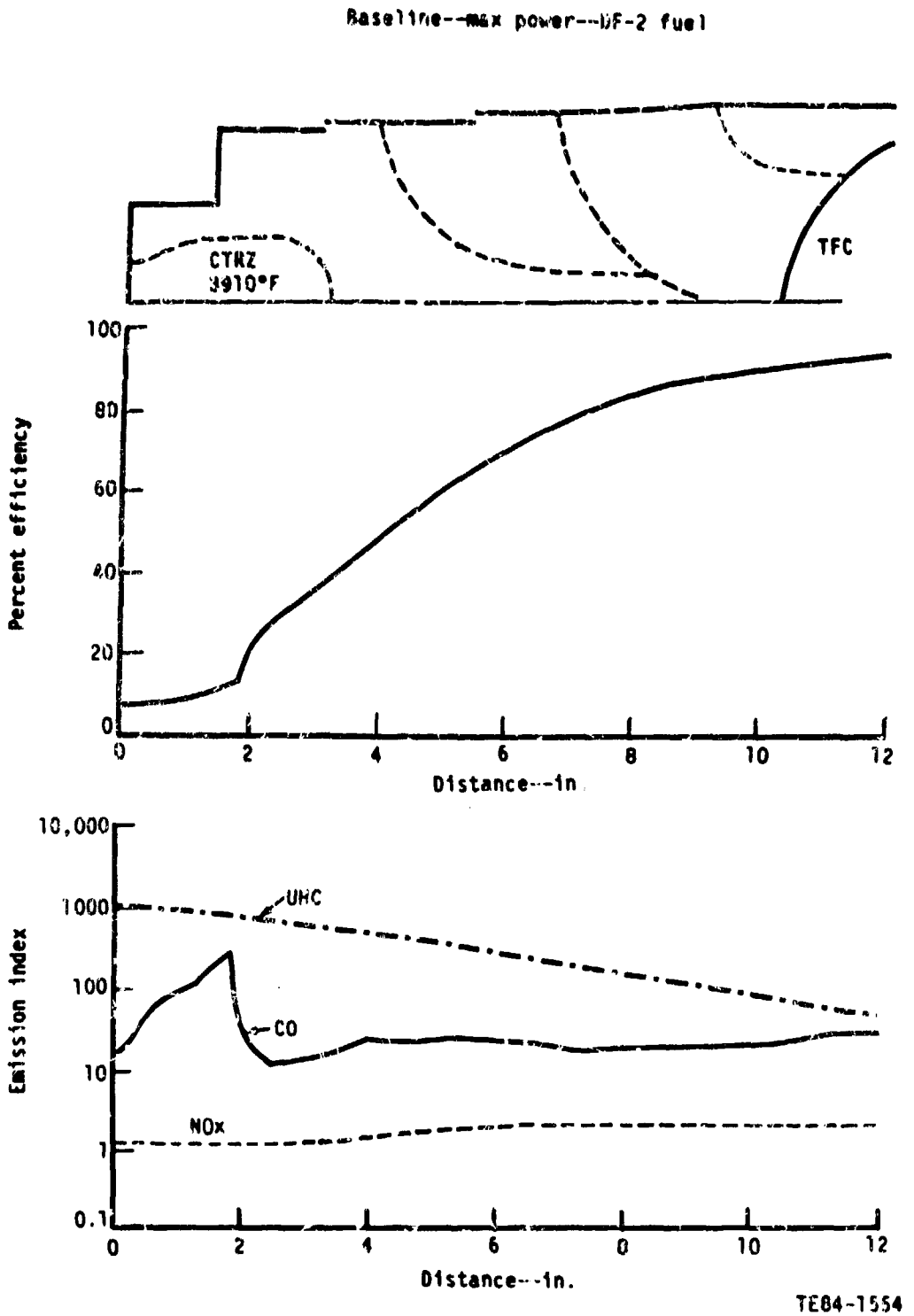

Figure 100. Baseline--maximum power with DF-2 fuel.

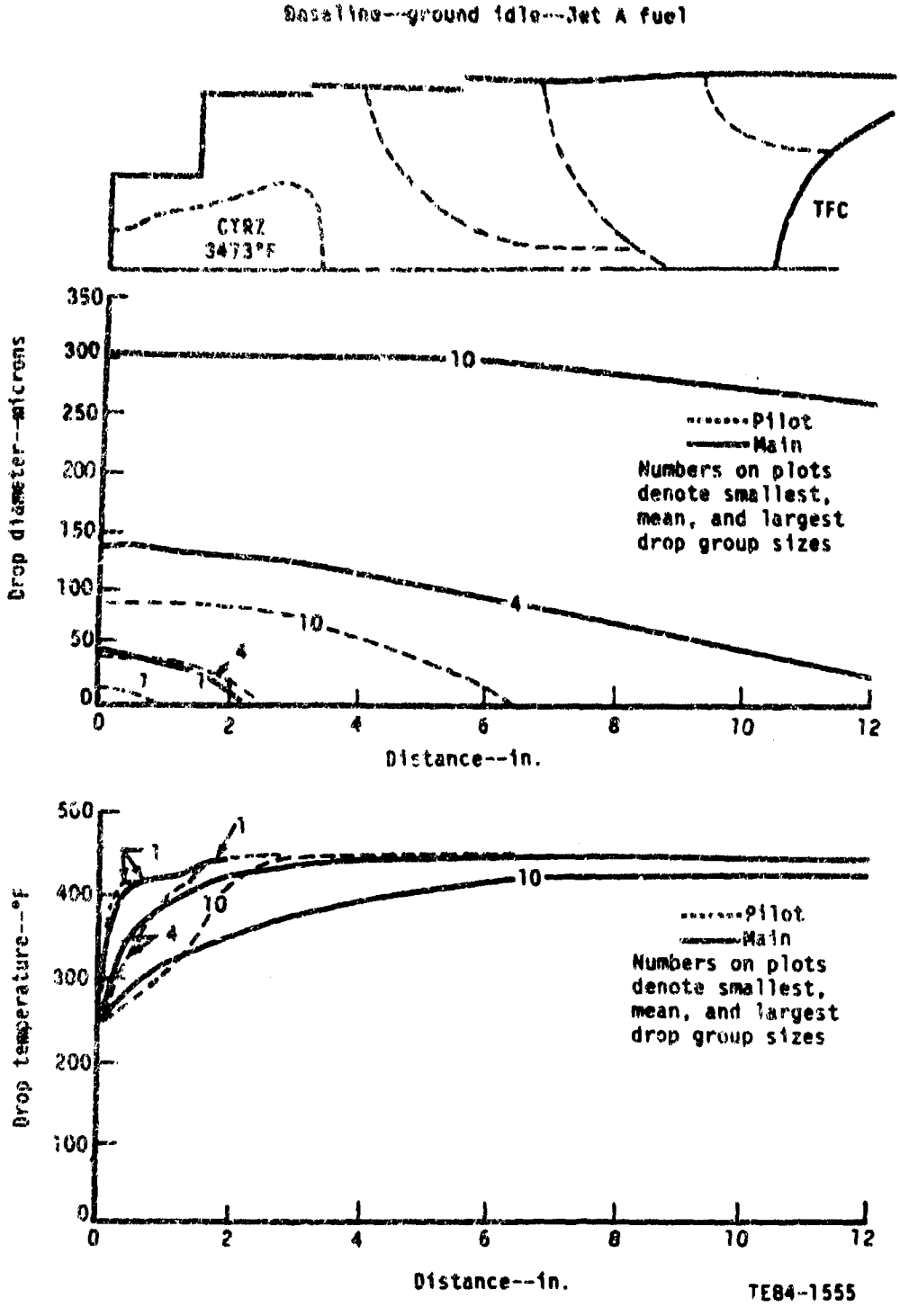

Figure 101. Baseline--ground idle with Jet A fuel.

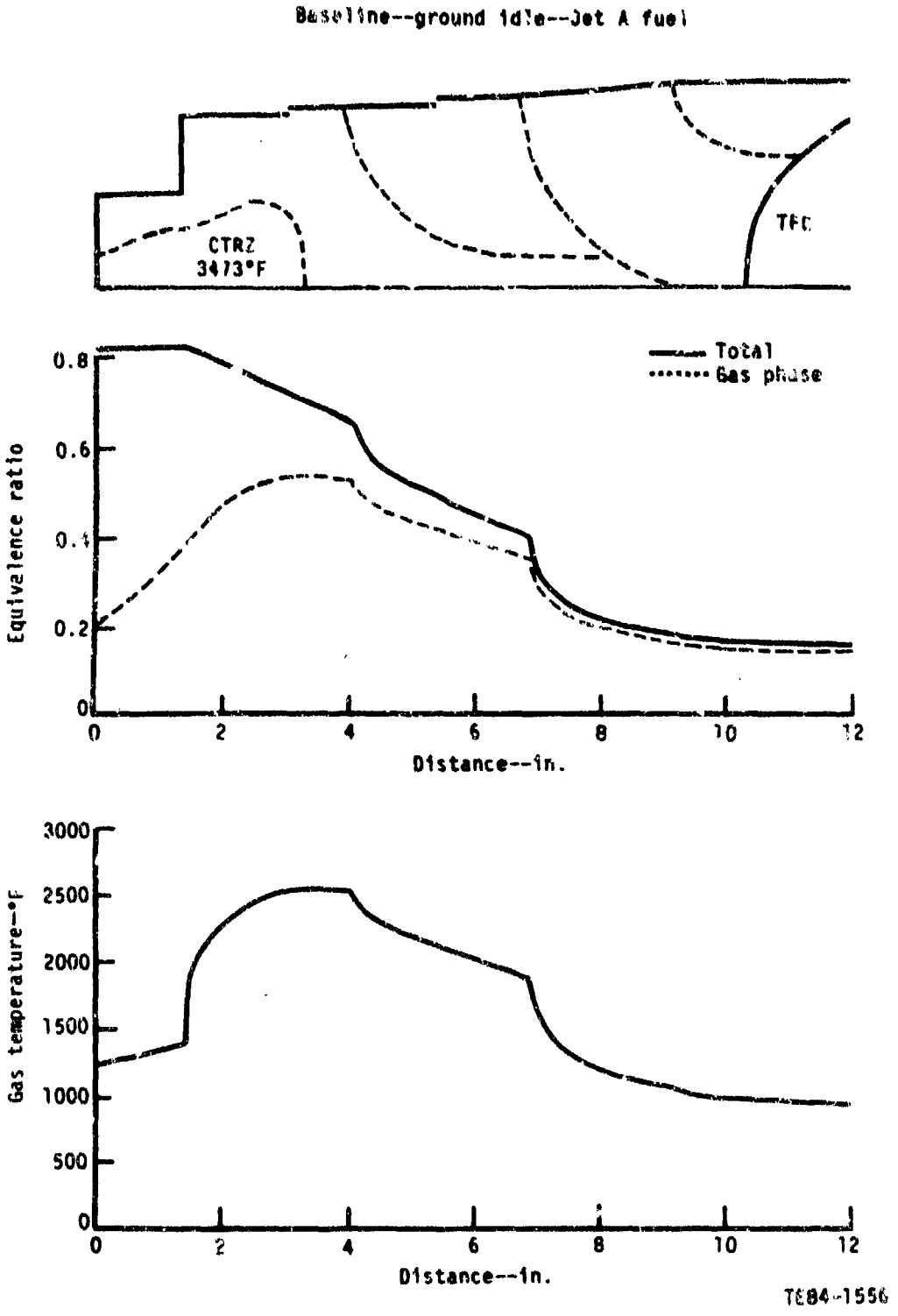

Figure 102. Baseline--ground idle with Jet A fuel.

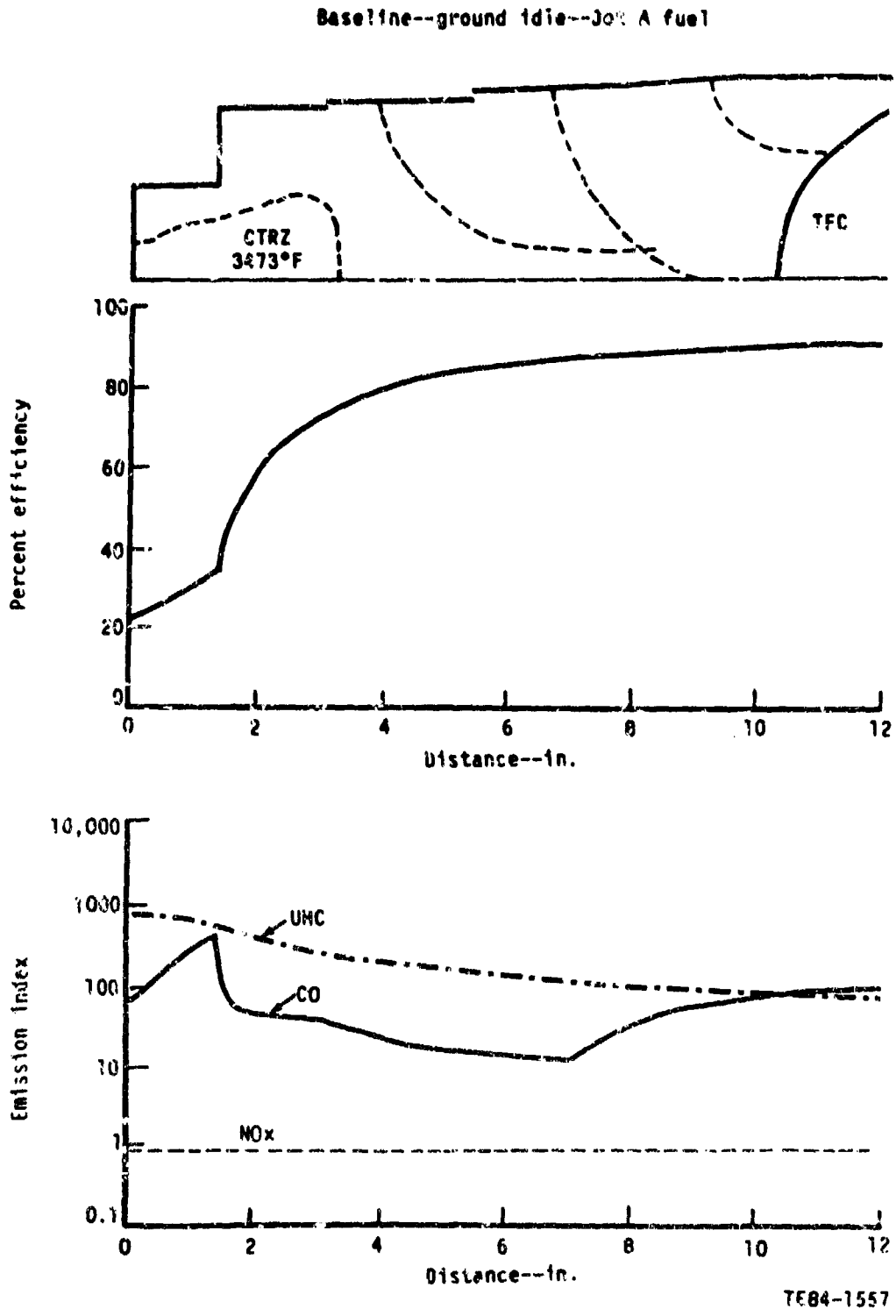

Figure 103. Baseline--ground idle with Jet A fuel.

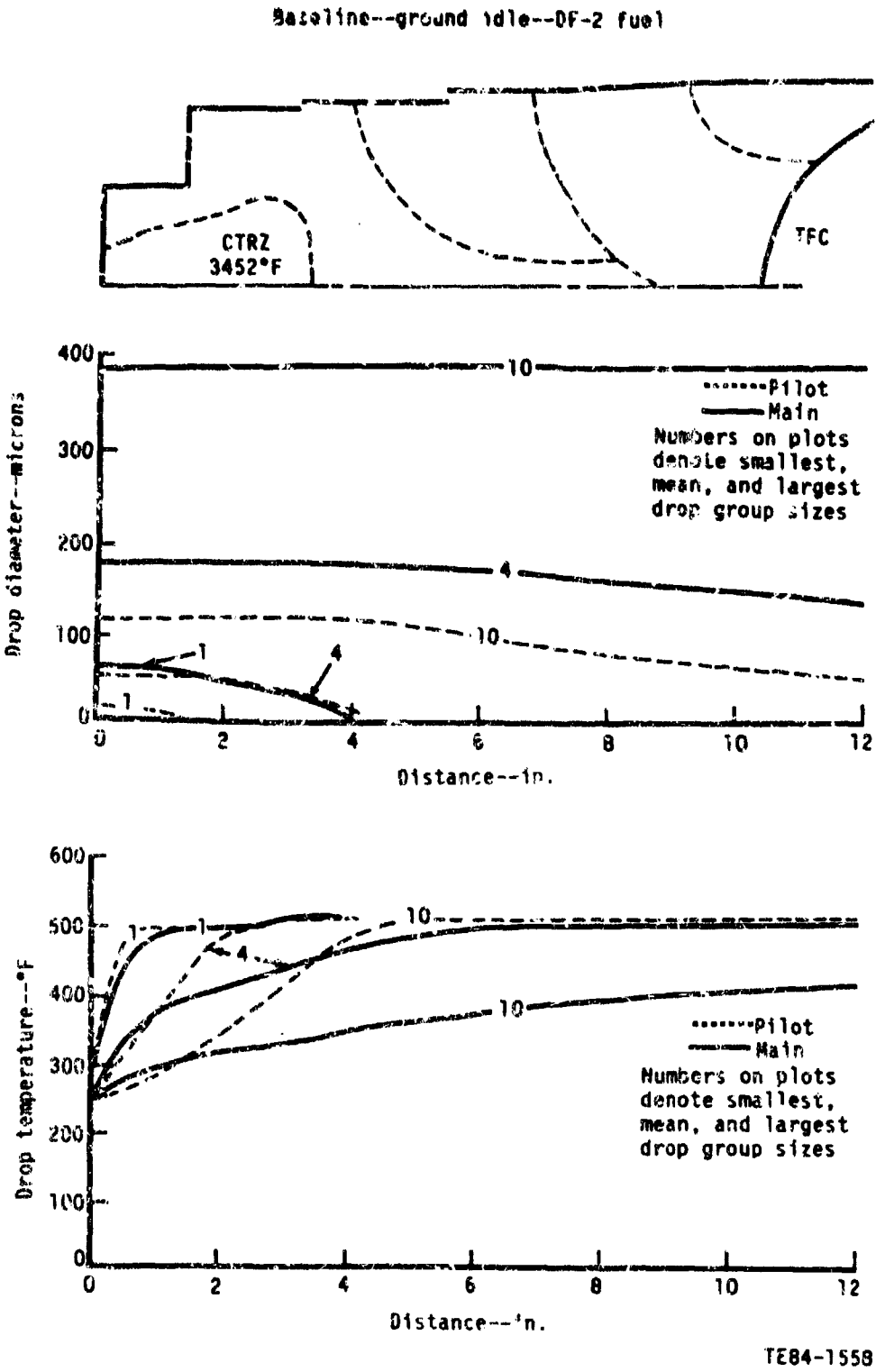

Figure 104. Baseline--ground idle with DF-2 fuel.

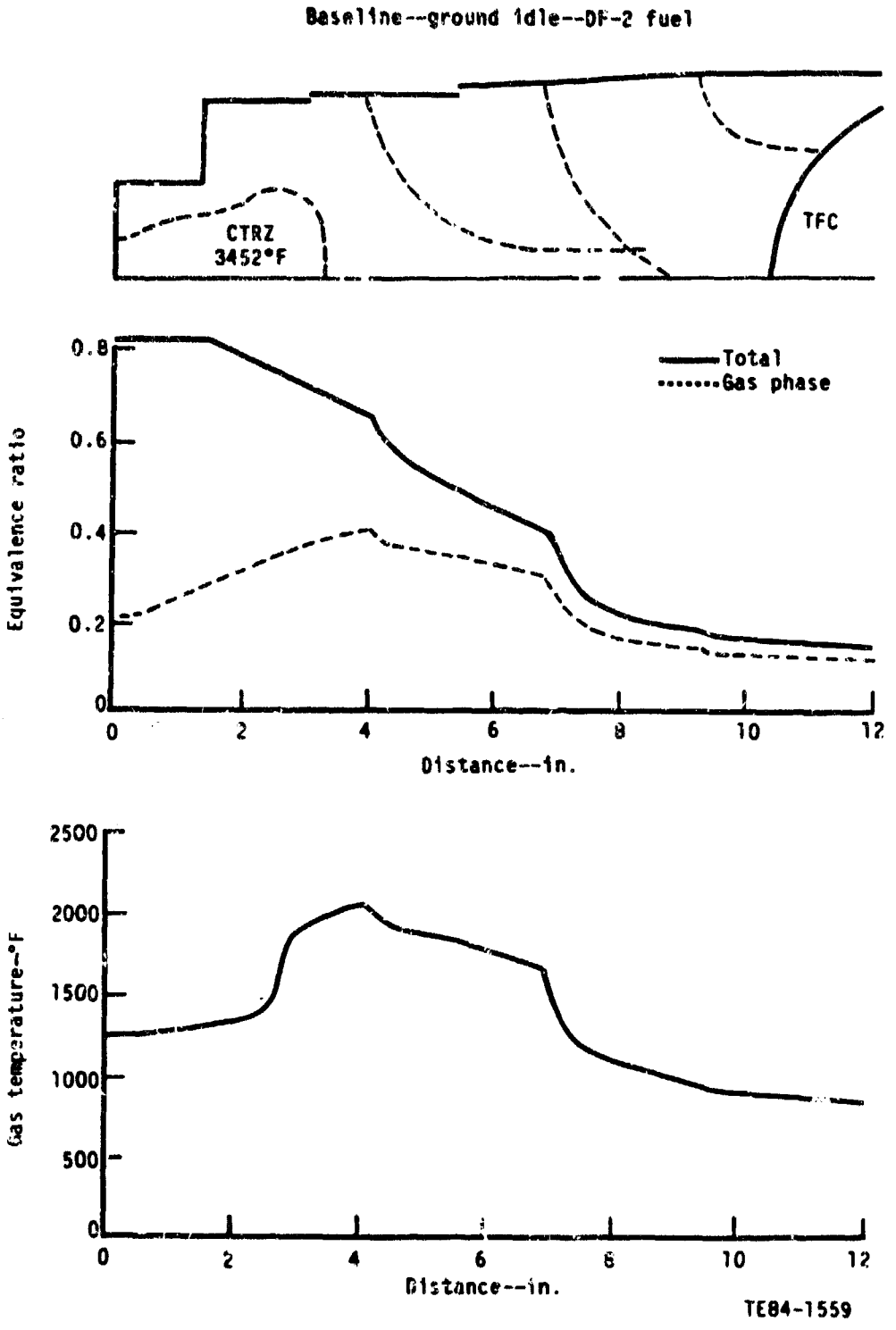

Figure 105. Baseline ground idle with DF-2 fuel.

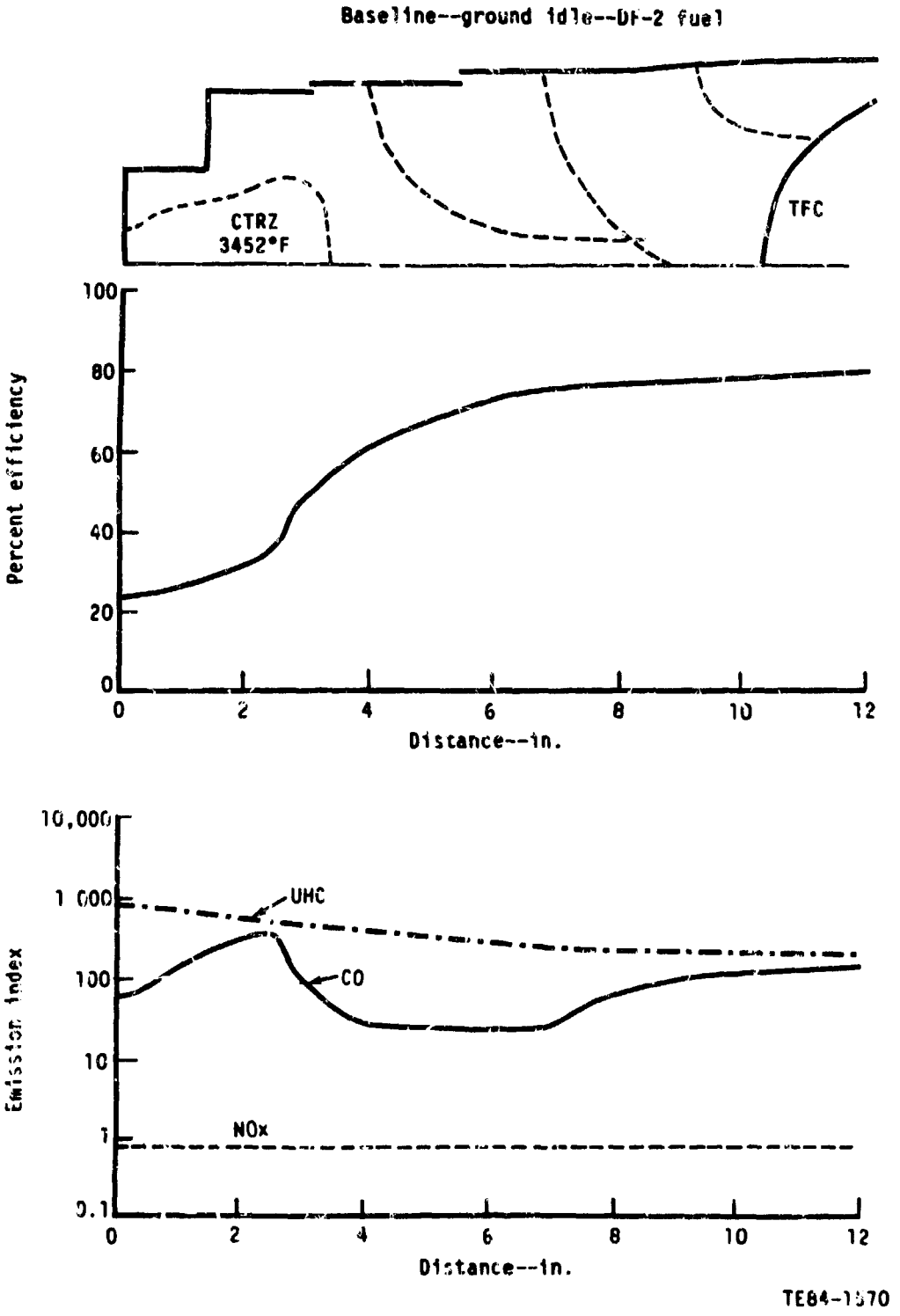

Figure 106. Baseline- ground idle with DF-2 fuel.

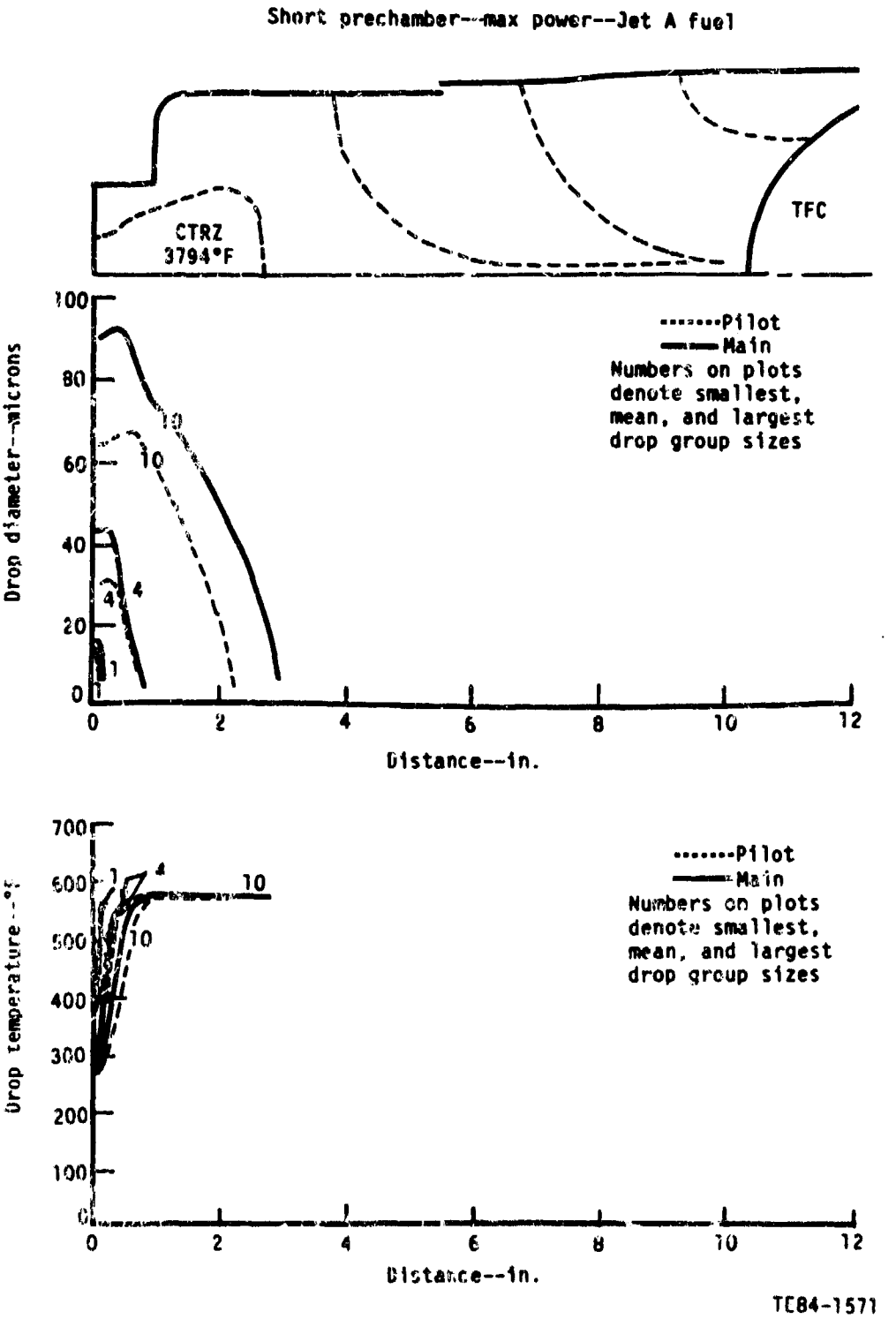

Figure 107. Short prechamber--maximum power with Jet A fuel.

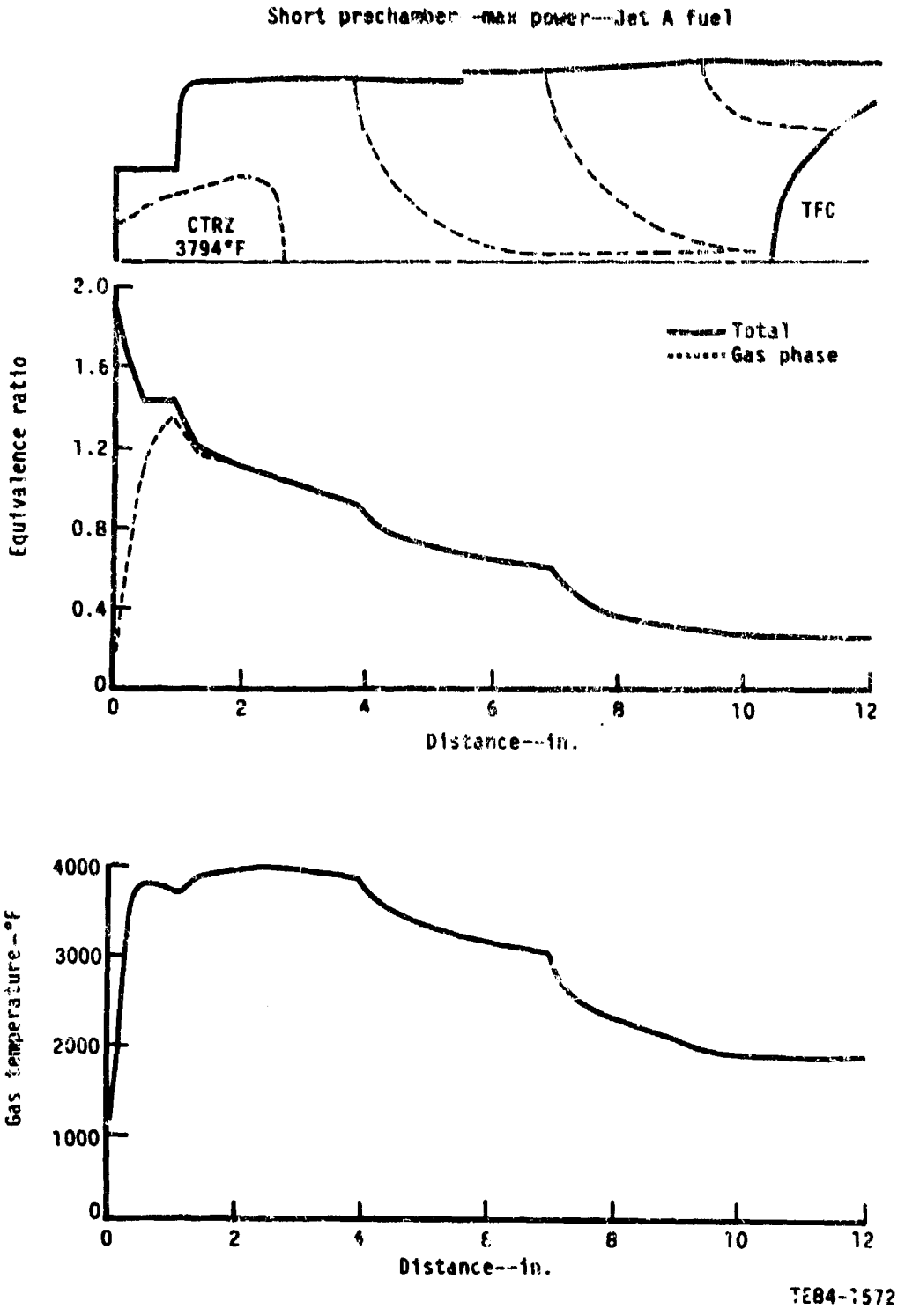

Figure 108. Short prechamber--maximum power with Jet A fuel

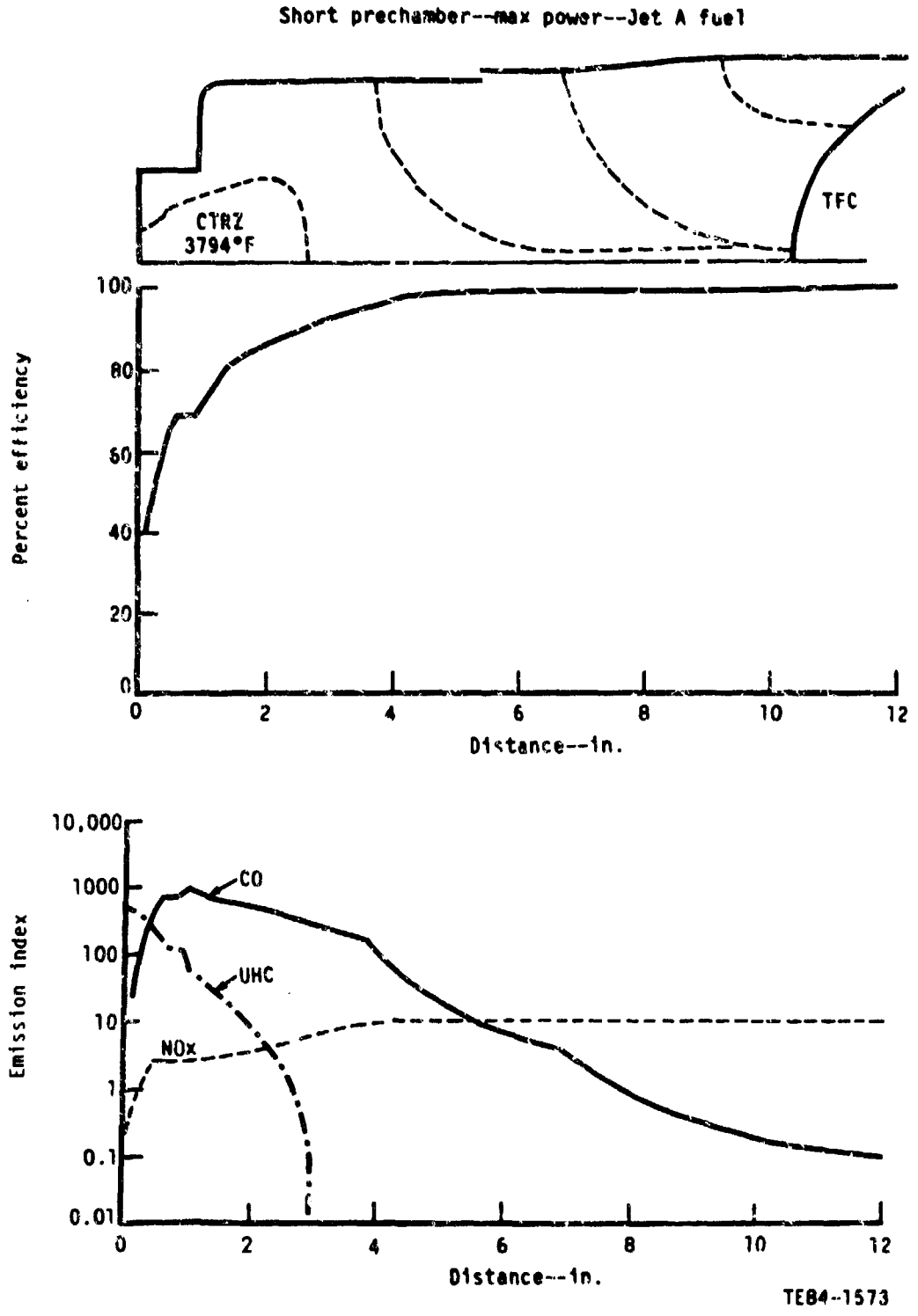

Figure 109. Short prechamber--maximum power with Jet A fuel.

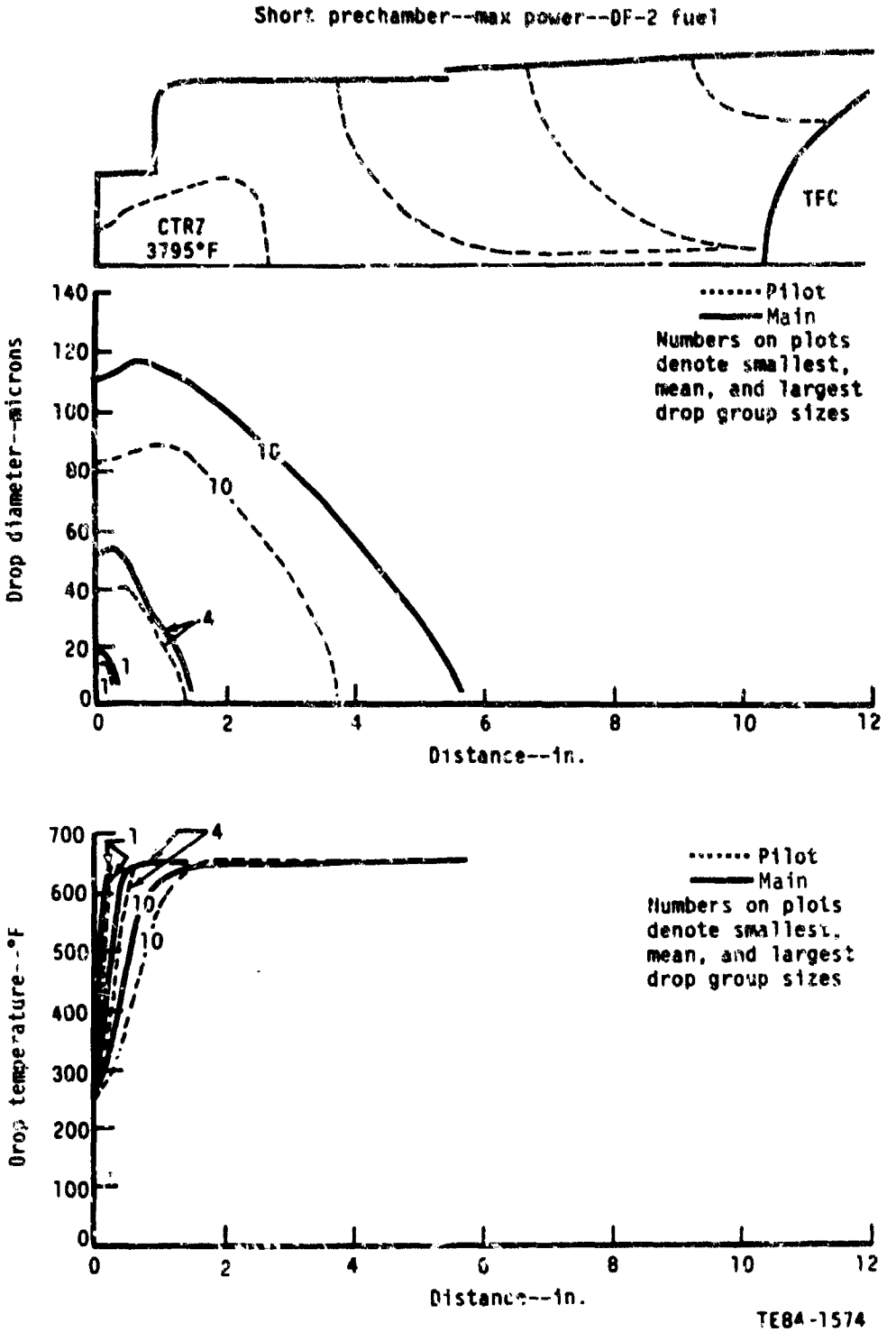

Figure 110. Short prechamber--maximum power with DF-2 fuel.

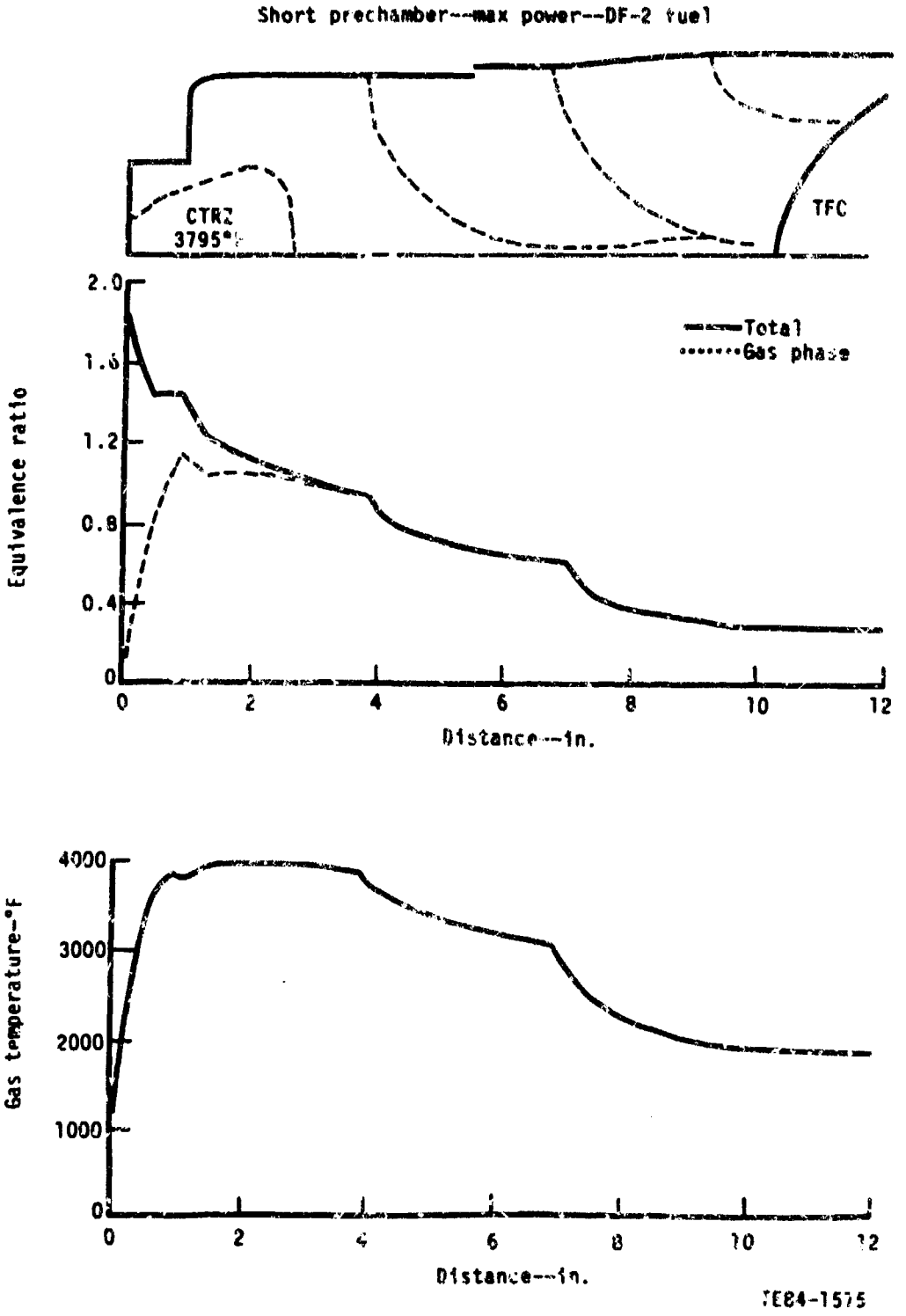

Figure 111. Short prechamber- maximum power with DF-2 fuel

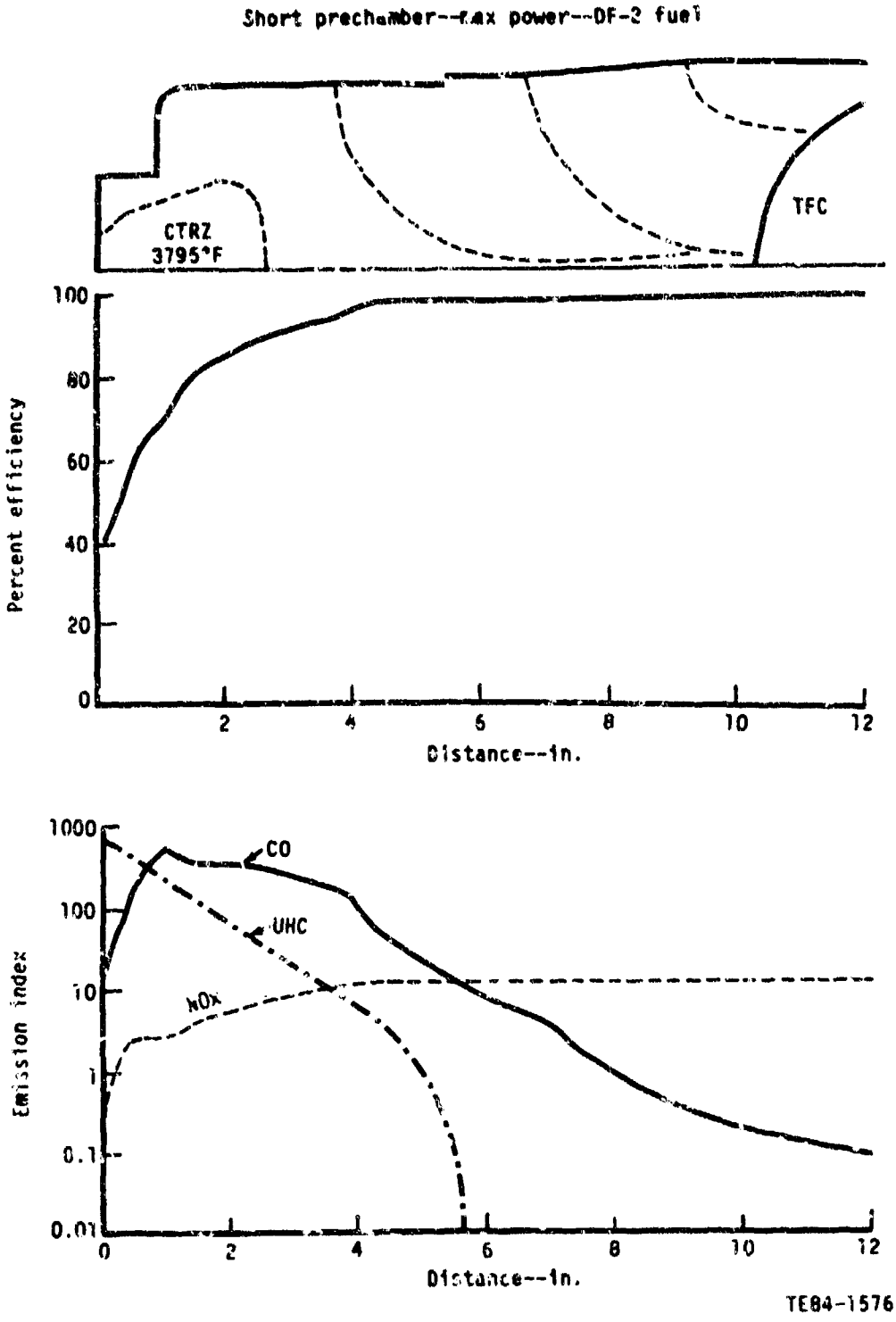

Figure 112. Short prechamber--maximum power with DF-2 fuel.

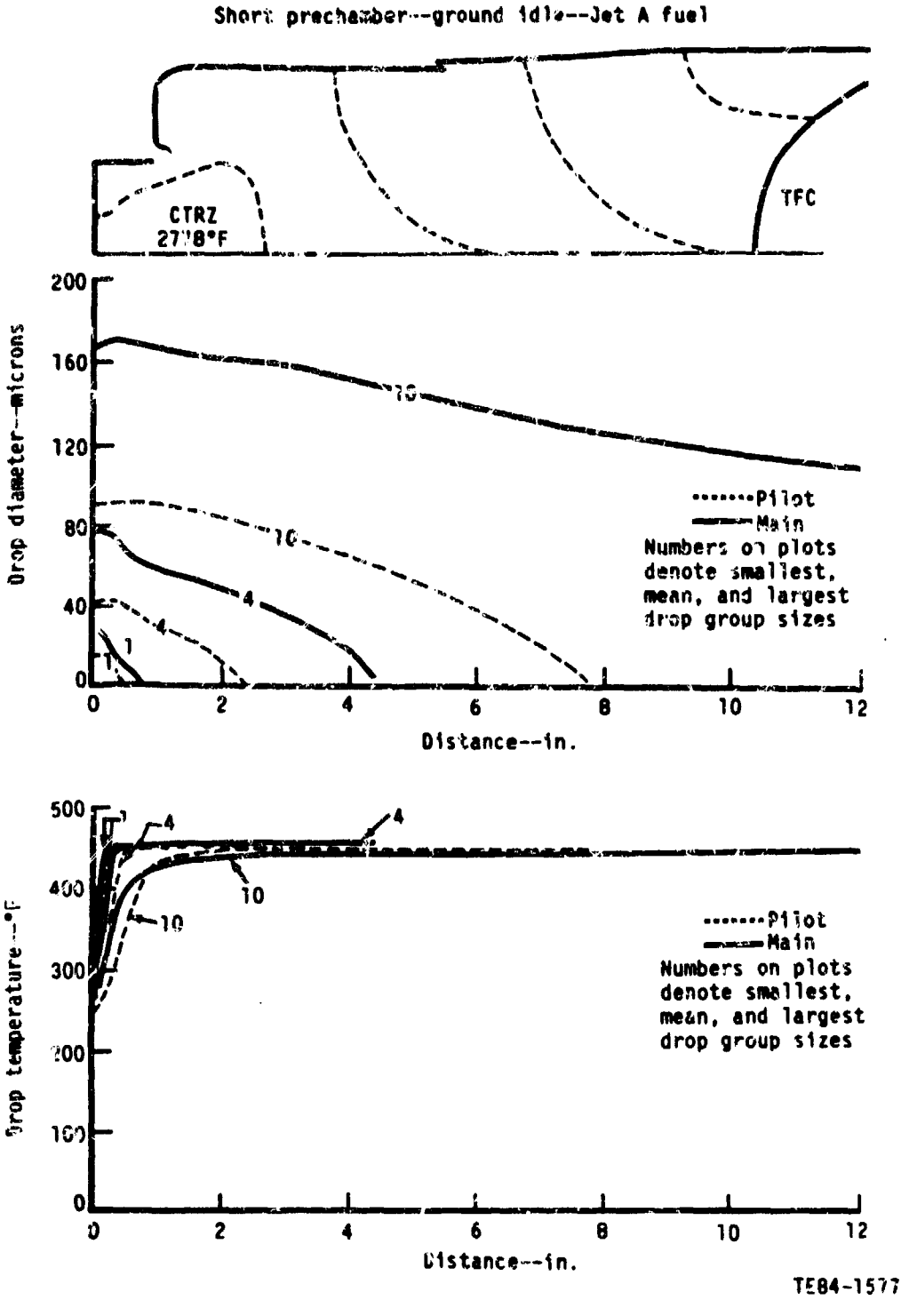

Figure 113. Short prechamber--ground idle with Jet A fuel.

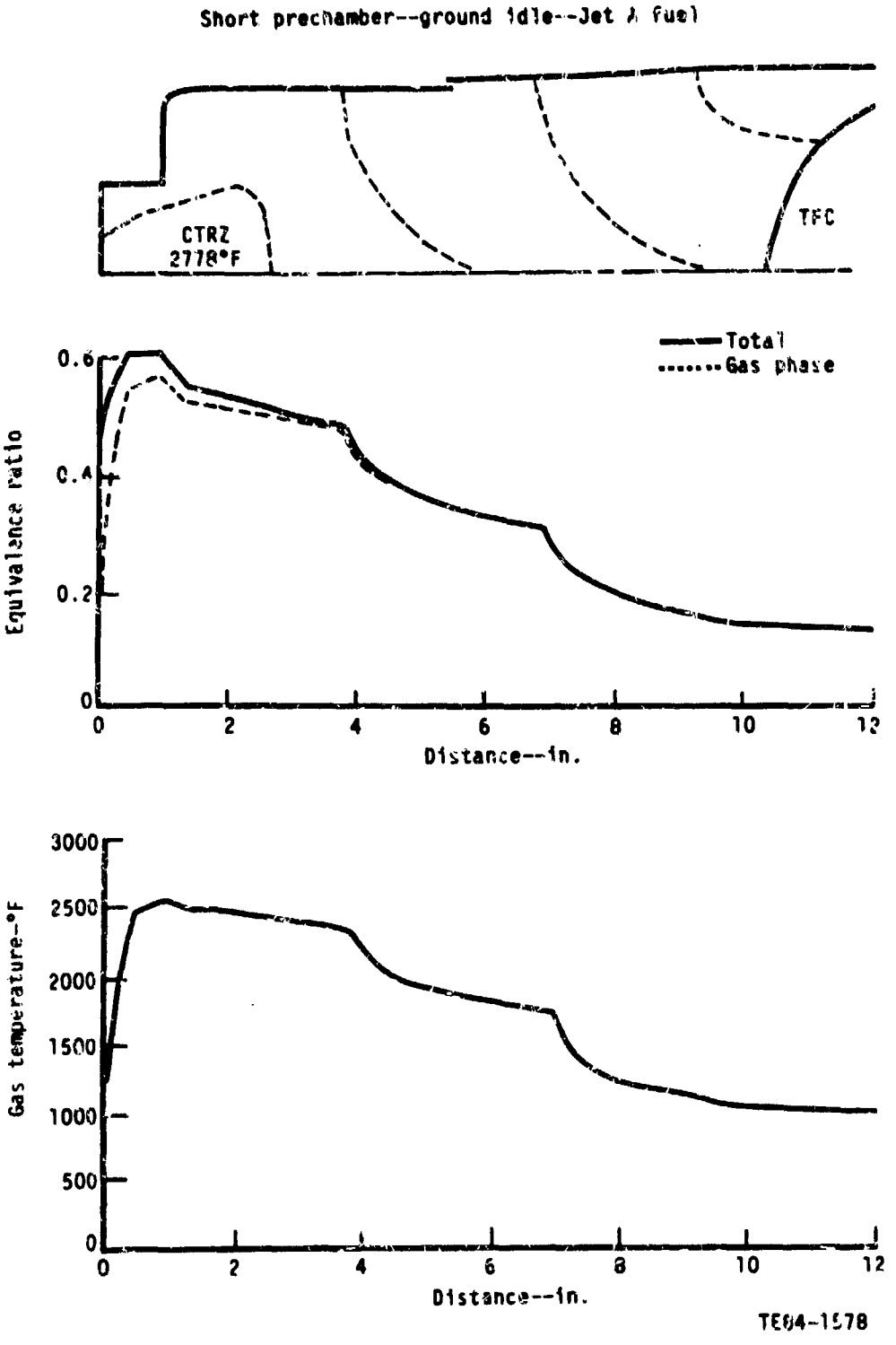

Figure 114. Short prechamber--ground idle with Jet A fuel.

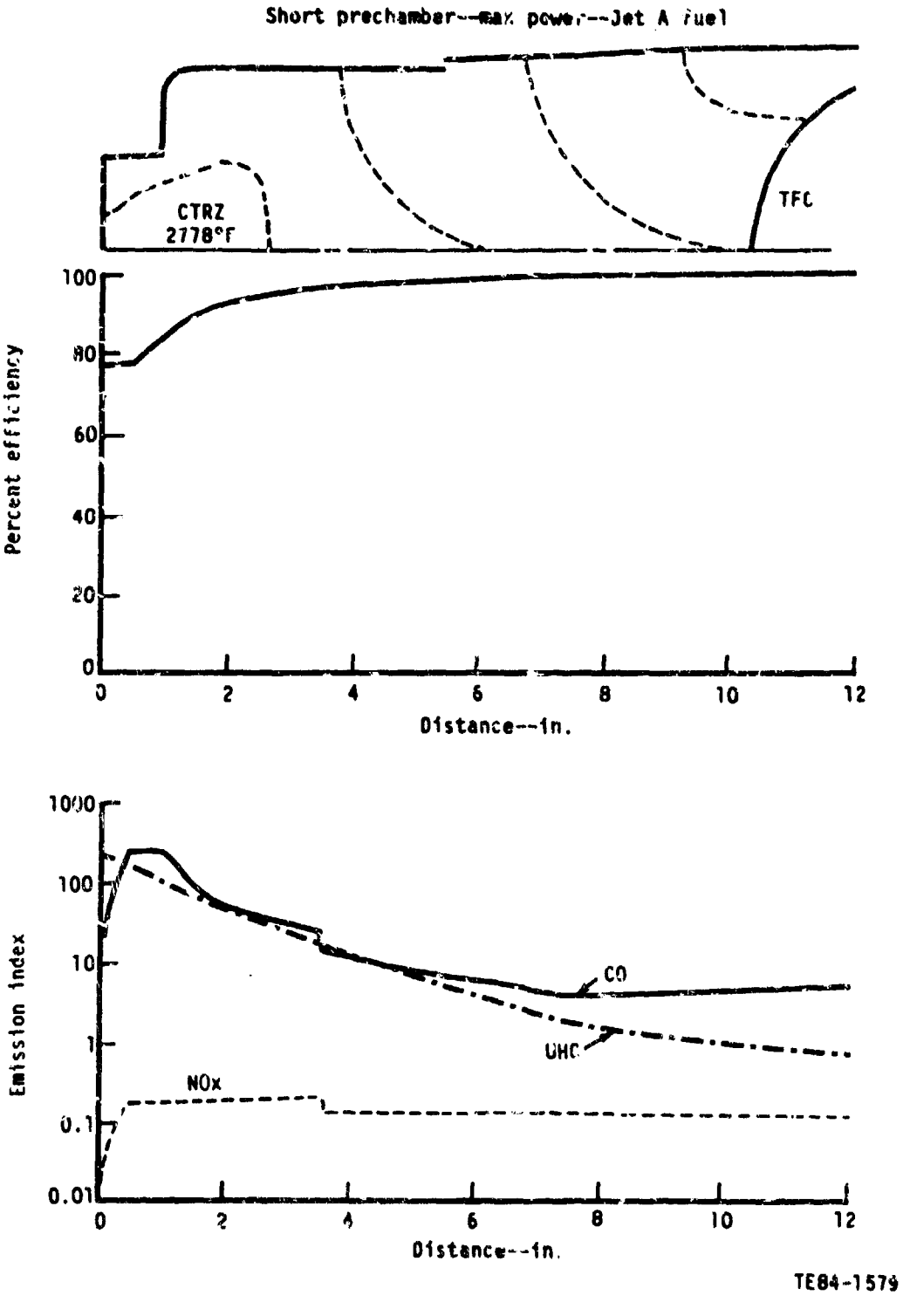

Figure 115. Short prechamber--ground idle with Jet A fuel

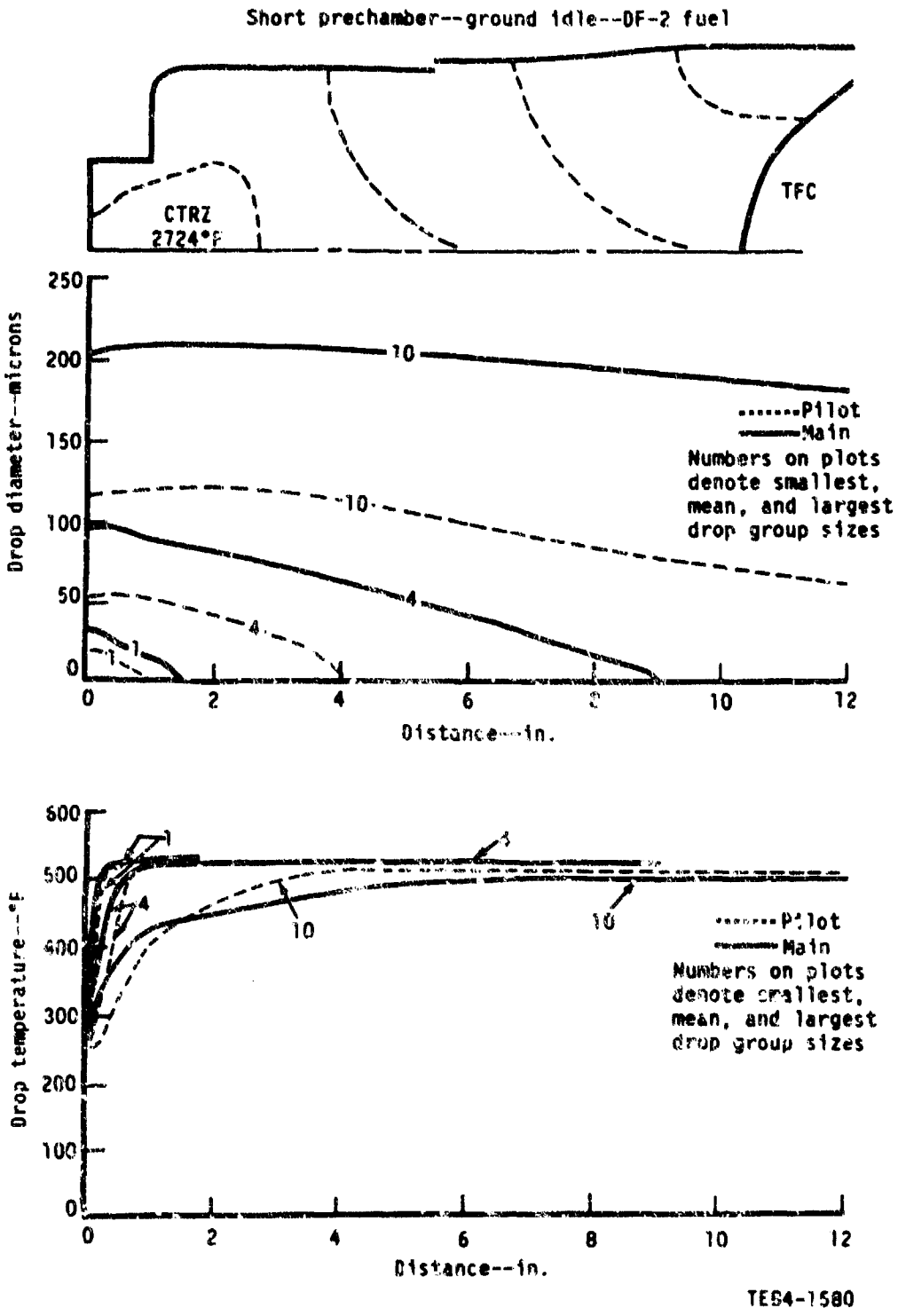

Figure 116. Short prechamber--ground idle with DF 2 fuel.

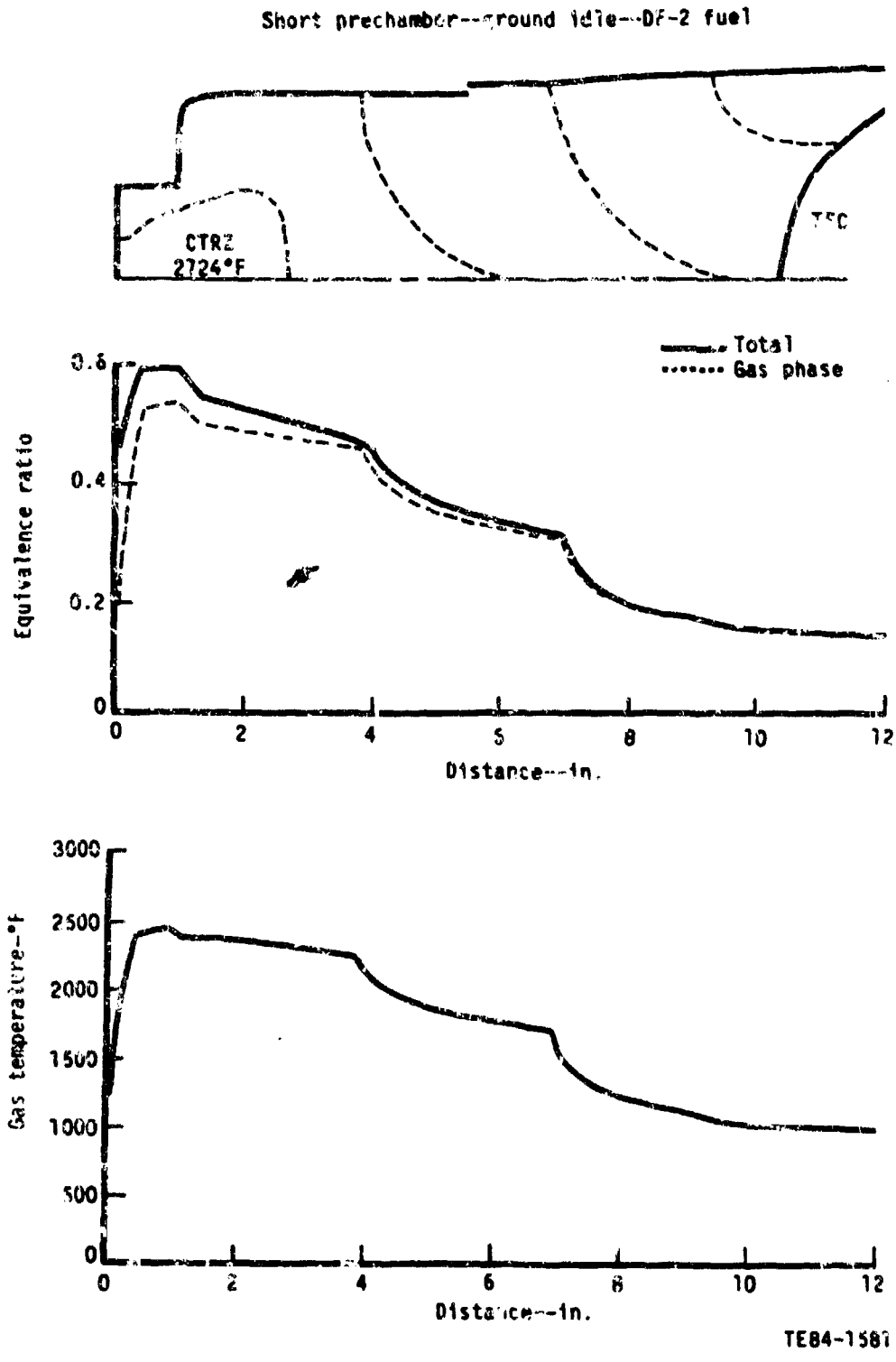

Figure 117. Short prechamber--ground idle with DF-2 fuel.

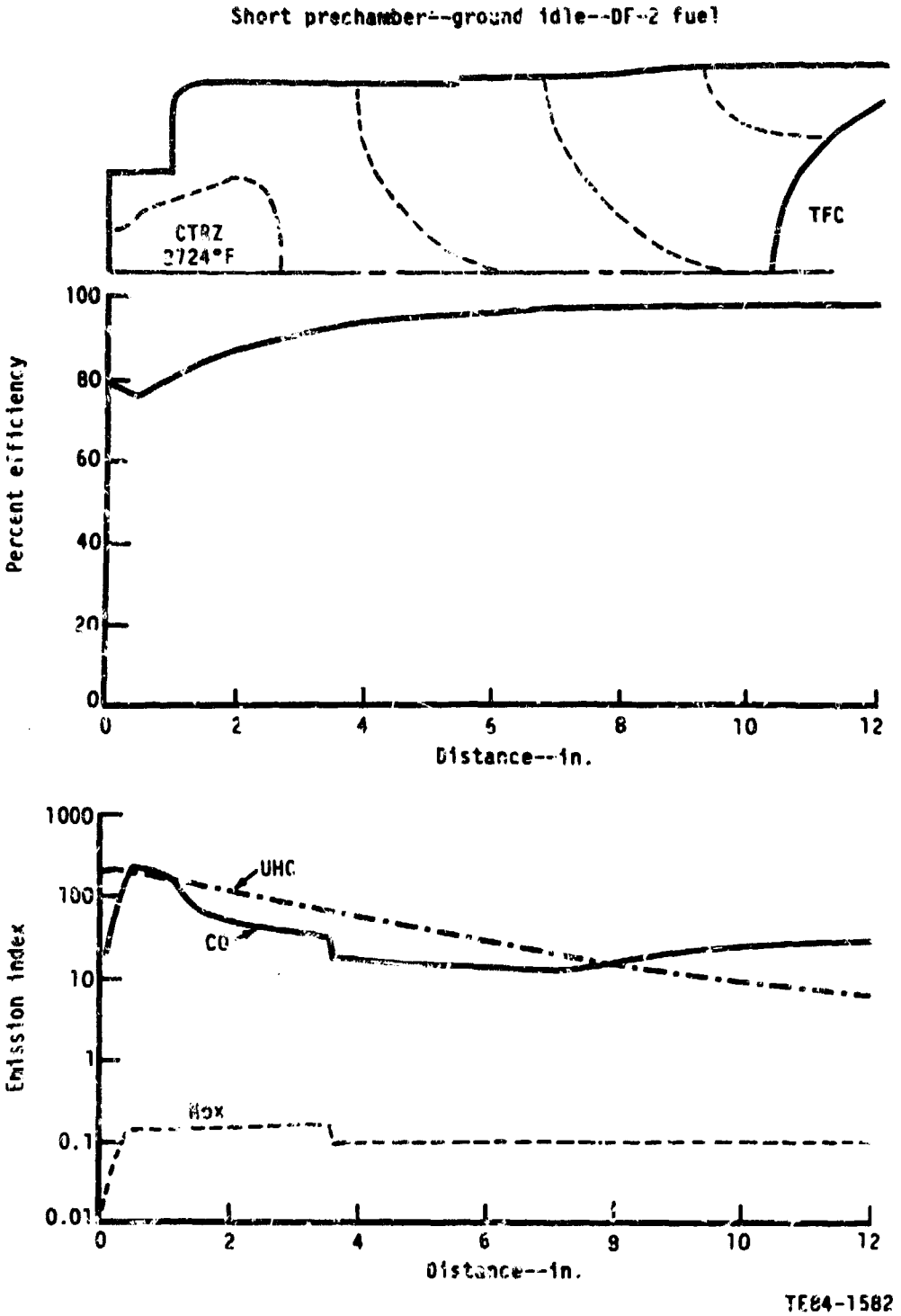

Figure 118. Short prechamber--ground idle with DF-2 fuel.

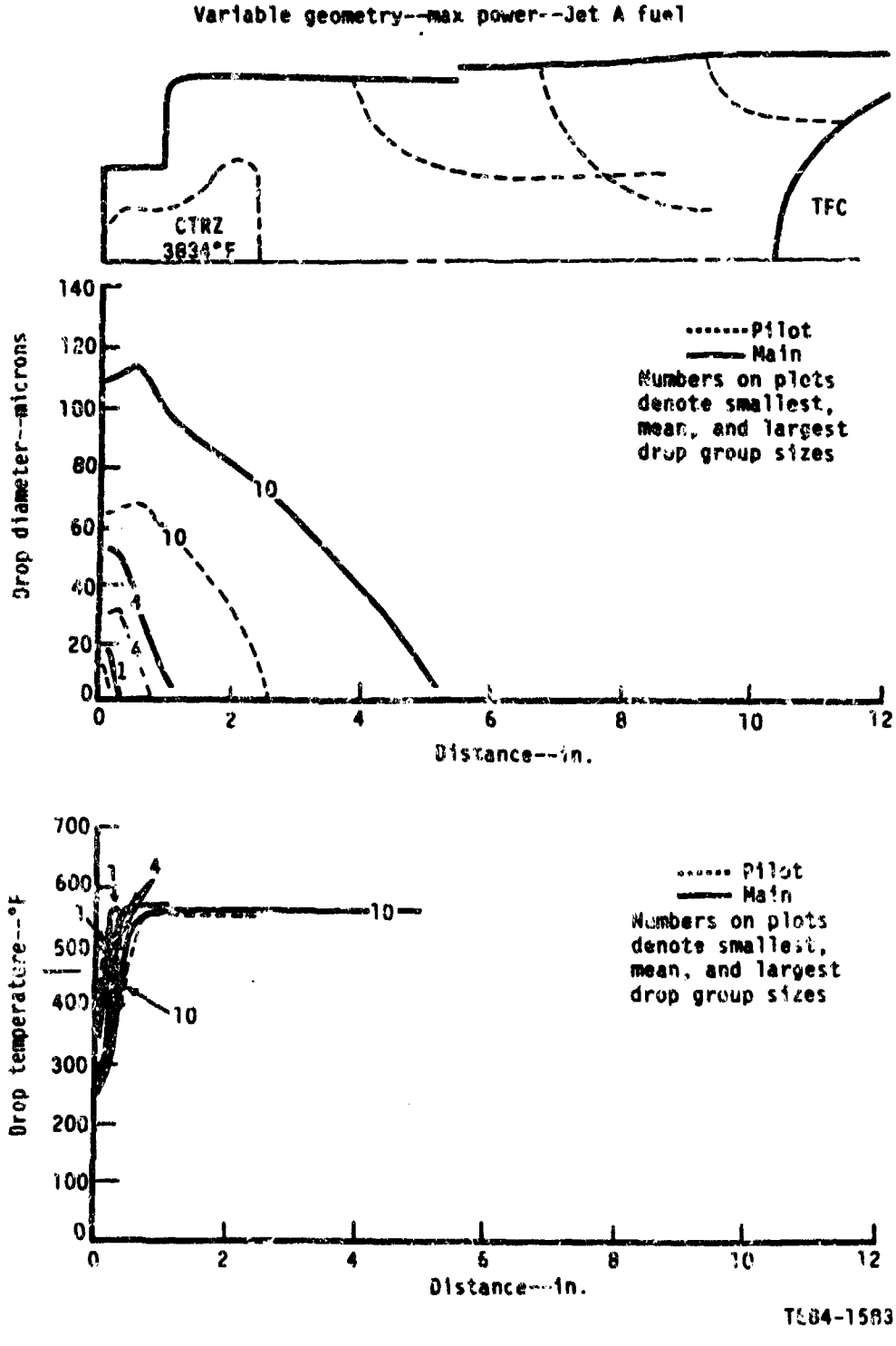

Figure 119. Variable geometry--maximum power with Jet A fuel.

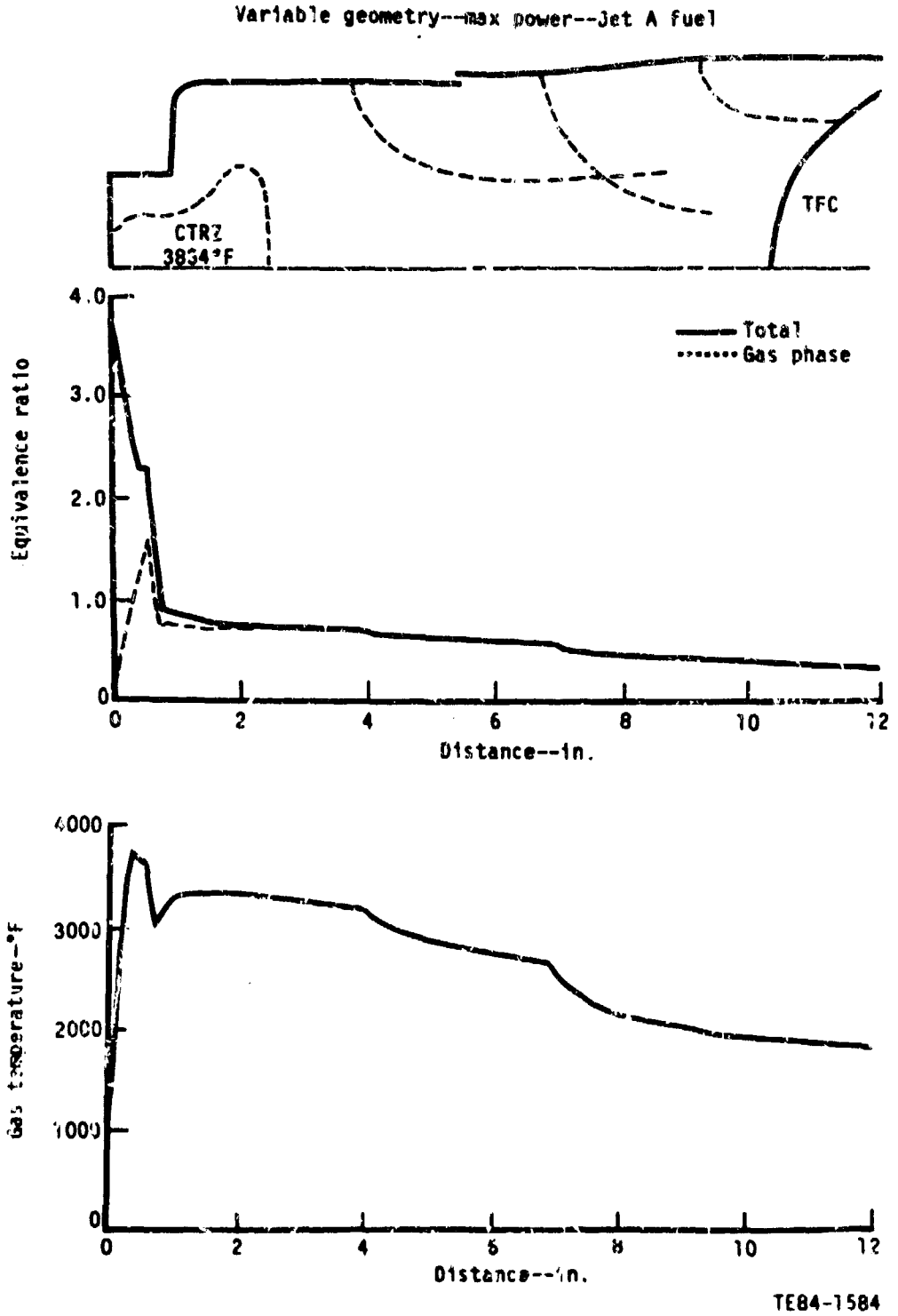

Figure 120. Variable geometry--maximum power with Jet A fuel.

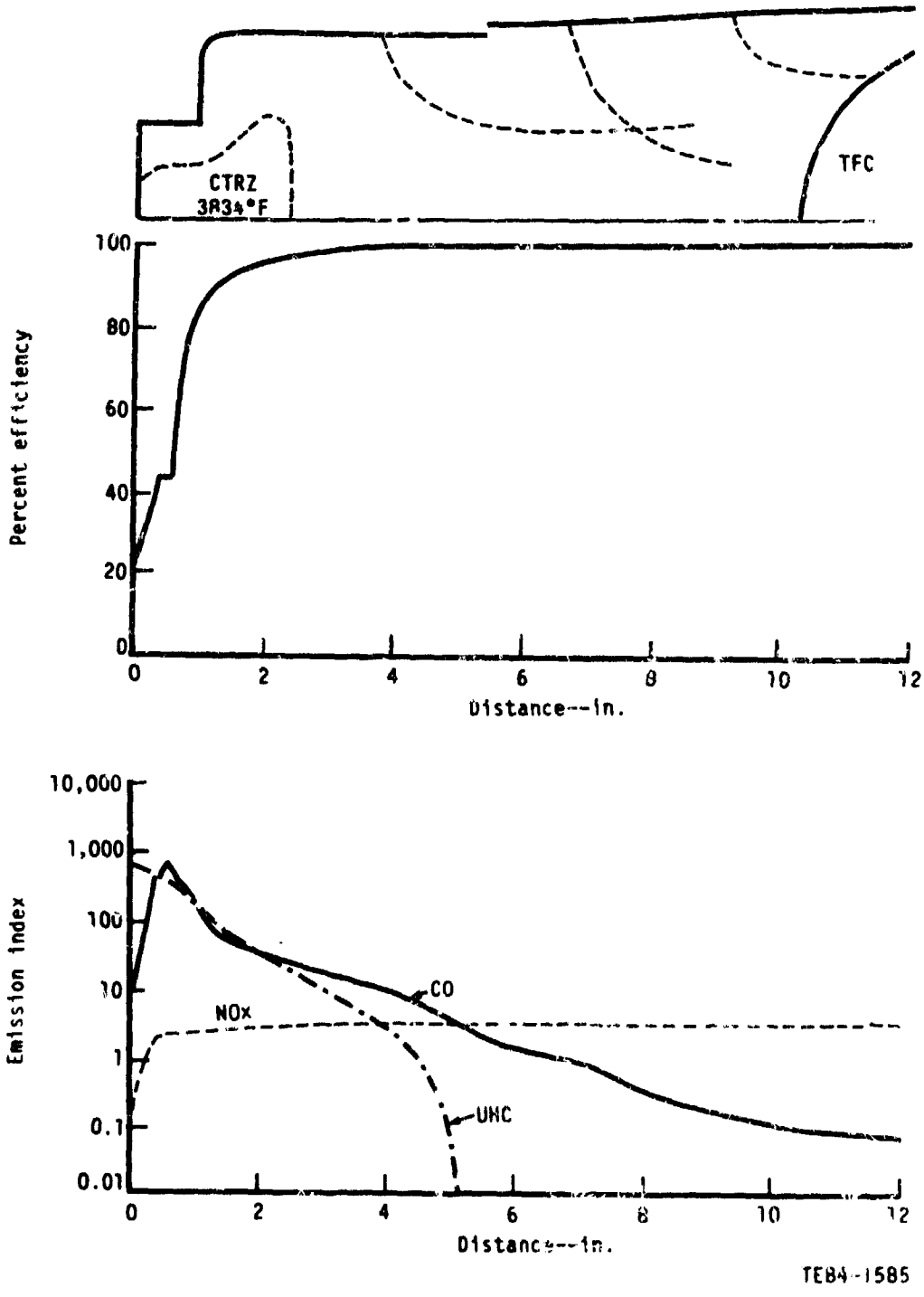

Figure 121. Variable geometry--maximum power with Jet A fuel.

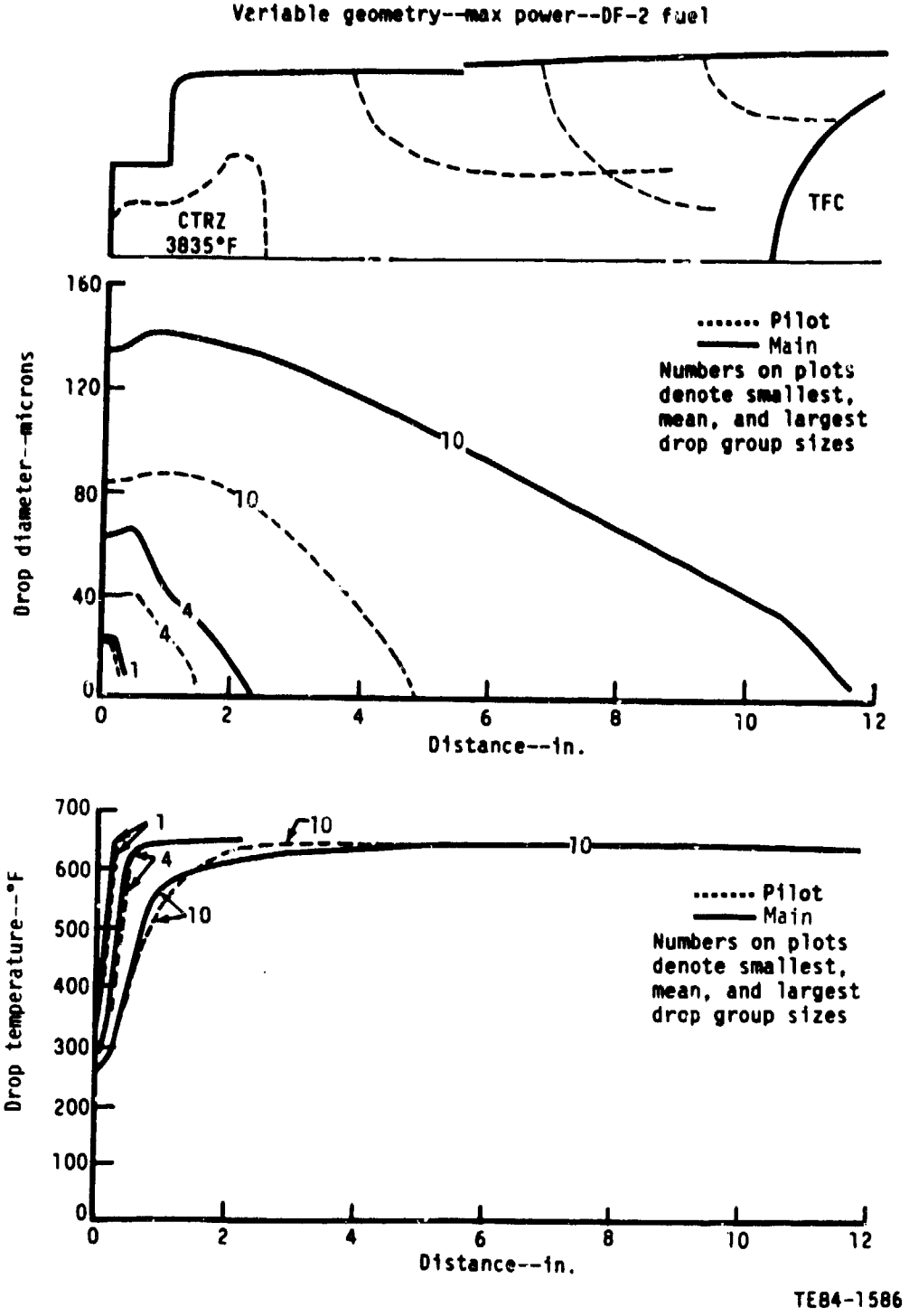

Figure 122. Variable geometry--maximum power with DF-2 fuel.

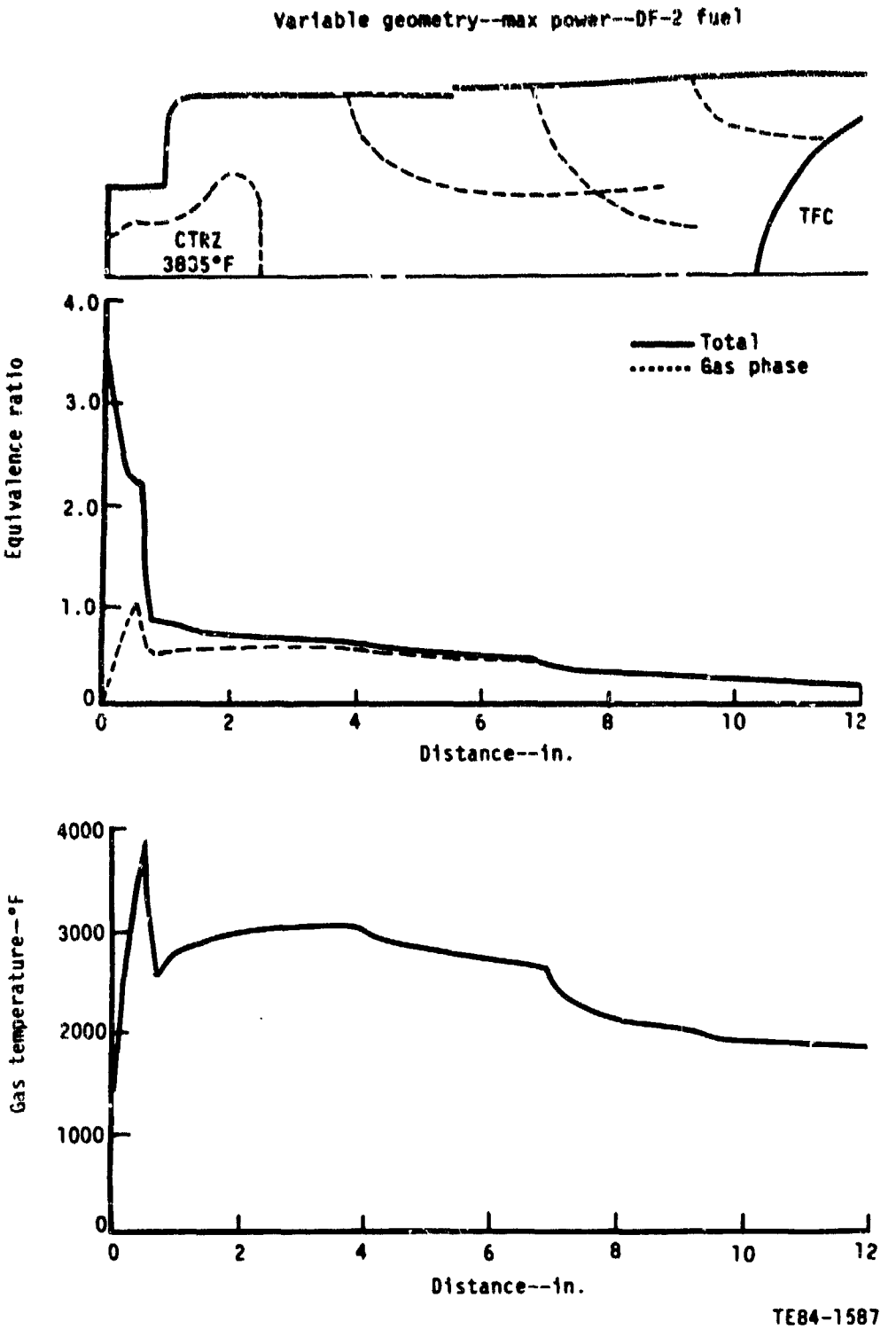

Figure 123. Variable geometry--maximum power with DF-2 fuel.

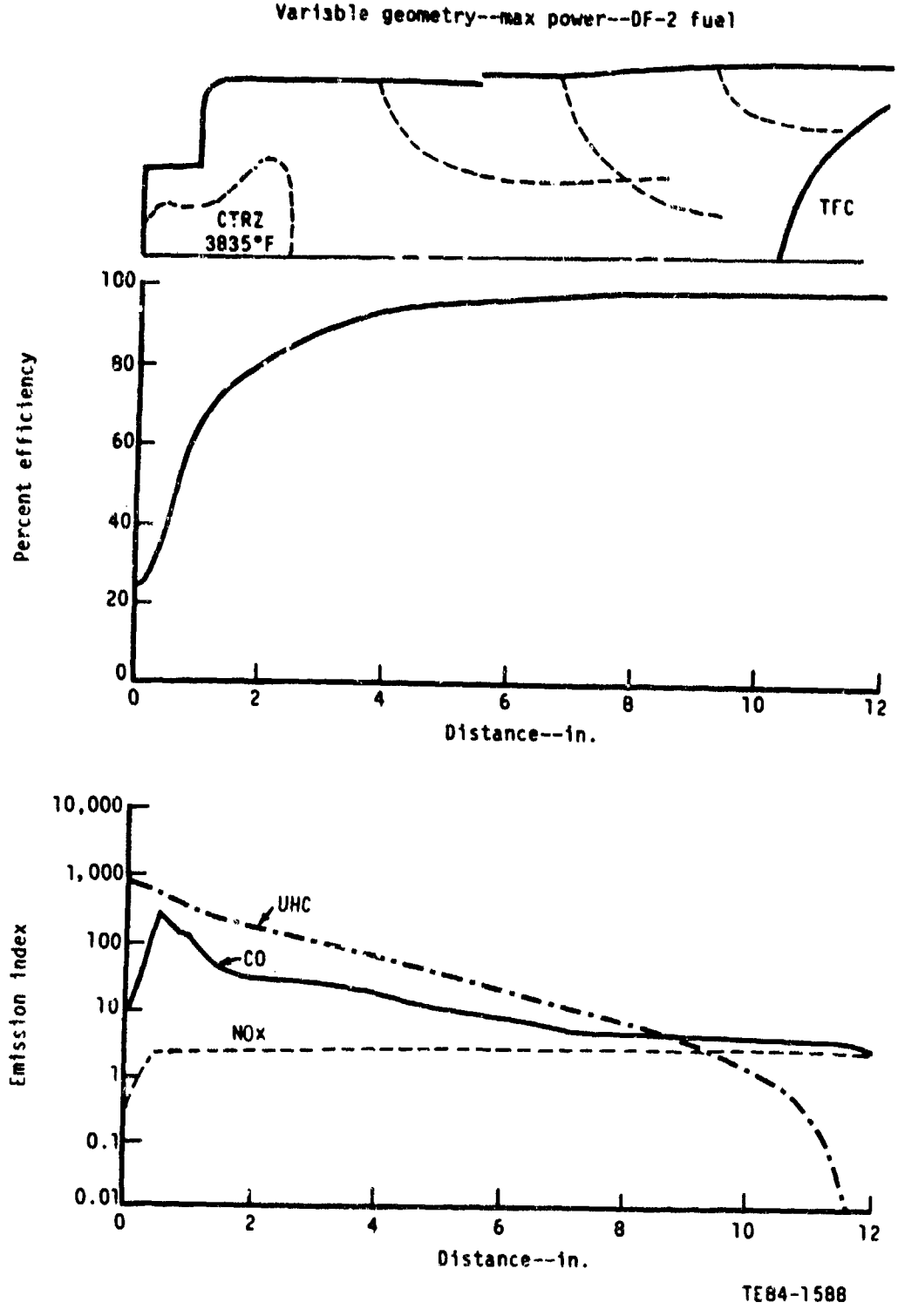

Figure 124. Variable geometry--maximum power with DF-2 fuel.

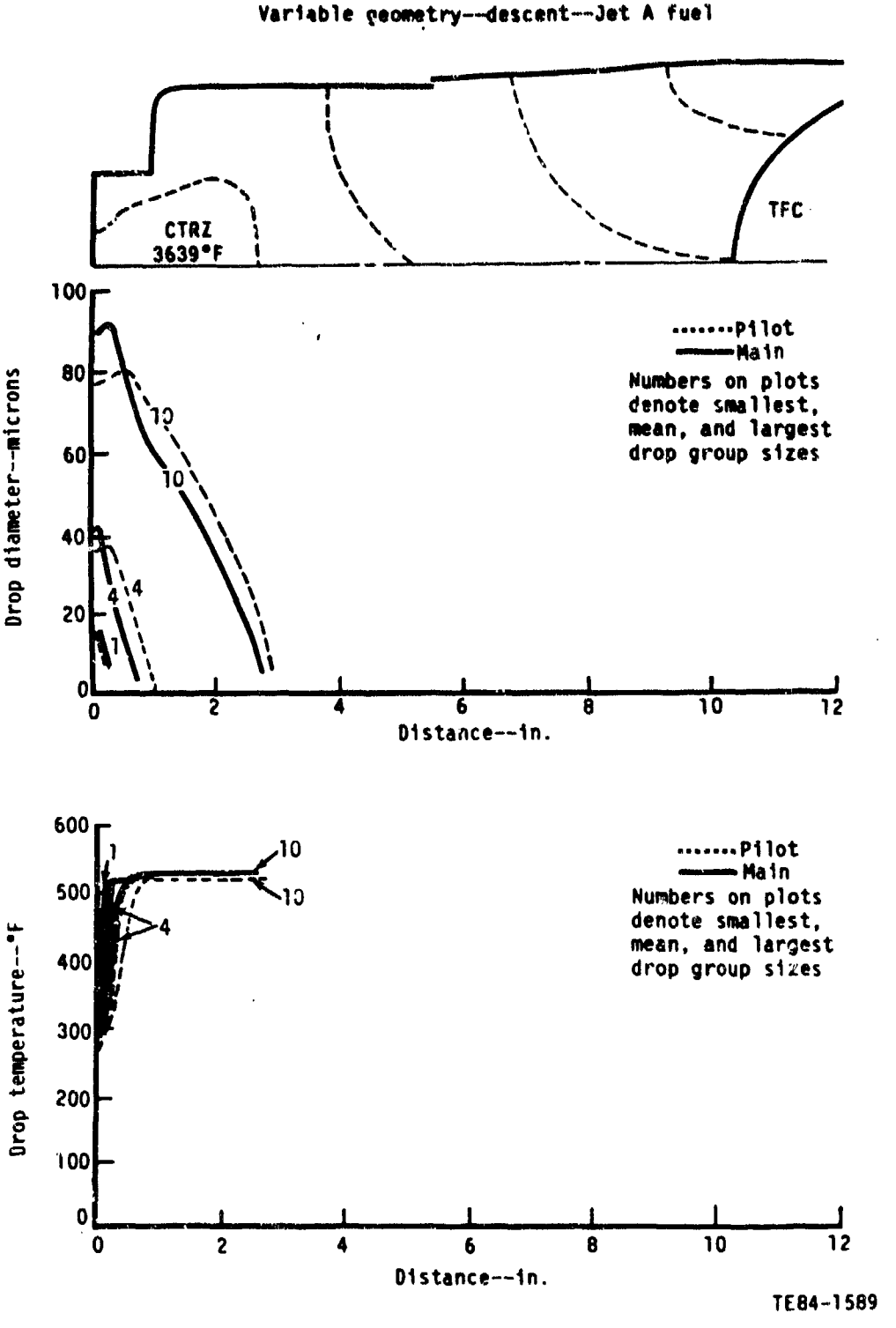

Figure 125. Variable geometry--descent with Jet A fuel.

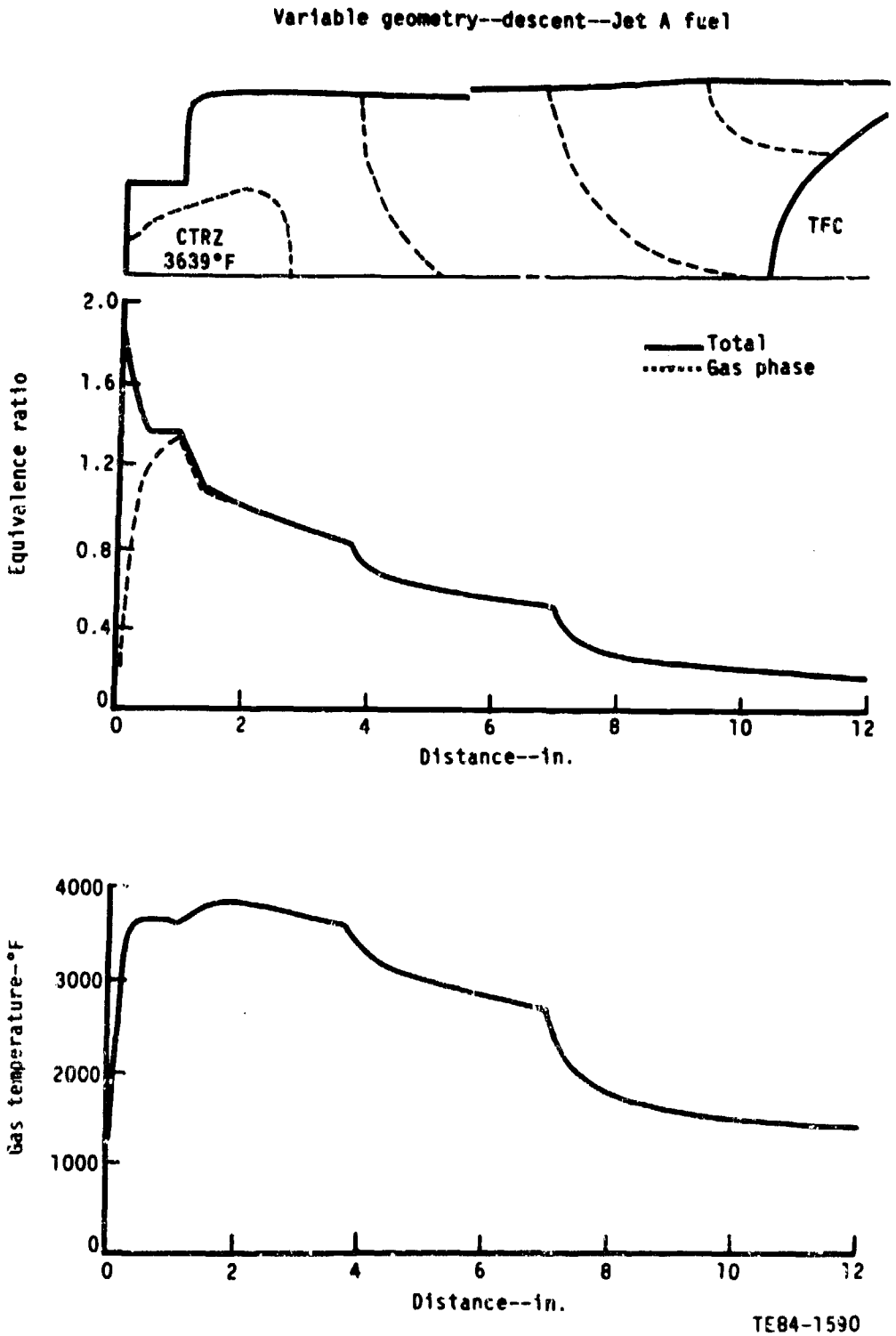

Figure 126. Variable geometry--descent with Jet A fuel.

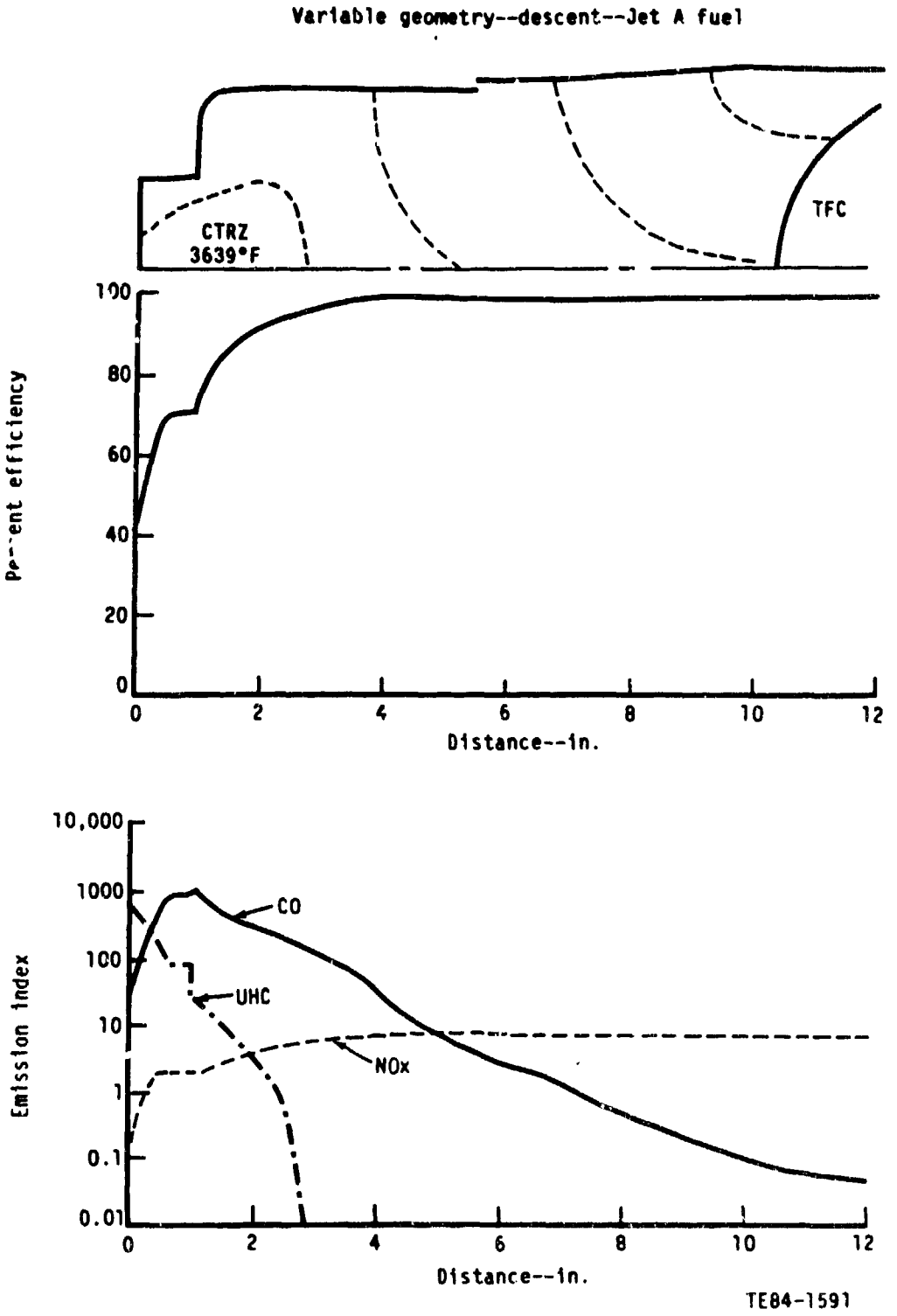

Figure 127. Variable geometry--descent with Jet A fuel.

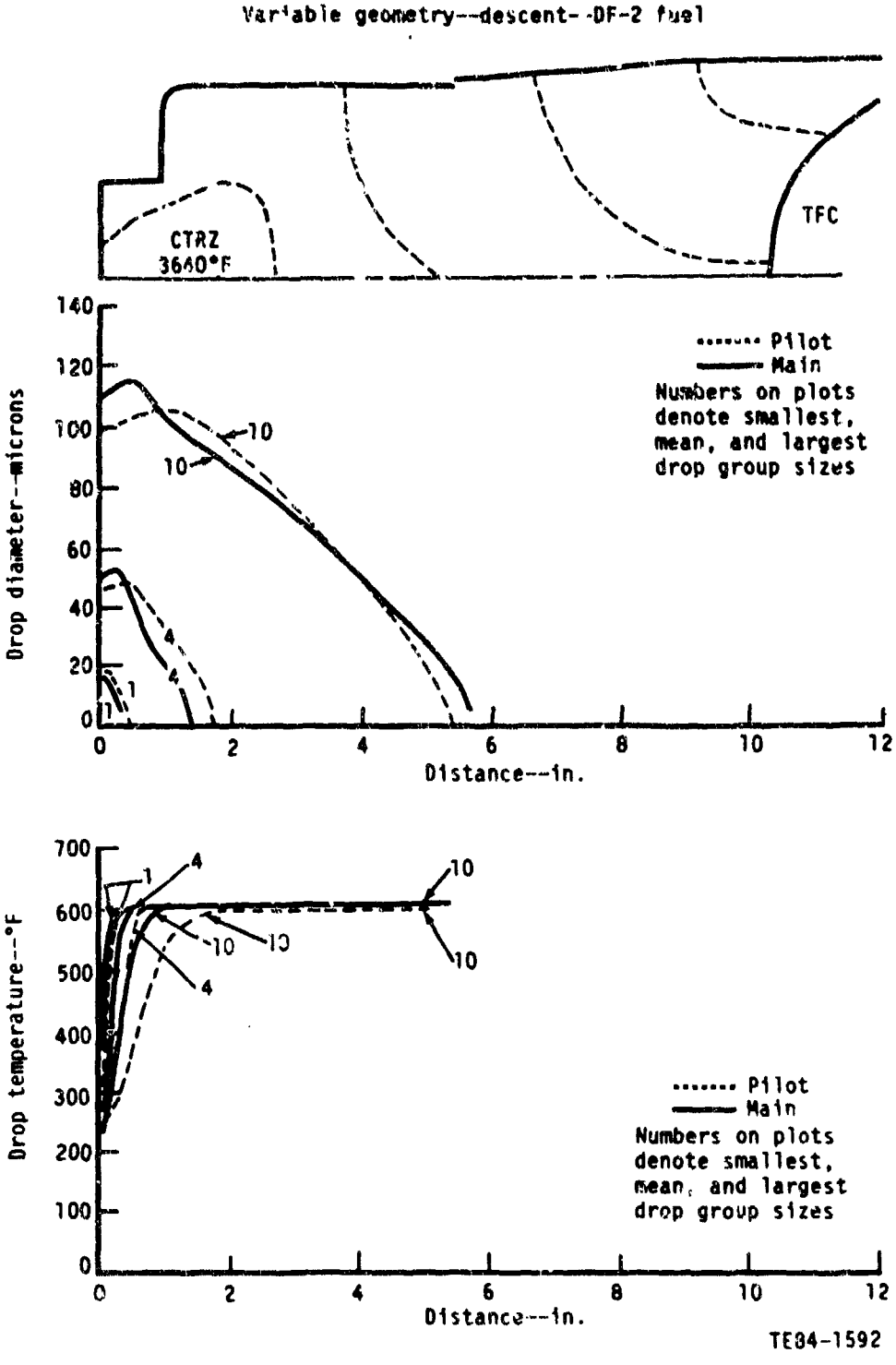

Figure 128. Variable geometry--descent with DF-2 fuel.

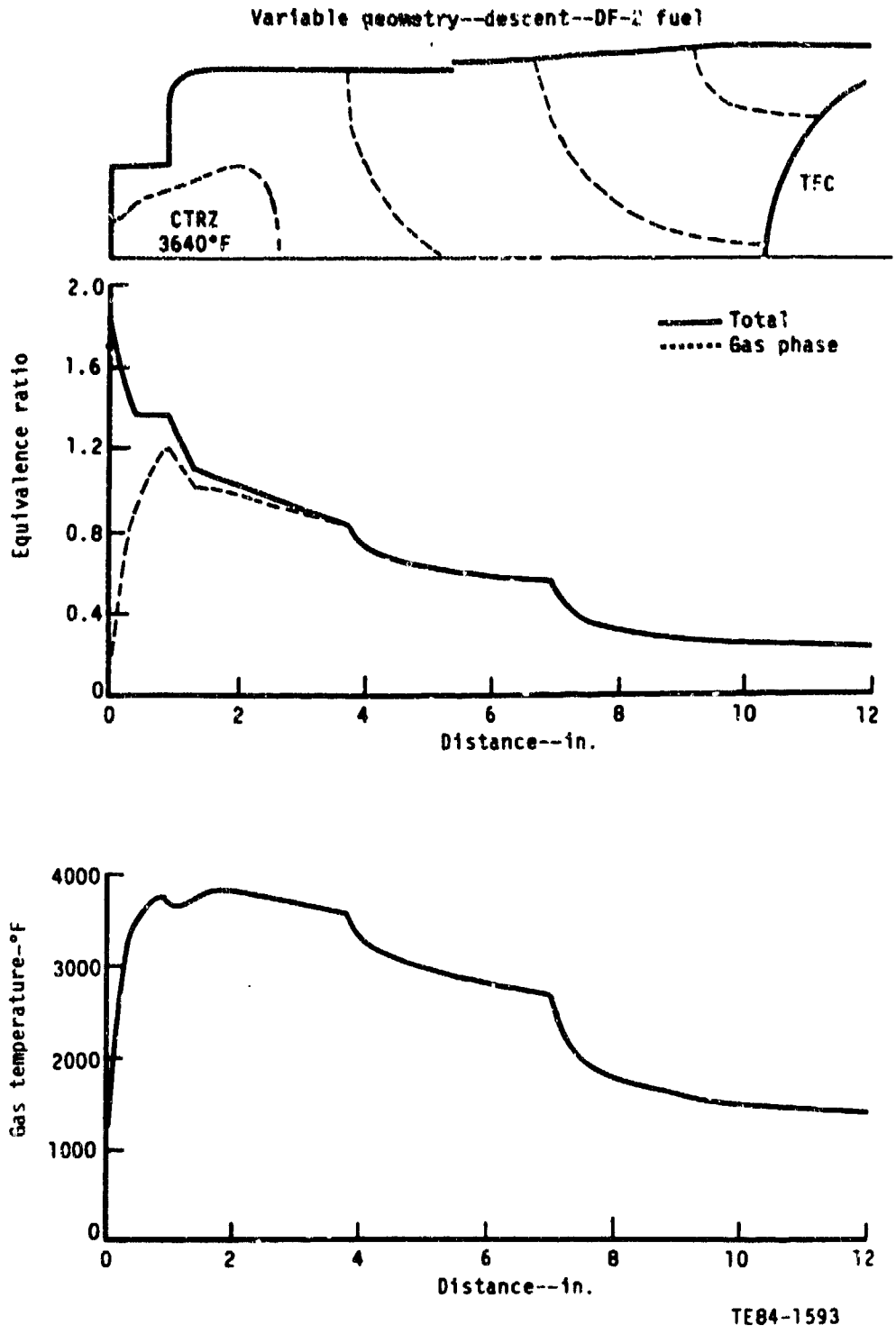

Figure 129. Variable geometry--descent with DF-2 fuel.

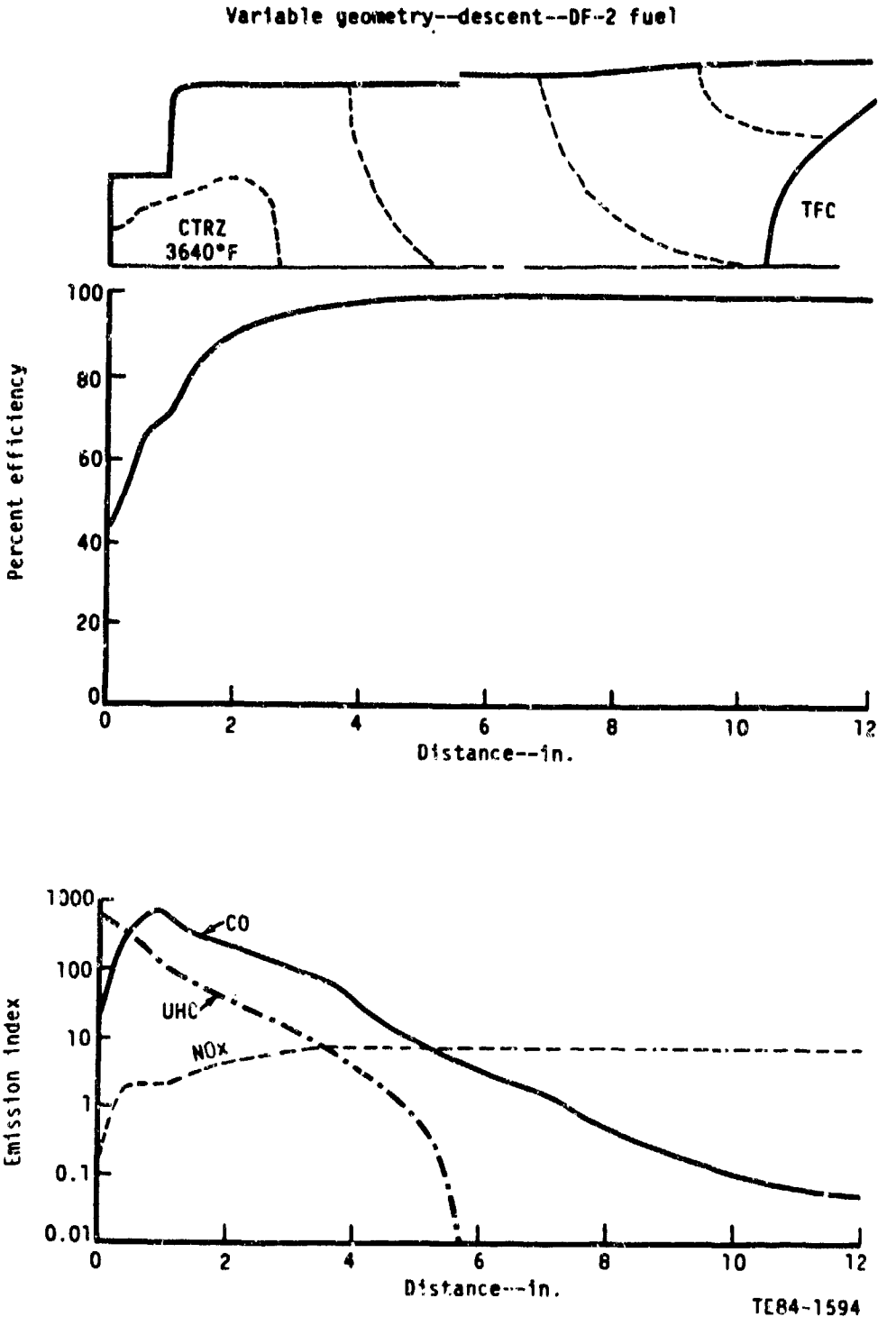

Figure 130. Variable geometry--descent with DF-2 fuel.

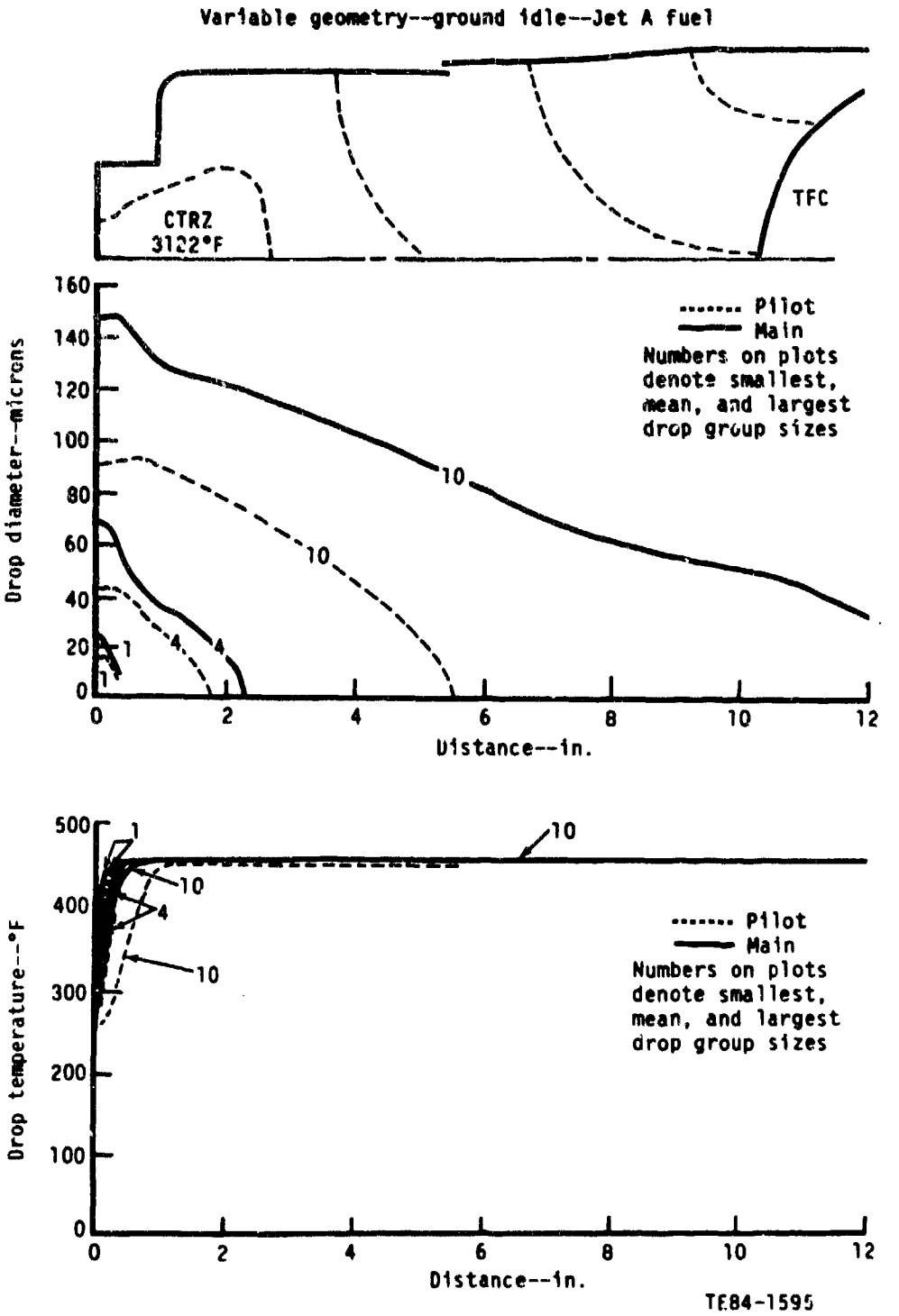

Figure 131. Variable geometry--ground idle with Jet A fuel.

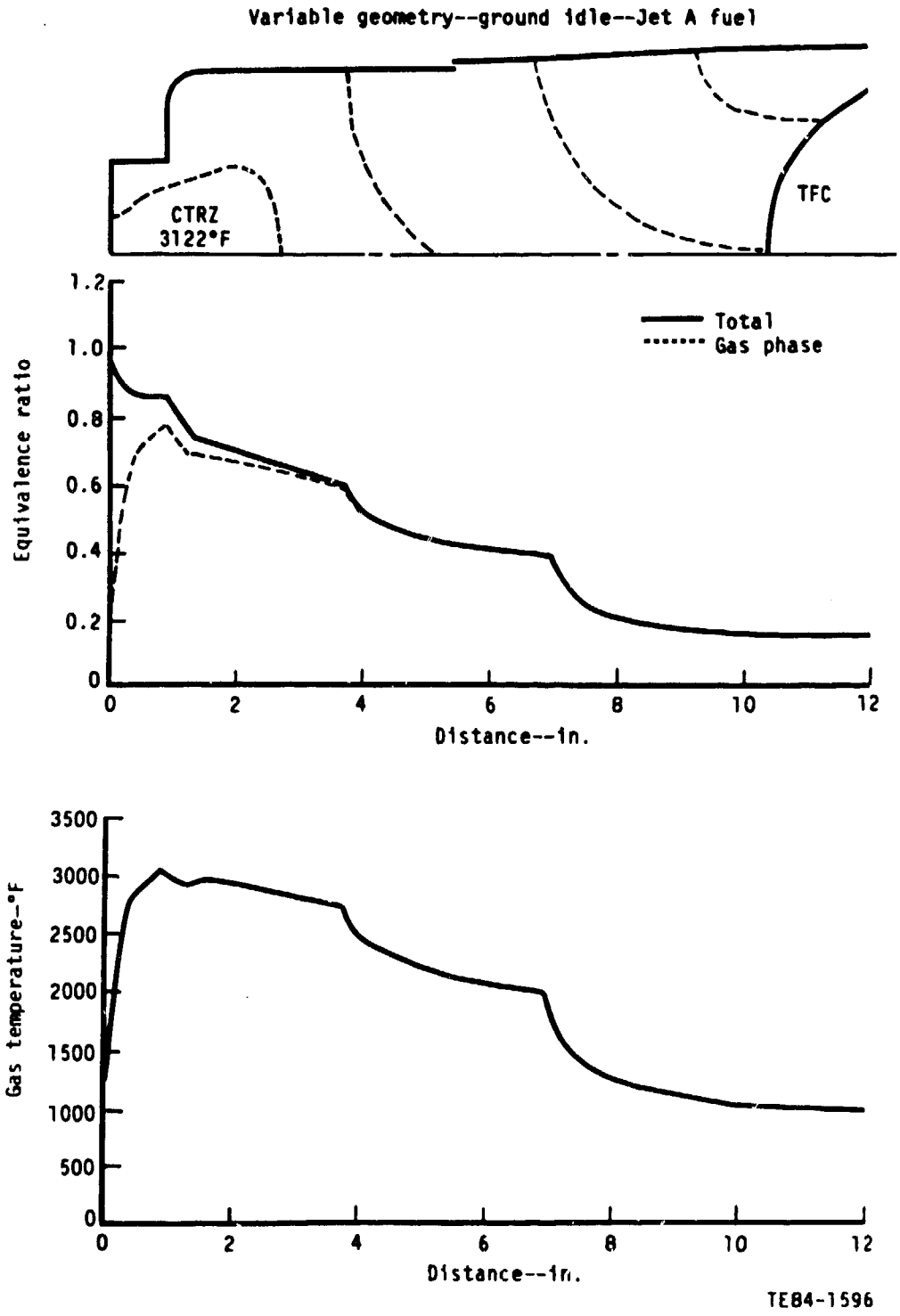

Figure 132. Variable geometry--ground idle with Jet A fuel.

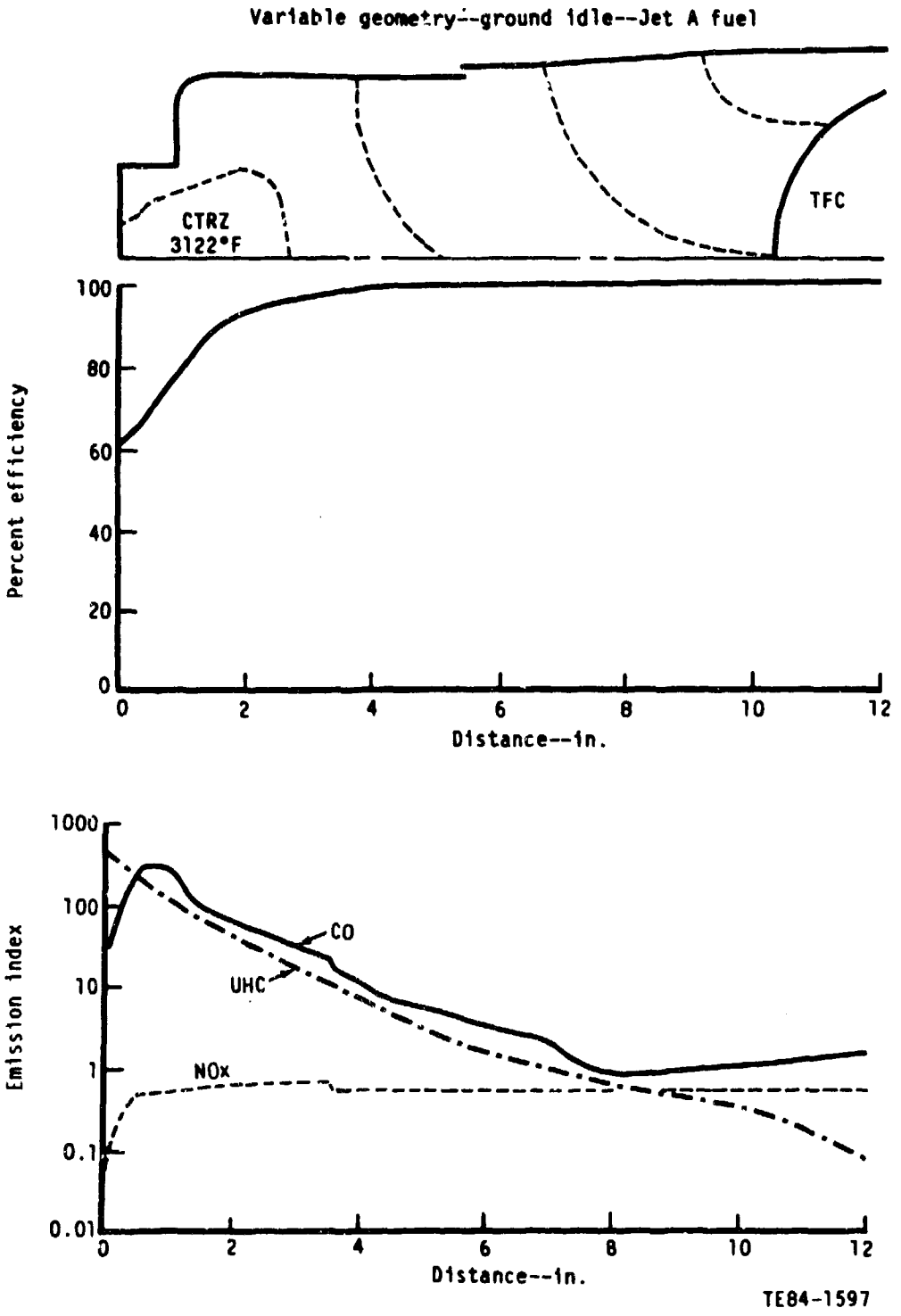

Figure 133. Variable geometry--ground idle with Jet A fuel.

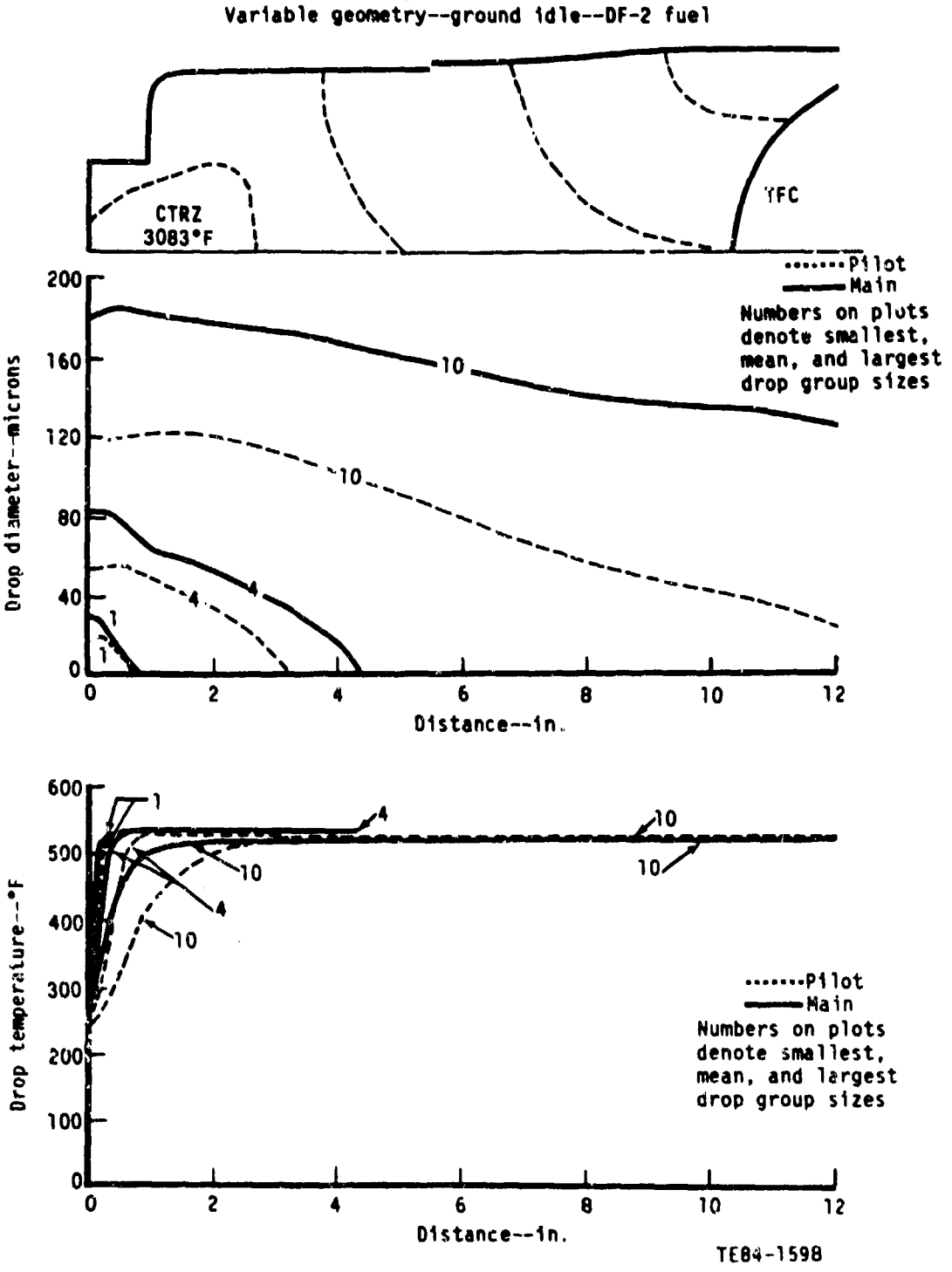

Figure 134. Variable geometry--ground idle with DF-2 fuel.

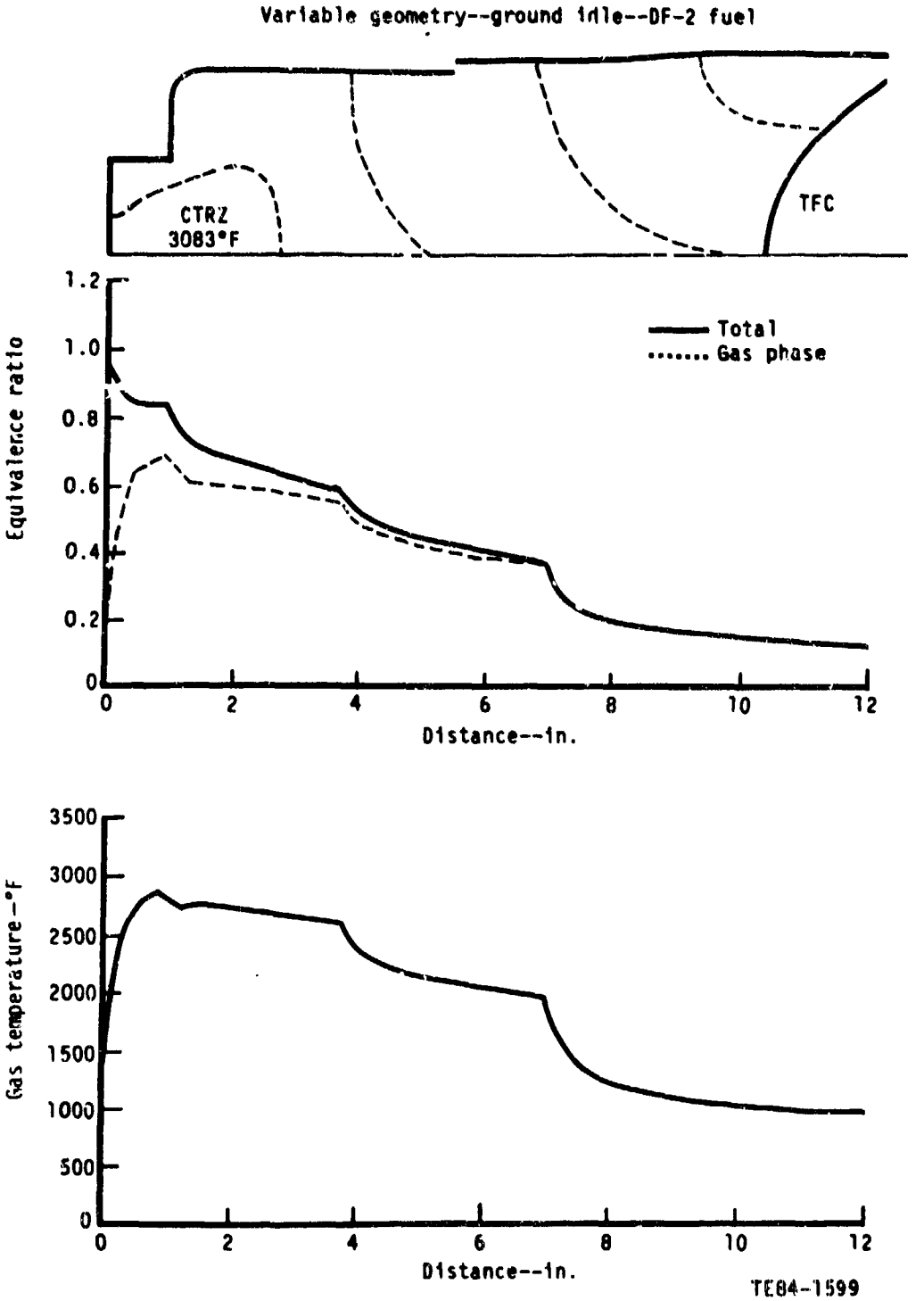

Figure 135. Variable geometry--ground idle with DF-2 fuel.

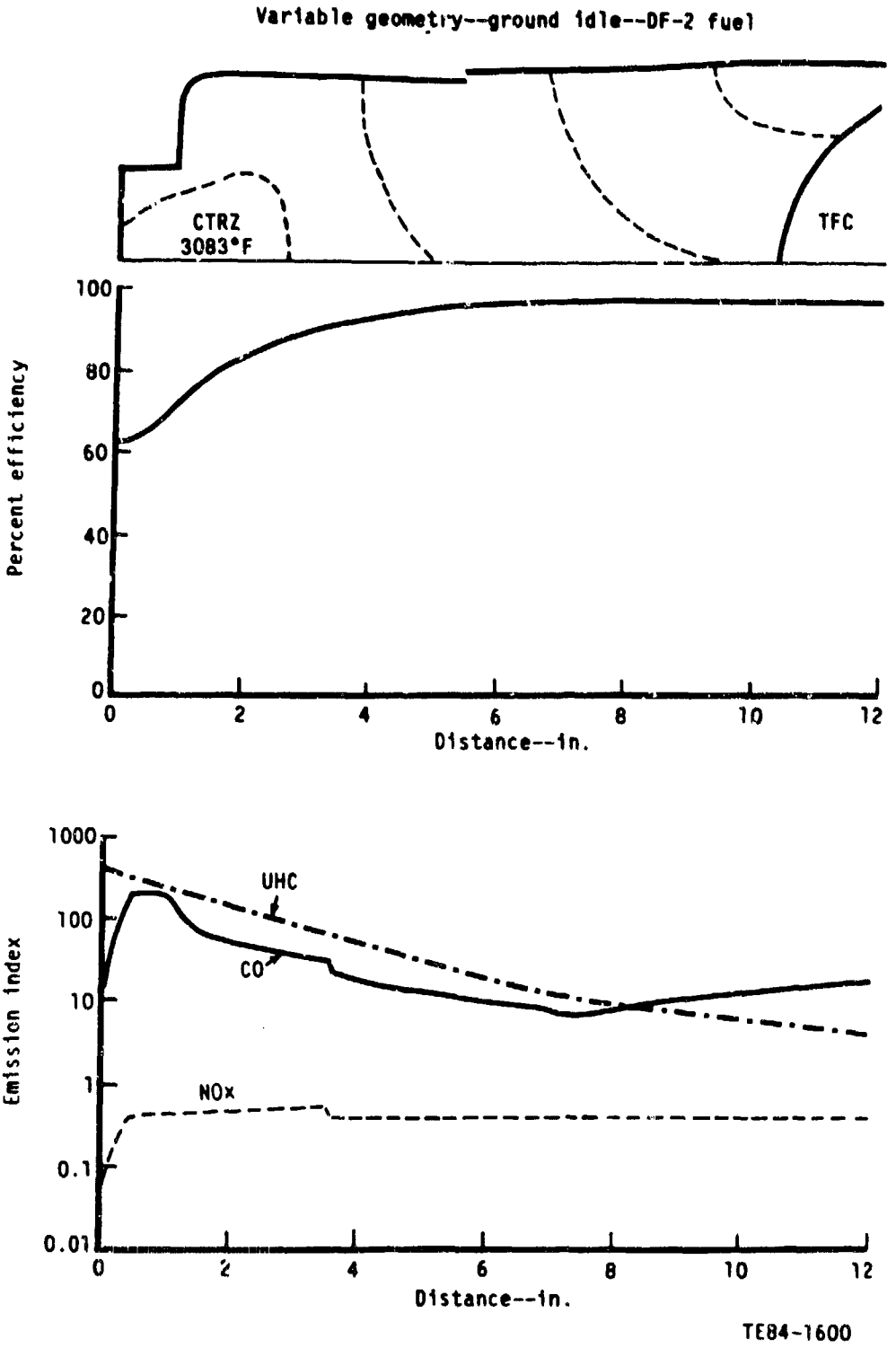

Figure 136. Variable geometry--ground idle with DF-2 fuel.

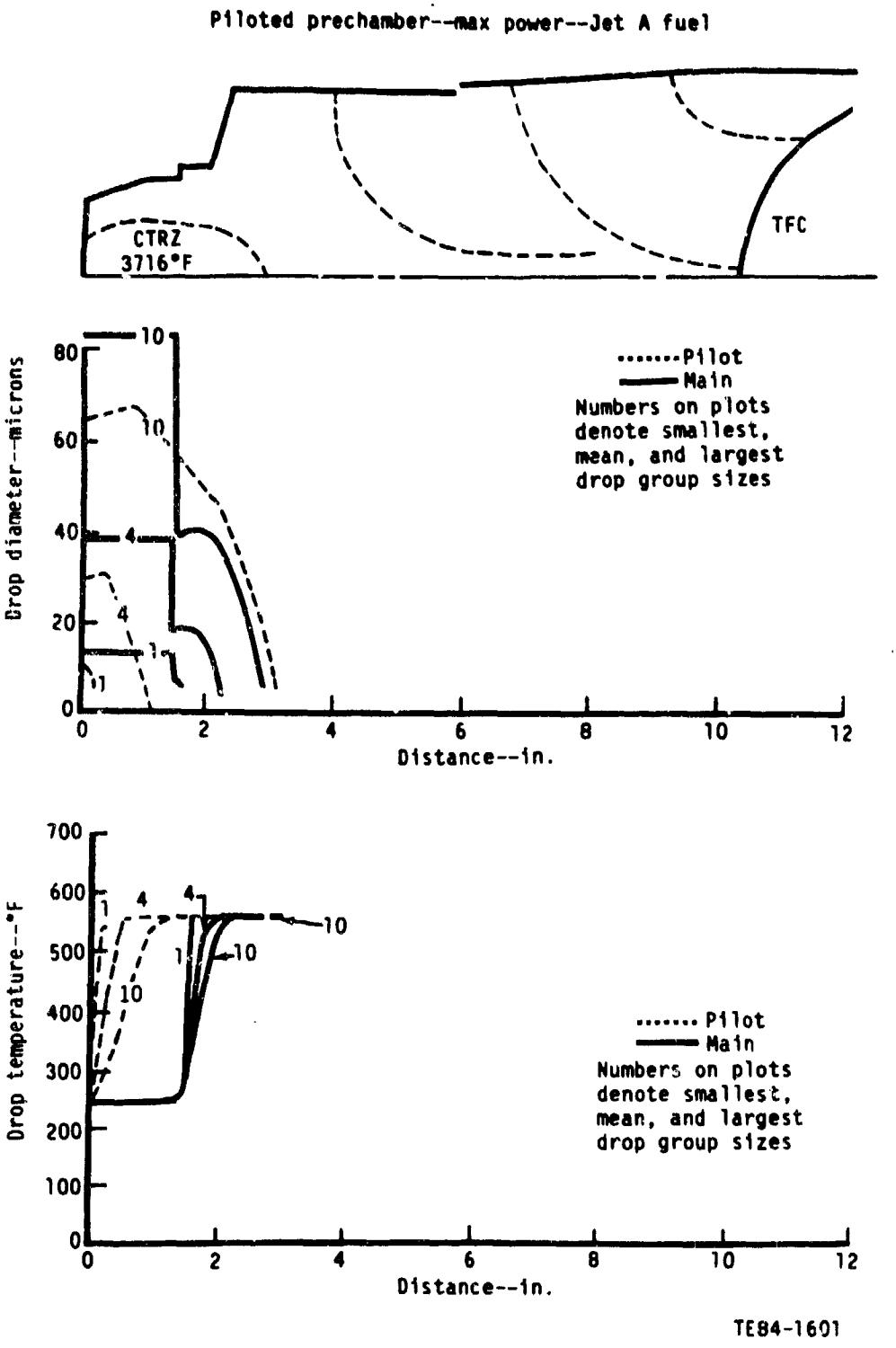

Figure 137. Piloted prechamber--maximum power with Jet A fuel.

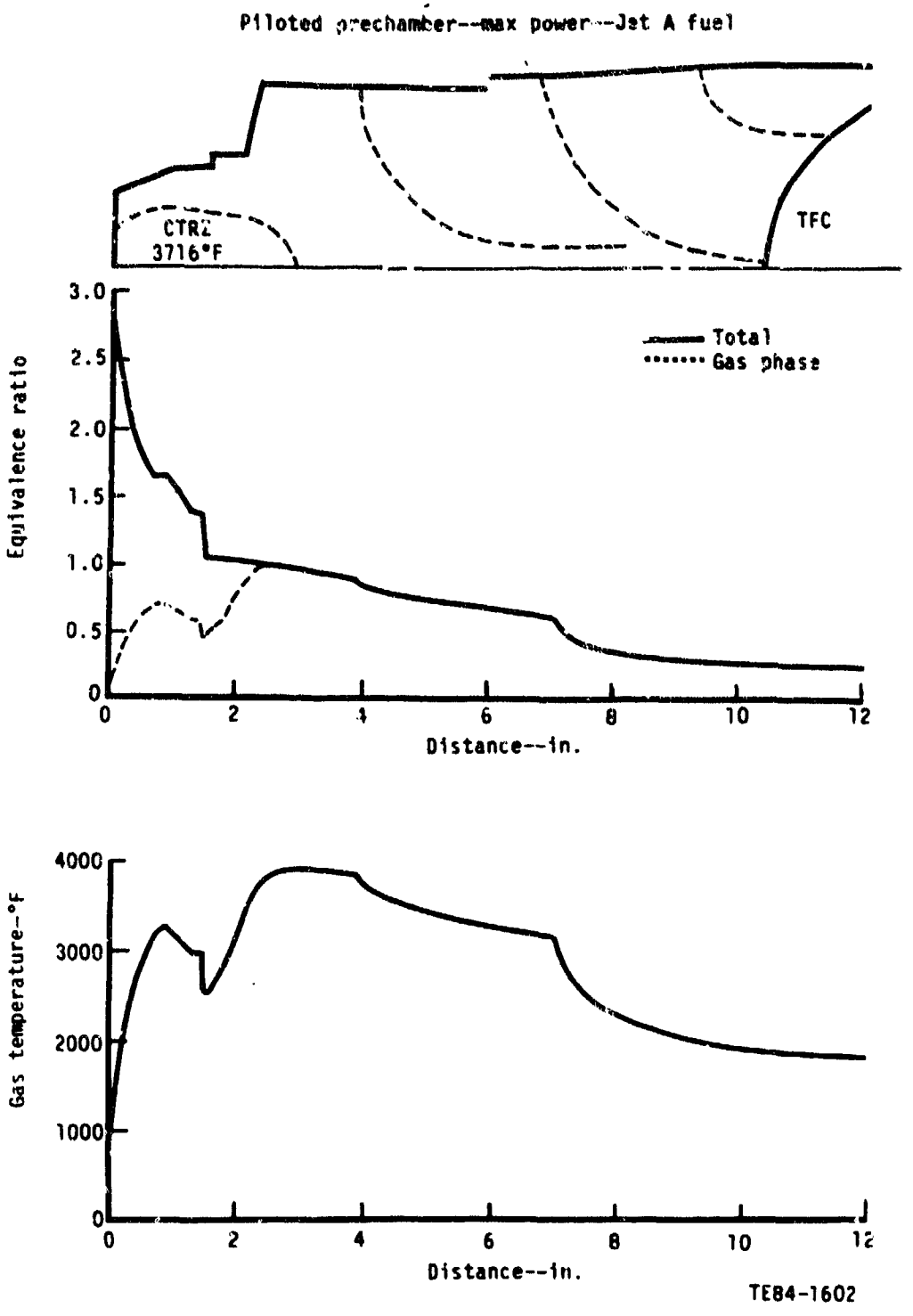

Figure 138. Piloted prechamber--maximum power with Jet A fuel.

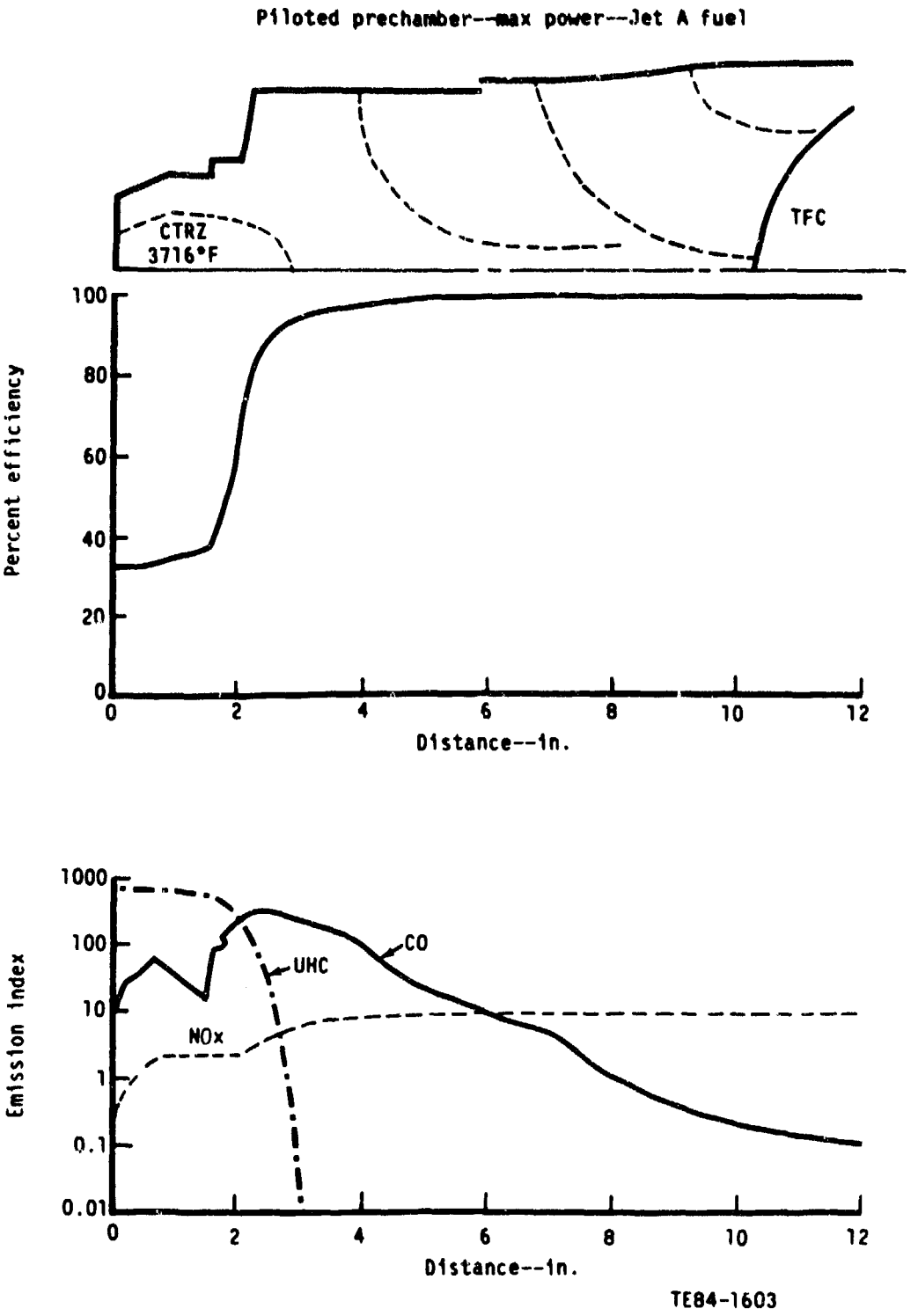

Figure 139. Piloted prechamber--maximum power with Jet A fuel.

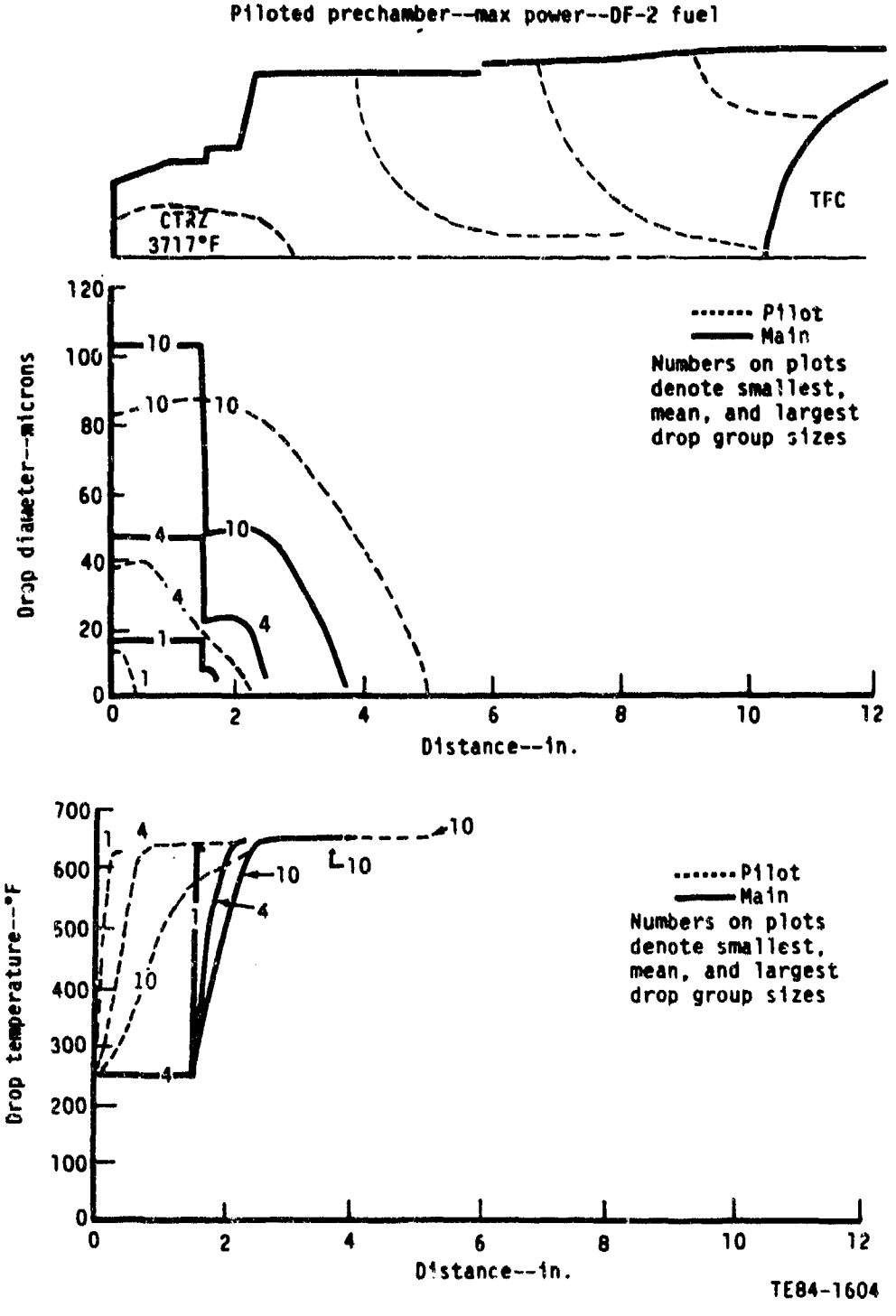

Figure 140. Piloted prechamber--maximum power with DF-2 fuel.

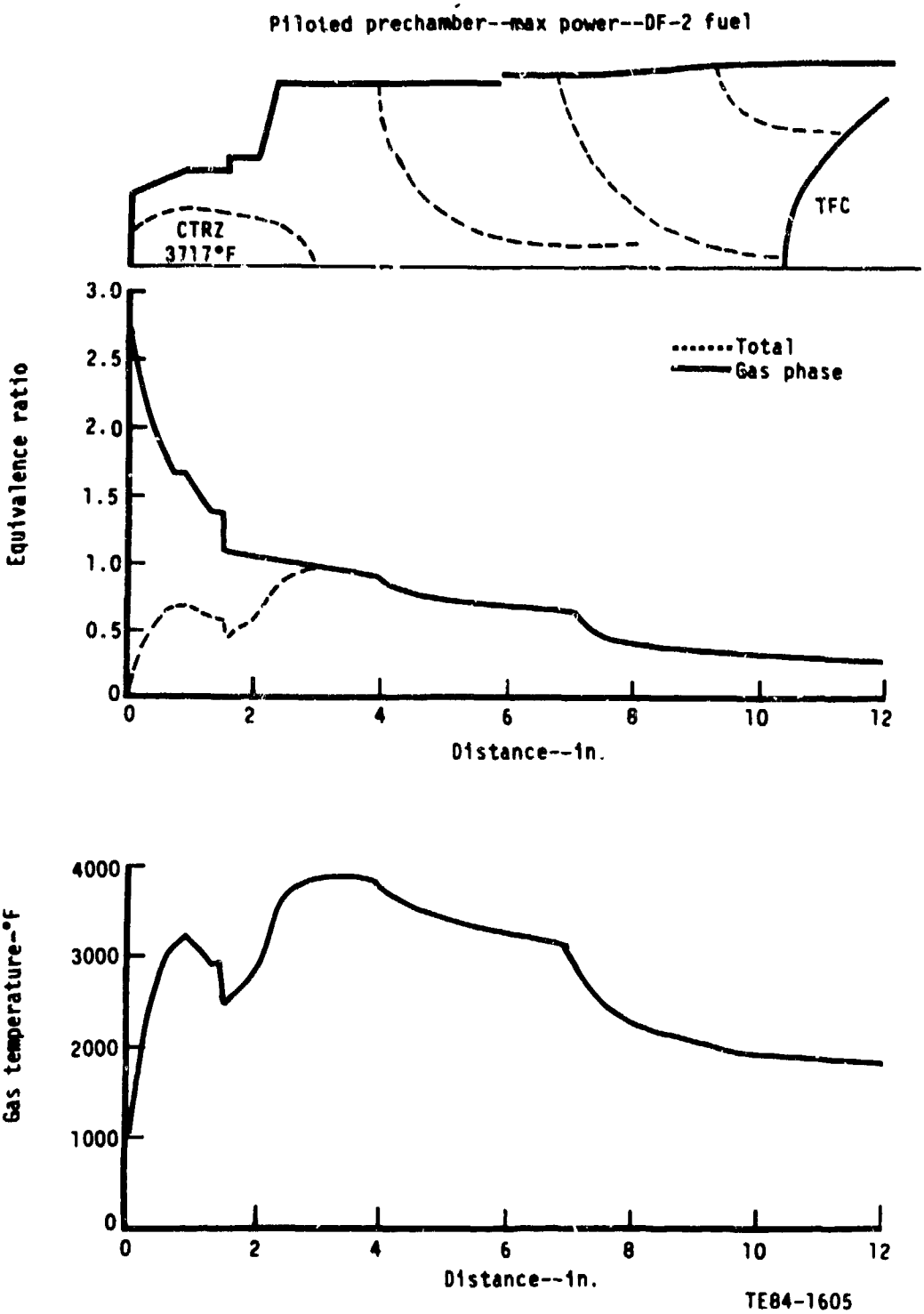

Figure 141. Piloted prechamber- maximum power with DF-2 fuel.

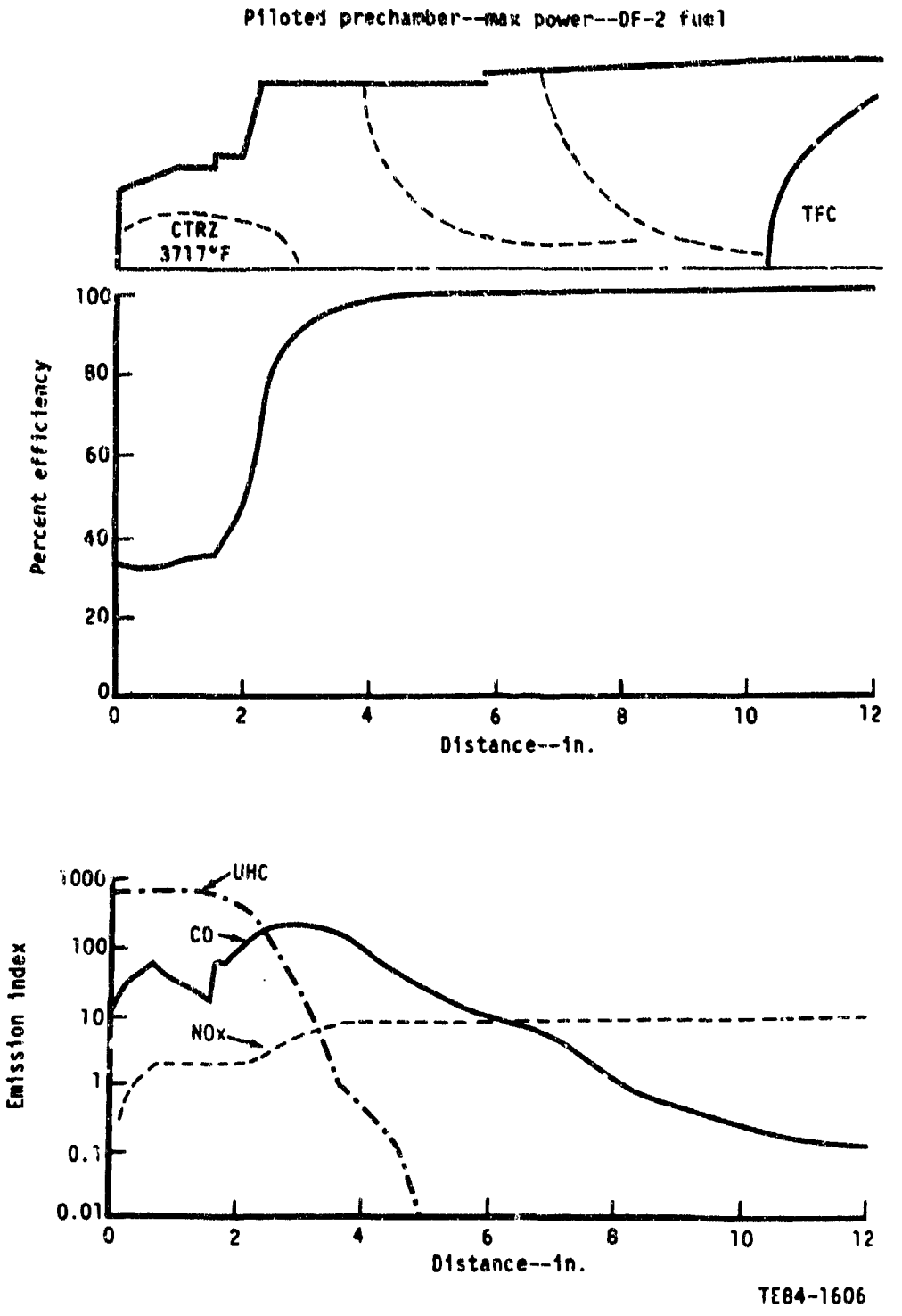

Figure 142. Piloted prechamber--maximum power with DF-2 fuel.

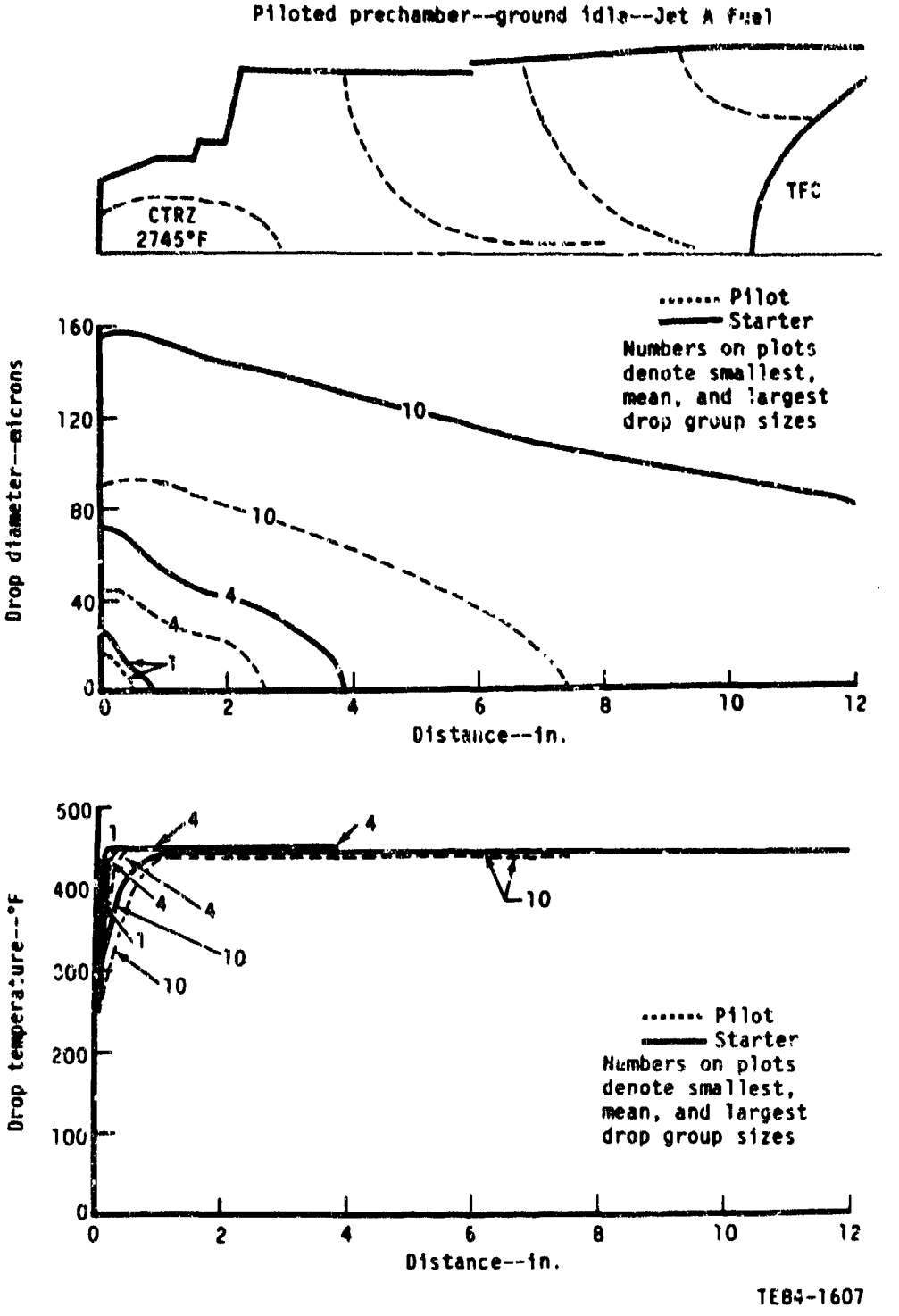

Figure 143. Piloted prechamber--ground idle with Jet A fuel.

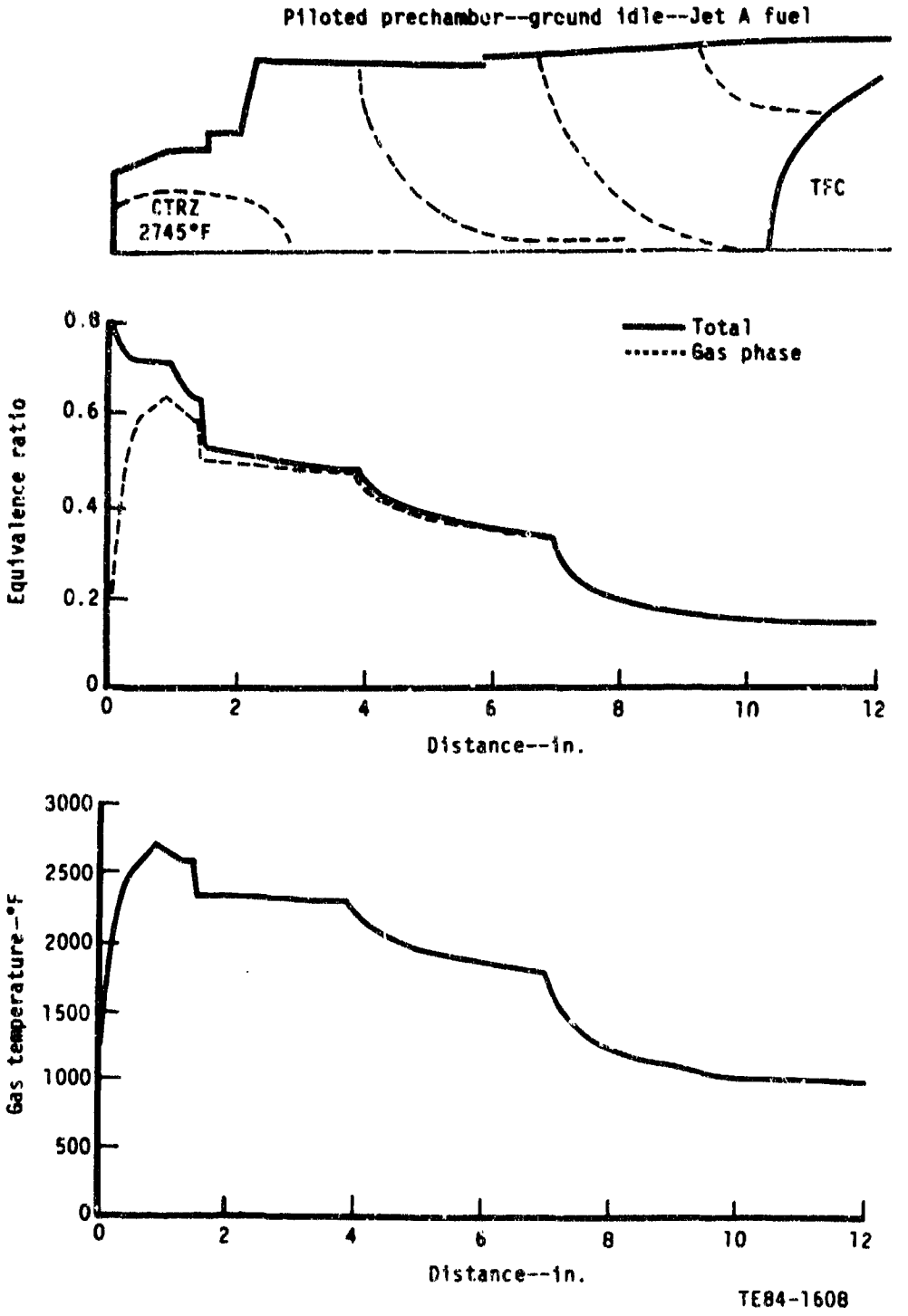

Figure 144. Piloted prechamber--ground idle with Jet A fuel.

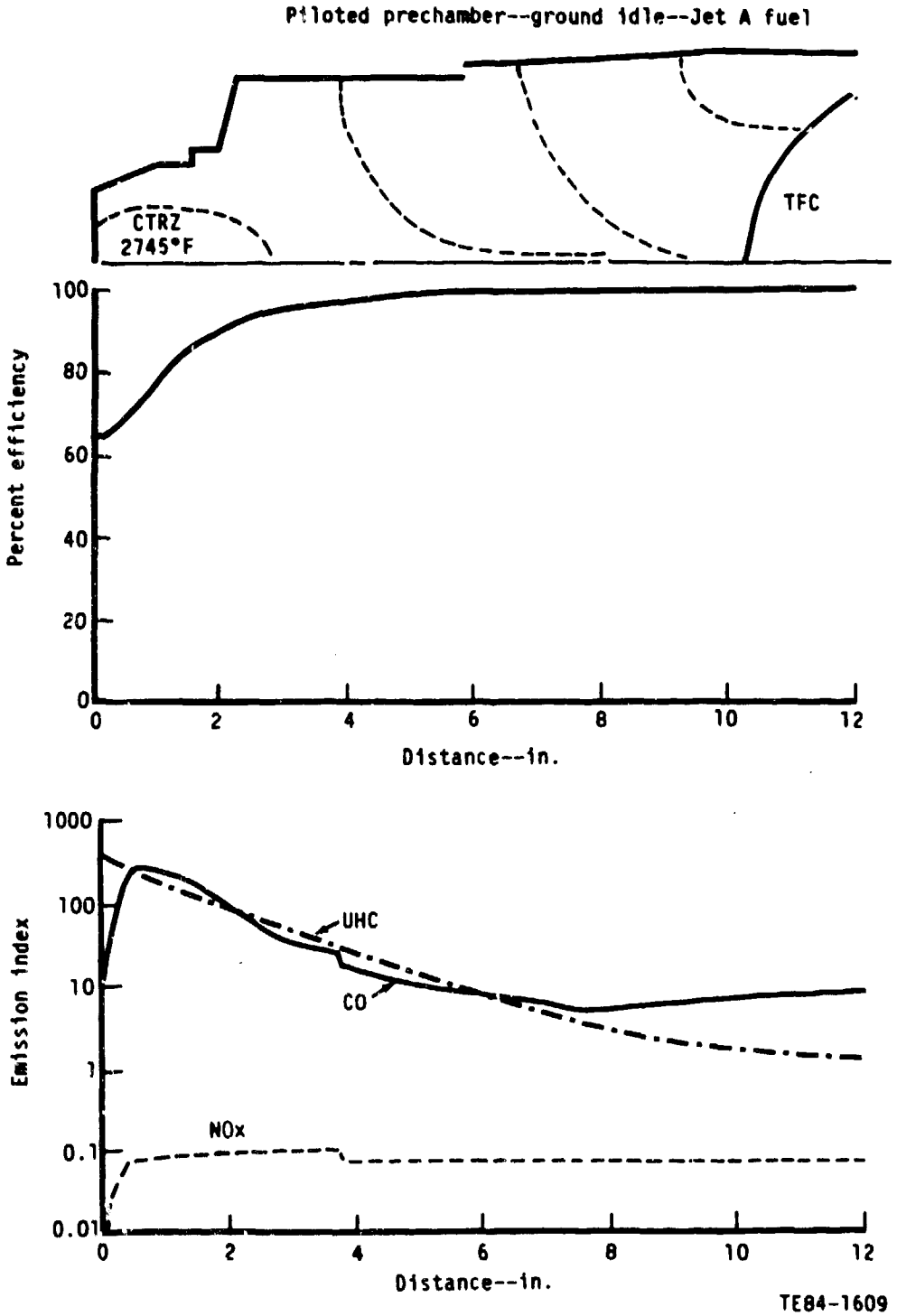

Figure 145. Piloted prechamber--ground idle with Jet A fuel.

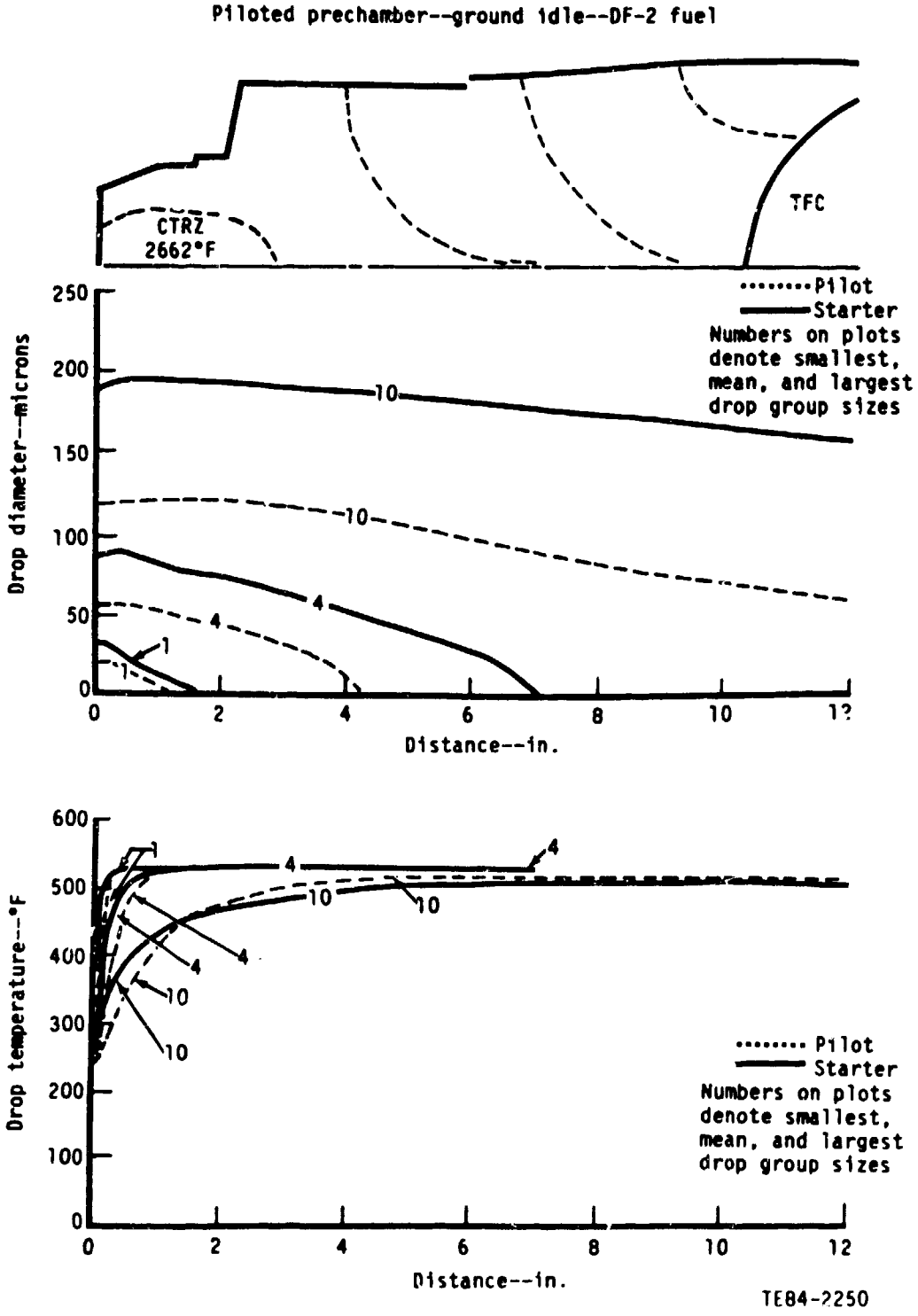

Figure 146. Piloted prechamber--ground idle with DF-2 fuel.

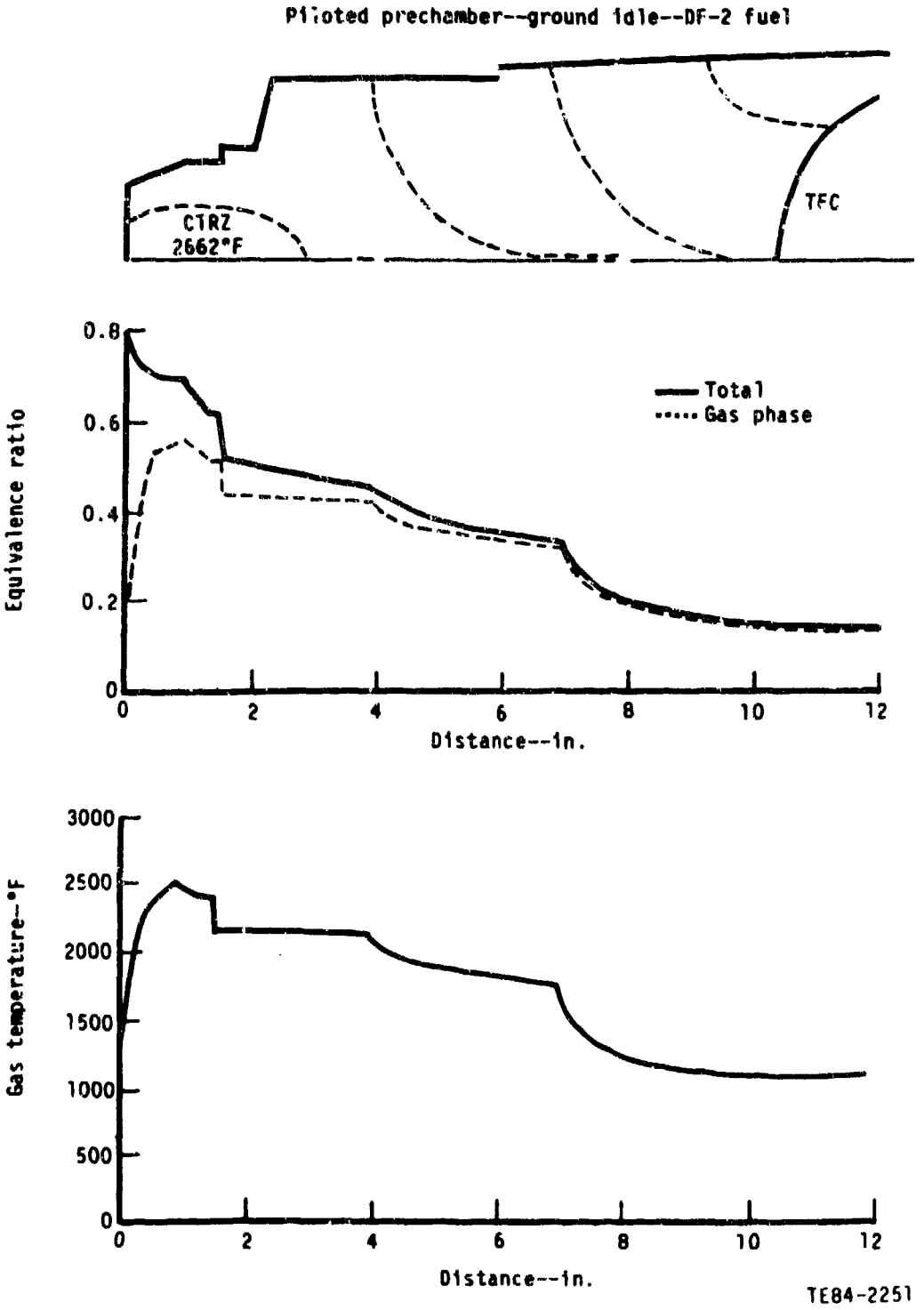

Figure 147. Piloted prechamber--ground idle with DF-2 fuel.

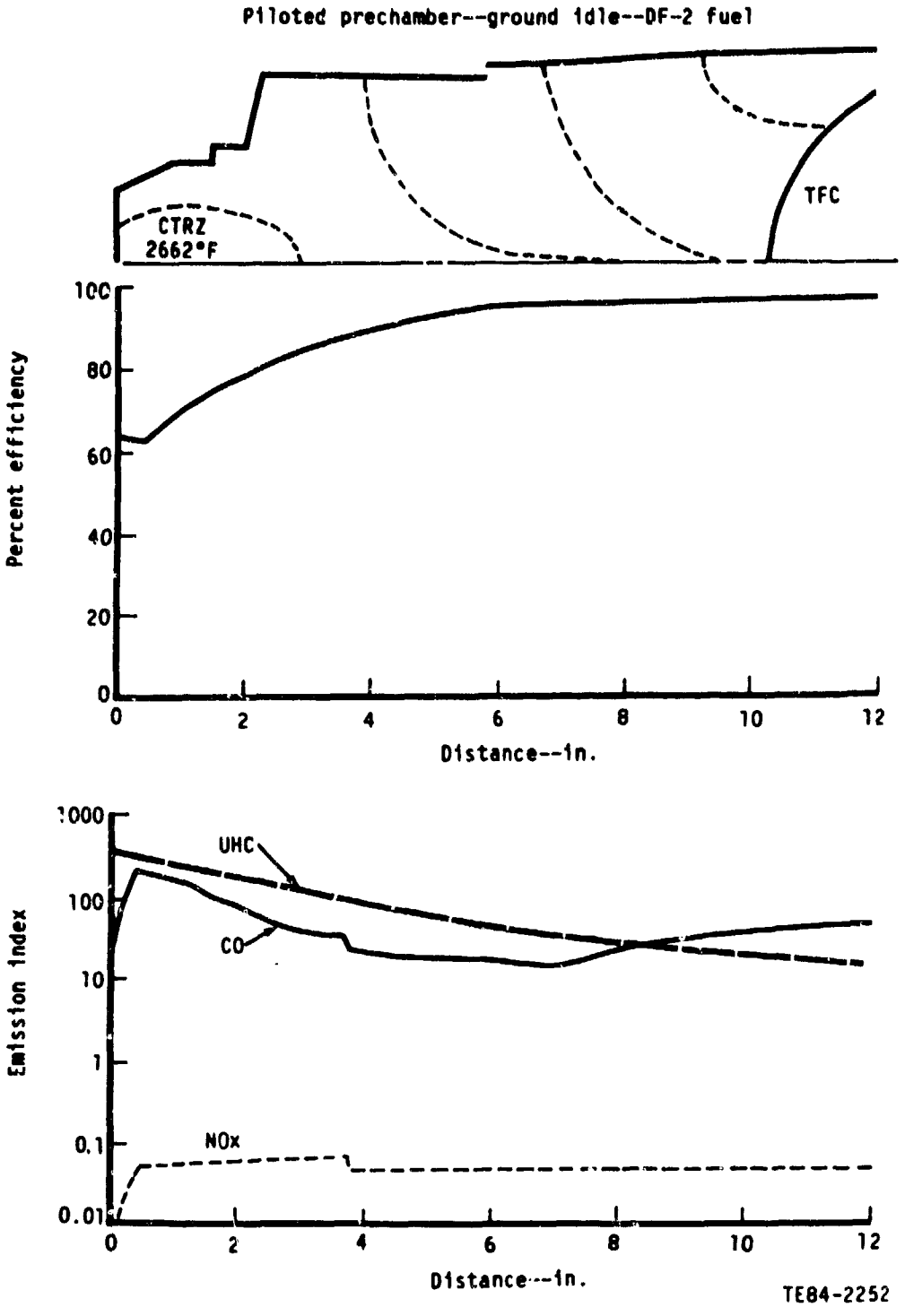

Figure 148. Piloted prechamber--ground idle with DF-2 fuel.

1. Report No.	2. Government Accession No.	3. Recipient's Catalog No.
NASA CR-174738 AVSCOM TR-84-C-14		

4. Title and Subtitle	5. Report Date
Analytical Fuel Property Effects-Small Combustors	October 1984
	6. Performing Organization Code

7. Author(s)	8. Performing Organization Report No.
R. D. Sutton, D. L. Troth, and G. A. Miles	EDR 11683
	10. Work Unit No.

9. Performing Organization Name and Address	11. Contract or Grant No.
General Motors Corporation Allison Gas Turbine Division P.O. Box 420 Indianapolis, Indiana 46206-0420	NASA-23165
	13. Type of Report and Period Covered
	Contractor Report

12. Sponsoring Agency Name and Address	14. Sponsoring Agency Code
NASA Lewis Research Center 21000 Brookpark Rd. Cleveland, Ohio 44135	

15. Supplementary Notes

Final Report. Project Manager, Steve Riddlebaugh. Aerothermodynamics and Fuels Division, NASA Lewis Research Center, Cleveland, Ohio 44135

16. Abstract

This report describes an analytical assessment of the consequences of using broad-property fuels in both conventional and advanced state-of-the-art small gas turbine combustors. Eight combustor concepts were selected for initial screening, of these, four final combustor concepts were chosen for further detailed analysis. These included the dual orifice injector baseline combustor (a current production 250-C30 engine combustor) two baseline airblast injected modifications, short and piloted prechamber combustors, and an advanced airblast injected, variable geometry air staged combustor.

Final predictions employed the use of the STAC-I computer code. This quasi 2-D model includes real fuels properties, effects of injector type on atomization, detailed droplet dynamics, and multistep chemical kinetics. In general, fuel property effects on various combustor concepts can be classified as chemical or physical in nature. Predictions indicate that fuel chemistry has a significant effect on flame radiation, liner wall temperature, and smoke emission. Fuel physical properties that govern atomization quality and evaporation rates are predicted to affect ignition and lean-blowout limits, combustion efficiency, unburned hydrocarbons, and carbon monoxide emissions. Nitric oxide formation is predicted to be dependent primarily on the combustion gas temperature and available oxygen concentration. Finally, STAC-I predicted results clearly indicate that any deteriorated performance characteristics of the alternate fuels are primarily due to the physical properties of the fuels as they affect atomization. As expected, the combustor candidates which employ hybrid airblast atomization are predicted to be less sensitive to the properties of alternate fuel type, and performance deterioration can be nearly negligible.

17. Key Words (Suggested by Author(s))	18. Distribution Statement
Small Gas Turbine; Combustor; Alternate Fuels; Fuel Property Effects; Combustor Performance; Combustion Emissions; Liner Wall Temperature; Analytical Predictions; Fuel Injector Effects	Unclassified-unlimited STAR Category

19. Security Classif. (of this report)	20. Security Classif. (of this page)	21. No. of Pages	22. Price*
Unclassified	Unclassified	222	

*For sale by the National Technical Information Service, Springfield, Virginia 22151